CIVIL ENGINEERING STUDIES

STRUCTURAL RESEARCH SERIES NO. 431

BEHAVIOR OF TEN-STORY REINFORCED CONCRETE WALLS SUBJECTED TO EARTHQUAKE MOTIONS

By

J. DARIO ARISTIZABAL-OCHOA

and

METE A. SOZEN

UNIVERSITY OF ILLINOIS
at URBANA-CHAMPAIGN
URBANA, ILLINOIS
OCTOBER 1976

BIBLIOGRAPHIC DATA SHEET	1. Report No. UILU-ENG-76-2017	2.	3. Recipient's Accession No.

4. Title and Subtitle

BEHAVIOR OF TEN-STORY REINFORCED CONCRETE WALLS SUBJECTED TO EARTHQUAKE MOTIONS

5. Report Date
October 1976

6.

7. Author(s)
J. Dario Aristizabal-Ochoa, Mete A. Sozen

8. Performing Organization Rept. No. SRS No. 431

9. Performing Organization Name and Address

University of Illinois at Urbana-Champaign
Urbana, Illinois 61801

10. Project/Task/Work Unit No.

11. Contract/Grant No.
ATA 7422962

12. Sponsoring Organization Name and Address

National Science Foundation
Washington, D. C. 20013

13. Type of Report & Period Covered

14.

15. Supplementary Notes

16. Abstracts

The response of ten-story reinforced concrete walls coupled by beams to earthquake base motions was investigated through experimental and analytical models.

The experimental work involved tests of small-scale ten-story reinforced concrete walls coupled by beams subjected to base motions, simulating one horizontal component of representative earthquake-motion records, on the University of Illinois Earthquake Simulator. Each test structure, consisting of two identical specimens parallel to each other and oriented such that the base motion caused them to bend about their strong axis, carried dead weight at each of the ten levels. The main variables in the experimental work were the strength of the test structures and the base motions. Measurements included horizontal acceleration at 22 locations and horizontal displacements at 20 locations.

17. Key Words and Document Analysis. 17a. Descriptors

17b. Identifiers/Open-Ended Terms

17c. COSATI Field/Group

18. Availability Statement

19. Security Class (This Report)
UNCLASSIFIED

20. Security Class (This Page
UNCLASSIFIED

21. No. of Pages
397

22. Price
10.75-3.00

FORM NTIS-35 (REV. 3-72)

THIS FORM MAY BE REPRODUCED

USCOMM-DC 14952-P72

BEHAVIOR OF TEN-STORY REINFORCED CONCRETE WALLS SUBJECTED TO EARTHQUAKE MOTIONS

by

J. Dario Aristizabal-Ochoa

and

Mete A. Sozen

UNIVERSITY OF ILLINOIS

URBANA, ILLINOIS

October, 1976

ii.

ACKNOWLEDGMENT

TABLE OF CONTENTS

LIST OF TABLES

viii

LIST OF FIGURES

1. INTRODUCTION

1.1 Object and Scope

The overall objective of this work was to investigate the response of multi-story reinforced concrete structures resisting earthquake forces primarily through "cantilever" rather than "frame" action. A secondary but important objective was to demonstrate the consequences of initial yielding in the wall or pier elements versus initial yielding in the beam elements.

The experimental work included tests of small scale perforated walls subjected to base motions simulating one horizontal component of representative earthquake records. These walls were designed using the principles of the "substitute-structure method" (Shibata, 1976)[*] for a given design spectrum.

The test results were used also to study the applicability of dynamic analyses based on linear response and "justify" the "substitute-structure method" as a procedure for determining the design forces of reinforced concrete frames.

---

[*] References are arranged in alphabetical order in the List of References. The numbers in parentheses refer to the year of publication.

1.2 Notation

All symbols used in the text are defined when they are first introduced. For convenient reference, they are listed below.

A = gross area of a cross section

A_s = area of tensile reinforcement; shear area

A_s' = area of compressive reinforcement

b = width of a cross section

c = depth to the neutral axis (kd)

C_c = compressive force in the concrete

C_s = force in the compressive reinforcement

d = effective depth of a cross section

d' = distance from the top concrete fiber to the centroid of the compressive reinforcement

D = total depth of a cross section

E_c = initial modulus of elasticity of concrete; Young's modulus of the columns

E_b = Young's modulus of the connecting beams

E_s = modulus of elasticity of steel

f_c = stress in the concrete

f_c' = compressive strength of the concrete

f_s = stress in the tensile reinforcement

f_s' = stress in the compressive reinforcement

f_{su} = ultimate stress of the reinforcement

f_t = tensile strength of the concrete (split cylinder)

f_r = modulus of rupture of the concrete

f_y = yield stress of the reinforcement (0.2% offset)

g = acceleration of gravity, 386 in./sec^2

G = shear modulus of concrete

I = moment of inertia of a cross section

I_a = moment of inertia of the transformed cracked section

L = length of a structural member

ℓ = half span of connecting beam

ℓ_a = anchorage length of reinforcement

M = bending moment

M_{ai}, M_{bi} = end moments of element i

n = modular ratio

p = tensile area ratio

P = axial force

P_i = strain energy of member i

r = radius of gyration

S_a = stiffness of actual structure (effective stiffness)

S_g = stiffness based on gross section

t = time

T_s = force in the tensile steel

Z = constant which defines the descending slope of the stress-strain curve of concrete

α = shear-deformation parameter (Eq. 2.11)

β = damping factor (fraction of critical damping)

β_b = damping factor for the connecting beams

β_c = damping factor for the columns

β_m = damping factor for mode m

γ = ratio of tensile- to compressive-steel area

δ = time increment

δ_y = yield deflection

ϵ_c = strain of concrete

ϵ_c^* = concrete strain of the extreme compressive fiber

ϵ_o = concrete strain at compressive strength

ϵ_s = strain of (tensile) steel

ϵ_s' = strain of compressive steel

ϵ_{su} = strain at ultimate strength of steel

ϵ_y = yield strain of steel

λ = (d'/d) in Eq. 2.7

θ = angle, indicated in Fig. 2.2

θ_s = rotation caused by slip of the reinforcement

μ = damage ratio, indicated in Fig. 2.2

ν = Poisson's ratio

ϕ = curvature

ϕ_y = curvature at yield

ϕ_{cr} = effect of cracking on flexural stiffness (Eq. 2.5)

ϕ_{sl} = effect of slip on flexural stiffness (Eq. 2.5)

2. TEST STRUCTURES

2.1 Introductory Remarks

This chapter describes the test structures, the geometric and mechanical properties of the structural components, as well as the general principles used in determining member sizes and relative strengths.

The ten-story test structure (Fig. 2.1) comprised two identical "frames" parallel to each other and to the direction of base motion. Each frame was made up of two walls (piers), 1 by 7 in. in cross section, connected at each level by 1 by 1.5-in. beams spanning 4 in. A steel weight of 1000 lb. was placed at each level. Story height was 9 in. The center of gravity of the weight at each level coincided with the elevation of that level and the geometric center of the beam section.

The test frames were not models of a particular prototype. They were designed primarily as physical tests of analytical concepts, with the proportions of the test frames governed by contraints created by the experimental facilities.

The general configuration of the test structure was chosen in order to investigate experimentally the response to strong ground motion of reinforced concrete multi-story structural-wall systems. The specific dimensions were determined by secondary objectives and experimental constraints.

The coupled-wall system was chosen because of questions with respect to the relative dissipation of energy in walls and

beams. Over and above the desire to simulate a multi-story sys-
tem, the use of many weights (stories) along the height of the
structure also makes it more convenient to observe continuously
the variation of structural response along the height.

The relationship between the input acceleration waveform
and the waveform reproduced by the earthquake simulator tends
to deteriorate at time compression ratios of five or higher
(Sozen,1970). Therefore, it was decided to use model ground mo-
tions having a time compression scale of 2.5 (model earthquake
duration was forty percent of prototype earthquake duration).
The choice of the time scale determined the shape of the accel-
eration response spectrum which had an approximately flat re -
sponse between 6 and 18 Hz, with the acceleration dropping off
rapidly above 18 Hz and gradually at frequencies below 6 Hz.
This constraint required that, in order to have an appreciable
effect, the second-mode frequency of the structure be in the
range from 6 to 18 Hz initially. The measured frequencies of
the "uncracked" test structure were approximately 4.5 for the
first mode and 18 Hz. for the second mode.

In the following portions of this report, the term "test
structure" will denote the entire structural system. The term
"frame" will refer to the combination of two walls (piers) con-
nected by beams in each level.

Two types of frames were built. These are referred to as
types D (the standard test frame) and M (the modified test
frame). Three structures with type-D frames and one structure

with type-M frames were contructed. The main difference between these two types of frames was the amount of steel reinforcement in the beams.

The following sections describe the basis for the proportioning of the frames of the test structure and the material properties.

2.2 Design Basis

The substitute-structure method (Shibata,1976) was used for determining the design forces. This method is explicitly a design method through which the minimum strengths of each com - ponent of a structure are determined so that a tolerable response displacement is not likely to be exceeded. The most significant feature of this method is that it takes into account the inelastic response of the structure using a linear-response model for dynamic analysis.

Given a design acceleration response spectrum, determination of the lateral forces by the substitute-structure method involves the following steps:

(1) Definition of the substitute structure: The flexural stiffnesses of the structural members are reduced in accordance with Eq. 2-1.

$$(EI)_{si} = (EI)_{ai}/\mu_i \qquad (2-1)$$

where $(EI)_{si}$ and $(EI)_{ai}$ are cross-sectional flexural stiffnesses of the member i in the substitute and actual structure, respectively, and μ is the selected tolerable "damage ratio" for el-

ement i.

Physical interpretation of the damage ratio, μ , and the stiffness of the actual structure, $(EI)_{ai}$, is illustrated in Fig. 2.2. The rigid portions at the ends of the beam are shown hatched. The solid curve in the figure represents the relationship between the end moment, M, and the rotation of the fixed support, θ , caused by flexural deformation within the span. The damage ratio, μ , is comparable to but not exactly the same as "ductility" based on the ratio of maximum to yield rotation. Damage and ductility ratio are numerically identical only for elastoplastic response.

Estimates of the stiffnesses of the structural members of the actual structure, denoted with the subscript a above, are discussed in section 2.3.

(2) Modal Responses: Periods (or frequencies), mode shapes and modal forces for the undamped substitute structure are ob - tained from a linear modal analysis.

(3) Damping factors: The damping factors for each mode are obtained by assuming that the overall damping for a particular mode can be obtained from the following expression

$$\beta_m = \Sigma \frac{P_i{}^*\beta_{si}}{\Sigma P_i} \qquad (2\text{-}2)$$

where $\qquad P_i = \frac{L}{6(EI)_{si}} \, (M_{ai}{}^2 + M_{bi}{}^2 - M_{ai}M_{bi}) \qquad (2\text{-}3)$

$$\beta_{si} = 0.2 \, (1 - (1/\mu_i)^{\frac{1}{2}}) + 0.02 \qquad (2\text{-}4)$$

where β_m = damping ratio for mode m

P_i = strain energy of structural member i

β_{si} = substitute viscous damping factor for structural member i

μ_i = damage ratio for structural member i

L = length of structural member

M_{ai} and M_{bi} = end moments of substitute-structure element i for mode m.

Expression (2-4) was derived from observed maximum inelastic response of single-degree-of freedom reinforced concrete systems under earthquake motions (Gulkan, 1974; Takeda, 1970). This expression provides an estimate of the amount of equivalent viscous damping required to simulate the observed effect of hys - teretic damping on the response of a reinforced concrete element to earthquake excitation.

Expression (2-3) assumes that each element of the substitute structure contributes to the modal damping in proportion to its relative flexural strain energy associated with the modal shape.

(4) Design Base Shear Force: The design base shear force is taken as the average of the root-sum-square value (RSS) and the maximum value for absolute sum of the effects of two modes.

(5) Member Design Forces: Normally the member design forces are obtained from the RSS combination modified by the ratio of the design base shear and the RSS value. However, because the characteristics of the base motion used in the tests could

be estimated with confidence, the member design forces of the structures were based only on the RSS combination.

2.3 Member Stiffnesses of Actual Structure

One of the most important steps in the calculation of the design forces, and corresponding displacements using the substitute-structure method is the determination of stiffnesses of the structural members of the actual structure.

In reinforced concrete members there are generally two effects that should be taken into account when the actual stiffness is required.

$$S_a = (\phi_{cr}) \ (\phi_{sl}) \ S_g \qquad\qquad (2-5)$$

where S_a = Stiffness of actual structure

S_g = Stiffness based on plain gross section

ϕ_{cr} = factor representing the effect of cracking

ϕ_{sl} = factor representing the effect of slip of the reinforcement

In the case of flexural stiffness the cracking effect is usually evaluated using the moment of inertia of the trans - formed cracked section and no tensile strength for concrete as shown in Fig. 2.3 . If strain and stress distributions are assumed as shown in the figure, the moment of inertia of the tranformed cracked section can be written as follows

$$I_a = \frac{1}{3} b(kd)^3 + nA_s (1-k)^2 d^2 + (n-1) A_s' (kd-d')^2 \quad (2-6)$$

where

I_a = moment of inertia of the transformed cracked section

b = width of cross section

d = distance from extreme compressive fiber to center of tensile reinforcement

kd = depth to neutral axis

d' = distance from extreme compressive fiber to center of compressive reinforcement

A_s = Area of tensile reinforcement

A_s' = Area of compressive reinforcement

n = (E_s/E_c) or modular ratio

From the compatibility and equilibrium conditions across the section

$$k = -pn(1 + \gamma) + [p^2 n^2 (1+\gamma)^2 + 2pn (1+\gamma\lambda)]^{1/2} \quad (2-7)$$

in which

p = A_s/bd or tensile area ratio

$\gamma = A_s' /A_s$

$\lambda = d'/d$

Variation of the factor representing the effect of cracking, $\emptyset_{cr}$, with the amount of reinforcement is given by Ferguson (1973, page 740).

The increase in flexibility due to slip of the reinforcement is particularly important in the connecting beams of the

test structures. Figure 2.4a shows half span of a connecting beam. If curvature along the span and strain along the anchorage of the reinforcement are assumed as shown in Fig. 2.4 the total deflection at yield can be written as follows

$$\delta_y \approx \phi_y \frac{\ell^2}{3} + \theta_s \ell \tag{2-8}$$

where δ_y = total end deflection at yield

ϕ_y = yield curvature

θ_s = end rotation caused by slip of reinforcement

Assuming linear strain distribution across the depth of the fixed end section and fixed neutral axis along the span

$$\delta_y = \frac{\epsilon_y}{d(1-k)} \frac{\ell^3}{3} + \frac{\epsilon_y \ell_a}{2} \frac{\ell}{d(1-k)} \tag{2-9}$$

where ℓ = half span of connecting beam

ℓ_a = anchorage length of beam reinforcement

ϵ_y = yield strain in reinforcement

Therefore

$$\phi_{sl} = 1/(1 + \frac{3}{2} \frac{\ell_a}{\ell}) \tag{2-10}$$

The factor "2" in expressions (2-9) and (2-10) is changed to "3" if a parabolic distribution is assumed for the strain along the anchorage length.

The slip effect becomes negligible in elements with small (ℓ_a/ℓ) values.

Another effect which is particularly important in the connecting beams is the shear deformation. Figure 2.2 shows the

deflected shape of a connecting beam. The flexibility of the beam increased by $(1+\alpha)$, where α is the shear-deformation pa - rameter (Przemieniecki, 1968). In the elastic range this pa - rameter is given by the expression shown below.

$$\alpha = \frac{12(EI)}{G A_s \ell^2} = 24(1+\nu) \frac{A}{A_s} (\frac{r}{\ell})^2 \tag{2-11}$$

where G = shear modulus $(= \frac{E}{2(1+\nu)})$

A_s = beam cross-sectional area effective in shear

$(= 5/6 \; A_{gross}$ for rectangular beams)

r = radius of gyration of section along flexural axis

ν = Poisson's ratio

If the ratio of radius of gyration to element length, (r/ℓ), is small by comparison with unity, as is the case with a slender beam, the shear deformation becomes negligible.

2.4 Design of the Standard Test Structure (Type D)

The critical sections of the test frames were reinforced to resist the lateral loads, based on a design response spectrum, and the gravity loads which acted at the geometric center of the walls. No load factors were used. Yield stress of the steel was based directly on the average value obtained from coupon tests (Fig. A.9). The assumed concrete strength was 4500 psi at 0.003 strain with a Young's modulus (E_c) of $3 * 10^6$ psi and Poisson's ratio of 0.15. No "understrength" factors were used in calcula- ting section resistances. Response spectrum A (Shibata, 1976,

Fig. 1), modified to a time scale of 1/2.5 (Fig. 2.5), was
used for the design of the test structures (maximum ground ac-
celeration= 0.5g). A detailed comparison between the assumed
and obtained spectra is described in chapter 6.

The design forces determined by the substitute-structure
method, corresponding to the assumed response spectrum, were
calculated as described below.

(1) Substitute structure: The model used for analysis of
lateral-force effects is shown in Fig. 2.6. A point of inflec-
tion was assumed to exist at beam mid-span. Axial deformation was
considered only in the walls. The walls were assumed to be
fixed at the base. The finite dimensions of the joints were
taken into consideration by inclusion of rigid portions at the
ends of the beam members, shown by hatched portions in Fig. 2.6b.
Each beam was assumed to be prismatic throughout its clear span.

The member stiffnesses of the actual structure were modi-
fied assuming damage ratios of one for the walls (μ_c=1) and
two for the connecting beams (μ_b=2). These specific damage
ratios were chosen with the intent (1) that energy should be
dissipated in the beams during the initial or design earthquake
motion and (2) that excessive displacements should be avoided
resulting from the high flexibility of the connecting beams
caused by the slip of the reinforcement, cracking of the con-
crete and shear deformation along the span.

To make calculations simple, the stiffnesses of the struc-
tural members of the substitute structure were obtained by mod-

ifying the Young's modulus of each member, E_i. The modifications are made taken into account the different stiffness reduction factors described in section 2.3.

Because the amount of steel reinforcement in the walls and beams was not known at the initial stage of the design, it was assumed for the first trial calculation that the ratio of cracked-to-gross-section moment-of-inertia was 1/2 for beams and columns. After a set of design forces were determined on this basis, the required amounts of reinforcement were selected and the dynamic analysis was repeated with the revised stiffnesses.

The calculations for the Young's modulus of the substitute frame for the first trial calculation are discribed below.

For the beams,

$$\phi_{cr} = 1/2 \quad \text{(assumed)}$$

$$\phi_{sl} = \frac{1}{(1+\frac{3}{2}*\frac{6.75}{2})} \approx \frac{1}{6} \quad \text{(assuming } \ell_a = 6.75 \text{ in.)}$$

$(1+\alpha)$ = effect of shear deformation
= 1.38 (assuming I_{gross} and $A_s = \frac{5}{6} A_{gross}$)

therefore

$$E_b = \frac{3*10^6 \text{ psi}}{2*6*1.38*\mu_b} = \frac{3*10^6 \text{ psi}}{33} \approx 91000 \text{ psi}$$

For the columns,

$$\phi_{cr} = 1/2 \quad \text{(assumed)}$$

$$\phi_{cl} = 1 \quad \text{(assuming } \ell \gg \ell_a\text{)}$$

$$(1+\alpha) = 1 \quad \text{(assuming } r/\ell \ll 1\text{)}$$

therefore

$$E_c = \frac{3*10^6 \text{ psi}}{2* \mu_c} = 1500,000 \text{ psi}$$

The moment of inertia of the transformed cracked section for the final calculation were determined using expressions (2-6) and (2-7) and the cross section properties shown in Fig. 2.16 and 2.17.

For the beams, $p = \frac{0.0206}{1.25} = 0.0165$

$$\lambda = \frac{0.25}{1.25} = 0.2$$

$$\gamma = 1.0 , \quad n \approx 10$$

therefore

$$kd = 0.48 \text{ in.} \quad \text{and} \quad I_{cracked} = 0.169 \text{ in}^4$$

$$\emptyset_{cr} = \frac{I_{cracked}}{I_{gross}} = \frac{0.169}{0.281} = 0.60$$

$$E_b = 91000* \frac{0.6}{0.5} \approx 110,000 \text{ psi}$$

For the first six columns,

$$p = \frac{4*0.0206}{6.25} = 0.0132$$

$$\lambda = \frac{0.75}{6.25} = 0.12$$

$$\gamma = 1.0 , \quad n \approx 10$$

therefore

$$kd = 2.13 \text{ in.} \quad \text{and} \quad I_{cracked} = 18.6 \text{ in}^4$$

$$\emptyset_{cr} = \frac{I_{cracked}}{I_{gross}} = \frac{18.6}{28.5} = 0.65$$

$$E_c = 3*10^6 *0.65 = 1950,000 \text{ psi}$$

For the top four columns,

$$p = \frac{2*0.0206}{6.34} = 0.0065$$

$$\lambda = \frac{0.66}{6.34} = 0.104$$

$$\gamma = 1.0 , \quad n \approx 10$$

therefore

$$kd = 1.7 \text{ in. and } I_{cracked} = 10.9 \text{ in}^4$$

$$\phi_{cr} = \frac{I_{cracked}}{I_{gross}} = 0.38$$

$$E_c = 3*10^6 * 0.38 = 114,000 \text{ psi}$$

(2) Modal Analysis: Linear modal analyses were made as-suming the structure as a ten-degree-of-freedom system, i.e. the stiffness matrix of the substitute structure was condensed to a matrix of 10 by 10 (Fig. 2.6c). No rotational inertia was considered for the structural members. Motion was considered only in one horizontal direction, parallel to the planes of the frames. Modal forces in the columns and beams were found from compatibility of deformations and equilibrium of forces at the structural joints.

Modal values, natural frequencies and participation factors for the base shear for the final calculation are listed in Table 2.1.

Modal shapes of the first three modes of the substitute structure for the final trial are plotted in Fig. 2.7.

(3) Damping Factors: The substitute viscous damping factors for the beams and columns were obtained from Eq. (2-4).

For the beams, $\beta_b = 0.02*(1-(1/2)^{\frac{1}{2}})+0.02 = 7.9\%$

For the columns, $\beta_c = 2\%$

The "smeared" damping factor for each mode was determined using Eq. (2-2) and (2-3) and the modal forces already calcu-lated above. The calculated "smeared" damping factor of the first three modes for the final trial are listed in Table 2.1.

It was assumed that the design response acceleration for any damping factor, β, could be related to the response for $\beta = 0.02$ using Eq. (2-12) (Shibata, 1976)

$$\frac{\text{Response Acceleration for } \beta}{\text{Response Acceleration for } \beta=0.02} = \frac{8}{6+100\beta} \qquad (2-12)$$

(4) Design Forces: Lateral forces, shear forces, over-turning moments and displacements at every level for the sub-stitute structure of the standard frame corresponding to the first three modes are plotted in Fig. 2.8, 2.9 and 2.10.

Variations of the shear forces, flexural moments and axial forces along the columns are plotted in Fig. 2.11, 2.12 and 2.13.

Flexural moments at the ends of the connecting beams are plotted in Fig. 2.14.

(5) Reinforcement: The amount and arrangement of rein-forcement in the structural frames was guided by the following considerations.

(a) Force distribution indicated by the substitute-damping method,

(b) Constructional and analytical need to maintain simi-

lar cross-sections.

The most convenient arrangement would have been to use uniform reinforcement throughout the walls. However, this option tends to be uneconomical particularly in full scale structures. Therefore, the lateral strength of the structure was changed at midheight (between levels 5 and 6) as shown in the reinforcement layout (Fig. 2.15).

All beams and walls had more transverse (shear) reinforcement than required by the substitute structure method to minimize the risk of primary failure in shear. The longitudinal reinforcement in the beams was extended all the way to the depth of the walls to develop sufficient anchorage (Fig. 2.17). To minimize reinforcement slip at the foundation the longitudinal reinforcement in the walls was welded to an anchor plate (Fig. 2.15). To improve the ductility capacity of the first three level columns, the longitudinal steel was confined by spiral reinforcement. The final amount and arrangement of the reinforcement in the walls and connecting beams of a standard frame is shown in Fig. 2.15, 2.16 and 2.17.

2.5 Design of the Modified Test Structure (Type M)

The design of the standard test structure, as described above, included frames with flexible beams and stiff walls. In order to permit investigation of the influence of the amount of steel reinforcement in the connecting beams on the structural system, the Type-M structure was reinforced such that it had

twice as much steel reinforcement in the connecting beams as the
standard structure (type D). The flexural steel reinforcement
in the walls was similar to that of the standard structure (Fig.
2.18). Therefore, more damage was expected to occur in the
piers than that in the standard structure.

The amount and arrangement of the steel reinforcement of
the modified frame is shown from Fig. 2.18, 2.19 and 2.20.

2.6 Material Properties and Calculated Force-Displacement Relationship of Frame Elements

Assumed properties for the concrete (because the design
calculations were made before casting the concrete) and mea -
sured properties of the steel as well as the calculated load-
deformation characteristics of the frame elements are briefly
described in this section. A detailed description of the mea-
sured material properties is given in Appendix A.

The deformation characteristics of the connecting beams
are described by Abrams (1976). Comparison of the assumed and
obtained stiffness is described in chapter 6.

The deformation characteristics of the piers described
here represent trends rather than individual results. They
are of importance only in order to describe the physical sig -
nifcance of the effect of the axial force on the strength of
the piers.

To simplify computations for the moment-curvature rela -
tionship and for the interaction diagram (axial load vs. bend-
ing moment) the stress-strain relationships of steel and con -

crete were idealized by mathematical functions.

(a) Concrete

The concrete used throughout this study was small-aggregate concrete similar to that used in previous experimental studies (Otani, 1974; Gulkan, 1974). A parabola combined with a straight line was adopted to define the stress-strain relationship of the concrete.

$$f_c = 0 \qquad\qquad\qquad\qquad \epsilon_c < 0$$

$$f_c = f'_c \left[2 \frac{\epsilon_c}{\epsilon_o} - \left(\frac{\epsilon_c}{\epsilon_o}\right)^2 \right] \qquad 0 \leq \epsilon_c \leq \epsilon_o \qquad (2\text{-}13)$$

$$f_c = f'_c \left[1 - Z(\epsilon_c - \epsilon_o) \right] \qquad \epsilon_o \leq \epsilon_c \leq \frac{1}{Z} + \epsilon_o$$

where

f_c = stress of the concrete

f'_c = compressive strength of the concrete (assumed to be 4500 psi)

ϵ_c = strain of the concrete

ϵ_o = strain at which f'_c is attained (assumed to be 0.003)

Z = constant which defines the descending slope of the stress-strain curve (assumed to be 100)

The resulting curve is shown in Fig. 2.21. Direct comparisons of the assumed curve and the measured data are provided in Fig. A.1.

(b) Steel Reinforcement

Number 8 gage wire (nominal diameter = 0.162 in. and cross sectional area = 0.0206 in.^{2}) was used as flexural reinforcement

in the piers and connecting beams of the test frames. The
mean yield stress, taken at a 0.2% offset from 68 coupons,
was 72 ksi with a coefficient of variation of 2.8%. The aver-
age stress-strain curve and the lower and upper bounds are
shown in Fig. A.7.

A bilinear relationship was adopted to define the stress-
strain curve of the flexural reinforcement.

$$f_s = E_s \epsilon_s \qquad\qquad 0 \le \epsilon_s \le \epsilon_y$$

$$f_s = f_y + (f_y - f_{su}) \frac{(\epsilon_s - \epsilon_y)}{(\epsilon_{su} - \epsilon_y)} \qquad \epsilon_y \le \epsilon_s \le \epsilon_{su} \qquad (2\text{-}14)$$

where

f_s = stress of the steel

f_y = yield stress of the steel (assumed to be 72 ksi)

f_{su}= ultimate stress of the steel (assumed to be 83 ksi)

ϵ_s = strain of the steel

ϵ_y = strain at which f_y is attained

ϵ_{su}= ultimate strain (assumed to be 0.08)

E_s = Young's modulus (assumed to be 29 * 10^3 ksi)

The proposed curve is shown in Fig.2.22, in comparison
with the measured mean stress-strain curve.

Number 16 gage wire (nominal diameter = 0.0625 in. and
cross-sectional area = 0.00307 in.^{2}) was used as transverse rein-
forcement throughout the test frames. A typical stress-strain
for this wire is shown in Fig. A.10. The average yield stress
was 106 ksi. (The actual yield stress of the transverse rein -

forcement was proportioned on a "saturation" basis with the
intent that the stress in such steel should not exceed 80 ksi
during the design earthquake).

(c) Moment-Curvature Relationship and Interaction Diagram

The moment-curvature relationship and interaction diagram
for the piers of the standard and modified structures were cal-
culated from the geometry of the sections, the amount of axial
load, the assumed stress-strain relationship of concrete and
flexural reinforcement described above, and Bernoulli's hypho-
thesis, which assumes a linear strain distribution across the
depth of the section.

If strain and stress distributions were assumed as shown
in Fig. 2.23, strains and curvature are related as follows

$$\phi = \epsilon_c^*/c = \epsilon_s'/(c-d') = \epsilon_s/(d-c) \qquad (2-15)$$

where

ϕ = curvature

ϵ_c^* = concrete strain of the extreme compressive fiber

ϵ_s = strain of tensile steel

ϵ_s' = strain of compression steel

c = depth of neutral axis

d = distance from the extreme compressive fiber to the
center of tensile steel

d' = distance from the extreme compressive fiber to the
center of compressive steel

From equilibrium conditions across the section

$$P = \int_{\frac{D}{2}-c}^{c} f_c b \, dx + A_s' f_s' - A_s f_s \qquad (2\text{-}16)$$

and

$$M = \int_{\frac{D}{2}-c}^{c} f_c b \, x \, dx + A_s' f_s' \,(D/2-d') + A_s f_s \,(d-D/2) \qquad (2\text{-}17)$$

where

f_c = stress in the concrete

f_s = stress in the tensile steel

f_s' = stress in the compression steel

b = width of the cross section

D = total depth of the section

A_s = area of the tensile steel

A_s' = area of the compression steel

P = axial load acting on the center line of the section

M = bending moment about center line of the section

Using Eq. (2-13) and (2-14) f_c, f_s and f_s' can be determined for given ϵ_c, ϵ_s and ϵ_s', respectively.

The moment-curvature relationships and interaction diagrams for the piers of the standard and modified frames are shown in Fig. 2.24 to Fig. 2.26. The flat portion in the bottom part of the interaction diagram represents the cutoff related to yield stress. Other parts of the curve reflect the distribution of strain hardening.

The RSS solution of the maximum end flexural moments (Fig. 2.12c) and net axial forces of the piers of the standard frame (Fig. 2.26a) were entered in the calculated interaction diagram

of the piers in Fig. 2.26b. As would be expected, the condi -
tions of tension in the base column controls the design of the
piers. Normally the most convenient solution from the "design"
point of view would have been to increase the amount of longi -
tudinal reinforcement to have the condition of tension within
the interaction diagram. However, this option would result in
a very conservatively proportioned test structure. Considering
that, with net tension on one pier and compression on the other,
the stiffness of and therefore the moment in the two piers would
be substantially different (the moment in the compressed pier
would be larger), the conditions shown in Fig. 2.26 were deemed
to be acceptable.

3. OUTLINE OF EXPERIMENTAL WORK

3.1 Experimental Variables

The experimental work included one series of four test struc-
tures described in Chapter 2 (Fig. 2.1). The main variables were
the relative beam stiffness and the base motions. The four test
structures were distributed with respect to the main variables as
shown below.

	Base Motion 1	Base Motion 2
Moderately reinforced beams	D1, D2	D3
Heavily reinforced beams	M1	-

The reinforcement of the connective beams, described in Chap-
ter 2, is shown in Fig. 2.17 (moderate) and 2.20 (heavy). The base
motions are described in section 3.4.

The target compressive strength for the small-aggregate con-
crete was 4500 psi (see Table A1 for measured values). Main rein-
forcement was provided by No.8 gage (0.162-in. round) wires with a
mean 0.2 percent-offset stress of 72000 psi.

3.2 Experimental Setup

Two identical frames were fastened onto the earthquake simu-
lator platform parallel to each other and to the direction of mo-
tion (Fig. 3.1 and 3.2). The distance between the two frames was
24 in. Steel weights of approximately 970 lb. were attached to
each floor level to develop horizontal inertia forces under simu-
lated earthquake motions. The weights were suspended in between
the frames using longitudinal and transversal fixtures. The steel

weights were concentrated at the wall center lines so that gravity forces were carried by the piers. Ball bearing con - nections were provided in the longitudinal fixtures at the wall center lines to minimize moment induced by the weights, in the plane of the frames (Fig. 2.1 and 3.4). Pin connect - ions were provided in the transversal fixtures to minimize any induced moment in the plane perpendicular to the frames (Fig. 2.1 and 3.1 b). In order to increase stiffness and prevent failure in the transverse direction the masses were connected at each floor level on both ends by steel "bellows" (Fig. 3.3). Including the weight of the frames and "bellows", the effective weight at each floor level was 1000 lb.

The base girders were prestressed to the earthquake simu- lator platform using longitudinal and transversal steel connec- tions (Fig. 3.1). To prevent slip of the specimen with respect to the test platform, steel angles were bolted to the platform and wedged against the base girders.

3.3 Instrumentation

Two kinds of fundamental responses were recorded during each motion: (1) displacements relative to the base and (2) ab- solute accelerations of each frame, at the ten floor levels par- allel to the motion.

The relative displacements were measured using linear volt- age differential transformers (LVDT's, Fig. 3.5) mounted on a rigid steel frame which was previously fastened on the earth - quake simulator platform (Fig. 3.2).

The absolute accelerations at the base level and at every floor level were measured using accelerometers (Fig. 3.4) mounted on the base girders of the frames (Fig. 3.3) and on the longitudinal fixtures of the steel masses at each floor level (Fig. 3.4). Details of the experimental setup are described in Appendix A.

LVDT's were set at their maximum limits to avoid saturating the records in case of large deflections. The accelerometers were set to read different magnitudes of acceleration in order to maintain necessary sensitivity without saturating the gages.

3.4 Base Motions

The base motions were scaled versions of the NS component of the 1940 Imperial Valley earthquake (recorded at El Centro, Calif.) and the N21E component of the 1952 Tehachapi earthquake (recorded at Taft, Calif.). In order to obtain a relation comparable to conditions for a full scale building between the natural frequencies of the test structures and the frequency content of the earthquake records, the time axis of the earthquake records were compressed by a factor of 2.5. Each test structure was subjected to a series of motions of increasing intensity. Details of the base motions are given in chapters 4 and 5.

4. OBSERVED BEHAVIOR OF TEST STRUCTURES

4.1 Introduction

Each of the four test structures was subjected to an initial earthquake selected to cause serious damage. If the structure survived this test, the "ground motion" was increased in intensity in successive tests until collapse was obtained. The measured spectrum intensity (Housner, 1959) was used as a basis for comparing the behavior of the test structures under different base motions. The values of the spectrum intensity should not be compared directly with those calculated from an actual earthquake because of the difference in time scale as well as, indirectly, the strength of the test structure relative to its total weight. Once again, it is important to emphasize that the test structures were not models of a particular or even of a class of buildings. Rather, they were physical models of idealized structural concepts.

Studies of behavior are based on recorded signals during each test run and on the crack pattern after each test run. The response signals were studied for their maximum values, waveform and frequency component.

4.2 General Remarks

(a) <u>Index to define the intensity of base motion</u>

Housner (1952) proposed the concept of spectrum intensity as a measure of the intensity of ground motion. The spectrum in-

tensity is defined to be the area under the velocity response
spectrum curve between periods of 0.1 and 2.5 sec.

$$(SI)_\beta = \int_{0.1}^{2.5} S_V(\beta,T) \, dT$$

in which

$(SI)_\beta$ = spectrum intensity at damping β

$S_V(\beta,T)$ = velocity response curve

β = damping ratio

T = period of a linear-elastic system

Spectrum intensities of measured base acceleration were cal-
culated between 0.04 and 1.0 sec. periods in order to be consis-
tent with the time scale of 1/2.5.

A damping of 20% is used to calculate the spectrum intensity
in this report although, as shown by the data in Fig. 5.3, any
value of damping factor would have yielded as good a relative
measure.

Since the difference between the measured base accelerations
of north and south frames during same test-runs was insignificant,
the spectrum intensity presented here refer to the south frame.

(b) Acceleration and Displacement Measurements

Behavior of a test structures was measured in terms of dis-
placements and accelerations at the ten different floor levels
of the north and south frames.

Deformation of the frames was measured at the ten floor levels relative to the steel A-frame (Fig. 3.2). The positions of the bases of the test frame and the A-frame were checked before and after each test run and found not to have moved. The natural frequency of the steel A-frame was 48 Hz. Inspection of the displacement records revealed no components of that frequency at any floor level. Therefore, the measured displacement records at the ten floor levels were assumed to represent the displacements relative to the base of the frame.

Accelerations were measured at the base and at each floor level of each frame in the direction of motion.

The sign convention used for the displacements and accelerations is shown in Fig. 2.1.

The waveforms reported in this Chapter were measured on the south frame in tests D1, D2 and D3. The choice of the frame was arbitrary. The waveforms measured on both walls were almost identical as it can be seen in the waveforms of test M1 (Fig. 4.27 and 4.28).

Maximum positive and negative values of the recorded wave - forms were picked automatically during the data reduction process.

(c) Frequency Measurements

The terms "first mode", "second mode", "third mode" and "high modes" were used to describe the phase relationship of ten dis - placement and acceleration signals and are defined below for the sake of clarity.

"First mode" refers to the condition with all ten floor level signals oscillating in the same phase. "Second mode" indicates that only one node, i.e. point that remains stationary with re - spect to the oscillatory motion of all the other points, is formed. "Third mode" refers to the case with two nodes. "High modes" refers to any combination of modes excluding the first one.

Frequencies associated with the first three modes were determined. The first-mode frequency was found on displacement signal traces. The second-mode frequency was more easily identified on the fifth or tenth floor level acceleration records. The third-mode frequency was identifiable on the eighth floor-level acceleration record for some cases.

(d) Crack patterns

Before the structure was first tested and after each run, a special solution*, which contains small fluorescent particles was sprayed on the surface of both frames. The small fluorescent particles penetrated into the concrete cracks and reflected "black light" showing the crack pattern clearly. The cracks in the concrete were marked and identified. The cracks patterns reported here refer to the south frame.

4.3 Observed Behavior of Test Structure D1

The base motion was patterned after the north component of El Centro earthquake (1940). The tests of this structure includ-

---

*Partek, P-1a Fluorescent, Magnafux Corporation, Chicago, Illinois.

ed two runs. The motion in the second run was approximately twice as strong as in the first.

Immediately before the first simulated earthquake, the first and second-mode frequencies of the structure were measured to be 4.5 Hz, and 18 Hz, respectively.

(a) Run D1-1

Response measurements and characteristic index values for this run are summarized below.

(1) Maximum base acceleration of 0.5g was measured at 1.02 sec.

(2) Base acceleration spikes during the first 2.5 sec. of motion were approximately twice as large as those measured in other periods.

(3) Spectrum intensity, calculated for a damping factor of 0.2, was 6.7 in.

(4) Response Spectra: Fig. 4.1 and 4.2

(5) Response displacements and accelerations: Fig. 4.3 and 4.4

(6) Crack pattern: Fig. 4.5 a and 4.6

(7) Response maxima: Table 4.1

The response displacement waveforms were generally smooth and were governed by the first-mode component, particularly in the top five-floor levels. Contribution of the second-mode components in the displacement records can be observed in the first five levels. Large displacements were measured during the first

four seconds. All measured maximum displacements occurred within a few thousands of a second of 2.62 sec. (positive, as shown in Fig. 4.3) in one direction and 2.43 seconds in the other direction. Maximum top displacements were 0.97 in. (positive) and 1.12 in. (negative) resulting in a double-amplitude value of 2.09 in. The displacement waveforms at the ten levels were similar.

The recorded absolute-acceleration waveforms were relatively smooth. The contribution of the high-frequency contents of the ground acceleration can be perceived from a qualitative study of the waveforms. The measured responses of the lower floors were dominated by high frequencies. This condition changed gradually to the eighth floor where the first mode dominates.

The frequencies associated with the first mode and second mode were measured to decrease with time. The changes in the frequencies are listed below.

Time from the beginning of the base motion (sec)	Measured Frequency		
	First mode (Hz)	Second mode (Hz)	Third mode (Hz)
1.0	4.3	17	--
2.0	2.7	13	30
3.0	2.7	12	--
4.0	2.3	11	--
6.0	2.1	10	--
8.0	2.0	10	--
10.0	--	10	--
12.0	2.0	10	26
end	2.0	10	--

No shrinkage cracks were observed in the frames before the structure was tested. After the first run, hairline (smaller than 0.002 in.) flexural cracks were observed at the ends of every beam at each floor level in both frames (Fig. 4.5 a and 4.6). No cracks were visible in the piers because of the "prestressing" effect of the dead load. No crushing or spalling of the concrete was observed in any portion of the test structure. No shear cracks were observed in any portion of the structure.

(b) <u>Run D1-2</u>

Response measurements and characteristic index values for this run are summarized below.

(1) Maximum base acceleration of 1.96g at 1.01 sec.

(2) Base acceleration spikes during the first 2.5 sec. of motion were approximately twice as large as those measured in other periods.

(3) Spectrum intensity (SI_{20}) was 14.2 in.

(4) Response Spectra: Fig. 4.7 and 4.8

(5) Response displacements and accelerations: Fig. 4.9 and 4.10

(6) Crack pattern: Fig. 4.5 b and 4.11

(7) Response maxima: Table 4.1

The response displacement waveforms were different from those obtained in the first run in that large displacements occurred throughout the duration of the test. Three distinct periods of relatively high-level response separated by two periods of low-

level response were observed in all records. The high-response periods occurred from 0.5 to 3.5 sec., when maximum values were recorded, from 5 to 9 sec., and from 10 sec. to the end of the test. Second-mode components were observed during the two low-response periods except in the eighth level where only first and third-mode components were observed.

The base acceleration waveform had more higher-frequency components than that of the first run (D1-1). As in the displacement waveforms, large accelerations occurred during the entire test duration and three periods of response can be distin - guished, particularly for the first three levels. The largest accelerations occurred in the first three levels and in the top level.

Changes in the first three frequencies during the second run are listed below.

Time from the beginning of the base motion (sec)	Measured Frequency		
	First mode (Hz)	Second mode (Hz)	Third mode (Hz)
2.0	2.6	--	--
4.0	2.0	--	20
6.0	2.0	--	20
8.0	1.9	9	19
10.0	1.9	9	19
12.0	1.6	9	19
end	1.6	9	--

Crushing of the concrete was observed at the lower level on the outside of the piers in both frames. Crushing and spalling

of the concrete were observed at the ends of second, third, fourth, fifth and sixth-floor beams in both frames. The damage in the beams looked more severe at fourth, fifth and sixth levels, as shown in Fig. 4.11. Additional flexural cracks were observed in the piers and beams, as recorded in Fig. 4.5 b. It appeared that the coupling provided by the beams was efficient since the piers were crushed extensively on the exterior edges.

4.4   Observed Behavior of Test Structure D2

The base motion was patterned after El Centro (1940) NS component. The tests of this structure included three runs. The motions in the second and third run were approximately twice and three times as strong as in the first, respectively.

Immediately before the first simulated earthquake, the first and second-mode frequencies were measured to be 4.8 Hz and 20 Hz.

(a)   Run D2-1 .

Response measuraments and characteristic index values for this run are summarized below.

(1)   Maximum base acceleration of 0.41g at 1.97 sec.

(2)   Base acceleration spikes during the first 2.5 sec. of motion were approximately 1.5 times as large as those measured in other periods.

(3)   Spectrum intensity (SI_{20}) was 6.5 in.

(4)   Response Spectra: Fig. 4.12 and 4.13

(5)   Response displacements and accelerations: Fig. 4.14 and 4.15

(6)   Crack pattern: Fig. 4.16 b

(7) Response maxima: Table 4.2

The response displacement waveforms for the first five levels, which were distorted by electronic noise with a frequency of about 17 Hz, are not reported. The rest of the displacements values and waveforms were similar to those in Test Run D1-1.

The base acceleration waveform is quite similar to that of Test Run D1-1. The main differences between base accelerations D1-1 and D2-1 were that the former had low-frequency and high-frequency components slightly stronger. The response acceleration waveforms were again similar to those in Test Run D1-1.

Changes in the frequencies are listed below.

Time from the beginning of the base motion (sec)	Measured Frequency		
	First mode (Hz)	Second mode (Hz)	Third mode (Hz)
1.0	4.2	17	--
2.0	2.7	13	--
3.0	2.7	13	--
4.0	2.4	11	--
6.0	2.1	--	--
8.0	2.0	--	26
10.0	2.0	10	--
12.0	2.0	10	--
end	2.0	10	--

Some shrinkage cracks were observed at the base piers and in the first level beam prior to the test. Hairline (smaller than 0.002 in.) flexural cracks were observed at the ends of each beam in both frames (Fig. 4.16 b). Some fine cracks were observed in the piers but almost none in the bottom piers except those due to the initial shrinkage. No crushing or spalling of

the concrete was observed in any portion of the test structure. No diagonal cracks were observed in any portion of the structure.

(b) Run D2-2

Response measurements and characteristic index values for this run are summarized below.

(1) Maximum base acceleration of 0.94g was measured at 1.08 sec.

(2) Base acceleration spikes during the first 2.5 sec. of motion were approximately twice as large as those measured in other periods.

(3) Spectrum intensity (SI_{20}) was 13.1 in.

(4) Response spectra: Fig. 4.17 and 4.18

(5) Response displacements and accelerations: Fig. 4.19 and 4.20

(6) Crack pattern: Fig. 4.16 c

(7) Response maxima: Table 4.2

The response displacement waveforms were similar to those obtained in Run D1-2. They were smooth and were dominated by the first-mode component. As it was for the displacements in Run D1-2, three different periods of response were observed at each floor level.

The measured base acceleration waveform had fewer very-high frequency components than that of test D1-2, and, as a result, the acceleration records at every level had fewer high frequencies than those of test D1-2. The response acceleration waveforms were relatively smooth. They were dominated by the first-mode compo -

nent in the top five floor levels, particularly in the eighth.
As it was for the displacement waveforms, large accelerations
occurred during the entire test duration and three periods of
response can be distinguished in the acceleration record for
each level.

Changes in the first three frequencies during the second
run are listed below.

Time from the beginning of the base motion (sec)	Measured Frequency		
	First mode (Hz)	Second mode (Hz)	Third mode (Hz)
2.0	2.6	11	--
8.0	2.0	10	--
12.0	1.9	10	20
end	1.9	9	20

Crushing of the concrete was observed at the lower level on
the outside of the piers in both frames. Crushing and spalling
of the concrete were observed at the ends of the second, third,
fourth, fifth and sixth-floor beams in both walls. The damage
in the beams looked more severe at second and third floor levels
in the north frame and at second, third, fourth and fifth floor
levels in the south frame. In general the damage in the beams
was not as severe as it was in test D1-2. Additional flexural
cracks were observed in the piers and beams as recorded in Fig.
4.16 c. The coupling provided by the beams was effective as in-
dicated by the fact that the piers were crushed on the exterior
and not on the interior edges.

(c) Run D2-3

Response measurements and characteristic index values for this run are summarized below.

(1) Maximum base acceleration of 1.72g at 0.88 sec.

(2) Base acceleration spikes during the first 2.5 sec. of motion were approximately twice as large as those measured in other periods.

(3) Spectrum intensity (SI_{20}) was 19.6 in.

(4) Response spectra: Fig. 4.21 and 4.22

(5) Response displacements and accelerations: Fig. 4.23 and 4.24.

(7) Crack pattern: Fig. 4.16 d.

(8) Response maxima: Table 4.2

As in the first two runs the response displacement waveforms were dominated by the first mode, particularly in the last five top levels. Second-mode components were observable in the first seven levels, particularly in the first three levels. Large excursions occurred throughout the test duration.

The base acceleration waveform was similar to those of the first two runs. The response acceleration waveforms were relatively smooth. They were governed by the first-mode in the seventh, eighth and ninth floor levels, particularly in the eighth. As in the displacements waveforms, large accelerations occurred during the entire test. The largest accelerations occurred in the first three floor levels and in the top floor level.

Changes in the first three frequencies during this run are listed below.

Time from the beginning of the base motion (sec)	Measured Frequency		
	First mode (Hz)	Second mode (Hz)	Third mode (Hz)
2.0	2.5	10	21
4.0	1.5	9	20
12.0	1.5	9	--
end	1.5	9	20

Additional crushing and spalling of the concrete were observed at the base on the exterior edges of the piers. No crushing or spalling of the concrete were observed at the interior edges of the piers. Additional crushing and spalling of the concrete occurred in each connecting beam. The damage in the beams looked more severe from the second to the eighth floor levels particularly at the second, third and fourth where diagonal cracks were observed (Fig. 4.17 d).

4.5 Observed Behavior of Test Structure M1

The base motion for structure M1 was patterned after the north component of the El Centro record (1940). The test structure was damage heavily in the first run which is the only one reported.

Immediately before the test the first and second-mode frequencies of the structure were measured to be 4.5 Hz, and 19 Hz.

(a) Run M1-1

Response measurements and characteristic index values for this run are summarized below.

(1)   Maximum base acceleration of 0.91g at 1.08 sec.

(2)   Base acceleration spikes during the first 2.5 sec. of motion were approximately twice as large as those measured in other periods.

(3)   Spectrum intensity (SI_{20}) was 12.9 in.

(4)   Response spectra: 4.25 and 4.26

(5)   Response displacements and accelerations: Fig. 4.27 and 4.28

(6)   Crack pattern: Fig. 4.29 a, 4.30 and 4.31

(7)   Response maxima: Table 4.3

The response displacement waveforms were similar to those obtained in Runs D1-2 and D2-2. They were smooth and were governed by the first-mode component. As in Runs D1-2 and D2-2, three different periods of response were observed at each floor level. Second-mode components were more visible in between these periods. They were relatively stronger in the first seven floor levels than in the last three top floor levels. All maximum positive displacements at every floor level occurred at 1.97 sec. The maximum positive top displacement was 2.05 in. All maximum negative displacement at each floor level occurred at 1.38 sec. The maximum negative top displacement was 1.47 in. The maximum double amplitude top displacement was 3.50 in. immediately before the maximum positive displacement.

The base acceleration waveform was similar to that of test D2-2. The acceleration records were relatively smooth. They were governed by the first-mode component in the top five floor

levels, particularly in the eighth. High-mode components were particularly strong in the first five floor levels. As in test D1-2 large accelerations occurred throughout the run and three periods of response can be distinguished in the acceleration histories.

Changes in the first three frequencies during this test run are listed below.

Time from the beginning of the base motion (sec.)	Measured Frequency		
	First mode (Hz)	Second mode (Hz)	Third mode (Hz)
1.0	4.2	15	--
2.0	2.5	13	--
3.0	2.5	12	30
6.0	2.1	11	24
8.0	2.1	10	--
10.0	2.1	10	23
end	2.1	10	--

Shrinkage cracks (less than 0.001-in. in width) were observed before the test in the piers and beams at every level, along the anchorage of the beam reinforcement in the piers and along the web reinforcement in the connecting beams (Fig. 4.29 a). These cracks were related to the minimal cover on the bars and stir - rups, which was less than 0.05 in. After the run, extensive damage was observed to be concentrated in the base piers and in the second, third, fourth, fifth and sixth-floor level beams. The damage in the beams was crushing of the concrete at the ends. That in the base piers was crushing of the concrete at the exterior edges (Fig. 4.29). The damage pattern was similar to that

observed after test Runs D1-2 and D2-2. The damage indicated that the coupling provided by the beams was strong since the piers were crushed extensively on the exterior and not on the interior edges.

4.6 Observed Behavior of Test Structure D3

The base motion for these tests was patterned after the N21E omponent of the 1952 Taft earthquake (Tehachapi shock). The tests included two runs. The motion in the second run was approximately twice as strong as in the first.

Immediately before the first simulated earthquake, the first and second-mode frequencies of the structure were measured to be 4.8 Hz and 19 Hz.

(a) Run D3-1

Response measurements and characteristic index values for this run are summarized below.

(1) Maximum base acceleration of 0.46g at 3.99 sec.

(2) Base acceleration spikes during the first six seconds of motion were approximately twice as large as those measured in other periods.

(3) Spectrum intensity (SI_{20}) was 6.8 in.

(4) Response spectra: Fig. 4.32 and 4.33

(5) Response displacements and accelerations: Fig. 4.34 and 4.35

(6) Crack pattern: Fig. 4.36 b

(7) Response maxima: Table 4.4

The response displacement waveforms were generally smooth and were governed by the first-mode component, particularly in the top five levels. Second-mode components in the displace- ment records were observed in the first five levels. Large dis- placements were measured during the first six seconds and during the last 5.5 seconds. All maximum positive displacements at each floor level were measured to occur at 3.37 sec. The maximum pos- itive top displacement was 0.72 in. All maximum negative dis- placements at each floor level were measured to occur at 3.20 sec., and immediately before the maximum positive displacements. The maximum negative top displacement was 0.95 in., resulting in a maximum double-amplitude displacement of 1.67 in. Two distinct periods of relatively high-level response separated by a period of low level response were observed in all records. The high-re- sponse periods occurred from 0.5 to 6.5 sec., when the maximum values recorded, and from 9.5 sec. to the end of motion. Second- and third-mode components were observed in between these two pe- riods, particularly in the first five floor levels. The displace- ments waveforms at the ten floor levels were similar.

The response acceleration waveforms were relatively smooth. They were governed by the first-mode components in the last five top floor levels, particularly in the eighth. The acceleration waveforms for levels 1 and 2 were very similar to that of the base motion. Large acceleration peaks occurred during the first six seconds. The largest acceleration which occurred at the top floor level, was 1.25g at 4.40 sec. Two different response periods were observed in the last four top floor-level acceleration waveforms

similar to those observed in the displacement waveforms. They were observed more clearly at these levels since the first mode-component is dominant in their waveforms.

Changes in the first three frequencies during this test run are listed below.

Time from the beginning of the base motion (sec)	Measured Frequency		
	First mode (Hz)	Second mode (Hz)	Third mode (Hz)
1.4	4.2	17	--
3.0	3.0	13	--
4.0	2.9	13	--
6.0	2.7	12	29
9.0	2.7	12	--
12.0	2.4	12	--
end	2.4	12	--

Shrinkage cracks were observed before the test in the bottom piers along the web reinforcement and in some of the beams of the north frame (Fig. 4.39 a). After the first test run, hairline (smaller than 0.002 in.) flexural cracks were observed at the ends of the beams in second, third, fourth, fifth and sixth floor levels (Fig. 4.39 b). No crushing or spalling of the concrete was observed in any portion of the test structure. No shear cracks were observed in any of the beams or piers.

(b) Run D3-2

Response measurements and characteristic index values for this run are summarized below.

(1) Maximum base acceleration of 1.06g at 4.26 sec.

(2) Base acceleration spikes during the first six seconds

were approximately 2.5 times as large as those mea-
sured in other periods.

(3) Spectrum intensity (SI_{20}) was 13.2 in.

(4) Response spectra: Fig. 4.37 and 4.38

(5) Response displacements and accelerations: Fig.4.39
and 4.40

(6) Crack pattern: 4.36 c.

(7) Response maxima: Table 4.4

The response displacement waveforms were smooth and were
governed by the first-mode component, particularly in the last
four top floor levels. As in the test Run D3-1, two distinct re-
sponse periods were observed at each floor level. Second-mode
components were observed during the first period and in between
the two response periods, particularly in the first seven floor
levels. All maximum positive displacements at each floor level
occurred at 2.07 sec. The maximum positive top displacement was
1.52 in. All maximum negative displacement at each floor level
occurred at 2.26 sec. and immediately after the maximum positive
displacements. The maximum negative top displacement was 1.13
in., resulting in a maximum double amplitude displacement of 2.59
in.

The response acceleration waveforms were relatively smooth.
They were governed by the first-mode component in the top four
levels. No second mode components were observed in the eighth
floor level. As in the displacement waveforms, high responses
occurred in the first 6.5 sec.

Changes measured in the first three frequencies during the second run are listed below.

Time from the beginning of the base motion (sec)	Measured Frequency		
	First mode (Hz)	Second mode (Hz)	Third mode (Hz)
4.0	2.7	12	--
6.0	2.3	11	--
12.0	2.3	--	21
end	1.8	10	20

Crushing of the concrete was observed after test run D3-2 at the lower level on the outside of the piers. No spalling of the concrete was observed in the piers. Additional cracks and widening of the previous cracks were observed at every floor level. The additional damage of the beams was observed to occur at the second, third, fourth, fifth and sixth floor levels. No crushing or spalling was observed in the beams. The amount of damage in the connecting beams at this stage was less than that after test runs D1-2 and D2-2.

5. GENERAL FEATURES OF OBSERVED BEHAVIOR

5.1 Introduction

This chapter summarizes the response maxima and discusses general characteristics of the response waveforms as well as the crack pattern and frequency changes of the test structures. Because the main variables in the experimental work were the characteristics of the base motion and the strength of the test structures, the discussions are based primarily on these two variables.

5.2 General Remarks

(a) Analysis of Frequency Content

The time-domain representation of the response of MDOF systems to any arbitrary input is completely general and traditionally used to evaluate the response of systems under dynamic loading. Another procedure, which is sometimes more convenient, of representing the response is through the frequency domain using the Fourier spectrum or Fourier Transform. This method involves expressing any transient-motion waveform in terms of harmonic components (series of sine or cosine waves) having all posible frequencies. The magnitudes and phase angles of these various components are adjusted so that, when superimposed, they once again add to give the original waveform. Because the magnitude and phase angle of each frequency component is determined using the Fourier Transform, the content of the

waveform between any two given frequencies is obtained by add-
ing the harmonic components having frequencies in the specified
range. Thus, the Fourier Transform is suitable for filtering.

As indicated above, the Fourier Transform of any waveform
is represented by two diagrams: (1) amplitude versus frequency
and (2)phase angle versus frequency. Usually information about
amplitude only is plotted because that is the one with informa-
tion of interest to engineers. Such plots (Fig. 5.1 and 5.2)
show that there are certain frequencies, represented by the
peaks, which are predominant within the duration of a record.
There are also other frequencies which, while present, are less
important.

Figures 5.1 and 5.2 give the amplitude Fourier spectra of
all the recorded signals of tests runs D1-1 and D1-2. The am-
plitudes shown in the figures are normalized with respect to the
maximum value. The Fourier spectra of the waveforms of all sig-
nals of only test runs D1-1 and D1-2 are reported, because they
are representative of the general characteristics of the wave-
forms of the rest of the test runs.

Similar to the response spectra already described in chap-
ter 4, it is possible to present the Fourier spectra of the mo-
tion of any floor mass of the test structures in terms of dis -
placements, in terms of velocities, or in terms of accelerations.
These spectra are related to each other in terms of the frequen-
cy. Figures 5.1a, 5.1b, 5.2a and 5.2b present the Fourier spec-
tra of the motion of the ten floor masses in terms of relative

displacement and absolute acceleration. Different frequency components become more important depending on whether displacements or accelerations are considered. In the case of accelerations amplitudes at higher frequencies may assume relatively more prominent positions than they would for displacement response.

A complete description of analysis through the frequency domain is given by Clough (1975) and Spiegel (1974).

(b) Filtering Program

To study the influence of the first- and higher-mode components in the waveforms, a Fourier analysis computer program was written to separate the harmonic content from frequencies 0 to 5.0 Hz of any record. Components between these two frequencies were denoted "first-mode" component or "low-frequency" components. The difference between the total record and the "first-mode" component was denoted "high-mode" components. The upper limit of 5.0 Hz was chosen to separate the first-mode components in the records as shown in Fig. 5.1 and 5.2. Studies of the values obtained through the filtering process using an upper limit of 7.0 Hz revealed that the "first-mode" component was not sensitive to the chosen upper frequency (between 5.0 and 7.0 Hz). This can be inferred from Fig. 5.1 and 5.2, since the fundamental frequency and the second-mode frequency of the test structures are far apart from each other during any test run. Because the first-mode and second-mode frequencies remain-

ed almost stationary (approximately 2.0 and 10 Hz) after the
large excursions of the first test run, the upper limit of 5.0
Hz was used for every signal of all test runs.

Details of the Fourier analysis computer program used for
the filtering process are given in Appendix B.

(c) <u>Shear and Moment Measurements</u>

Shear forces and overturning moments at each level for a
single frame were calculated from the measured acceleration
signals at the ten floor levels combined with the story weight
(0.5 kip) and the story heights. Shear force in a particular
floor level was defined as the lateral force acting on the frame
at that floor level. It was calculated at each time step (0.004
sec) as the algebraic sum of the products of the story masses
and the acceleration amplitudes of every higher floor levels.
Overturning moment in a particular floor level was defined as
the moment acting on the frame at that floor level. It was
calculated as the algebraic sum of the products of the story
masses, the acceleration amplitudes and the height with respect
to that particular level of every higher floor levels. The
overturning effect of gravity load acting through the sidesway
displacements (P-Δ effect) was included in calculating the over-
turning moment at each floor level. At the base, this effect
was less than two percent in all test runs.

As in the previous chapter, only the waveforms correspond-
ing to the south frame are reported.

The sign convention used for the waveforms is shown in Fig. 2.1.

5.3 Base Motions

The response spectrum and the measured spectrum intensity (Housner, 1959) were used as a basis for comparing the different base motions as well as for comparing the behavior of the test structures. The spectrum intensity at 20% damping was chosen as the medium of comparison, although, as shown in Fig. 5.3, any damping factor would have yield as good a relative measure. The maximum base acceleration would not have been a good basis for normalizing the base motions since the earthquake simulator tends to distort the input acceleration waveform when the maximum ground acceleration is greater than approximately 1.0g, as indicated by the data in Fig. 5.4. Similar distortion was observed by Otani (1974).

(a) The Simulated El Centro Earthquake Record

The acceleration signals of the El Centro (1940) NS component were used in all runs of test structures D1, D2 and M1 as input to the earthquake simulator.

Response spectra and spectrum intensities for the total and for three specific time intervals of the base acceleration records were calculated for each test run. The time intervals are (i) the first three seconds (ii) the intermediate six seconds and (iii) the final three seconds. Measurements and characteristic index values for the base accelerations are summa -

rized below.

(1) Maximum positive and negative acceleration values
and spectrum intensities at different damping fac-
tors: Tables 5.1 to 5.3

(2) Comparison of acceleration response spectrum of each
time interval (damping factor=0.02): Fig. 5.5a to 5.5f

(3) Waveforms and filtered components below 5.0 Hz: Fig.
5.6a to 5.6f.

Salient characteristics of the base accelerations are:

The response spectra for the first three seconds were
identical to those for the total test duration (except for small
differences occurring between periods of 0.24 and 0.29 sec. and
frequencies of 36 and 42 Hz in some spectra), as shown in Fig.
5.5a to 5.5f.

The response spectra for the intermediate six seconds and
final three seconds show a progressive and noticeable diminish-
ing of contents at frequencies lower than 3 Hz (Fig. 5.5).

The spectrum intensities for the first three seconds at
damping factors greater than 10% are identical to those for the
total duration (Tables 5.1 to 5.3).

The spectrum intensities for the intermediate six seconds
and final three seconds are approximately 2/3 and 1/3 of those
for the total test duration (Tables 5.1 to 5.3).

The waveforms and the filtered "low-frequency" components
(Fig. 5.6) show that the low-frequency content is mainly concen-

trated in the first three seconds, as it can also be concluded from the response spectra for the three periods (Fig. 5.5). The filtered acceleration records also revealed two relatively high "low-frequency" oscillations at 4.7 sec. and 10.5 sec.

(b) The Simulated Taft Earthquake

The acceleration signals of Taft (1952) N21E component were used in the two runs of test structure D3 as input to the earthquake simulator. Response spectra and spectrum intensities for the total duration and for two specific time intervals of the base acceleration were calculated for both runs. The time intervals are (i) the first 6.5 seconds (first half) and (ii) the final 6.5 seconds (final half). Measurements and characteristic index values for the base accelerations are summarized below.

(1) Maximum positive and negative acceleration values and spectrum intensities at different damping factors: Table 5.4

(2) Comparison of acceleration response spectrum of each time interval (damping factor=0.02): Fig. 5.7

(3) Waveforms and filtered components below 5 Hz: Fig. 5.8

Significant properties of the base acceleration are:

Response spectra for the first half were identical to those for the total record, as shown by Fig. 5.7.

Response spectra ordinates and spectrum intensities for the final half were approximately 50% of those for the first half (Fig. 5.7).

Spectrum intensities for the first half at damping factors greater than 2% were identical to those for the total record (Table 5.4).

Waveforms and filtered "low-frequency" components during the final 6.5 sec. were less than half of those measured during the first 6.5 sec. (Fig. 5.8). The low- and high-frequency contents were mainly excited in the first half.

5.4 Frequencies of Test Structures

(a) Frequencies Measured in Initial Free Vibration Tests

The initial free vibration of the test structures was obtained by a very small amplitude and sudden movement of the test platform immediately before the first test run. The natural frequencies of the "uncracked" structure were determined from the free-vibration waveforms for the tenth floor displacement and acceleration plotted on oscillograph paper during the tests. A period of three to ten cycles of clearly identified free oscillations was measured, and the average frequency was deter - mined. The amplitudes of the top displacement and acceleration were approximately 0.05 in. and 0.1g, respectively. Only the first- and second-mode frequencies were identifiable on the plotted signals.

It was a general characteristic of all test structures that the measured natural frequencies were smaller than the frequencies calculated for the "uncracked" structural model shown in Fig. 2.6 (using the gross moment of inertia of the structural

members and a Young modulus of $3 * 10^6$ psi). The measured fundamental frequency varied from 83% to 89% of the calculated "uncracked" value. Frequencies associated with the first three modes calculated for the uncracked and cracked test structures (taking into account the shear deformation in the connecting beams as described in section 2.3) are listed in Table 5.5 along with the measured frequencies. The measured frequencies of the test structures were in between those values of the cracked structure and those of the uncracked struture.

Possible sources of discrepancy between the calculated uncracked natural frequencies and the measured values are discussed below. This discussion is based on considerations related to the initial effective stiffness as well as on the base fixity and conceptual modeling of the test structures. It is important to emphasize that the measured "uncracked" frequencies are not a significant characteristic of the test structures. As a matter of fact they are of trivial interest for response to strong ground motion.

Base Fixity

As described in chapter 3, the base girders of the test structures were prestressed to the test platform (Fig. 3.1 to 3.3). Making conservative assumptions about the fixity of the base girder (Fig. 5.9) it was estimated that the error in the measured fundamental frequency created by the flexibility of the base girder would be of the order of 2%.

Figure 5.10 shows a conservative estimate of the stiffness of the test platform in the vertical direction as well as an estimate of the rocking frequency of the test structure plus the platform (details of the test platform are given by Gulkan, 1971). The estimated frequency of the structure-platform system (120 Hz) suggests that the influence of the flexibility of the test platform in the measured frequencies is very small.

Stiffness of Test Structures

Figures 5.11a anb 5.11b show the variation in the first two natural frequencies of the structural model (Fig. 2.6) with beam stiffness (continuous line) and with base column stiffness (broken line). The stiffness variation is represented by the ratio of the gross flexural stiffness and the assumed value. As would be expected, softening of the base column causes greater changes in the fundamental frequency than softening of the connecting beams (Fig. 5.11a) whereas the contrary can be ob - served for the second-mode frequency (Fig. 5.11b) because of the modal shape.

Figures 5.12a and 5.12b show the influence of the shear stiffness of the connecting beams on the first two natural frequencies. For intance, if shear deformation of the beams is included (A_{shear}/A_{gross}= 5/6) the first- and second-mode fre - quencies of the structure are 5.4 and 23 Hz. Note that reduction in shear stiffness of the beams causes similar effects as reduction in flexural stiffness of the beams (section 2.3) but

at lower rates as shown by Fig. 5.12a and 5.12b.

Variation of the first two nartural frequencies with the axial stiffness of the piers is shown in Fig. 5.13. If axial deformation of the piers is neglected the structure as a whole appears much stiffer than that assuming gross section area.

Previous experimental results on reinforced concrete frames (Gulkan, 1971; Otani, 1974) indicate that the measured initial stiffness was less than the calculated based on uncracked sections. For instance, Otani (1974) reported a 20% discrepancy between the initial measured fundamental frequency and that calculated on the basis of gross sections.

From the preceding discussion it is estimated that due to cracking (caused by shrinkage in the concrete, by handling during the setup or during the free vibration of the test struc - tures) the error in the measured frequencies of the test structures could be as much as 10%. (If all elements are assumed to be fully cracked, the calculated reduction in frequency is over 20%.)

Conceptual Modeling

Another possible source of discrepancy between the calculated and measured frequencies is the eccentricity between the center of inertia and the center of rigidity of the test structure in the direction of motion. Figure 5.14 show the influence of this effect on the natural frequency of a single mass connected by two springs in parallel. For instance, a difference of

20% between the stiffness of the springs makes the funda - mental frequency 0.94 times that of a symmetric system. Fig - ure 5.14b shows that the fundamental frequency is rather insensitive to the mass eccentricity. Based on the values shown in Fig. 5.14, it is estimated that the error in the fundamental frequency created by differences in stiffness between the frames of the test structure is probably of the order of 2%.

Figure 5.15 shows a model of the test structure for the calculation of vertical frequencies. Vertical frequencies are induced by the rotational inertia of the story masses and by axial deformation of the piers. The estimated fundamental frequency (45 Hz) is relatively high to have strong influence on the lateral frequencies of the test structure.

Concluding Remarks

There are some other sources of discrepancy between the calculated and measured frequencies (damping within the structure, friction in the different connections used in the setup, air resistance, etc.) which are not discussed above because of their undetermined characteristics and trivial significance. It is important to note, however, that they all reduce the natural frequencies of the test structures. In general, it is difficult to ascribe the reason for the observed discrepancy to a single cause conclusively, but it appears that most of the observed difference is caused by the stiffness (softening of the test frames).

(b) Changes in Apparent Frequency during Test Runs

Measured frequencies associated with the first three modes during each test run were reported in chapter 4. The variation of these frequencies throughout the duration of the first and second test runs are plotted in Fig. 5.16 through 5.18 (data are shown at midpoints of the time intervals given in chapter 4). The measured frequencies associated with the first two modes, obtained from free vibration tests at low amplitudes, were plotted against the double-amplitude displacement measured at the tenth level of the south frame in Fig. 5.19.

One of the critical characteristics of the response of the test structures, observed throughout the simulated earthquake motions, was the reduction in the natural frequencies. Reductions in the natural frequencies ocurred very early during the first test run of each test structure: a reduction of approximately 50% in the fundamental frequency was indicated immediately after the initial maximum excursions. A reduction of approximately 40% was indicated in the second natural frequency. Observed reductions were a little higher in test structures using El Centro (1940) than in that using Taft (1952) as shown by Fig. 5.16 and 5.18. The frequency reduction was expected to occur very early since both types of motion (El Centro 1940, and Taft 1952) contained relatively strong low- and high-frequency acceleration pulses at the beginning of their durations (during the first three seconds and during the first six seconds for El Centro and for Taft, respectively), as shown by Fig. 5.6 and 5.8.

Further reductions in the natural frequencies occurred during subsequent test runs, but at lower rates, as shown by the data in Fig. 5.18.

5.5 Crack Patterns

The cracks observed on the test structures after each test run were described and reported in chapter 4. The significant characteristics of the observed crack patterns on each struc-ture type are summarized below.

(a) Test Structure D

Flexural cracks were concentrated at the ends of the con-necting beams during the first test run of structures D1, D2 and D3 (Fig. 4.5a, 4.16b and 4.36b). No damage was visible in the piers, except some shrinkage cracks previously detected (Fig. 4.16a, 4.36a). No crushing, spalling or shear cracks were observed in any part of the test structures.

When the test structures were then subjected to a base mo-tion approximately twice as strong as the first motion (Test Runs D1-2, D2-2 and D3-2) crushing and sometimes spalling of the concrete were concentrated on the exterior edges of the base piers (Fig. 4.5b, 4.16c and 4.36c). Severe damage consist-ing of crushing and spalling of the concrete was concentrated at the ends of the connecting beams, particularly in those between levels three and six.

Finally, when the test structures were subjected to a base motion approximately three times as strong as the first motion

(Test Run D2-3), additional crushing and spalling of the con - crete were concentrated at the base level on the exterior edges of the piers and at the ends of the connecting beams (Fig. 4.16 d). It is important to note that no crushing or spalling of the concrete was observed at the interior edges of the piers.

(b) Test Structure M

As described in section 4.5, the crack pattern observed in test structure M was similar to that in test runs D1-2 and D2-2 (Fig. 4.29). Crushing and spalling of the concrete on the exterior edges of the base piers were much more severe than that observed after the second run of test structure D, as shown by Fig. 4.30, while the damage in the connecting beams was less extensive, as shown by Fig. 4.31.

5.6 Response Waveforms

(a) Filtered Waveforms

Measured response histories for displacements and accelerations for all test runs at all levels are included in this report and described in chapter 4. Records filtered using the Fourier Transform are given for even numbered levels including the base level for all test runs in Fig. 5.20 through 5.46. A key to these figures is provided in Table 5.6.

(b) Characteristics of the Waveforms

Description of the waveforms observed in each particular test run was given in the previous chapter. The general char -

acteristics of the waveforms for test structures D and M are
summarized bellow.

The displacement waveforms indicate that the test struc-
tures oscillated primarily in the first mode during each test
run. High-mode components are visible in the displacement
records for the lower levels. Influence of the high-mode com-
ponents was less than 7% in the maximum top displacement.

During any particular test run the maximum displacement
at each level occurred virtually at the same time (within a
few thousands of a second).

Test structures D did not suffer permanent lateral defor -
mation immediately after the first test run (Fig. 4.3, 4.14 and
4.34). Moreover, the first-mode shape of test structure D was
insensitive to the damage caused in the structures during the
first run. Table 5.7 and Fig. 5.47 show calculated and measured
first-mode shapes for various stiffnesses and at different times
during test run D1-1. The calculated values shown in Table 5.7
indicate that uniform reduction of the stiffness for the beams
and piers along the height of the structure does not have much
influence on the first-mode shape.

Test structures D suffered permanent lateral deformation
of the order of 1/4 in. immediately after the second test run
(Fig. 4.19), which made difficult to measure the first-mode
shape of the test structures from the displacement records.
Permanent lateral deformation was observed in test structure M

immediately after the first run (Fig. 4.27).

The acceleration waveforms show a gradual change in their frequency content along the height of the structure (Fig. 5.1b and 5.2b). The contribution of the high-frequency contents of the imparted base motion can be visualized from the figures. The acceleration response at the lower levels was dominated by high-mode components. This condition changes gradually to the eighth floor, the node position for the second-mode shape, where the first-mode component dominates.

An interesting aspect of the response of the test struc - tures during all imparted base motions was the stationry posi- tion of the node corresponding to the second-mode shape of the structure. This can be observed in the eighth level accelera- tion waveform (Fig. 5.20) or in its corresponding amplitude Fourier Spectrum (Fig. 5.1b). Identical stationary character- istics of the second-mode node were obtained for analytical models of test structure D as shown in Fig. 5.47b.

The moment at the base was dominated by the first-mode component. The relative contributions of the first and second modes at higher levels varied as anticipated by the modal dis- tributions shown in Fig. 2.8 through 5.10 based on the design model.

The first-mode component represented approximately two thirds of the maximum base shear. The relative contributions to shear of the first and higher modes also varied as indicated

in Fig. 2.8 through 2.10.

Because the displacement and moment records were dominated by the first-mode component the waveforms were quite similar to each other and the maximum values tended to occur at the same time.

There was a noticeable difference between the characteristics in the waveforms of the first runs and those of the subsequent runs of test structures D. During the first run the maximum excurtions occurred very early and then remained relatively low for the rest of the duration of the motion. This behavior was due to the characteristics of the base motions. As described in section 5.4, a drastic reduction in the natural frequencies of the test structures was observed immediately after the maximum excurtions of the first run. During the following runs the test structures behaved very much as a linear system with first- and second-mode frequencies of approximately 2 and 10 Hz. As described in chapter 4, the waveforms corresponding to additional runs show distinct periods of relatively high-level response separated by periods of low-level response, which is consistent with characteristics of the imparted base motion.

The characteristics of the waveforms corresponding to test structure M (Fig. 5.37 through 5.40) were quite similar to those observed in test run D2-2 (Fig. 5.31 through 5.33).

5.7 Response Maxima

Values and characteristics of response maxima are summariz-

ed bellow.

(1) The "low-frequency" and "high-frequency" components of the response maxima, as well as the times of their occur - rence (in 0.004 of a second) are listed in Tables 5.8 through 5.15.

(2) The distribution of lateral forces, shears and moments corresponding to the instant of the base overturning moment max- imum for the first run of all test structures are plotted in Fig. 5.48 through 5.51.

(3) Relation of the maximum top level displacement with spectrum intensity (SI_{20}) value of the different time intervals described in section 5.2 is plotted in Fig. 5.52 for each test structure.

Salient characteristics of the response maxima are:

The maximum positive and negative responses indicate that the test structures were subjected to excurtions of the same order of magnitude in both directions (Tables 5.8 through 5.15).

The distributions of the first-mode component of lateral forces, shears and moments shown in Fig. 5.48 through 5.50 are quite similar to those based on the design model (Fig. 2.8).

The relation of spectrum intensity (SI_{20}) of the base ac - celeration and the maximum top level displacement (Fig. 5.52) is reasonably linear. As can be observed from Fig. 5.52a and 5.52b there is a gradual softening of the test structures in successive runs.

6. DISCUSSION OF OBSERVED RESPONSE

6.1 Introductory Remarks

This chapter compares the response maxima of the test structures with results of linear dynamic analyses based on spectral response, particularly in relation to the design procedure described in chapter 2.

Only the first three modes are considered in the linear dynamic analyses. The test frames are assumed to be plane frames as described in section 2.4.

Because the primary objective is to interpret the observed response in terms of linear spectral-response analyses, the chapter is organized as follows:

(1) Response spectra corresponding to the first run for each test structure are compared with that used in design (Fig. 2.5) to rationalize the use of a simple smooth response spectrum for all motions considered.

(2) The moment-displacement relationships of test struc - tures D and M (reconstructed from the measured dynamic response) and the moment-rotation relationships of the connecting beams (Abrams, 1976) are presented. The main intent of this section is to provide a framework for assessing the amount of damage caused in the test structures.

(3) Influence of variations in effective stiffness of

beams and columns on dynamic properties of the test
structure is discussed to prepare a basis for inter-
preting the measured response.

(4) The maximum responses of test structures D and M are
evaluated in relation to calculations based on linear
models and the assumed response spectrum.

6.2 Response Spectra

Figures 6.1 and 6.2 contain the calculated response spec-
tra for all four initial test runs (D1-1, D2-1, D3-1 and M1-1).
Response data are shown for damping factors of 0.02, 0.05 and
0.10.

Acceleration response spectra for runs D1-1, D2-1, and
D3-1 have similar shapes. As indicated by the values in Table
6.1 for structures D, the spectrum intensities are quite simi-
lar as are the maximum accelerations corresponding to the "low-
frequency" content (between 0-5 Hz). The values for test run
M1-1 are approximately twice those for test runs D1-1, D2-1,
and D3-1. Figures 6.1 and 6.2 also compare the spectrum used
in design (section 2.4, Fig. 2.5) with the obtained spectra.
In general, the spectrum used in design shows better agreement
with the obtained spectra at damping factors of five and ten
percent (Fig. 6.1b, 6.1c, 6.2b and 6.2c) and at frequencies
less than 25 Hz.

6.3 Stiffness and Strength of Test Structures

   (a) Moment-Rotation Relationships of Connecting Beams

   Static loading tests of the connecting beams were made by Abrams (1976). The spinal force-displacement relationships for the beams of structures D and M described in this section are taken from Abrams. The purpose of this section is to estimate the amount of damage suffered by the connecting beams of structures D and M during the first test run.

   Figures 6.3a and 6.3b show the measured spinal curves (given in terms of moment at face of wall vs. end rotation) of the connecting beams of structures D and M. The slope of the broken line represents the effective stiffness used in design and in different analyses described in this chapter. Measured effec - tive stiffnesses of the beams of test structures D and M were approximately 1/10 and 1/6 of the stiffnesses based on gross section (or approximately 1/6 of the stiffnesses based on cracked sections for both test structures D and M). Most of the flexibility was due to slip of the reinforcement (section 2.3).

   The maximum end rotations suffered by the connecting beams of the test structures during the first run were estimated from (1) the story displacements measured at the time of the maximum top level deflection, and (2) the calculated axial deformations in the columns. The first term was estimated by fitting a parabola through three consecutive floor levels. The second term was estimated by determining the axial forces in the columns at each level using the measured lateral forces and a linear model

of the structure with stiffnesses as described in Section 2.4.
The first term was typically four times as large as the second term.

Figures 6.4a and 6.4b show the calculated maximum end
rotations of the connecting beams of test structures D and M.
The "assumed" rotations shown in the figures correspond to an
approximate damage ratio of two ($\mu_b = 2$) for both types of
structures, as can be inferred from Fig. 6.3a and b. This
damage ratio corresponds to an equivalent damping factor of
approximately 8%, according to Eq. 2.4.

(b) Force-Displacement Relationships of Test Structures

In the case of multistory structures there is no unique
way to describe the force-displacement relationship without
assuming a specific force or displacement distribution and
without an arbitrary decision as to what forces and displace-
ment should be reported. Moreover, any chosen force-displace-
ment relationship for a determined force distribution repre-
sents only a limited and sometimes misleading source of infor-
mation about the energy dissipation characteristics of a struc-
ture as a whole. However, for multistory buildings incorpo -
rating walls resisting lateral loading the relationship be-
tween the base moment and the top-level deflection provides a
good source of information because usually the base moment is
a critical factor.

In this section, the base moment-top level deflection characteristics (spinal force-displacement relationship) of the test structures are discussed. The main purpose for constructing these curves is to provide a basis for judging the amount of damage suffered by the test structures as a whole during the first test run.

Direct information on the static response of the test structures was not obtained in the course of the experimental work. An indirect method was used to obtain information about the base moment-top level displacement relationship from the dynamic response as follows.

(1) The "force" quantity was chosen as the base moment corresponding to the first mode, which had been obtained from the total base moment waveform by filtering out all components higher than 5 Hz. as plotted in Fig. 5.23.

(2) The displacement quantity was chosen as the total lateral deflection at the tenth level (because the contribution of higher modes was negligible).

(3) Coordinates of the force-displacement relationship were obtained by scaling simultaneous maximum values of (1) and (2), and plotting them as shown in Fig. 6.5. In compiling the data, only those peak values which exceeded the previously attained values were considered. Dynamic responses of all three structures D were used to obtain Fig. 6.5a which was based on data from runs 1 and 2 of each test structure. The data

in Fig. 6.5b refers to the first run of structure M.

The broken lines in Fig. 6.5 passing through the origin refer to linear-response analyses for various assumptions about the stiffness of the structure as described in the figures. "Effective stiffness" refers to a model which includes the reduction in stiffness of the connecting beams resulting from slip of reinforcement. The "minimum effective slope" was obtained by drawing a straight line through the origin and the coordinates measured at the time of the maximum moment obtained in the first run. Comparison of these slopes and the curves leads to the following observations.

(1) A notable characteristic of the curves shown in Fig. 6.5 is that the stiffness of the test structures were less than those based on gross sectional properties and also less than those based on fully cracked sections for all structural elements.

(2) For top-level displacements less than 0.4 in., both spinal curves (Fig. 6.5a and 6.5b) are almost identical. The overall stiffnesses in this range were close to those based on effective stiffnesses of the beams.

(3) Both branches of the spinal curve of test struc - ture D (Fig. 6.5a) were almost identical for displacements less than approximately one inch (this corresponds to the range of displacements obtained during the first run). Because of the drift in the displacements waveforms obtained during the

second run, the two branches were not identical for displace -
ments exceeding one inch. The two branches of the spinal curve
of test structure M were almost identical.

(4) The overall damage ratio for the test structures
may be defined as the ratio of the slope indicated by the elas-
tic solution corresponding to the "effective" stiffness to the
"minimum effective" slope shown in Fig. 6.5. The overall dam-
age ratio obtained during the first test run of structures D
and M were approximately 1.5 and 2, respectively.

(c) Base Moment Capacity of Test Structures

Comparisons of the maximum base moment measured during the
second run of test structures D (test runs D1-2, D2-2 and D3-2)
and during the only run of test structure M (test run M1-1) with
calculated values for different yield mechanisms of the test
structures are presented in this section. The measured maximum
base moments of a single frame (half of the test structure) are
first compared with the limiting condition of the yield base-
moment calculated for the test frames assumed as a single "can-
tilever" projecting vertically. Then comparisons are made with
values calculated from the mechanism shown in Fig. 6.6a, which
consists of hinges at the ends of each connecting beam and the
bases of the columns.

The yield base moment calculated for a single frame of
test structures D and M as a "cantilever" projecting vertically
taking into account the gravity force (5 Kips at the base level)

was approximately 220 Kip-in.

The maximum base moment measured for a single frame of test structures D during the second run ranged from 185 to 200 Kip-in with an average value of 192 Kip-in (Tables 5.9, 5.11 and 5.15). The yield base moment calculated for the mechanism shown in Fig. 6.6a was 166 Kip-in. The yield moment of the connecting beams was calculated to be 1.6 Kip-in (assuming f_c' = 4500 psi and f_y = 72000 psi and the cross sectional properties shown in Fig. 2.17a) which is in fairly good agreement with experimental data on beam strength (Fig. 6.3a). The yield moments of the piers were taken from the interaction diagram of the base piers shown in Fig. 2.26. The difference between the measured base moment and the calculated value (based on the yield moments of the beams and base piers) was caused mainly by the strain hardening of the steel reinforcement as described below. It is important to note also that the obtained strength of the concrete of test structures D was higher than the assumed value of 4500 psi as shown in Table A.1 and Fig. A.1.

A reasonable "upper bound" of the base moment of the mechanism shown in Fig. 6.6a based on the average strength of the steel (f_{su} = 83000 psi) and on the assumptions described below was calculated to be 191 Kip-in for test structures D. The ultimate moment of the connecting beams was assumed to be 1.8 Kip-in which is comparable to the experimental data (Fig. 6.3a). Note that the actual strength of the connecting beams may be

increased at large deformations because of the restraining effect of the connections used in the setup (Fig. 4.11). The ultimate moments of the base piers were calculated using the cross sectional properties shown in Fig. 2.16a and assuming that only the "confined flanges" are working as shown in Fig. 6.6b. The calculated ultimate forces on the base piers are shown in Fig 6.6c and 6.6d.

The maximum base moment measured for a single frame of test structure M was 200 Kip-in (Table 5.13). The base moment for the mechanism shown in Fig. 6.6a was 215 Kip-in. The yield moment of the connecting beams for the mechanism was calculated to be 3.0 Kip-in (assuming f'_c = 4500 psi and f_y = 7200 psi and the cross sectional properties shown in Fig. 2.20a) which is comparable to the experimental data on beam strength (Fig. 6.3 b). The yield moments of the piers were taken from the interaction diagram (Fig. 2.26). Note that the yield moment in the connecting beams and "full" yield tension force in one of the piers occurred virtually simultaneously in the failure mechanism (Fig. 6.6a, that was why the moment capacity of the pier under tension was taken as zero).

The values obtained above lead to the following observations:

(1) The yield base moment calculated for the yield mechanism of a single frame of test structure D (166 Kip-in) was not reached during the first test runs (D1-1, D2-1 and D3-1).

The maximum base moment measured during the first run of test structures D ranged from 137 to 152 Kip-in with and average value of 145 Kip-in (Tables 5.8, 5.10 and 5.14). Therefore, heavy damage in the piers was unlikely to have taken place in the first runs of test structures D.

(2) The condition of almost simultaneous yield in the connecting beams and "full" yield tension force in one of the piers was likely to have happened during the only run of test structure M. This is indicated by the proximity of the measured maximum base moment (200 Kip-in) to that calculated for the yield mechanism (215 Kip-in).

6.4 Effect on Dynamic Response of Variations in Effective Stiffness

Before attempting to study the measured response using models, it is helpful to discuss the effects on calculated dynamic response of variations in the stiffness configurations of such models.

Natural frequencies associated with the first three modes for different configurations are summarized in Table 5.5. As would be anticipated, the highest fundamental frequency , 6.3 Hz., corresponds to a structural model with rigid connecting beams (cantilever beam with lumped masses). The ratio of the natural frequencies of the structural model working as a cantilever system is approximately 1:6:17 (first mode:second mode: third mode). The lowest fundamental frequency corresponds to

a structural model with infinitely flexible beams (two uniform cantilevers with no coupling beams).

The overall calculated response of the test structures could be grossly classified as that of a "flexure beam" or a cantilever projecting vertically from the base.

In the case of structure D, the structural system responded as a pair of cantilevers working in series, with coupling provided by the connecting beams.

In the case of structure M, which had strong beams, the system response was essentially that of a single cantilever.

Analyses made to study changes in the dynamic characteristics of the structural model (Fig. 2.6b) due to changes in the stiffnesses of different elements of the test structure are described below.

(a) Effects of Changes in the Stiffness of
     Connecting Beams

This study was made to determine the changes in natural frequencies, maximum top-level displacement and other charac - teristic (for a constant 1.0g response spectrum) of a struc - tural model corresponding to test structure D (section 2.4). The flexural stiffness of all connecting beams were varied uni- formly along the height of the structure from zero (no coupling) to that corresponding to the gross cross section. Calculations were made with three different assumptions about column stiff- ness: (1) gross section, (2) transformed cracked section

(μ_c = 1), and (3) modified transformed section (μ_c = 1.5).

Variations of the first- and second-mode frequencies and the corresponding top-level deflections are plotted in Fig. 6.7a and 6.7b against the ratio of the gross beam stiffness to the assumed stiffness, λ, with increase in λ. The figures indicate that (1) reduction in the first two natural frequencies is high for $\lambda < 5$ becoming small for $\lambda > 20$, (2) the second-mode frequency is relatively less sensitive to the beam stiffness than the first-mode frequency for $\lambda > 5$. As a result the ratio of second-mode to first-mode frequencies (f_2:f_1) increases with the flexibility of the connecting beams (for $\lambda > 5$), and (3) the top-level displacements for a constant 1.0g response spectrum increases significantly with the stiffness of the beams.

Figure 6.8 shows the effect of "coupling factor" in the first-mode base moment. The "coupling factor" is defined as the percentage of the total first-mode base moment generated by the axial forces in the piers at the base level. Figure 6.9 shows the distribution of flexural moment along a single pier for various values of the ratio of the flexural stiffness of the base column and that of the beams, α. Figures 6.8 and 6.9 indicate that even very small relative beam flexural stiffness will have palpable coupling effect. Note that the rate of change of the coupling factor with λ shown in Fig. 6.8 is similar to that of the fundamental frequency (Fig. 6.7a).

(b) <u>Effects of Changes in the Stiffness of Piers</u>

This study was made to determine the changes in natural frequencies and maximum top-level deflections (for a constant 1.0g response spectrum) of a structural model corresponding to test structure M (section 2.5). The structural model is identical to that shown in Fig. 2.6b with the following stiffness values for the beams,

$$I_{gross} = 0.2813 \text{ in}^4 \text{ ,}$$

$$E = 3 \times 10^6 \text{ psi}$$

for the first six columns,

$$I_{gross} = 0.2858 \text{ in}^4 \text{ ,} \quad \text{Axial Area} = A = 7.0 \text{ in}^2$$

$$E = (I_{cracked}/ I_{gross}) \times 3 \times 10^6 \text{ psi}$$

$$= 0.65 \times 3 \times 10^6 \text{ psi}$$

$$= 1.95 \times 10^6 \text{ psi}$$

for the top four columns,

$$I_{gross} = 0.2858 \text{ in}^4 \text{ ,} \quad \text{Axial Area} = A = 7.0 \text{ in}^2$$

$$E = (I_{cracked}/ I_{gross}) \times 3 \times 10^6 \text{ psi}$$

$$= 0.60 \times 3 \times 10^6 \text{ psi}$$

$$= 1.8 \times 10^6 \text{ psi}$$

Young's modulus of the two piers over the height of the first story is varied from 1.95×10^6 psi (denoted as $\mu = 1$ in Fig. 6.10) to 3.25×10^5 ($\mu = 6$). Calculations were made with

two different assumptions about beam stiffness based on: (1) effective stiffness (Fig. 6.3b, μ = 1), and (2) modified actual stiffness (μ = 2).

The variations of the first- and second-mode frequencies and the corresponding top-level displacements are plotted in Fig. 6.10. Figures 6.10a and 6.10b indicate that the variation of the natural frequencies and top-level displacement with the damage ratio in the base columns, μ, is approximately linear over the range considered.

6.5 Measured and Calculated Response

(a) Test Structure D

Response maxima obtained during test runs D1-1, D2-1 and D3-1 are compared with the values calculated in the design stage (section 2.4) in Fig. 6.11, 6.12 and 6.13. Measured and calculated first- and second-mode frequencies are listed in Fig. 6.11a. The measured frequencies were obtained from the waveforms recorded during the period of maximum excurtions.

Figures 6.11 through 6.13 indicate that the story displacements, shears and moments calculated assuming damage ratios of two for the beams (μ_b = 2) and one for the columns (μ_c = 1) corresponds fairly well to the maximum measured response of test structures D. Moreover, the first- and second-mode frequencies (Table 2.1 and Fig. 6.11a) calculated using the substitute-structure model are in good agreement with the measured values.

Results of the analysis of the model for structure D assum-

ing a uniform damage ratio of 1.5 ($\mu_c = \mu_b = 1.5$) using the response spectrum in Fig. 2.5 are summarized below.

(1) Modal shapes, frequencies, participation factors and damping factors: Table 6.2

(2) Distribution of flexural moments in the beams and piers: Fig. 6.14 and 6.15.

(3) Distribution of axial load in the piers: Fig. 6.16

(4) Comparison of displacements, shears, and moments with measured values: Fig. 6.17, 6.18 and 6.19.

Figures 6.17 through 6.19 and the calculated frequencies indicate that the results obtained assuming a uniform damage ratio for all elements are not as good as those obtained for the design model. While the calculated displacements for the model based on a uniform damage ratio represent an upper bound to the measured values (Fig. 6.17), the shears and moments represent a lower bound to the measured values (Fig. 6.19).

It is of some interest to observe the change in the calculated (RSS) base column moments as the model is changed from that used for design (damage ratio for columns = 1, for beams = 2) to one with a damage ratio of 1.5 for both the columns and the beams. As would be expected, the calculated total base moment is approximately the same for the two models (less than 10% difference) but the base columns moments for the design model are approximately 35% higher. (Compare Fig. 2.14 and 6.15.)

Another interesting point that should be mentioned is the

ratio of second-mode to first-mode frequencies $(f_2:f_1)$ for the two models described above and their relation with the measured values. The measured $f_2:f_1$ ratio varied from an average value of 4.1 (during the initial free vibration tests) to 4.9 (in the final part of the first test runs). During the maximum excur - sions of the first runs this ratio was 4.4. For the design mod- el $f_2:f_1$ was calculated to be 4.3 and for the model assuming a uniform damage ratio $f_2:f_1$ was 4.1. The frequencies from the design model were in better agreement with the measured data than that with a uniform damage ratio. Note that assuming a uniform damage causes a reduction in all calculated frequencies by $1/\mu^{\frac{1}{2}}$.

(b)   Test Structure M

Two types of analyses were made to study the observed re- sponse of test structure M. These two analyses were based on the assumptions of the substitute structure method (section 2.2). A response spectrum with effective peak acceleration of 1.0g (Fig. 6.2) was used in both analyses.

The first analysis was based on a damage ratio of two for the connecting beams $(\mu_b = 2)$, four for both columns at base level $(\mu_c = 4)$, and one for the rest of the columns $(\mu_c = 1)$. Results of this analysis are summarized below.

(1) Modal values, frequencies, participation factors and damping factors: Table 6.3.

(2) Modal shapes: Fig. 6.20.

(3) distribution of flexural moments in the connecting

beams and columns: Fig. 6.21 and 6.22.

(4) Distribution of axial load in the columns: Fig. 6.23.

(5) Location of calculated forces in the columns with respect to the interaction diagram: Fig. 6.24.

(6) Comparison of displacements, shears and moments with the measured values: Fig. 6.25, 6.26 and 6.27.

The comparisons shown in Fig. 6.25 through 6.27 indicate that the calculated displacements, shears and moments represent good estimates of the response maxima of test structure M. The calculated first- and second-mode frequencies (Table 6.3 and Fig. 6.25) show good agreement with the measured values. The assumed damage ratio (μ_b = 2) for the beams was justified in section 2.3. The damage of the piers only at the base level is compatible with the observations immediately after test run M1-1 (Fig. 4.30).

An interesting point that was briefly mentioned in section 2.5 (c) is the apparent redistribution of flexural moments in the piers. Figures 2.27 and 6.24 show the locations in the interaction diagrams of the calculated actions on the piers of test structures D and M, respectively. The conditions of tension force appeared to be critical at the lower piers for both test structures. However, considering that the stiffnesses of the pier under compression is larger than those of the pier under tension, a redistribution of moments is most likely to have happened.

The second analysis was based on a uniform damage ratio of two for the entire structure ($\mu_b = \mu_c = 2$). Results of this analysis are summarized below.

(1) Modal shapes, frequencies, participation factors and damping factors: Table 6.4.

(2) Distribution of flexural moments in the connecting beams and piers: Fig. 6.28 and 6.29.

(3) Distribution of axial load in the piers: Fig. 6.30.

(4) Comparison of displacements, shears and moments with the measured values: Fig. 6.31, 6.32 and 6.33.

As shown in Fig. 6.31 through 6.33, the calculated displacements, shears and moments agree reasonably well with the measured values. It is important to note, however, that the calculated second natural frequency (10.4 Hz) is relatively low compared with the apparent measured value (approximately 12Hz).

In both analyses the calculated double-amplitude displacement shows better agreement than the single-amplitude displacement. This is because of the final drift in the measured waveforms (Fig. 4.27).

The measured ratio of second-mode to first-mode frequencies (f_2:f_1) varied from 4.2 (during the initial free vibration test) to 5.0 (in the final part of test run M1-1). During the maximum excursions in test run M1-1 this ratio was measured to be about 4.8. For the structural model with uniform damage ratio of two f_2:f_1 was calculated to be 4.1 and for the model with a

damage ratio of four for the piers at the base level and two for all connecting beams $f_2:f_1$ was calculated to be 4.8. The first analysis set of assumptions led to results in better agreement with the measured response than the second set of assumptions.

7. SUMMARY AND CONCLUSIONS

7.1 Object and Scope

Tall reinforced concrete structures resist lateral forces as frames (shear beams) or as cantilevers (flexure beams). The tests discussed in this report were designed to investigate the earthquake response of reinforced concrete systems resisting lateral forces primarily in the flexure-beam mode. The small-scale test structures represented slender walls coupled by beams.

A secondary but important objective of the experimental program was to demostrate the consequences of flexural yielding in the wall prior to yielding of the beams.

Studies of the experimental data were made with a view to the development of procedures to determine design forces using modified linear-response models.

(a) Experimental Program

A total of four small scale ten-story test structures (Fig. 3.1) were built and tested using the University of Illinois Earthquake Simulator.

Each test structure (Fig. 2.1) comprised two identical perforated walls parallel to each other and oriented such that the base motion caused them to bend about their strong axis. (See Fig. 2.6 for overall dimensions.)

The test structures carried a mass of 1000 lb. at each of the ten levels.

The small-scale steel reinforcement used for constructing the model had a yield stress of 72,000 psi (Fig. A.7). The compressive strength of the concrete was nominally 4500 psi. Details of the material properties are given in Table A.1 and Fig. A.1 to A.10 (section A.2).

The main variables in the experimental work were the strength of the test structures and the base motions.

Structure M (one only) differed from structures D (three) primarily in that its beams had more reinforcement (see Fig. 2.15 and 2.18).

The base motions were scaled versions of the NS component of the 1940 Imperial Valley earthquake (recorded at El Centro, Calif.) and the N21E component of the 1952 Tehachapi earthquake (recorded at Taft, Calif.). In order to obtain a relation comparable to conditions for a full scale building between the natural frequencies of the test structures and the frequency content of the earthquake records, the time axis of the earthquake records were compressed by a factor of 2.5. Each test structure was subjected to a series of motions of increasing intensity. Details of the base motions are given in section 5.3.

The principles of the substitute-structure method (Shibata, 1976) were used in determining the relative amounts of reinforcement in the beams and piers of the test structures D.

To permit investigation of the influence of the amount of

reinforcement in the beams, test structure M was reinforced arbitrarily with twice as much beam reinforcement as test structures D. Details of the design of the test structures are given in chapter 2.

Acceleration Response Spectra A (Shibata, 1976; Fig. 1) for the base motion was used in the design of test structures D with the time axis compressed by 2.5. Comparisons of the obtained response spectra with that used in design are shown in Fig. 6.1 and 6.2.

(b) Instrumentation and Data

Measurements included horizontal acceleration at 22 locations and horizontal displacements at 20 locations (see sections A.4b, A.5 and Fig. 3.4 and 3.5). Crack patterns were recorded after each test run (chapter 4 and section 5.5).

Continuously recorded data are presented in two forms. Displacements and accelerations are presented as obtained directly from the measurements modified by appropiate calibration factors (chapter 4). Selected displacement and acceleration data as well as all shear and moment records are shown in filtered form (chapter 5).

Natural frequencies inferred from free vibration tests and from the response waveforms in every test run are reported in chapter 4 and discussed in section 5.4.

Spectrum intensities, peak values, and response spectra for the base accelerations for every test run are reported in sec -

tion 5.3 (Tables 5.1 to 5.4 and Fig. 5.3 to 5.8).

Fourier Spectra of selected displacement and acceleration records are shown in Fig. 5.1 and 5.2.

(c) Studies

Natural frequencies obtained from free vibration tests were compared with calculated values based on different stiffness assumptions (Table 5.5, section 5.4).

The moment-displacement relationships of test structures D and M (constructed from the measured dynamic response) and the moment-rotation relationships of the connecting beams were used to provide a framework for assessing the amount of damage caused in the test structures (section 6.3a and 6.3b).

Comparison of the maximum base moment measured during the second runs of test structures D and during the only run of structure M with calculated values for different failure mechanisms are presented in section 6.3c.

Influence of variations in effective stiffness of beams and piers on dynamic properties (natural frequencies, ratio of the natural frequencies, etc.) is discussed in section 6.4.

Comparative studies of the observed response with linear analyses based on spectral response were made for the first run of the test structures (section 6.5). The comparisons were based on response maxima, natural frequencies and ratio of the natural frequencies during maximum excursions.

7.2 Conclusions

(a) Conclusions Related to Behavioral Considerations

*A critical characteristic of the observed response was the reduction in the natural frequencies inferred from the displacement and acceleration waveforms. Reductions in natural frequencies occurred very early during the first run: a reduction of approximately 50% in the fundamental frequency was observed immediately after the initial maximum excursions. A reduction of approximately 40% was observed in the second natural frequency. The observed reductions in the inferred frequencies were a little higher in test structures subjected to El Centro (1940) than in the structure subjected to Taft (1952). Further reductions in natural frequencies occurred during subsequent test runs, but at lower rates (Fig. 5.16 and 5.18).

*Spectrum intensity (Housner, 1959) served as a better index to define the intensity of the base motions for a given waveform than the maximum base acceleration values (Tables 5.1 to 5.3). The top-level displacement increased almost linearly with spectrum intensity (Fig. 5.52).

*The displacements were dominated by the first mode. Influence of higher-mode components in the maximum top displacements was less than 7 percent.

*The overturning effect of gravity load resulting from lateral displacement (P-Δ effect) was less than two percent in

all test runs.

*For all test structures the displacement waveforms were quite similar to the base moment waveform and the maximum values tended to occur at the same time (Chapter 5).

*The apparent centroids of the lateral forces on the test structures corresponding to maximum base moment were located at 0.70 H or higher where H is the height of the structure from the base.

*In runs with "design earthquakes" the maximum top displacements in terms of the height of the structure, H, did not exceed 1.3% for the D structures. The maximum inter-story deflection was less than 0.12 in. or 1.3% of the story height.

*The acceleration responses for all test structures at the lower levels were observed to be dominated by the high-frequency components of the imparted base motions. This condition was observed to change gradually to the eighth level, node position for the second mode, where the first-mode component dominated (Chapter 5).

*For test structures D, the observed damage consisted of flexural cracks at the ends of the connecting beams during the first test run ("design earthquake"). No structural distress was observed in the piers. During subsequent test runs, additional damage consisted of spalling of the concrete on the exterior edges of the piers and at the ends of the connecting beams, particularly in the beams between levels three and six (Fig. 4.5, 4.6 and 4.11).

*For test structure M, the observed damage in run 1 consisted of severe spalling of the concrete on the exterior edges of the base piers. There was some spalling at the ends of the connecting beams at levels two to six (Fig. 4.29, 4.30 and 4.31).

*Similar waveforms and response maxima were observed for test structures D and M when subjected to comparable base motions (Test runs D2-2 and M1-1). However, the type of failure and extent of the observed damage in the two types of test structures were completely different. The critical damage for test structure M was concentrated at base of the piers. Failures for test structures D were characterized by the complete formation of a failure mechanism which consisted of hinges at the ends of each connecting beam and finally at the bases of the piers.

*For all test structures the shear in the piers was not critical because of the basic design. The "nominal" shear stress (total shear force at the base level divided by the gross area of the piers) did not exceed $4\sqrt{f'_c}$.

(b) Conclusions Related to the Use of Linear Models for Design

*For all test structures the natural frequencies determined in the initial free vibration tests were smaller than the calculated frequencies for a linear model based on gross sectional properties of the structural members. The fundamen-

tal frequency varied from 83% to 89% of the calculated value
based on gross sections. (See Table 5.5 and Section 5.4a).
Whereas all factors, ranging from lack of perfect fixity at
base to air resistance, would tend to reduce the natural fre-
quency in relation to the calculated value, sensitivity studies
indicated that the main reason for the discrepancy was the
existence of shrinkage cracks in the test structures (section
5.4).

*Linear analyses based on spectral response and on plau-
sible reductions in the stiffness of the structural components
provided an adequate basis for interpreting the observed re-
sponse maxima (story shears, moments and lateral deflections),
the natural frequencies (f_1, f_2) and the ratio between the nat-
ural frequencies $(f_2 : f_1)$.

The stiffnesses of the beams and piers used in linear
analyses (Chapter 6) were determined taking into account the
effects of flexural cracking, shear deformation, and slip of
the reinforcement (axial deformation was considered only in
the piers). The stiffness of the beams and piers were further
reduced on the basis of damage ratios determined with the help
of the overall moment-displacement relationships of the test
structures plus data from static tests of the connecting beams
(Chapter 6).

*The relative amounts of reinforcement in the beams and
piers of structures D were determined using a linear-response

model for dynamic analysis (the substitute structure method) with explicit criteria about structural response: (a) maximum story displacements and (b) a damage pattern with the connecting beams providing the main source of energy dissipation in the nonlinear range of response. The behavior of structures D, during the base motions corresponding to the "design earthquake," was as anticipated by the design calculations. The displacements did not exceed the design values (Fig. 6.11). Yielding was limited to the connecting beams (Section 6.3).

*Two features of the process by which design forces in the structural elements were determined deserve special mention.

The initial cracked-section stiffness of the beams included the effect of slip of the beam reinforcement anchored in the pier. The inclusion of the effect of slip reduced the cracked-section stiffness by a factor of six. This stiffness reduction is not limited to small-scale structures (Sozen, 1971).

At a given level, the linear model results in equal moments in both piers which are subjected to different axial loads. Strict adherence to the design premises would require that reinforcement be provided, in both piers, to resist the moment in conjunction with the lower compressive (or higher tensile) axial load. In determining the required reinforcement an arbitrary amount of redistribution was assumed. The section was proportioned for the calculated moment acting in

conjunction with the dead load. A check was then made to make certain that the surplus flexural strength for the compressed pier would offset the apparent insufficiency in resistance for the pier in tension.

LIST OF REFERENCES

1. Abrams, D. and M. A. Sozen, "Measured Hysteresis Relation-
    ships for Small-Scale Beams," Civil Engineering Studies,
    Structural Research Series No. 432, University of Illinois,
    Urbana, November 1976.

2. Clough, R. W. and J. Penzien, Dynamics of Structures,
    McGraw-Hill, 1975.

3. Ferguson, P. M., Reinforced Concrete Fundamentals, Third
    Edition, John Wiley, 1973.

4. Gulkan, P. and M. A. Sozen, "Inelastic Response of Reinforc-
    ed Concrete Structures to Earthquake Motions," Journal of
    the American Concrete Institute, V. 71, No. 12, November
    1974, pp. 601-609.

5. Gulkan, P. and M. A. Sozen, "Response and Energy-Dissipa-
    tion of R/C Frames Subjected to Strong Base Motions,"
    Civil Engineering Studies, Structural Research Series No.
    377, University of Illinois, Urbana, May 1971.

6. Housner, G. W., "Spectrum Intensities of Strong Motion
    Earthquakes," Proceedings of 1952 Symposium on Earthquake
    and Blast Effects on Structures, Earthquake Engineering
    Research Institute, 1952.

7. Housner, G. W., "Behavior of Structures during Earthquakes,"
    Journal of the Engineering Mechanics Division, ASCE, Vol.
    85, No. EM4, October 1959, pp. 108-129.

8. Otani, S. and M. A. Sozen, "Behavior of Multistory Reinforc-
    ed Concrete Frames during Earthquakes," Civil Engineering
    Studies, Structural Research Series No. 392, University of
    Illinois, Urbana, 1972.

9. Otani, S. and M. A. Sozen, "Simulated Earthquake Tests of
    R/C Frames," Journal of the Structural Division, ASCE, Vol.
    100, No. ST3, March 1974, pp. 687-701.

10. Przemienieki, J. S., Theory of Matrix Structural Analysis,
    McGraw-Hill, 1968.

11. Shibata, A. and M. A. Sozen, "Substitute Structure Method
    for Seismic Design in R/C," Journal of the Structural
    Division, ASCE, Vol. 102, No. ST1, January 1976, pp. 1-18.

12. Sozen, M. A. and S. Otani, "Perfomance of the University of Illinois Earthquake Simulator in Reproducing Scaled Earthquake Motions," Proceedings, U.S.-Japan Seminar on Earthquake Engineering with Emphasis on the Safety of School Buildings, Sendai, September 1970, pp. 278-302.

13. Sozen, M. A., "Five Easy Pieces," Structural Concrete Symposium, University of Toronto, May 1971.

14. Spiegel, M. R., Fourier Analysis, Schaum's Outline Series, McGraw-Hill, 1974.

15. Staffier, S. R. and M. A. Sozen, "Effect of Strain Rate on Yield Stress of Model Reinforcement," Civil Engineering Studies, Structural Research Series No. 415, University of Illinois, Urbana, Febraury 1975.

16. Takeda, T., Sozen, M. A., and Nielsen, N. M., "Reinforced Concrete Response to Simulated Earthquakes," Journal of the Structural Division, ASCE, Vol. 96, No. ST12, Dec. 1970, pp. 2557-2573.

17. Thomson, W. T., Theory of Vibration with Applications, Prentice-Hall, 1972.

Table 2.1 Modal Shapes and Characteristic Values
Used in Design

Level	First Mode	Second Mode	Third Mode
10	1.000	1.000	1.000
9	0.887	0.457	-0.092
8	0.768	-0.066	-0.869
7	0.643	-0.458	-0.996
6	0.516	-0.746	-0.463
5	0.392	-0.817	0.299
4	0.275	-0.750	0.904
3	0.170	-0.568	1.096
2	0.083	-0.328	0.831
1	0.023	-0.106	0.325
Natural Frequency (Hz)	2.8	12	28
Damping Factor	5.0%	3.7%	2.8%
Participation Factor for the Base Shear	68.1%	15.9%	7.1%

Table 4.1

Response Maxima of Test Structure D1

Level	TEST RUN D1-1 Acceleration (g) (+)	(-)	Displacement (in.) (+)	(-)	TEST RUN D1-2 Acceleration (g) (+)	(-)	Displacement (in.) (+)	(-)
10	1.20	-1.67	0.97	-1.12	2.27	-1.62	1.82	-1.72
9	0.86	-1.12	0.83	-0.98	1.28	-1.15	1.63	-1.55
8	0.70	-0.70	0.72	-0.82	0.97	-0.88	1.45	-1.34
7	0.82	-0.82	0.61	-0.70	1.33	-1.43	1.23	-1.20
6	0.92	-0.97	0.50	-0.56	1.46	-1.50	1.05	-1.01
5	0.86	-0.97	0.40	-0.43	1.33	-0.98	0.80	-0.80
4	0.81	-0.92	0.29	-0.33	1.22	-1.04	0.59	-0.62
3	0.76	-0.78	0.19	-0.22	1.48	-1.17	0.40	-0.42
2	0.60	-0.66	0.11	-0.13	1.46	-1.15	0.22	-0.25
1	0.53	-0.48	0.05	-0.05	1.76	-1.63	0.09	-0.10
Base	0.50	-0.44	---	---	1.94	-1.29	---	---

Table 4.2

Response Maxima of Test Structure D2

	TEST RUN D2-1				TEST RUN D2-2				TEST RUN D2-3			
Level	Acceleration (g)		Displacement (in.)		Acceleration (g)		Displacement (in.)		Acceleration (g)		Displacement (in.)	
	(+)	(-)	(+)	(-)	(+)	(-)	(+)	(-)	(+)	(-)	(+)	(-)
10	1.25	-1.66	0.97	-1.16	2.00	-1.58	2.13	-1.74	2.36	-2.38	1.98	-2.96
9	0.92	-1.12	0.86	-1.00	1.37	-1.14	1.92	-1.58	1.20	-1.47	1.83	-2.70
8	0.73	-0.75	0.74	-0.86	1.00	-0.92	1.57	-1.38	0.99	-1.11	1.40	---
7	0.73	-0.72	0.61	-0.71	1.07	-0.98	1.41	-1.18	1.18	-1.31	1.35	-1.99
6	0.84	-0.85	0.47	-0.58	1.12	-1.07	1.16	-0.97	1.23	-1.47	1.12	-1.73
5	0.79	-0.86			1.07	-0.99	0.94	-0.76	1.26	-1.46	0.91	-1.35
4	0.79	-0.82			1.11	-0.95	0.70	-0.60	1.48	-1.38	0.68	-1.06
3	0.71	-0.67			0.96	-1.05	0.49	-0.41	1.48	-1.23	0.47	-0.74
2	0.56	-0.57	Not		0.93	-0.90	0.27	-0.25	1.46	-1.26	0.27	-0.45
1	0.45	-0.47	Reported (because of noise)		0.96	-0.78	0.12	-0.11	1.40	-1.49	0.11	-0.20
Base	0.40	-0.41			0.94	-0.75	---	---	1.44	-1.72	---	---

Table 4.3

Response Maxima of Test Structure M1

TEST RUN M1-1				
Level	Acceleration (g)		Displacement (in.)	
	(+)	(-)	(+)	(-)
10	1.58	-1.84	2.05	-1.47
9	1.24	-1.24	1.92	-1.33
8	1.00	-0.87	1.69	-1.20
7	1.10	-1.00	1.43	-1.02
6	1.31	-1.17	1.18	-0.87
5	1.27	-1.23	0.94	-0.69
4	1.11	-1.19	0.71	-0.55
3	1.09	-1.10	0.50	-0.39
2	1.00	-0.80	0.28	-0.21
1	0.94	-0.69	0.13	-0.10
Base	0.91	-0.71	---	---

Table 4.4

Response Maxima of Test Structure D3

	TEST RUN D3-1				TEST RUN D3-2			
Level	Acceleration (g)		Displacement (in.)		Acceleration (g)		Displacement (in.)	
	(+)	(-)	(+)	(-)	(+)	(-)	(+)	(-)
10	1.21	-1.26	0.72	-0.95	1.76	-1.61	1.48	-1.11
9	0.77	-0.85	0.64	-0.84	1.07	-0.96	1.36	-1.00
8	0.61	-0.75	0.56	-0.75	0.91	-0.76	1.23	-0.88
7	0.65	-0.77	0.48	-0.63	1.00	-0.91	1.06	-0.73
6	0.72	-0.72	0.40	-0.53	1.19	-1.11	0.90	-0.62
5	0.71	-0.78	0.31	-0.40	1.24	-1.11	0.70	-0.47
4	0.76	-0.85	0.22	-0.30	1.25	-1.18	0.54	-0.35
3	0.75	-0.82	0.14	-0.21	1.19	-1.00	0.37	-0.23
2	0.54	-0.58	0.09	-0.12	0.96	-0.80	0.22	-0.13
1	0.45	-0.47	0.04	-0.04	0.95	-0.87	0.09	-0.05
Base	0.43	-0.46	---	---	0.99	-1.06	---	---

Table 5.1

Maximum Base Acceleration and

Spectrum Intensities . Test Structure D1

Time (sec) from-to	TEST RUN D1-1								TEST RUN D1-2						
	Max. Acc. (g)		Spectrum Intensity (in.)						Max. Acc. (g)		Spectrum Intensity (in.)				
	$(+)$	$(-)$	SI_0	SI_2	SI_5	SI_{10}	SI_{20}		$(+)$	$(-)$	SI_0	SI_2	SI_5	SI_{10}	SI_{20}
0 - 12	0.50,	-0.44	19.1	12.2	9.9	8.1	6.7		1.94,	-1.29	37.9	24.3	19.7	16.5	14.0
0 - 3	0.50,	-0.44	13.9	11.2	9.6	8.1	6.7		1.94,	-1.29	27.9	22.5	19.2	16.5	14.0
3 - 9	0.27,	-0.27	9.9	7.1	5.9	5.0	4.1		1.10,	-0.88	19.9	14.2	12.0	10.4	8.8
9 - 12	0.24,	-0.26	4.6	3.7	3.1	2.6	2.2		0.59,	-0.77	9.0	7.2	6.1	5.3	4.5

(SI_β) = spectrum intensity at $\beta(\%)$ damping

Table 5.2

Maximum Base Acceleration and
Spectrum Intensities.   Test Structure D2

	TEST RUN D2-1							TEST RUN D2-2						
Time (sec)	Max. Acc. (g)		Spectrum Intensity (in.)					Max. Acc. (g)		Spectrum Intensity (in.)				
from-to	(+)	(−)	SI_0	SI_2	SI_5	SI_{10}	SI_{20}	(+)	(−)	SI_0	SI_2	SI_5	SI_{10}	SI_{20}
0 - 12	0.40,	−0.41	18.7	12.0	9.6	7.9	6.5	0.94,	−0.75	37.2	23.6	18.9	15.5	13.0
0 - 3	0.40,	−0.41	13.6	10.7	9.4	7.8	6.5	0.94,	−0.75	26.7	21.6	18.3	15.5	13.0
3 - 9	0.20,	−0.30	9.5	6.8	5.7	4.9	4.0	0.41,	−0.50	18.9	13.7	11.5	9.7	8.0
9 - 12	0.19,	−0.18	4.3	3.5	2.9	2.4	2.0	0.35,	−0.38	8.6	6.9	5.8	4.9	4.1

TEST RUN D2-3

Time (sec)	Max. Acc. (g)		Spectrum Intensity (in.)				
from-to	(+)	(−)	SI_0	SI_2	SI_5	SI_{10}	SI_{20}
0 - 12	1.44,	−1.72	55.0	35.0	28.3	23.3	19.5
0 - 3	1.44,	−1.72	39.7	32.1	27.3	23.3	19.4
3 - 9	0.65,	−0.76	28.0	20.2	17.0	14.5	11.9
9 - 12	0.56,	−0.60	12.8	10.2	8.6	7.3	6.0

(SI_β) = spectrum intensity at $\beta(\%)$ damping

Table 5.3

Maximum Base Acceleration and
Spectrum Intensities.   Test Structure M1

TEST RUN   M1-1

Time (sec)	Max. Acc. (g)		Spectrum Intensity (in.)				
from-to	(+)	(-)	SI_0	SI_2	SI_5	SI_{10}	SI_{20}
0 - 12	0.91,	-0.71	36.9	23.4	18.9	15.5	12.9
0 - 3	0.91,	-0.71	26.6	21.6	18.3	15.5	12.9
3 - 9	0.42,	-0.54	18.9	13.6	11.5	9.8	8.0
9 - 12	0.36,	-0.38	8.5	6.8	5.7	4.8	4.0

(SI_β) = spectrum intensity at $\beta(\%)$ damping

Table 5.4

Maximum Base Acceleration and
Spectrum Intensities.   Test Structure D3

| Time (sec) | TEST RUN D3-1 | | | | | | | TEST RUN D3-2 | | | | | | |
| | Max. Acc. (g) | | Spectrum Intensity (in.) | | | | | Max. Acc. (g) | | Spectrum Intensity (in.) | | | | |
from-to	(+)	(−)	SI_0	SI_2	SI_5	SI_{10}	SI_{20}	(+)	(−)	SI_0	SI_2	SI_5	SI_{10}	SI_{20}
0 - 13	0.43,	−0.46	19.5	12.6	10.2	8.4	6.8	0.99,	−1.06	38.5	24.7	19.9	16.5	13.2
0 - 6.5	0.43,	−0.46	17.8	12.6	10.2	8.4	6.8	0.99,	−1.06	35.1	24.7	19.9	16.5	13.2
6.5-13	0.20,	−0.18	9.0	6.2	4.8	3.9	3.1	0.40,	−0.36	17.7	12.2	9.5	7.7	6.0

(SI_β) = spectrum intensity at $\beta(\%)$ damping

Table 5.5 Comparison of Calculated and Measured
Frequencies of the Test Structures

Structure	Frequencies (Hz)		
	First Mode	Second Mode	Third Mode
(A) Calculated			
Uncracked* (Types D&M)	5.4	23	52
Cracked Type D	4.2	17	38
Type M	4.4	19	44
Substitute Structure Type D	2.8	12	28
Structure as two uncracked piers(no beams)	2.2	13	37
Structure with fully coupled uncracked piers	6.3	39	107
(B) Measured			
"Uncracked" (during initial free vibration)			
Test Structure D1	4.5	18	--
D2	4.8	20	--
D3	4.8	19	--
M1	4.5	19	--
"Cracked" (during end of first test run)			
Test Run D1-1	2.0	10	26
D2-1	2.0	10	--
D3-1	2.4	12	--
M1-1	2.1	10	23

*Assuming a Young Modulus of 3×10^6 psi
and gross section properties

Table 5.6 Key to the Figures of Filtered Waveforms

Test Structure	Test Run	Displs.	Accels.	Shears	Moments
D1	D1-1	5.20	5.21	5.22	5.23
	D1-2	5.24	5.25	5.26	5.27
D2	D2-1	----	5.28	5.29	5.30
	D2-2	----	5.31	5.32	5.33
	D2-3	----	5.34	5.35	5.36
M1	M1-1	5.37	5.38	5.39	5.40
D3	D3-1	----	5.41	5.42	5.43
	D3-2	----	5.44	5.45	5.46

Table 5.7

Comparison of Calculated and Measured First-Mode Shape of Test Structure D

Level	Cantilever[a]	Uncracked Structure[b]	Design Values[c]	Measured Values At[d]		
				0.87 sec	2.43 sec	3.66 sec
10	1.00	1.00	1.00	1.00	1.00	1.00
9	0.86	0.88	0.89	0.88	0.88	0.89
8	0.73	0.76	0.77	0.77	0.76	0.74
7	0.59	0.63	0.64	0.66	0.65	0.65
6	0.46	0.51	0.52	0.54	0.53	0.52
5	0.34	0.39	0.39	0.42	0.40	0.41
4	0.23	0.27	0.28	0.31	0.30	0.31
3	0.14	0.17	0.17	0.20	0.20	0.20
2	0.06	0.09	0.08	0.10	0.11	0.11
1	0.02	0.03	0.02	0.04	0.04	0.04

[a] First-mode shape of clamped-free beam (lumped masses)

[b] Using the structural model in Fig. 2.6 based in gross-sectional properties

[c] Used in design of structure D (see Table 2.1)

[d] Values are normalized with respect to top-level deflection (Test Run D1-1)

Table 5.8

Low- and High-Frequency Components of Response Maxima in Test Run D1-1

| | DISPLACEMENTS (in.) | | | | | | ACCELERATIONS (g) | | | | | |
| | Maximum Positive | | | Maximum Negative | | | Maximum Positive | | | Maximum Negative | | |
Level	Time*	First Mode	High Modes	Time*	First Mode	High Modes	Time*	First Mode	High Modes	Time*	First Mode	High Modes
10	655	0.92	0.05	607	-1.04	-0.08	658	0.70	0.50	527	-0.64	-1.03
9	655	0.80	0.03	607	-0.92	-0.06	657	0.62	0.24	609	-0.70	-0.42
8	655	0.70	0.01	611	-0.80	-0.03	655	0.54	0.16	611	-0.61	-0.09
7	655	0.60	0.00	611	-0.69	-0.02	488	0.40	0.42	517	-0.30	-0.52
6	655	0.50	0.00	611	-0.56	-0.01	488	0.32	0.59	517	-0.24	-0.73
5	653	0.38	0.01	614	-0.41	-0.02	488	0.27	0.59	517	-0.18	-0.79
4	653	0.28	0.01	614	-0.31	-0.02	486	0.23	0.59	518	-0.13	-0.78
3	650	0.17	0.02	616	-0.20	-0.03	485	0.18	0.59	324	-0.16	-0.62
2	651	0.10	0.01	616	-0.11	-0.02	485	0.13	0.47	325	-0.15	-0.51
1	652	0.04	0.01	616	-0.04	-0.01	275	0.01	0.52	325	-0.14	-0.34
Base		---	---		---	---	273	(0.01)	(0.49)	510	(-0.04)	(-0.40)

* Time in 0.004 of a second

Table 5.8 (Contd)

Low- and High-Frequency Components of Respone Maxima in Test Run D1-1

	SHEAR FORCES (Kips)						OVERTURNING MOMENTS (Kip-in.)					
	Maximum Positive			Maximum Negative			Maximum Positive			Maximum Negative		
Level	Time*	First Mode	High Modes	Time*	First Mode	High Modes	Time*	First Mode	High Modes	Time*	First Mode	High Modes
10		---	---		---	---		---	---		---	---
9	658	0.35	0.25	527	-0.32	-0.52	609	3.6	3.8	658	-3.2	-2.2
8	657	0.66	0.36	609	-0.75	-0.63	609	10.5	9.4	658	-9.2	-5.5
7	657	0.93	0.36	609	-1.06	-0.63	609	20.2	15.1	658	-17.7	-8.7
6	655	1.17	0.33	610	-1.33	-0.47	609	32.4	19.3	657	-28.5	-10.9
5	655	1.36	0.22	610	-1.55	-0.22	609	46.7	20.8	657	-41.0	-12.3
4	655	1.50	0.33	604	-1.59	-0.24	610	62.6	19.7	655	-54.9	-14.3
3	488	1.37	0.72	602	-1.60	-0.56	610	79.7	16.2	655	-69.7	-16.8
2	487	1.49	0.89	602	-1.70	-0.74	610	97.5	10.5	655	-85.7	-18.4
1	487	1.54	1.09	617	-1.66	-1.00	610	115.9	3.2	655	-100.7	-19.3
Base	486	1.62	1.20	617	-1.74	-1.02	604	124.5	12.9	655	-116.5	-19.6

* Time in 0.004 of a second

Table 5.9

Low- and High-Frequency Components of Response Maxima in Test Run D1-2

| | DISPLACEMENTS (in.) | | | | | | ACCELERATIONS (g) | | | | | |
| | Maximum Positive | | | Maximum Negative | | | Maximum Positive | | | Maximum Negative | | |
Level	Time*	First Mode	High Modes	Time*	First Mode	High Modes	Time*	First Mode	High Modes	Time*	First Mode	High Modes
10	505	1.73	0.09	355	-1.78	0.06	285	0.53	1.73	242	-0.61	-1.00
9	505	1.51	0.11	356	-1.58	0.02	499	0.75	0.53	242	-0.54	-0.62
8	505	1.33	0.12	355	-1.37	0.03	509	0.62	0.34	350	-0.79	-0.09
7	505	1.13	0.11	358	-1.17	-0.03	290	0.45	0.88	284	0.31	-1.74
6	505	0.95	0.10	358	-0.97	-0.04	278	0.08	1.38	284	0.24	-1.74
5	505	0.73	0.07	358	-0.76	-0.04	276	0.04	1.29	449	-0.26	-0.73
4	505	0.54	0.06	357	-0.58	-0.04	275	0.00	1.22	448	-0.20	-0.84
3	505	0.36	0.04	357	-0.39	-0.03	273	-0.01	1.49	446	-0.15	-1.02
2	505	0.20	0.02	357	-0.22	-0.02	272	0.01	1.11	961	-0.04	-1.11
1	505	0.08	0.01	357	-0.09	-0.01	271	0.02	1.74	278	0.01	-1.62
Base		---	---		---	---	270	0.04	1.90	277	-0.01	-1.28

* Time in 0.004 of a second

114

Table 5.9 (Contd)

Low- and High-Frequency Components of Response Maxima in Test Run D1-2

Level	SHEAR FORCES (Kips)						OVERTURNING MOMENTS (Kip-in.)					
	Maximum Positive			Maximum Negative			Maximum Positive			Maximum Negative		
	Time*	First Mode	High Modes	Time*	First Mode	High Modes	Time*	First Mode	High Modes	Time*	First Mode	High Modes
10		---	---		---	---		---	---		---	---
9	285	0.27	0.87	242	-0.31	-0.50	242	2.8	4.5	285	-2.5	-7.8
8	499	0.81	0.81	242	-0.57	-0.81	242	8.1	11.9	499	-11.4	-12.3
7	499	1.12	0.76	242	-0.80	-0.91	242	15.5	20.2	499	-21.8	-19.2
6	497	1.31	0.58	241	-0.91	-0.93	242	24.7	27.4	499	-34.6	-23.2
5	507	1.63	0.50	350	-1.99	-0.11	242	35.3	32.1	498	-48.2	-24.9
4	507	1.80	0.75	344	-1.96	-0.38	350	80.5	3.6	497	-62.1	-25.3
3	507	1.90	0.81	344	-2.16	-0.44	351	103.5	0.6	403	-80.0	-21.1
2	505	1.97	0.75	358	-2.27	-0.57	350	125.9	3.4	507	-103.2	-16.0
1	294	1.92	1.14	356	-2.41	-0.61	352	151.0	4.2	507	-121.3	-20.7
Base	294	1.96	1.54	354	-2.51	-0.77	352	174.8	9.7	407	-129.1	-34.6

Fig. 5.10

Low- and High-Frequency Components of
Response Maxima in Test Run D2-1

	ACCELERATIONS (g)					
	Maximum Positive			Maximum Negative		
Level	Time*	First Mode	High Modes	Time*	First Mode	High Modes
10	654	0.75	0.50	525	-0.64	-1.02
9	653	0.66	0.25	607	-0.75	-0.37
8	651	0.58	0.15	609	-0.66	-0.09
7	487	0.39	0.34	516	-0.31	-0.41
6	487	0.33	0.52	515	-0.23	-0.61
5	487	0.25	0.54	534	-0.13	-0.73
4	646	0.21	0.59	517	-0.14	-0.68
3	524	0.03	0.67	532	-0.00	-0.68
2	524	0.00	0.56	324	-0.14	-0.43
1	483	0.11	0.35	324	-0.13	-0.34
Base	249	0.06	0.34	494	-0.03	-0.38

* Time in 0.004 of a second

Table 5.10 (Contd)

Low- and High-Frequency Components of Response Maxima in Test Run D2-1

| | SHEAR FORCES (Kips) | | | | | | OVERTURNING MOMENTS (Kip-in.) | | | | | |
| | Maximum Positive | | | Maximum Negative | | | Maximum Positive | | | Maximum Negative | | |
Level	Time*	First Mode	High Modes	Time*	First Mode	High Modes	Time*	First Mode	High Modes	Time*	First Mode	High Modes
10		---	---		---	---		---	---		---	---
9	654	0.37	0.25	525	-0.32	-0.51	525	3.0	4.6	654	-3.4	-2.3
8	653	0.71	0.37	525	-0.60	-0.77	525	8.4	11.6	654	-9.9	-5.5
7	653	1.00	0.39	607	-1.13	-0.56	525	16.0	18.6	653	-19.0	-8.9
6	653	1.25	0.33	607	-1.42	-0.45	607	34.8	16.7	653	-30.5	-11.9
5	651	1.44	0.27	608	-1.66	-0.25	607	50.0	19.1	653	-43.9	-13.6
4	651	1.59	0.21	609	-1.83	-0.12	607	66.9	19.1	653	-58.6	-14.2
3	649	1.66	0.25	615	-1.69	-0.43	607	85.1	17.0	653	-74.3	-13.5
2	486	1.41	0.74	617	-1.55	-0.51	608	103.1	15.8	652	-90.0	-13.0
1	486	1.47	0.90	615	-1.74	-0.47	608	121.6	13.8	652	-106.0	-11.9
Base	485	1.55	1.00	615	-1.76	-0.54	608	140.5	11.0	651	-121.5	-11.5

* Time in 0.004 of a second

117

Table 5.11

Low- and High-Frequency Components of
Response Maxima in Test Run D2-2

	ACCELERATIONS (g)					
	Maximum Positive			Maximum Negative		
Level	Time*	First Mode	High Modes	Time*	First Mode	High Modes
10	499	1.12	0.88	339	-0.63	-0.96
9	500	0.97	0.41	241	-0.47	-0.68
8	403	0.71	0.28	350	-0.84	-0.08
7	299	0.55	0.52	349	-0.74	-0.24
6	298	0.45	0.67	331	-0.25	-0.82
5	296	0.35	0.72	330	-0.25	-0.74
4	295	0.27	0.84	445	-0.27	-0.68
3	294	0.15	0.80	444	-0.23	-0.82
2	272	0.01	0.93	445	-0.14	-0.76
1	271	0.03	0.93	225	-0.26	-0.52
Base	270	0.04	0.89	224	-0.29	-0.45

* Time in 0.004 of a second

Table 5.11 (Contd)
Low- and High-Frequency Components of Response Maxima in Test Run D2-2

| | SHEAR FORCES (Kips) | | | | | | OVERTURNING MOMENTS (Kip-in.) | | | | | |
| | Maximum Positive | | | Maximum Negative | | | Maximum Positive | | | Maximum Negative | | |
Level	Time*	First Mode	High Modes	Time*	First Mode	High Modes	Time*	First Mode	High Modes	Time*	First Mode	High Modes
10		---	---		---	---		---	---		---	---
9	499	0.56	0.44	339	-0.32	-0.48	339	2.9	4.3	499	-5.1	-4.0
8	499	1.04	0.63	339	-0.60	-0.75	339	8.4	11.1	499	-14.8	-9.7
7	500	1.46	0.63	252	-1.33	-0.32	339	16.5	18.1	499	-28.1	-15.3
6	501	1.82	0.46	253	-1.65	-0.33	252	40.8	9.5	500	-45.1	-19.0
5	503	2.08	0.25	350	-2.12	-0.10	252	57.9	12.1	500	-64.3	-20.2
4	506	2.18	0.42	350	-2.35	-0.22	252	76.4	13.6	501	-85.8	-19.4
3	507	2.25	0.63	350	-2.54	-0.34	350	108.9	0.9	502	-108.1	-19.0
2	296	1.93	0.92	350	-2.59	-0.54	350	132.8	5.9	503	-129.9	-20.5
1	295	1.97	1.16	350	-2.68	-0.61	350	157.5	11.3	503	-152.1	-21.6
Base	295	2.02	1.31	350	-2.73	-0.65	350	182.5	17.2	503	-173.8	-22.9

* Time in 0.004 of a second

Table 5.12

Low- and High-Frequency Components of
Response Maxima in Test Run D2-3

	ACCELERATIONS (g)					
	Maximum Positive			Maximum Negative		
Level	Time*	First Mode	High Modes	Time*	First Mode	High Modes
10	310	0.41	1.96	276	-0.52	-1.87
9	312	0.43	0.77	276	-0.46	-1.01
8	225	0.63	0.35	369	-0.75	-0.37
7	527	0.23	0.94	379	-0.49	-0.83
6	322	0.27	0.96	287	-0.15	-1.32
5	322	0.15	1.11	286	-0.15	-1.31
4	470	0.23	1.25	285	-0.14	-1.24
3	470	0.28	1.21	264	0.02	-1.25
2	469	0.37	1.08	227	-0.29	-0.97
1	272	0.00	1.39	225	-0.38	-1.12
Base	270	0.07	1.37	225	-0.44	-1.29

* Time in 0.004 of a second

Table 5.12   (Contd)

Low- and High-Frequency Components of Response Maxima in Test Run D2-3

| | SHEAR FORCES (Kips) | | | | | | OVERTURNING MOMENTS (Kip-in.) | | | | | |
| | Maximum Positive | | | Maximum Negative | | | Maximum Positive | | | Maximum Negative | | |
Level	Time*	First Mode	High Modes	Time*	First Mode	High Modes	Time*	First Mode	High Modes	Time*	First Mode	High Modes
10		---	---		---	.---		---	---		---	---
9	310	0.25	0.98	276	-0.26	-0.94	276	2.4	8.4	310	-1.9	-8.9
8	311	0.42	1.32	276	-0.49	-1.44	276	6.9	21.5	311	-6.0	-20.6
7	311	0.60	1.29	275	-0.73	-1.50	276	13.4	35.3	311	-11.6	-32.3
6	227	1.35	0.50	368	-1.67	-0.62	275	22.9	45.3	311	-18.8	-40.3
5	224	1.64	0.51	369	-1.88	-0.61	275	33.2	51.5	311	-27.4	-43.6
4	224	1.70	0.68	367	-2.02	-0.46	369	79.2	23.7	226	-65.4	-16.7
3	222	1.77	0.82	379	-1.70	-0.96	369	98.7	24.2	224	-85.4	-17.4
2	221	1.70	0.94	264	-1.66	-1.13	369	118.6	21.1	221	-106.0	-18.5
1	321	1.22	1.51	264	-1.62	-1.76	369	138.1	14.8	221	-120.8	-28.1
Base	320	1.14	1.60	264	-1.55	-2.41	610	165.3	7.9	221	-133.9	-37.6

* Time in 0.004 of a second

121

Table 5.13

Low- and High-Frequency Components of Response Maxima in Test Run M1-1

| | DISPLACEMENTS (in.) | | | | | | ACCELERATIONS (g) | | | | | |
| | Maximum Positive | | | Maximum Negative | | | Maximum Positive | | | Maximum Negative | | |
Level	Time*	First Mode	High Modes	Time*	First Mode	High Modes	Time*	First Mode	High Modes	Time*	First Mode	High Modes
10	494	1.97	0.08	343	-1.48	0.01	305	0.53	1.05	337	-0.71	-1.13
9	494	1.83	0.09	347	-1.38	0.07	498	0.99	0.25	338	-0.71	-0.52
8	494	1.62	0.06	346	-1.22	0.02	493	0.88	0.13	249	-0.77	-0.10
7	495	1.39	0.04	346	-1.02	0.00	295	0.55	0.56	346	-0.69	-0.30
6	495	1.15	0.03	346	-0.86	-0.02	295	0.46	0.85	347	-0.62	-0.55
5	493	0.89	0.05	346	-0.66	-0.03	295	0.36	0.90	347	-0.52	-0.71
4	493	0.67	0.03	346	-0.51	-0.04	295	0.28	0.83	327	-0.29	-0.91
3	493	0.46	0.03	346	-0.35	-0.04	274	0.04	1.05	326	-0.27	-0.83
2	493	0.23	0.01	346	-0.17	-0.02	273	0.03	0.96	327	-0.28	-0.52
1	493	0.13	0.00	346	-0.09	-0.01	272	0.03	0.91	261	0.12	-0.81
Base	---	---		---	---		270	0.05	0.86	509	-0.09	-0.62

* Time in 0.004 of a second

Table 5.13 (Contd)

Low- and High-Frequency Components of Response Maxima in Test Run M1-1

	SHEAR FORCES (Kips)						OVERTURNING MOMENTS (Kip-in.)					
	Maximum Positive			Maximum Negative			Maximum Positive			Maximum Negative		
Level	Time*	First Mode	High Modes	Time*	First Mode	High Modes	Time*	First Mode	High Modes	Time*	First Mode	High Modes
10		---	---		---	---		---	---		---	---
9	305	0.26	0.52	337	-0.36	-0.56	337	3.3	5.1	305	-2.4	-4.7
8	498	1.04	0.35	337	-0.70	-0.82	337	9.7	12.5	498	-14.5	-5.3
7	498	1.47	0.37	338	-1.06	-0.78	337	19.1	19.7	498	-28.1	-8.6
6	497	1.85	0.29	249	-1.66	-0.34	338	32.5	23.7	498	-45.1	-11.1
5	493	2.18	0.25	249	-1.91	-0.20	338	47.7	26.5	497	-65.6	-12.0
4	493	2.41	0.31	348	-2.18	-0.17	250	78.5	13.1	497	-87.6	-12.2
3	295	1.87	1.10	347	-2.40	-0.49	249	97.8	11.7	496	-112.1	-9.8
2	295	1.98	1.44	346	-2.59	-0.75	249	118.4	7.3	493	-137.4	-11.6
1	295	2.05	1.69	346	-2.73	-0.96	348	148.5	2.8	493	-162.6	-12.3
Base	295	2.09	1.81	346	-2.89	-1.03	346	174.1	11.0	493	-188.1	-11.0

* Time in 0.004 of a second

Table 5.14

Low- and High-Frequency Components of
Response Maxima in Test Run D3-1

	ACCELERATIONS (g)					
	Maximum Positive			Maximum Negative		
Level	Time*	First Mode	High Modes	Time*	First Mode	High Modes
10	1131	0.34	0.86	1099	-0.44	-0.82
9	840	0.63	0.14	805	-0.66	-0.18
8	928	0.34	0.27	800	-0.59	-0.16
7	1141	0.30	0.35	800	-0.50	-0.26
6	1141	0.24	0.48	1093	-0.19	-0.53
5	924	0.16	0.55	1091	-0.12	-0.65
4	924	0.11	0.65	1090	-0.09	-0.75
3	923	0.06	0.69	1090	-0.06	-0.76
2	1120	0.04	0.50	1120	-0.04	-.054
1	1008	-0.07	0.52	778	-0.11	-0.35
Base	751	0.15	0.29	998	-0.10	-0.35

* Time in 0.004 of a second

Table 5.14 (Contd)

Low- and High-Frequency Components of Response Maxima in Test Run D3-1

| | SHEAR FORCES (Kips) | | | | | | OVERTURNING MOMENTS (Kip-in.) | | | | | |
| | Maximum Positive | | | Maximum Negative | | | Maximum Positive | | | Maximum Negative | | |
Level	Time*	First Mode	High Modes	Time*	First Mode	High Modes	Time*	First Mode	High Modes	Time*	First Mode	High Modes
10		---	---		---	---		---	---		---	---
9	1131	0.17	0.43	1099	-0.22	-0.41	1099	2.0	3.7	1131	-1.6	-3.9
8	1131	0.32	0.64	1099	-0.41	-0.59	1099	5.7	9.1	1131	-4.5	-9.7
7	840	0.94	0.21	805	-0.99	-0.27	1099	11.0	14.1	1131	-8.7	-15.4
6	840	1.17	0.13	802	-1.28	-0.24	805	30.3	7.9	840	-28.5	-6.5
5	842	1.36	-0.01	802	-1.48	-0.31	803	44.6	9.0	840	-40.9	-6.4
4	845	1.46	0.08	800	-1.63	-0.38	802	59.8	11.4	841	-55.0	-4.8
3	846	1.52	0.21	800	-1.75	-0.43	802	76.0	14.7	841	-69.8	-2.8
2	846	1.57	0.32	800	-1.82	-0.43	802	92.5	17.7	842	-85.0	-1.3
1	847	1.55	0.43	800	-1.86	-0.39	802	109.4	20.2	843	-99.9	-1.3
Base	847	1.56	0.49	796	-1.79	-0.47	802	126.2	21.6	844	-113.9	-3.4

* Time in 0.004 of a second

125

Table 5.15

Low- and High-Frequency Components of
Response Maxima in Test Run D3-2

	ACCELERATIONS (g)					
	Maximum Positive			Maximum Negative		
Level	Time*	First Mode	High Modes	Time*	First Mode	High Modes
10	1072	0.57	1.19	1103	-0.40	-1.21
9	1072	0.48	0.59	472	-0.60	-0.37
8	1495	0.61	0.30	1533	-0.45	-0.32
7	1083	0.16	0.84	1026	-0.17	-0.74
6	1083	0.10	1.09	1025	-0.12	-0.98
5	1082	0.04	1.20	1093	0.00	-1.11
4	1081	-0.03	1.27	1093	0.00	-1.19
3	1080	-0.09	1.28	463	-0.34	-0.67
2	1080	-0.15	1.11	464	-0.30	-0.49
1	753	0.24	0.71	1068	-0.16	-0.71
Base	752	0.28	0.72	1067	-0.18	-0.89

* Time in 0.004 of a second

Table 5.15 (Contd)

Low- and High-Frequency Components of Response Maxima in Test Run D3-2

| | SHEAR FORCES (Kips) | | | | | | OVERTURNING MOMENTS (Kip-in.) | | | | | |
| | Maximum Positive | | | Maximum Negative | | | Maximum Positive | | | Maximum Negative | | |
Level	Time*	First Mode	High Modes	Time*	First Mode	High Modes	Time*	First Mode	High Modes	Time*	First Mode	High Modes
10		---	---		---	---		---	---		---	---
9	1072	0.29	0.60	1103	-0.20	-0.61	1103	1.8	5.5	1072	-2.6	-5.4
8	1072	0.53	0.89	1103	-0.37	-0.88	1103	5.2	13.4	1072	-7.5	-13.4
7	1071	0.73	0.89	472	-0.90	-0.55	1102	9.3	21.8	1072	-14.2	-21.5
6	521	1.69	0.09	472	-1.14	-0.47	472	27.3	16.3	1072	-22.2	-27.3
5	519	2.10	0.00	565	-1.39	-0.34	472	39.9	18.7	525	-53.9	-8.0
4	519	2.34	0.15	566	-1.49	-0.49	472	54.1	18.7	522	-80.0	-3.4
3	518	2.51	0.30	462	-1.64	-0.68	564	72.7	14.8	522	-101.8	-5.1
2	518	2.68	0.36	462	-1.81	-1.00	565	86.6	21.2	519	-132.0	-0.6
1	518	2.76	0.43	462	-1.96	-1.22	566	99.8	29.2	519	-157.0	-4.7
Base	515	2.92	0.41	462	-2.11	-1.34	566	114.4	35.8	519	-182.1	-8.4

127

* Time in 0.004 of a second

Table 6.1

Characteristic Values of The Base Acceleration Corresponding to First Runs

Test Run	Peak Acceleration (g)	Maximum * "Low-Frequency" Acceleration (g)	Spectrum Intensity (in.)				
			SI_0	SI_2	SI_5	SI_{10}	SI_{20}
D1-1	0.50	0.19	19.1	12.2	9.9	8.1	6.7
D2-1	0.41	0.19	18.7	12.0	9.6	7.9	6.5
D3-1	0.46	0.17	19.5	12.6	10.2	8.4	6.8
M1-1	0.91	0.36	36.9	23.4	18.9	15.5	12.9

* Maximum value corresponding to the content between 0-5 Hz

Table 6.2   Modal Shapes and Characteristic Values
            Calculated for Model of Test Structure D
            Assuming $\mu_b = \mu_c = 1.5$

Level	First Mode	Second Mode	Third Mode
10	1.000	1.000	1.000
9	0.893	0.482	-0.054
8	0.779	-0.032	-0.837
7	0.657	-0.468	-1.000
6	0.532	-0.740	-0.500
5	0.408	-0.831	0.246
4	0.289	-0.776	0.858
3	0.180	-0.598	1.070
2	0.090	-0.351	0.825
1	0.026	-0.116	0.328
Natural Frequency (Hz)	2.6	11	24
Damping Factor	5.7%	5.7%	5.7%
Participation Factor for the Base Shear	69.1%	15.6%	6.6%

Table 6.3   Modal Shapes and Characteristic Values
            Calculated for Model of Test Structure M
            Assuming $\mu_b = 2$ and $\mu_c = 4$

Level	First Mode	Second Mode	Third Mode
10	1.000	1.000	1.000
9	0.900	0.539	0.077
8	0.797	0.080	-0.664
7	0.688	-0.333	-0.969
6	0.577	-0.648	-0.739
5	0.463	-0.828	-0.126
4	0.350	-0.858	0.563
3	0.241	-0.742	1.006
2	0.139	-0.514	1.012
1	0.049	-0.231	0.626
Natural Frequency (Hz)	2.5	12	29
Damping Factor	8.7%	5.4%	4.0%
Participation Factor for the Base Shear	73.8%	15.6%	5.6%

Table 6.4   Modal Shapes and Characteristic Values
Calculated for Model of Test Structure M
Assuming $\mu_b = \mu_c = 2$

Level	First Mode	Second Mode	Third Mode
10	1.000	1.000	1.000
9	0.893	0.513	0.035
8	0.780	0.021	-0.732
7	0.661	-0.418	-0.993
6	0.539	-0.738	-0.653
5	0.415	-0.893	0.064
4	0.296	-0.872	0.764
3	0.186	-0.693	1.085
2	0.094	-0.418	0.891
1	0.027	-0.143	0.370
Natural Frequency (Hz)	2.5	10	24
Damping Factor	7.9%	7.9%	7.9%
Participation Factor for the Base Shear	69.6%	16.5%	5.9%

132
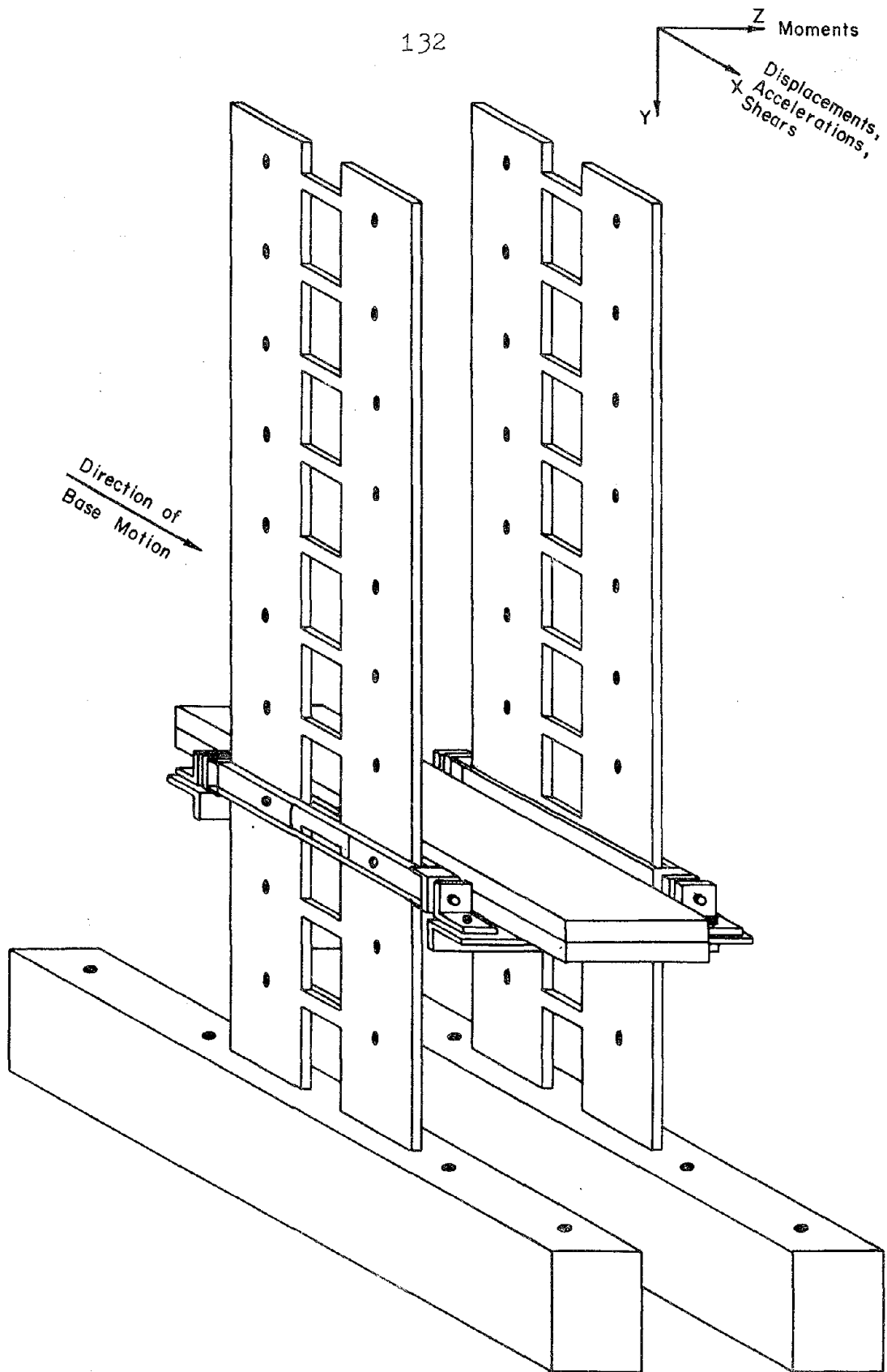
Fig. 2.1   Test Structure

$$\theta = \frac{M}{EI} \times \frac{\ell^2(1+\alpha)}{6(\ell+2a)}$$
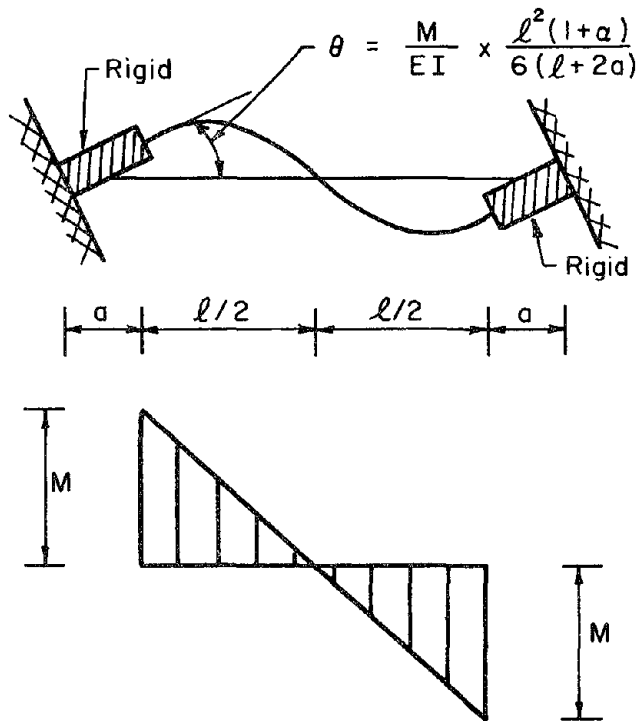
Where α = Shear-Deformation Parameter = $\dfrac{12EI}{GA_s \ell^2}$

(See Przemieniecki, 1968, Page 70)

$M-\theta$, Uncracked Section

$M-\phi$, "Actual" Stiffness

$(EI)_a \dfrac{6(\ell+2a)}{\ell^2(1+\alpha)}$

$(EI)_s \dfrac{6(\ell+2a)}{\ell^2(1+\alpha)} = \dfrac{(EI)_a}{\mu} \dfrac{6(\ell+2a)}{\ell^2(1+\alpha)}$
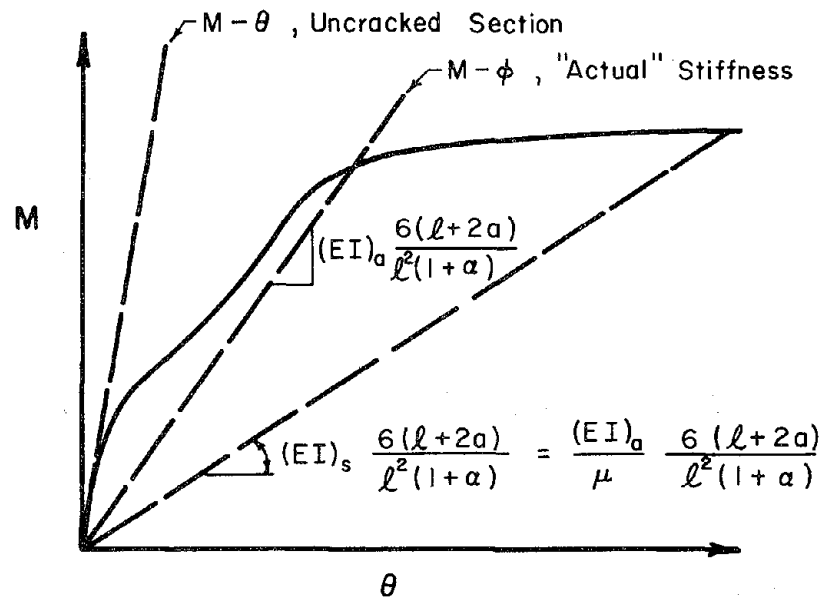
Fig. 2.2   Interpretation of Damage Ratio
and Stiffness of Actual Structure

133

(a)	(b)	(c)	(d)
Cross Section	Transformed Section	Strain and Stress Distributions	Forces
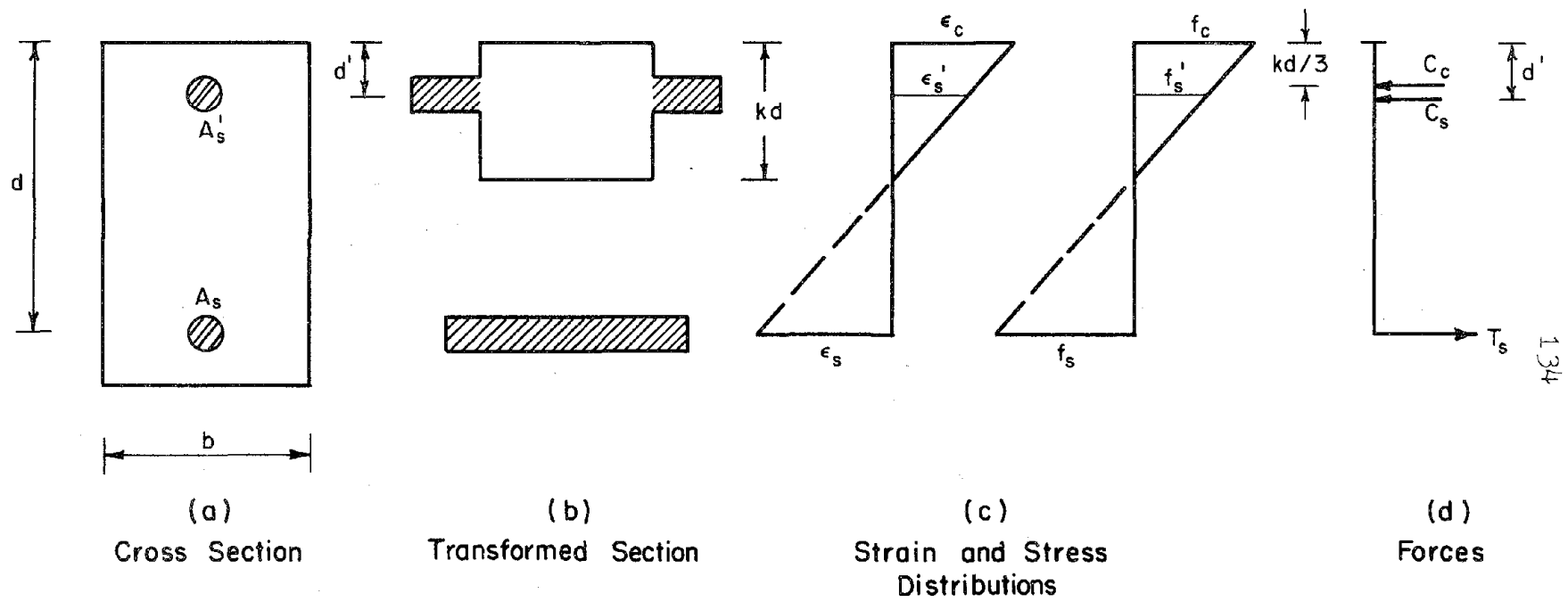
Fig. 2.3 Cracked Transformed Section

(a)

2ℓ = Span of Connecting Beam

ℓ_a = Anchorage Length

ϕ_y = Yield Curvature

ϵ_y = Yield Strain in Steel

(b)

(c)
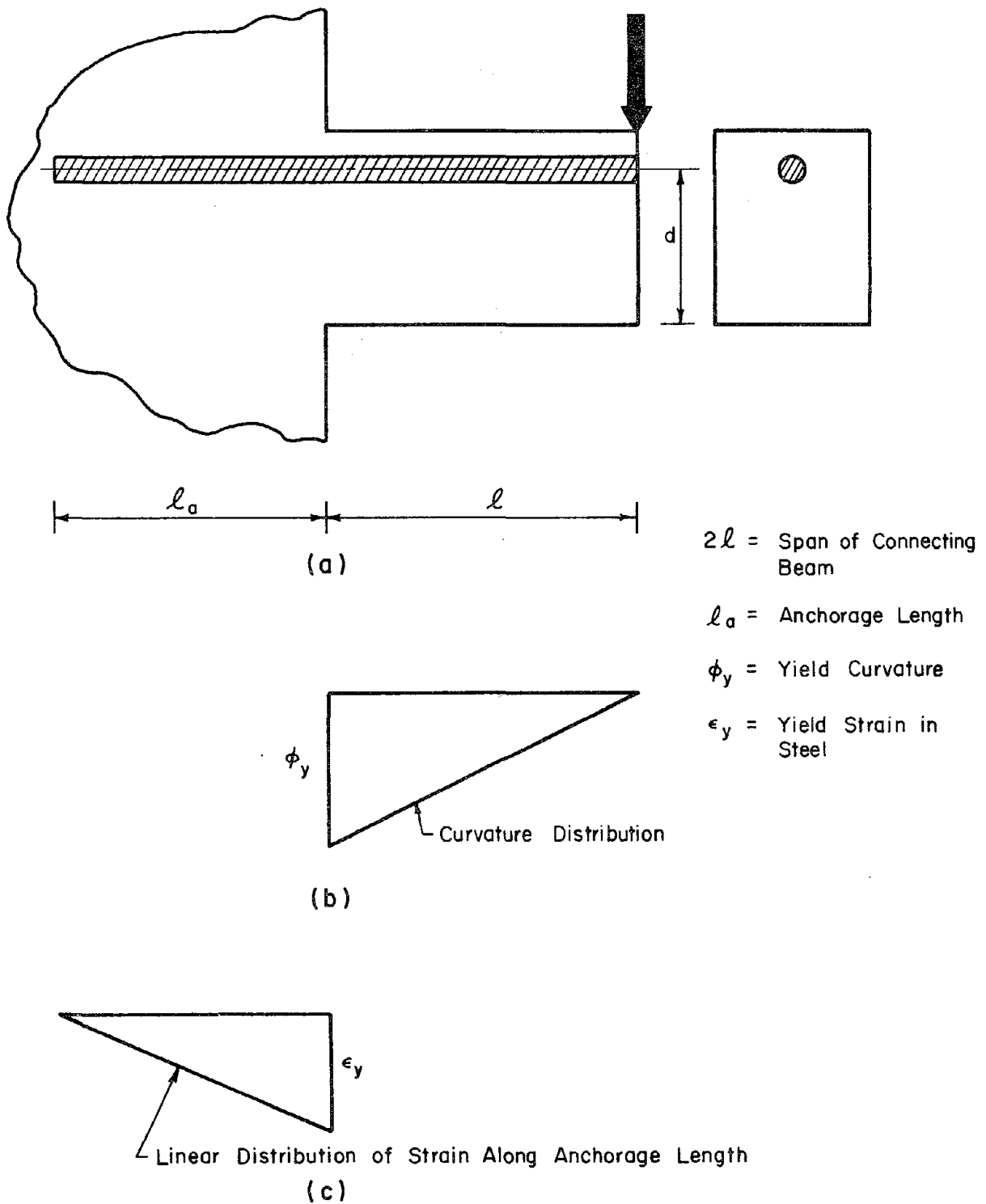
Fig. 2.4   Curvature and Strain Distribution in Connecting Beam
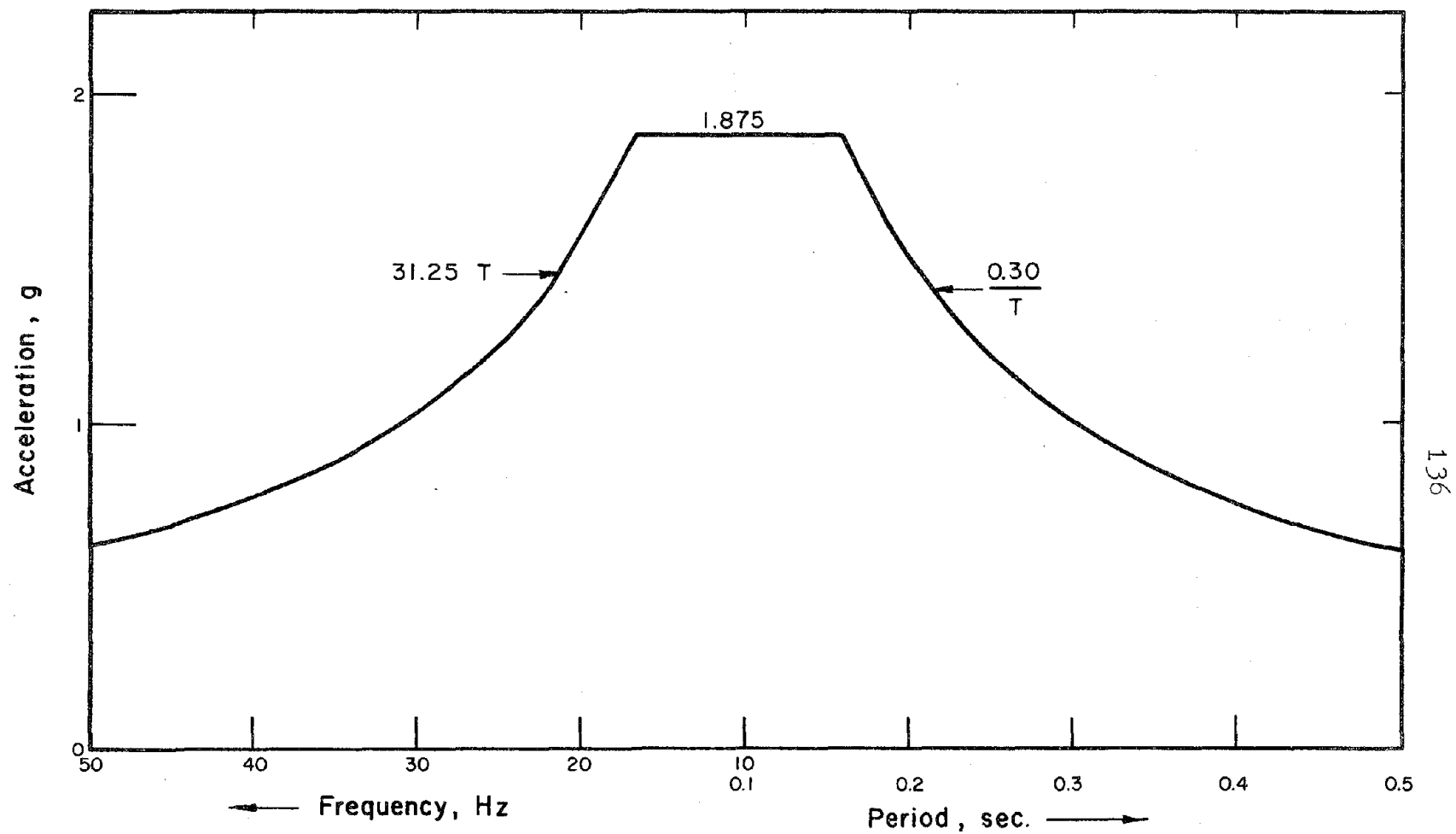
Fig. 2.5 Design Response Spectrum for
Standard Structure (Type D)
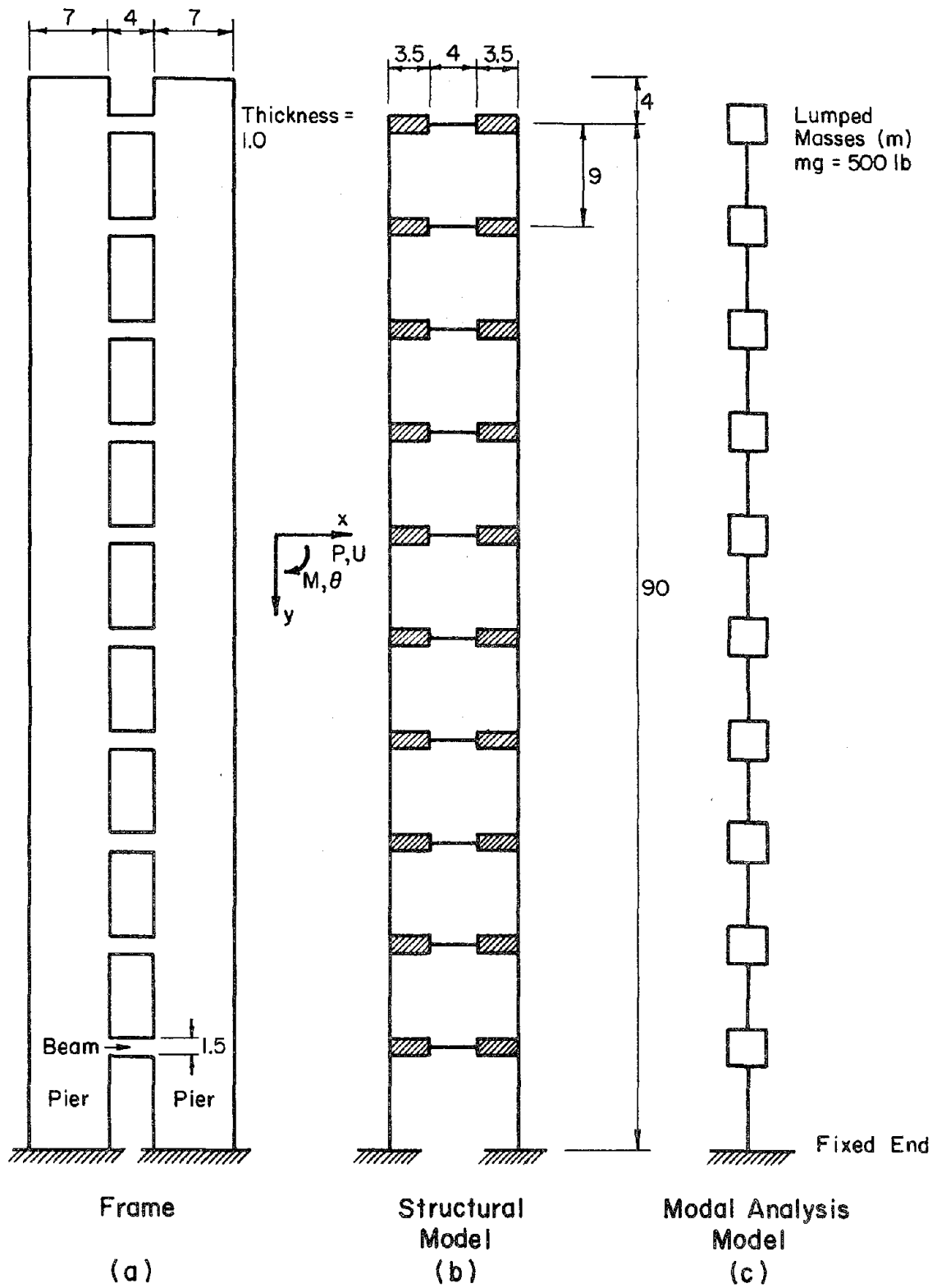
Fig. 2.6 Models Used for Design Calculations

Level
10 —
9 —
8 —
7 —
6 —
5 —
4 —
3 —
2 —
I —

Base —

(a) First Mode

(b) Second Mode

(c) Third Mode

138
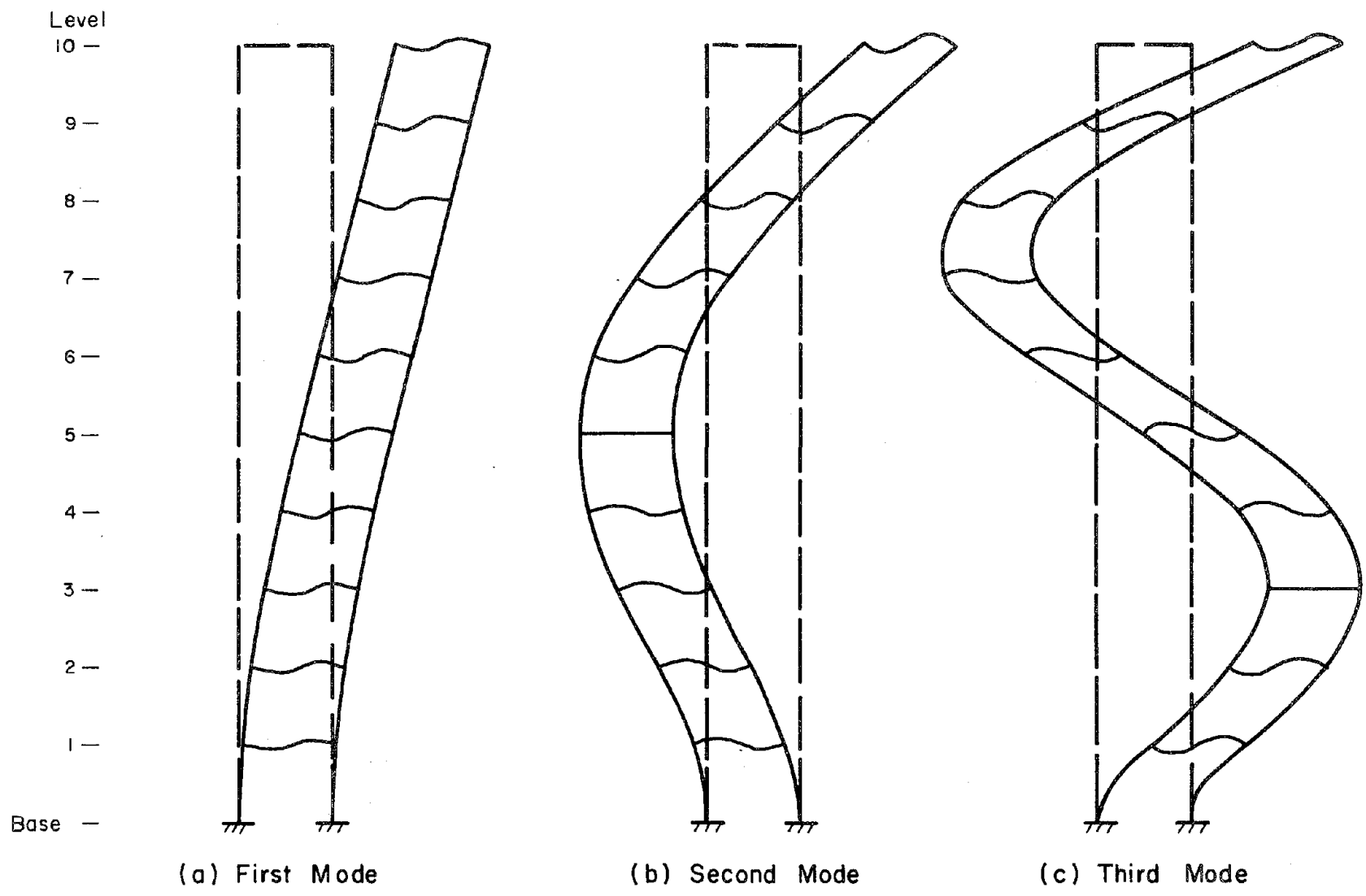
Fig. 2.7   Modal Shapes Used for Design

Level

0.432	10
0.384	9
0.322	8
0.278	7
0.223	6
0.170	5
0.119	4
0.073	3
0.036	2
0.010	1

Shear forces: 0.43, 0.82, 1.15, 1.43, 1.65, 1.82, 1.94, 2.01, 2.05, 2.06

0 1 2

Overturning Moments: 3.9, 11.2, 21.6, 34.4, 49.2, 65.6, 83.1, 101.2, 119.6, 138.1

0   50   100   150

Displacements: 1.10, 0.97, 0.84, 0.71, 0.57, 0.43, 0.30, 0.19, 0.09, 0.03

(a) Lateral Forces (Kips)   (b) Shear Forces (Kips)   (c) Overturning Moments (Kip - in.)   (d) Displacements (in.)
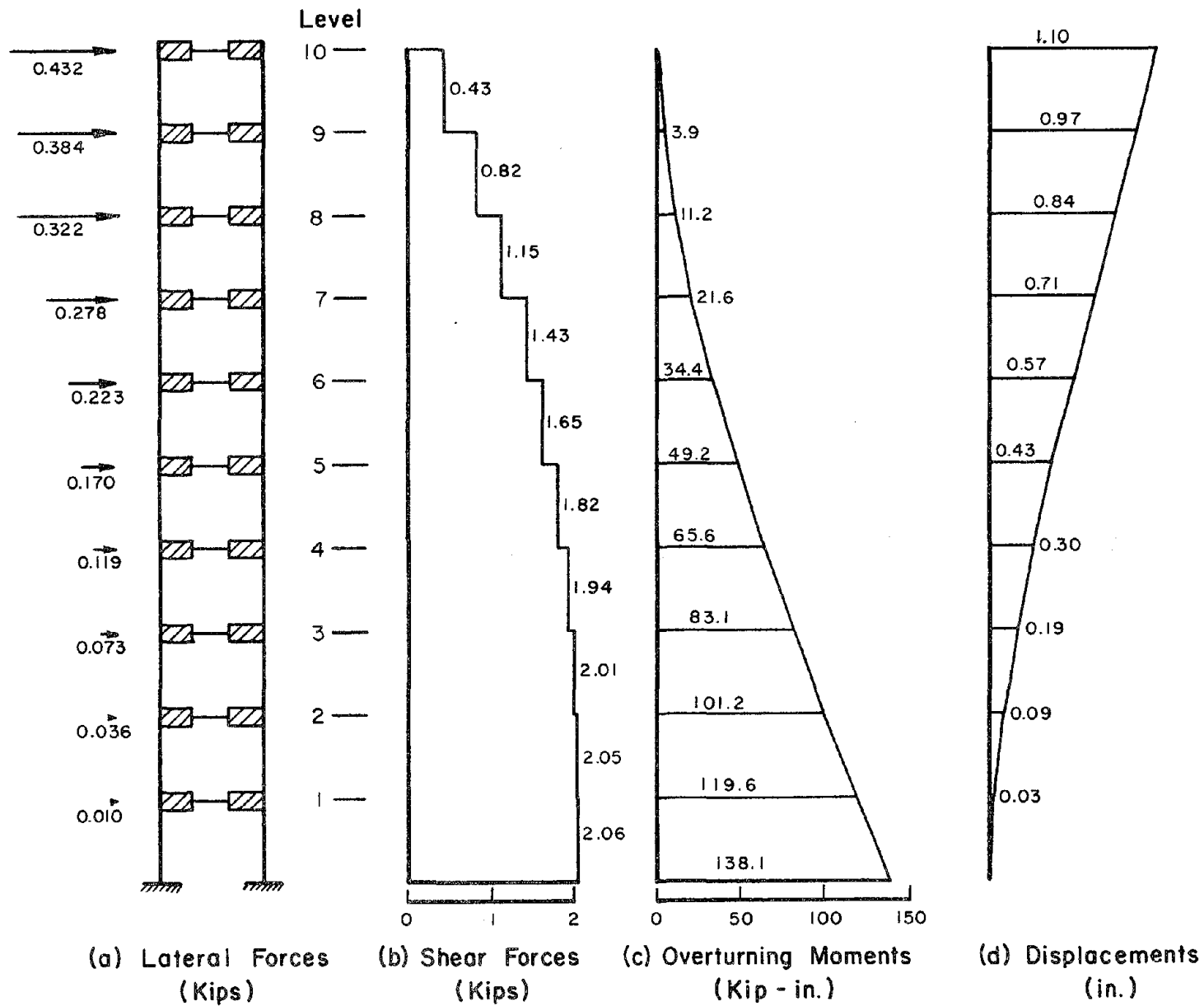
Fig. 2.8   Lateral Forces, Shears, Moments and Displacements
Used for Design (First Mode)

(a) Lateral Forces
(Kips)

(b) Shear Forces
(Kips)

(c) Overturning Moments
(Kip — in.)
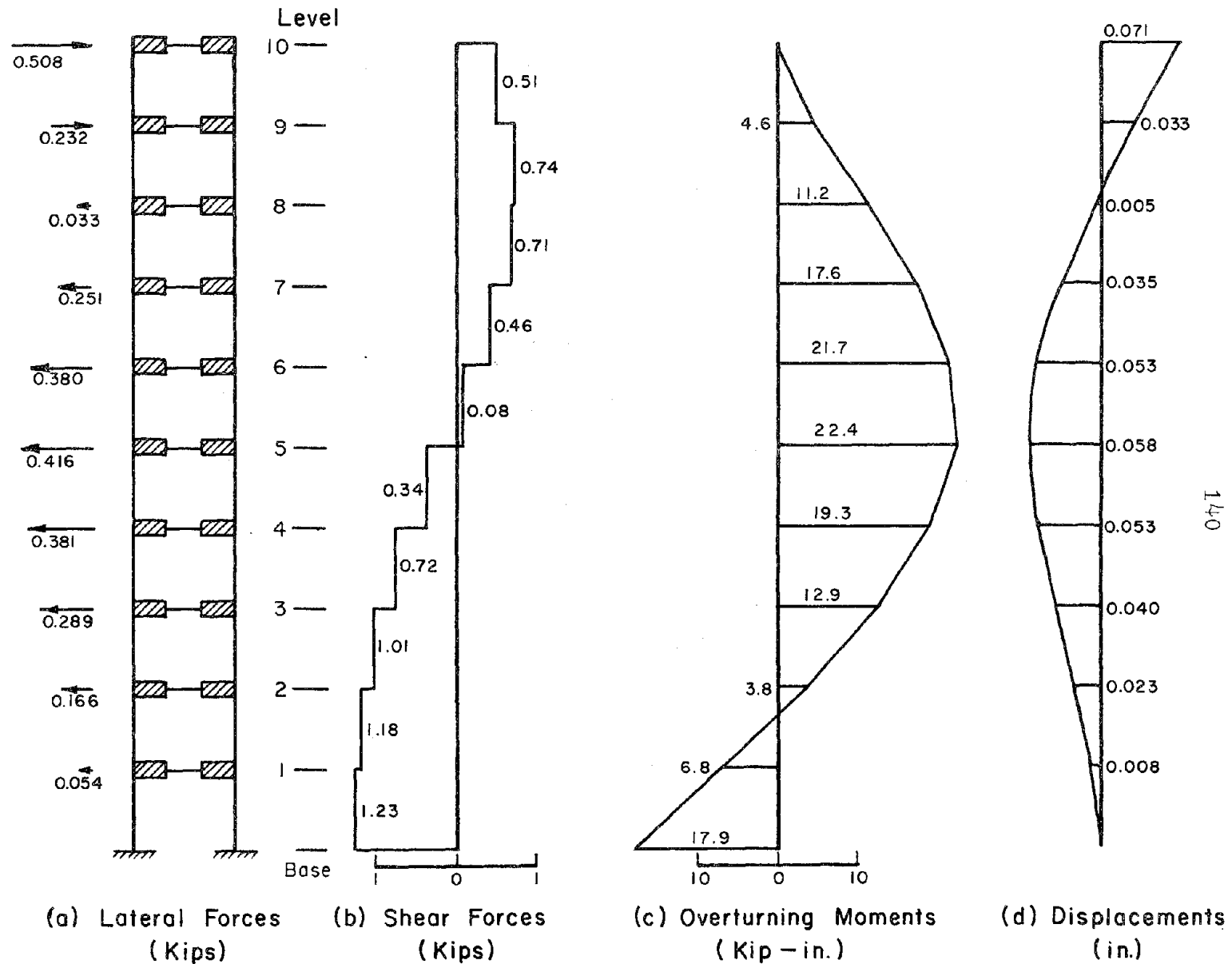
(d) Displacements
(in.)

Fig. 2.9 Lateral Forces, Shears, Moments and Displacements
Used for Design (Second Mode)

140
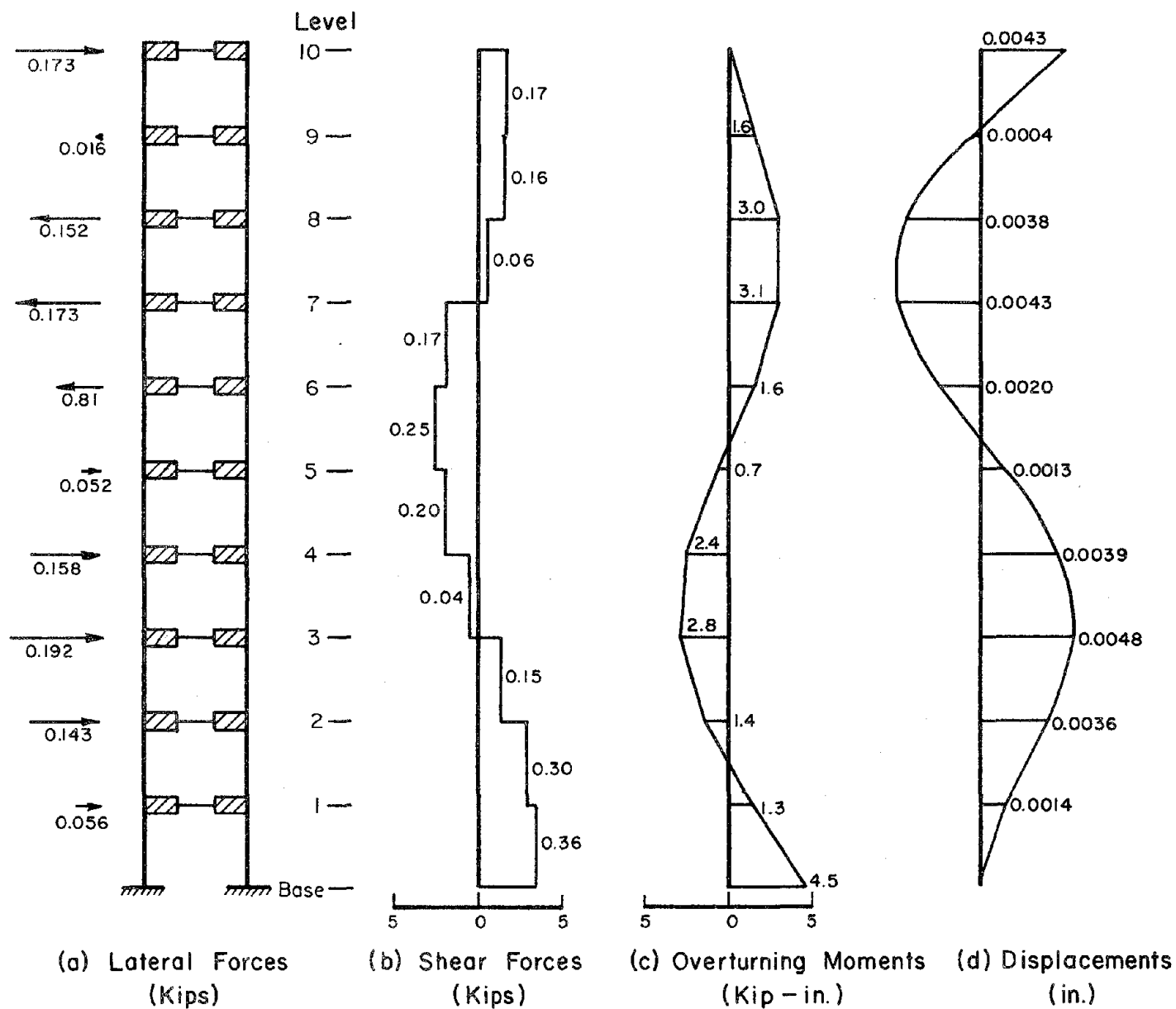
Fig. 2.10   Lateral Forces, Shears, Moments and Displacements
Used for Design (Third Mode)

141

Level

10

9

8

7

6

5

4

3

2

1

Base

(Forces in Kips)

0.94

1.56

1.85

1.88

1.73

2.16

2.66

3.02

3.22

3.29

0   1   2   3

(a) Absolute Sum Of First
And Second Modes

0.69

1.11

1.35

1.51

1.67

1.86

2.07

2.25

2.38

2.42

0   1   2   3

(b) RSS (Three Modes)

$$\frac{RSS + \{|1| + |2|\}}{2 \times RSS} = 1.175$$

Design Base Shear $= 1.175 \times 2.42$
$= 2.85$ Kips

142
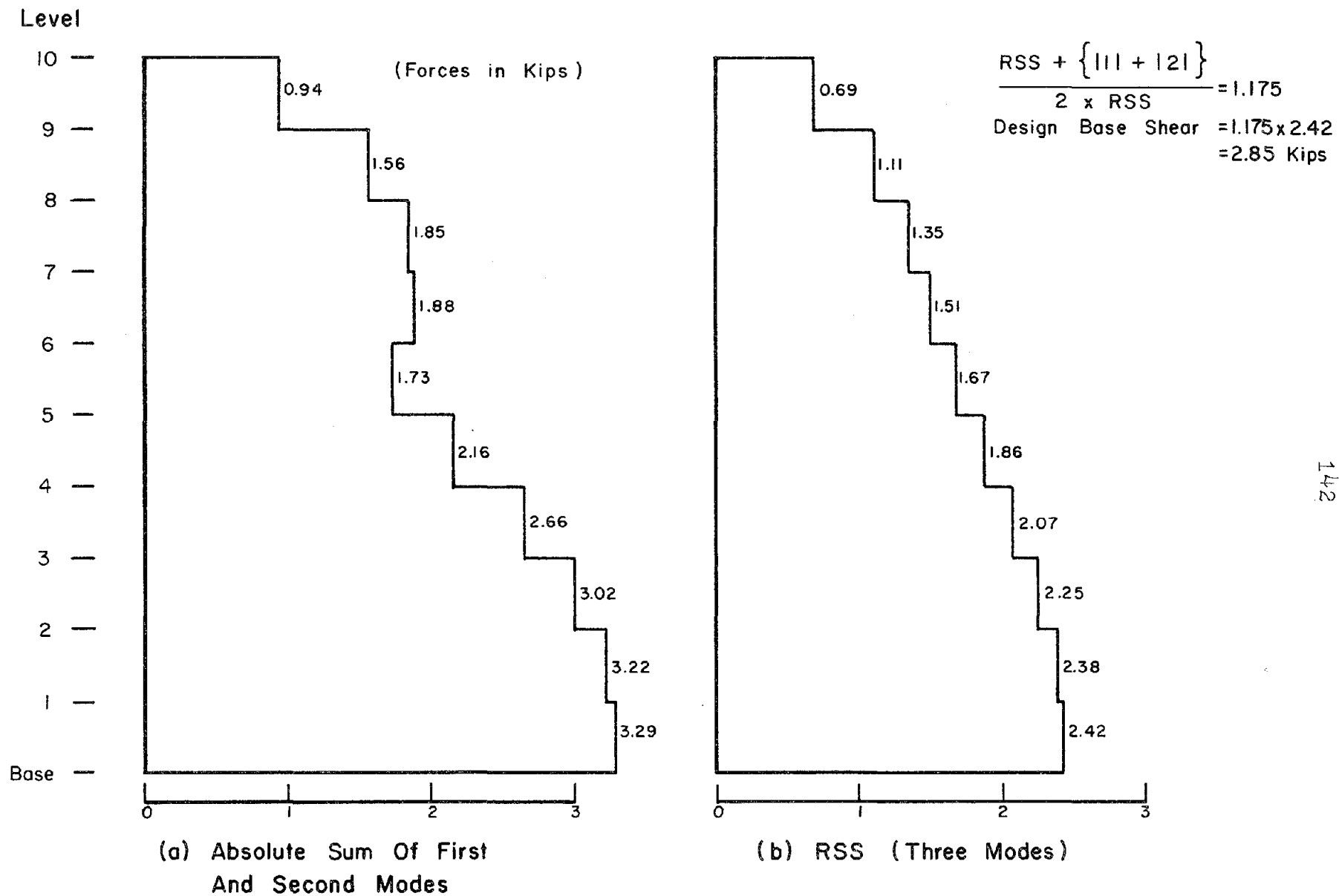
Fig. 2.11   Shear Forces Used for Design

Level

10 —	3.0
9 —	-4.4, -1.1
8 —	-4.3, -0.7
7 —	-3.0, 0.9
6 —	-0.7, 3.4
5 —	2.7, 6.8
4 —	7.1, 11.0
3 —	12.5, 15.9
2 —	19.0, 21.6
1 —	26.7, 28.2
Base —	36.0

(Moments In Kips − in.)

0   10   20   30   40

(a) First Mode

1.2	
-1.1, 0.1	
-3.3, -2.2	
-5.4, -4.7	
-6.7, -6.5	
-7.0, -6.8	
-5.9, -5.4	
-3.28, -2.6	
0.6, 1.3	
5.4, 5.9	
10.9	

0   10

(b) Second Mode
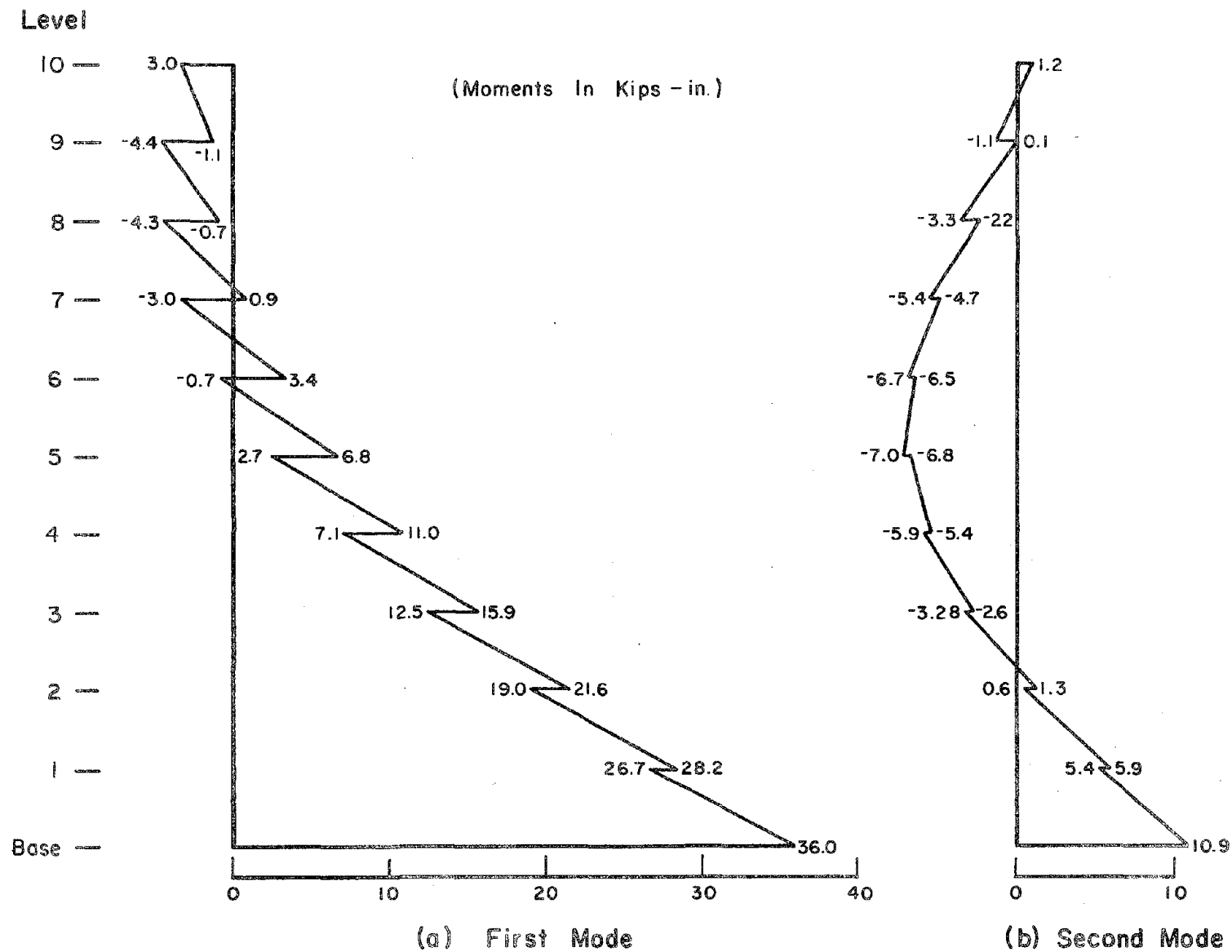
Fig. 2.12   Moments Used for Design of Piers

143
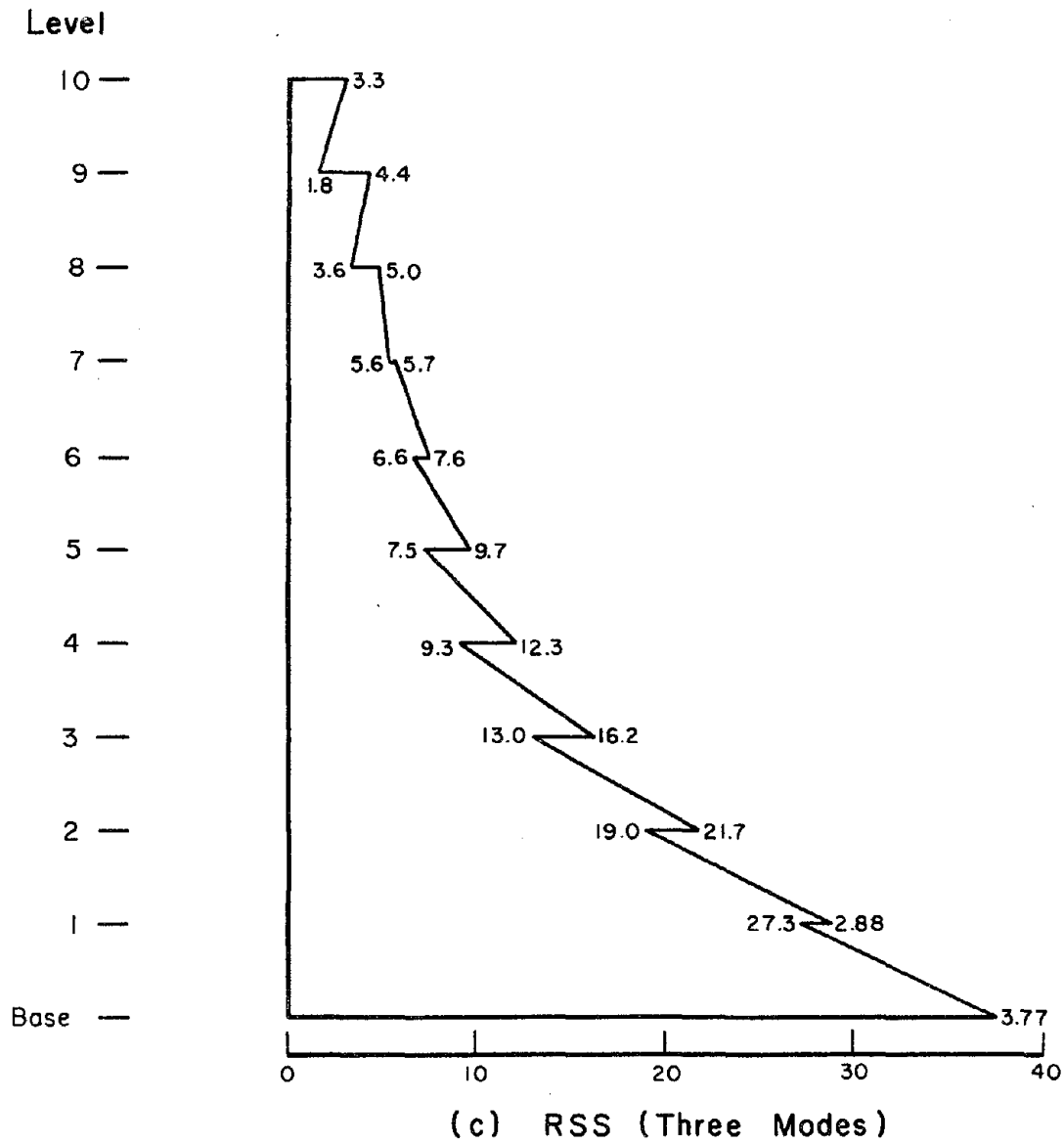
(c) RSS (Three Modes)

Fig. 2.12 (Cont.) Moments Used for Design of Piers
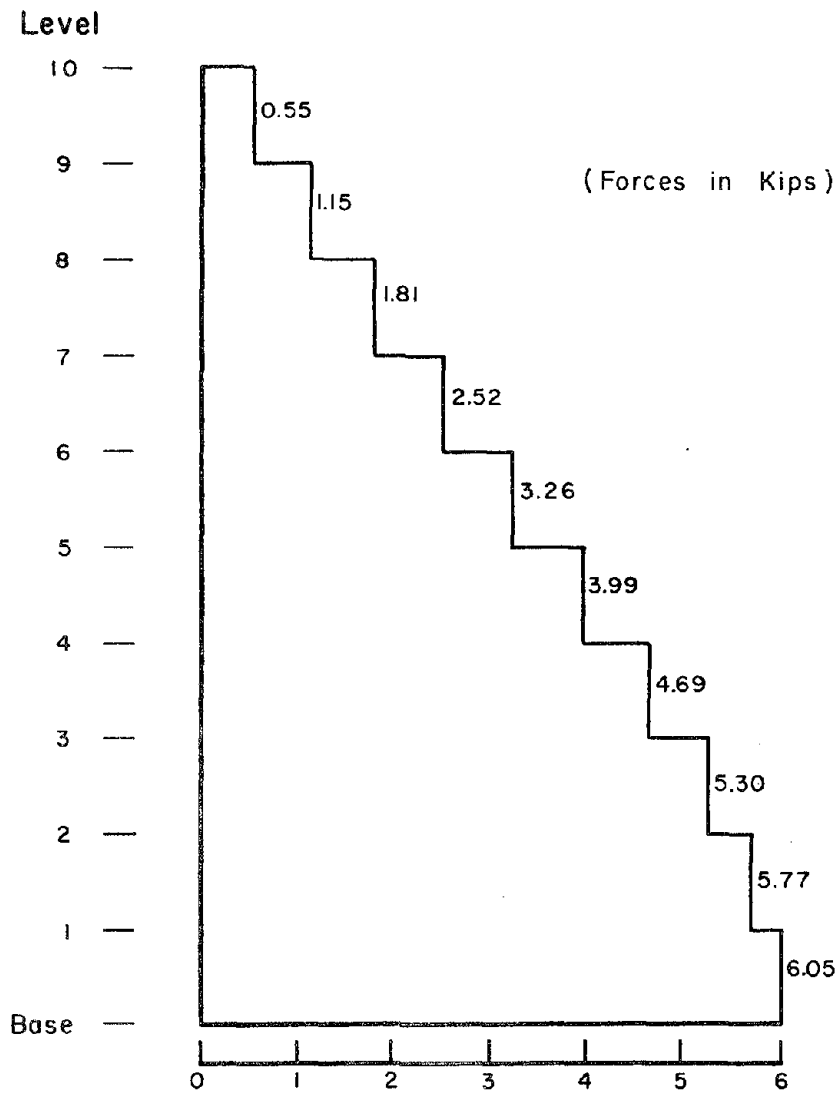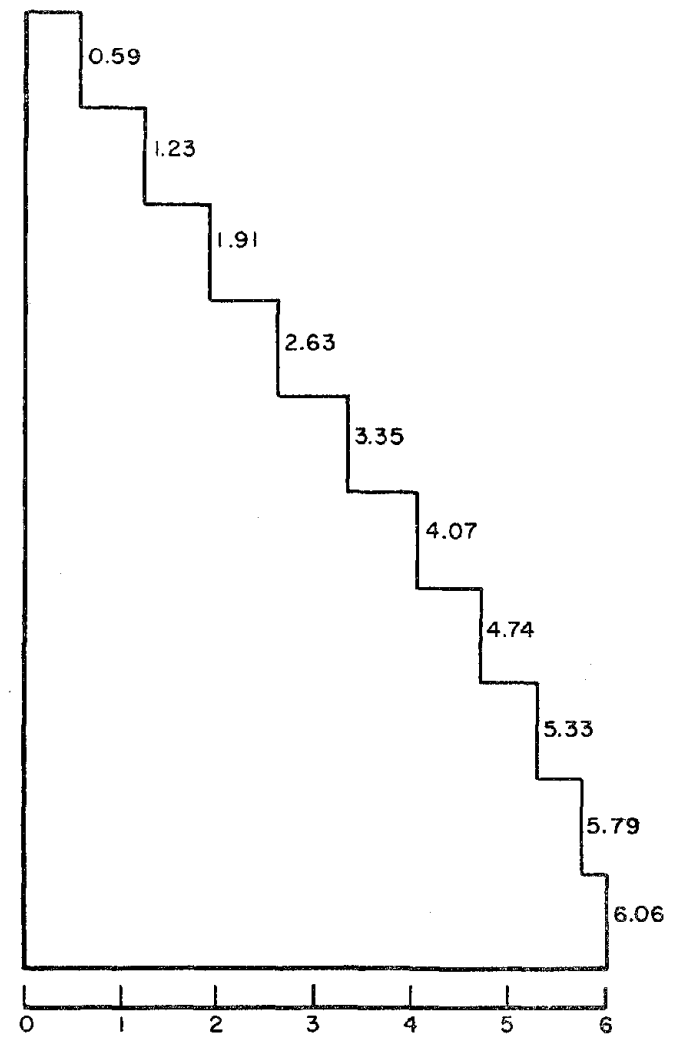
Fig. 2.13 Axial Forces Used for Design of Piers
(Not Including Dead Loads)

145
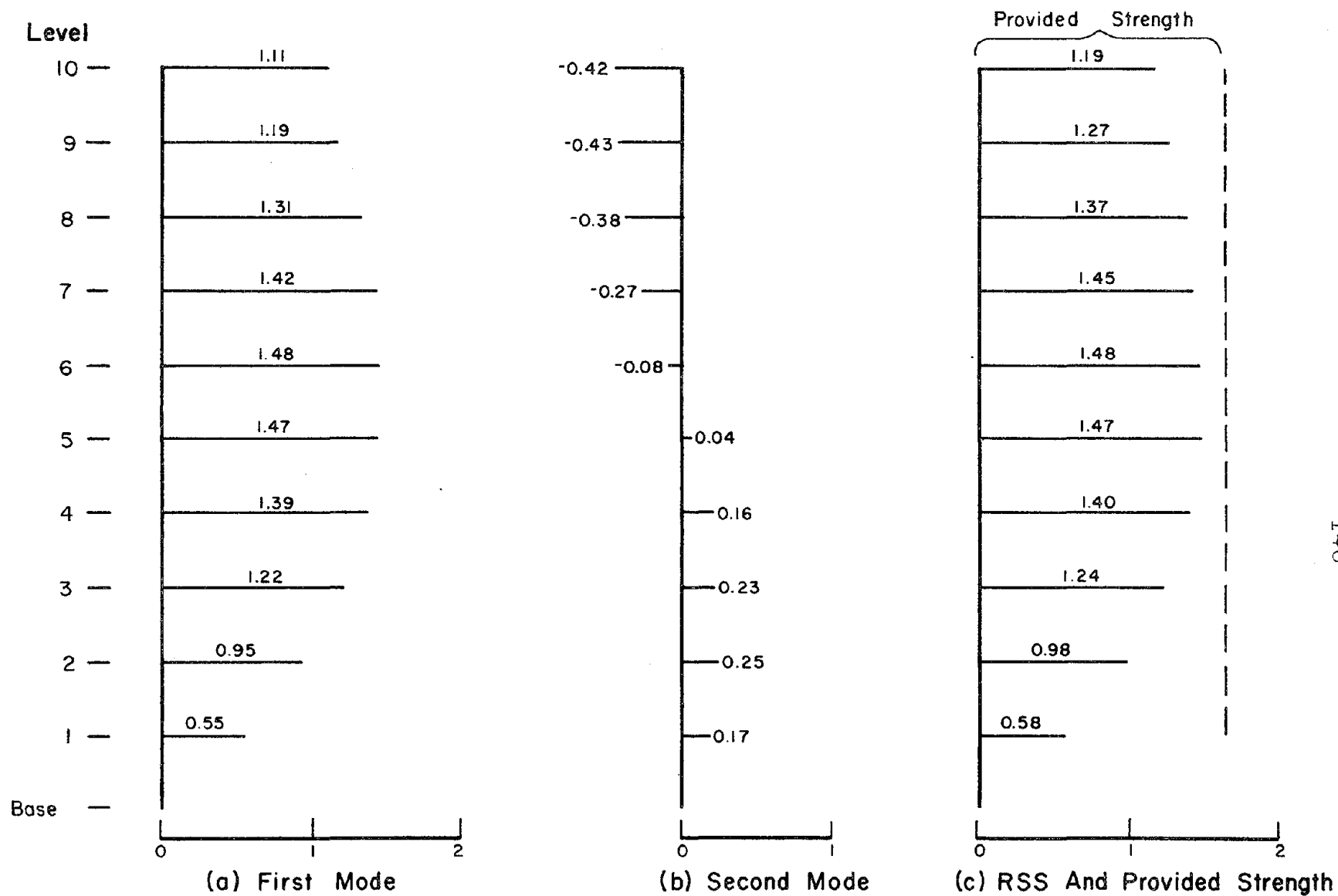
Fig. 2.14 End Moments of Connecting Beams Used for Design
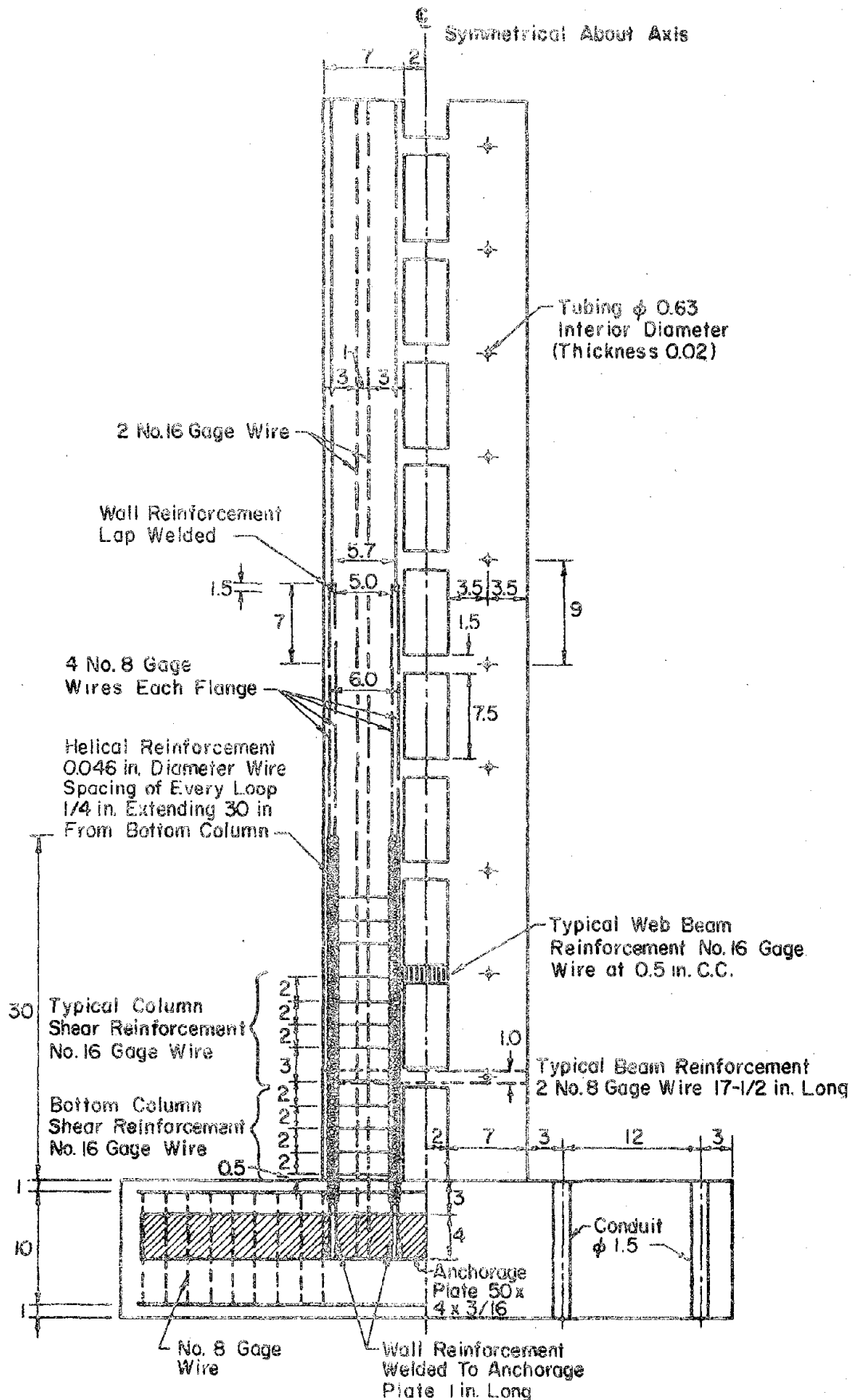
Fig. 2.15   Reinforcement in Test Structure D
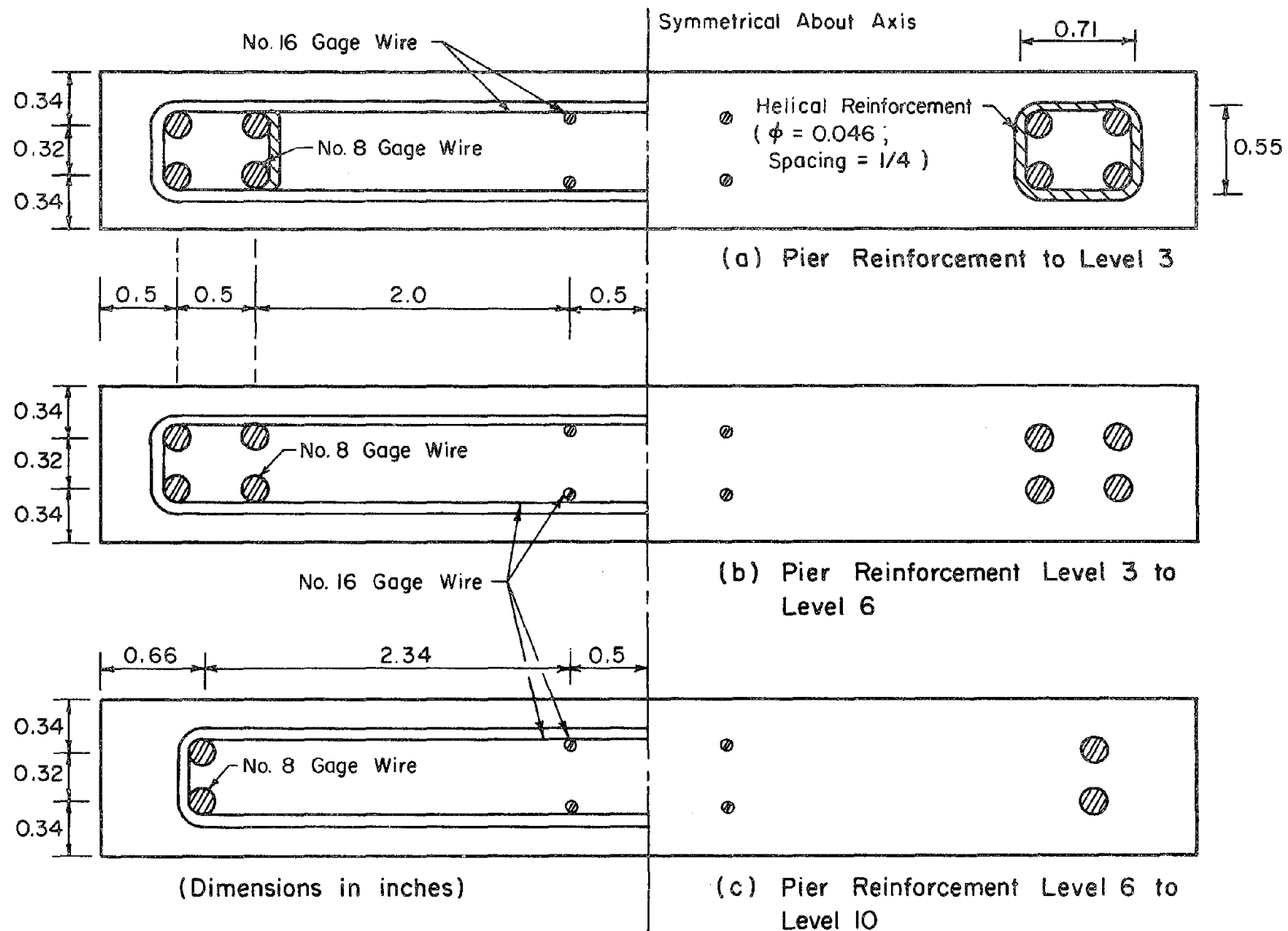
Fig. 2.16 Cross-Sectional Properties of Piers
(Structure D)
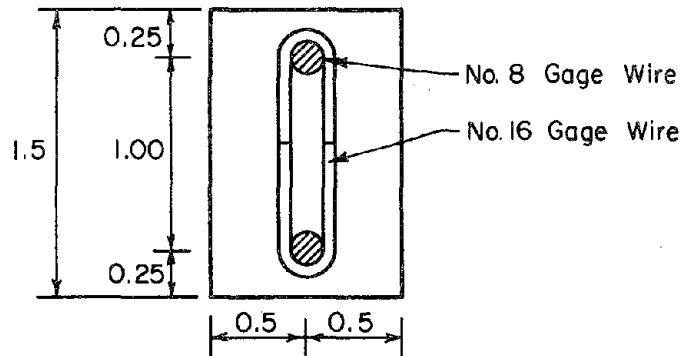
(a) Cross Section of a Typical Beam
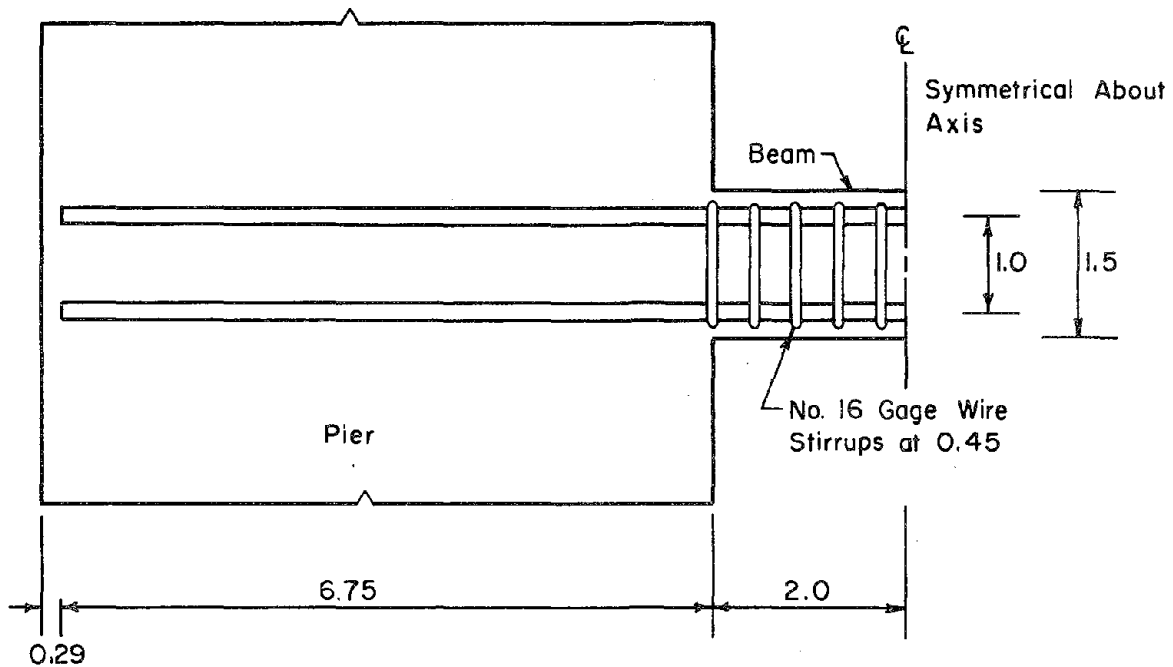
(b) Pier - Beam Connection

(Dimensions in inches)

Fig. 2.17 Beam Reinforcement (Structure D)
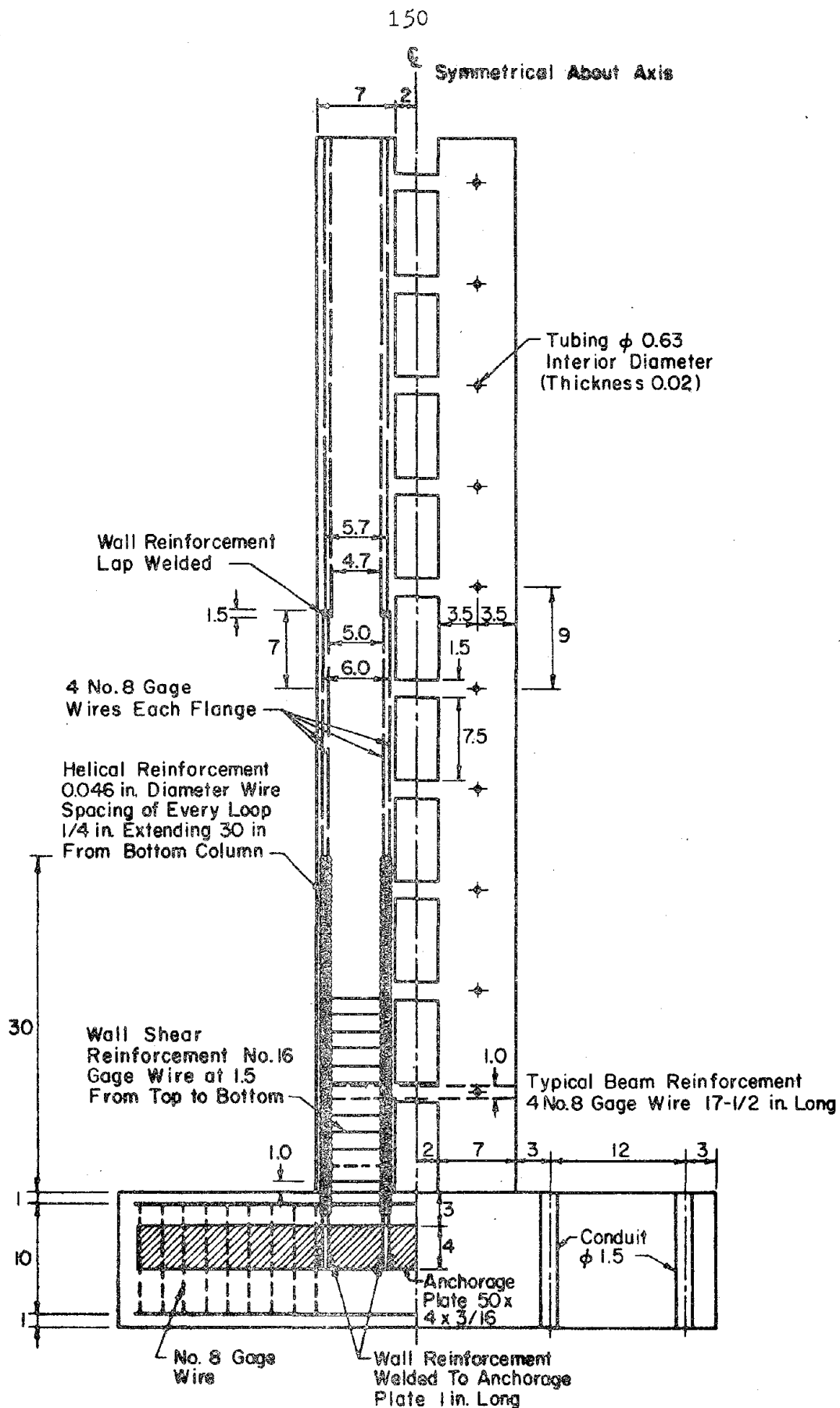
Fig. 2.18 Reinforcement in Test Structure M
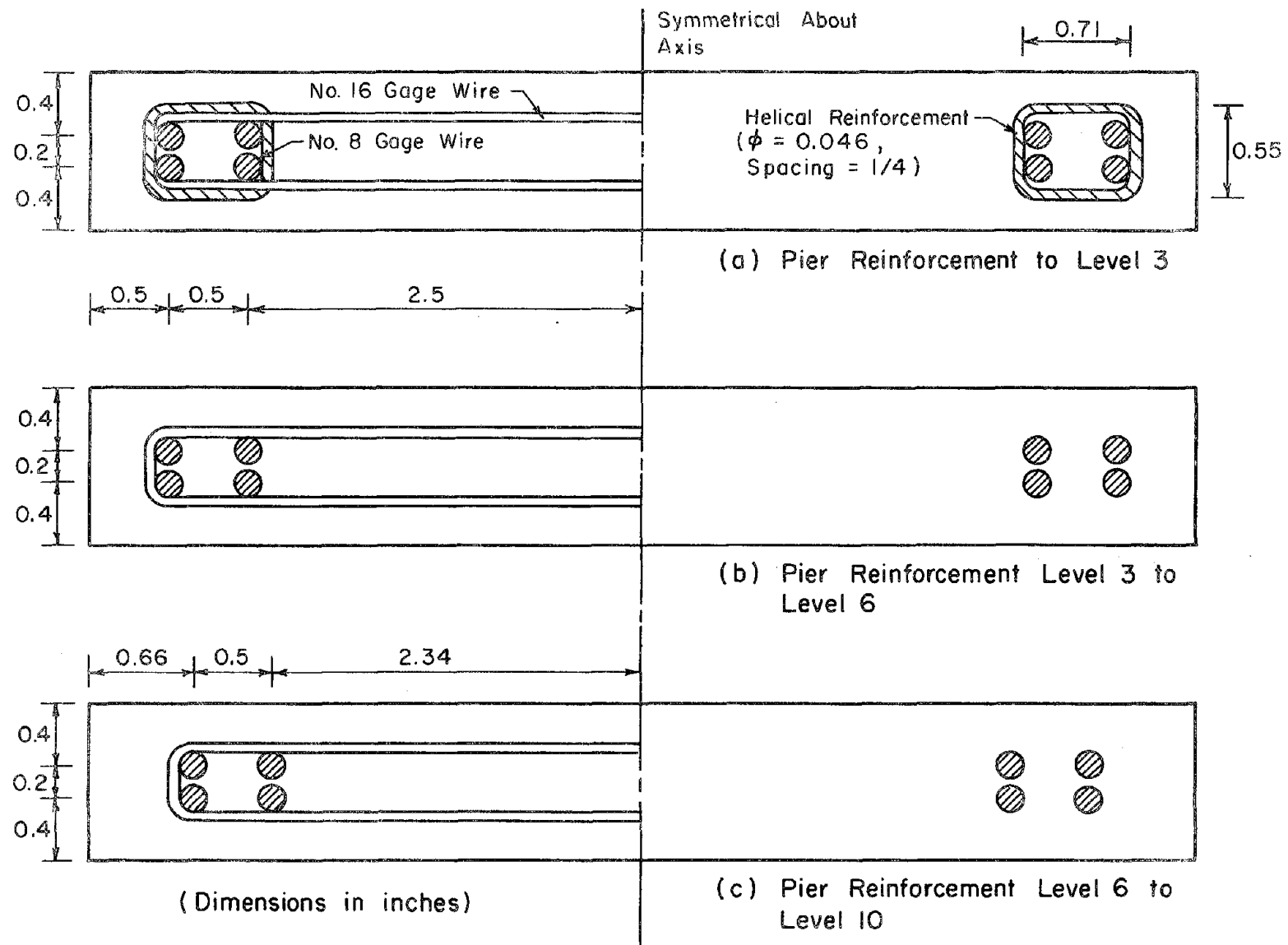
Fig. 2.19   Cross-Sectional Properties of Piers
(Structure M)

(a) Cross Section of a Typical Beam

- No. 8 Gage Wire
- No. 16 Gage Wire

0.25 1.00 0.25 1.5

0.2 0.6 0.2

(b) Wall-Beam Connection

(Dimensions in inches)

0.75 in. Long Cross Bar Welded
to the Beam Reinforcement

Symmetrical About
Axis

Beam

1.0 1.5

No. 16 Gage Wire (20 Stirrups
Along the Span Evenly Spaced)

5.0

Wall

6.75 2.0

0.25

Fig. 2.20 Beam Reinforcement (Structure M)

Axial Stress, ksi

E_c

$f_c = 0$ $\epsilon_c < 0$

$f_c = f_c' \left[2\left(\frac{\epsilon_c}{\epsilon_0}\right) - \left(\frac{\epsilon_c}{\epsilon_0}\right)^2 \right]$ $0 \le \epsilon_c \le \epsilon_0$

$f_c = f_c' \left[1 - 100\,(\epsilon_c - \epsilon_0) \right]$ $\epsilon_0 \le \epsilon_c \le \epsilon_0 + 0.01$

$f_c' = 4500$ psi

$\epsilon_0 = 0.003$

$E_c = 3 \times 10^6$ psi

Strain $\times 10^3$
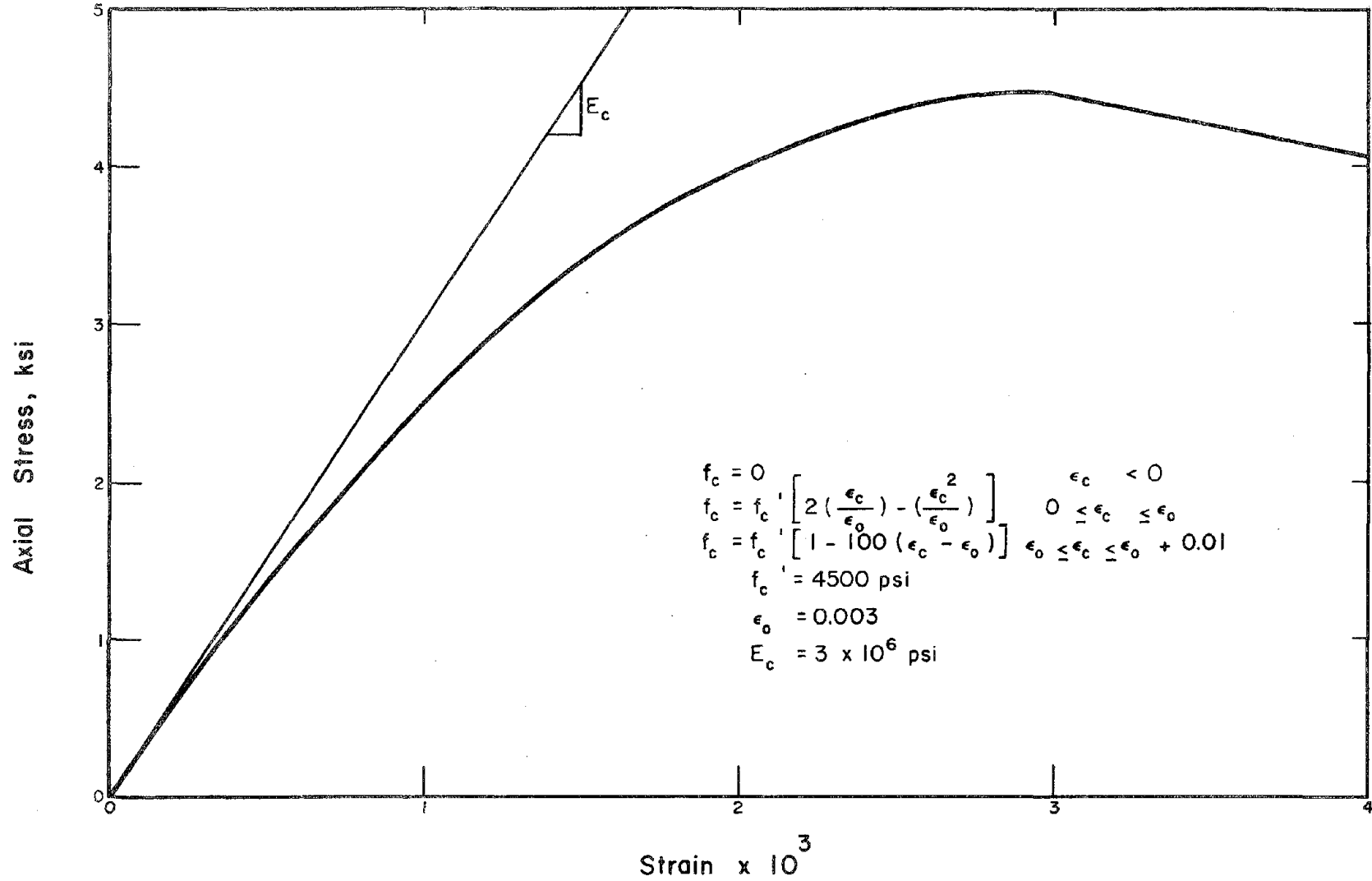
Fig. 2.21   Assumed Stress-Strain Relationship for Concrete
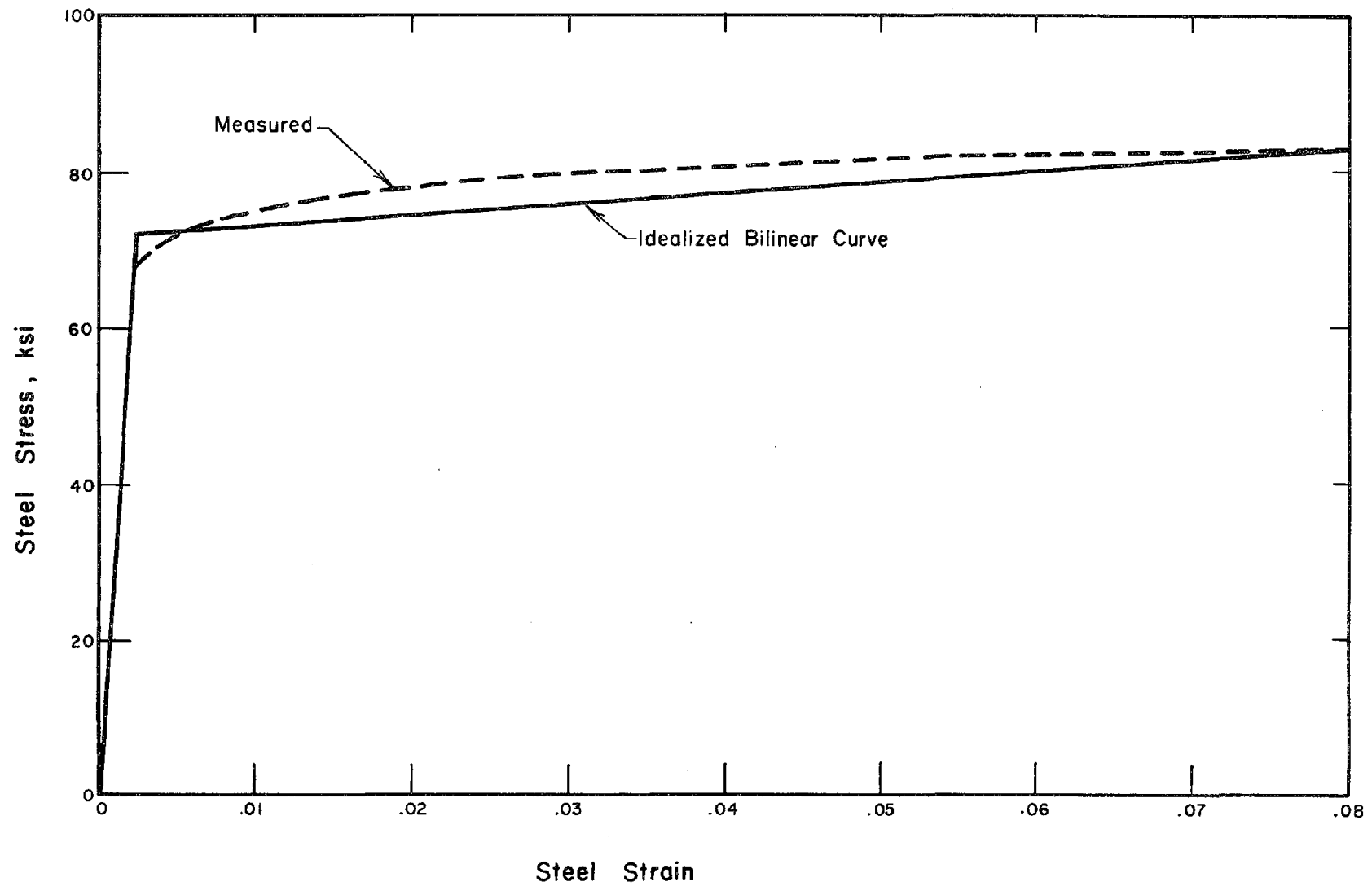
Fig. 2.22   Idealized and Measured Stress-Strain Relationships
            for No. 8 Gage Wire
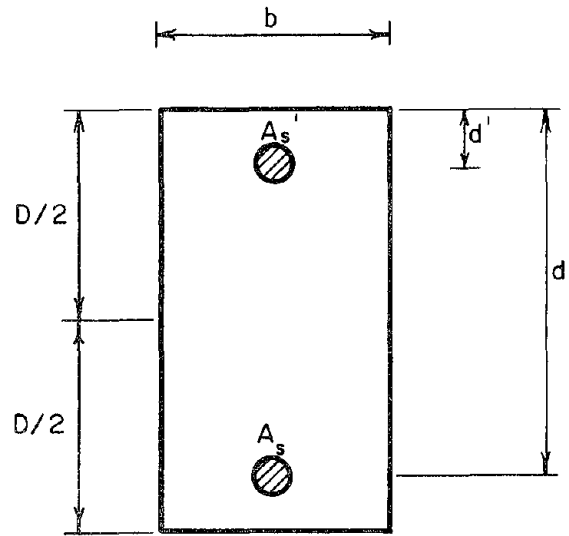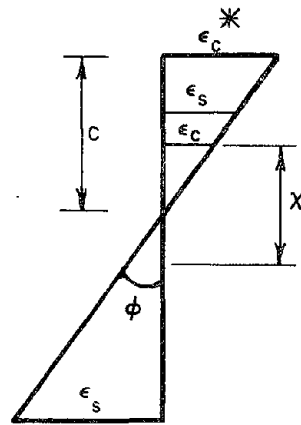
(a) Cross Section   (b) Strain Distribution   (c) Force Distribution
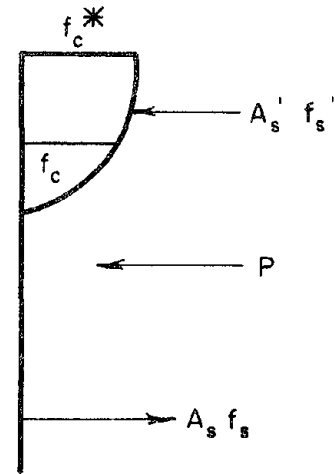
Fig. 2.23   Distribution of Strain and Stress over a Cross Section
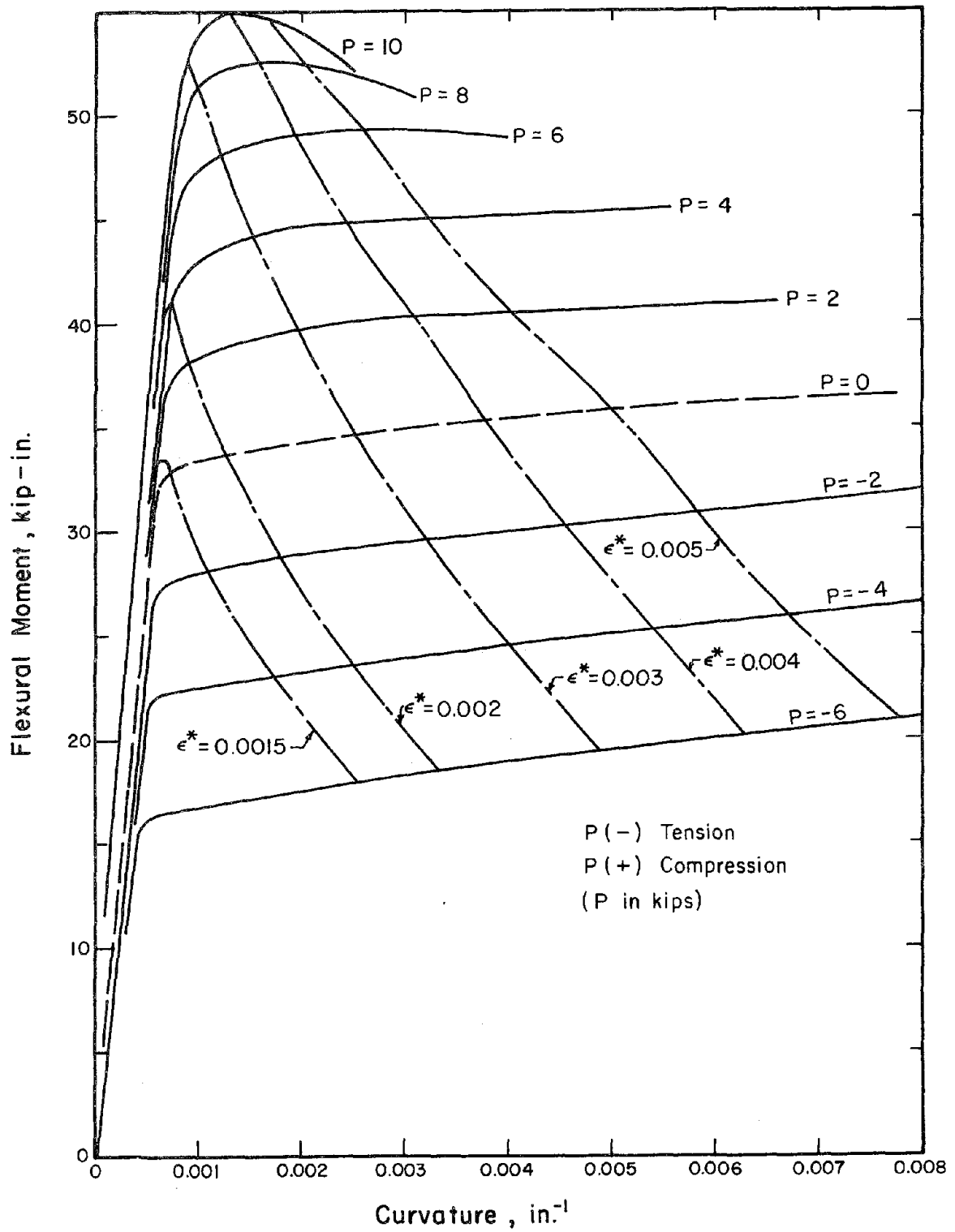
Fig. 2.24 Moment-Curvature Relationships for Piers
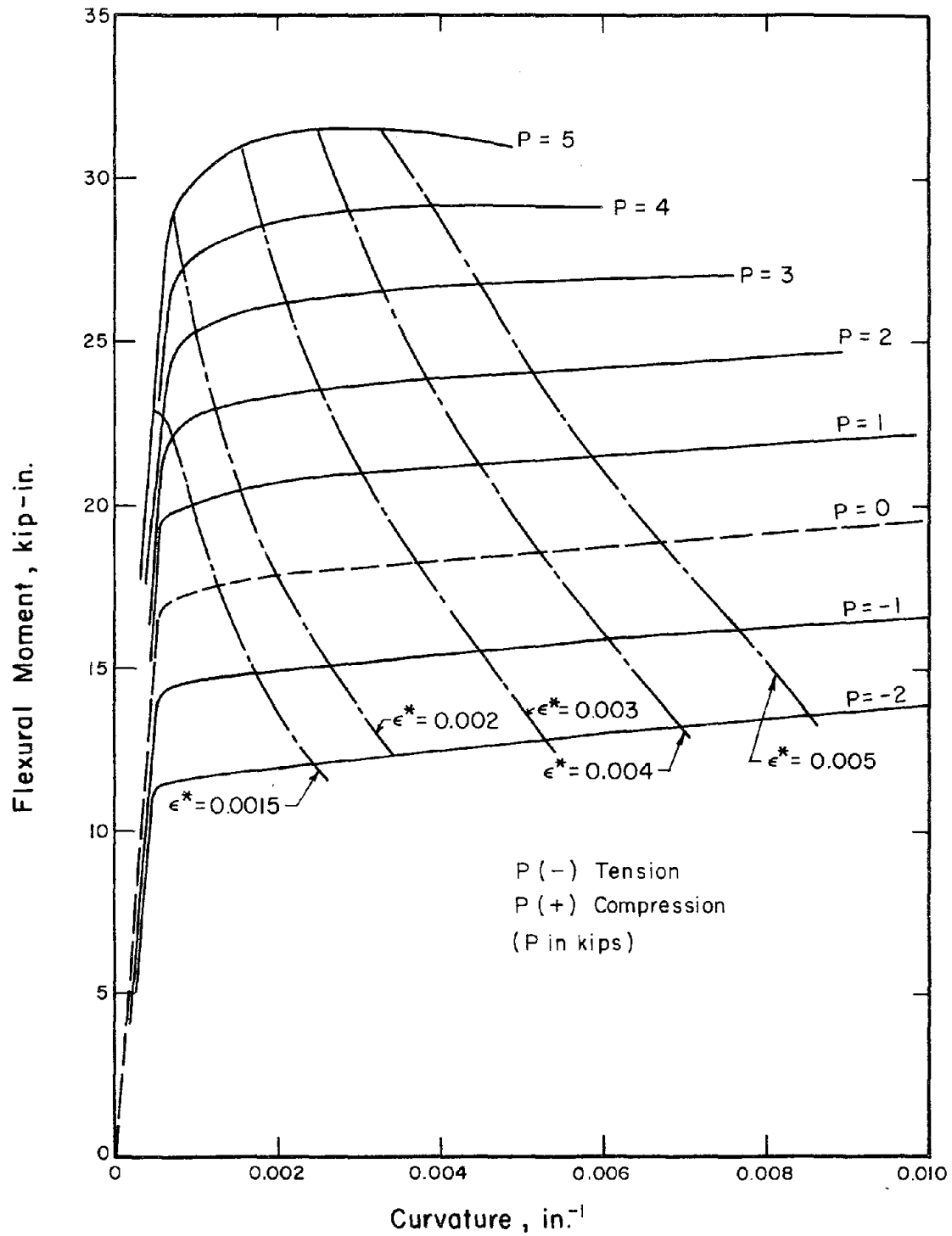
Fig. 2.25 Moment-Curvature Relationships for Piers (Level 6 to 10)
(Structure D)
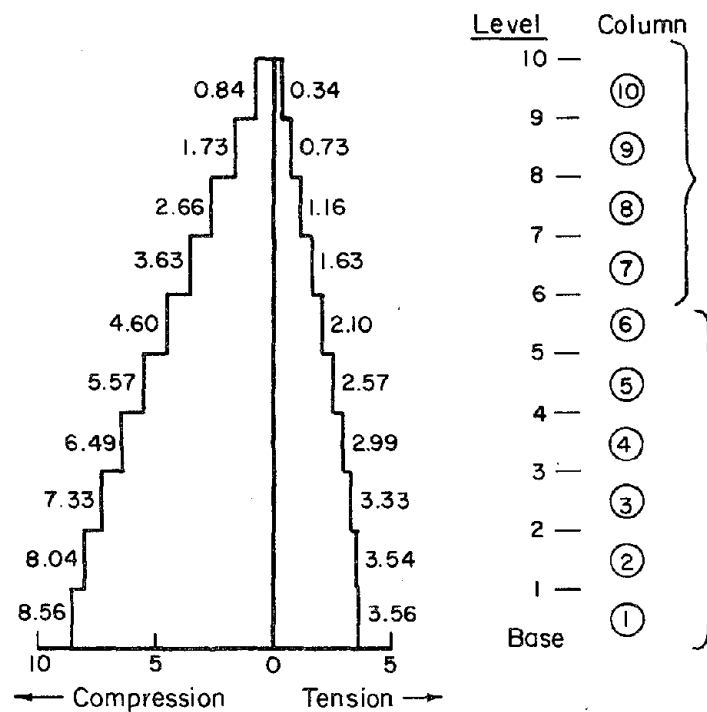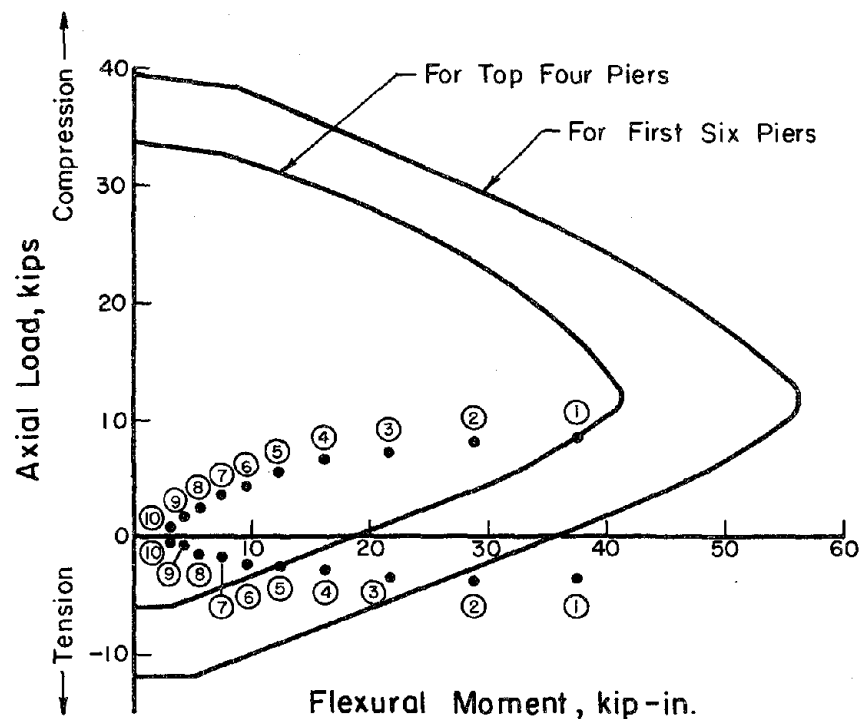
Fig. 2.26 Interaction Diagram of Piers and Corresponding
Design Moments-vs-Axial Forces of Each Pier

158
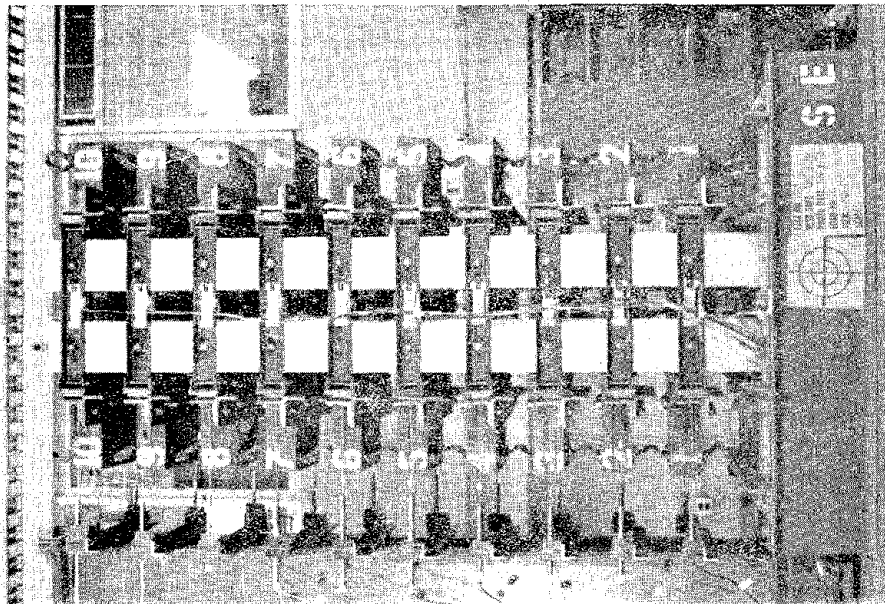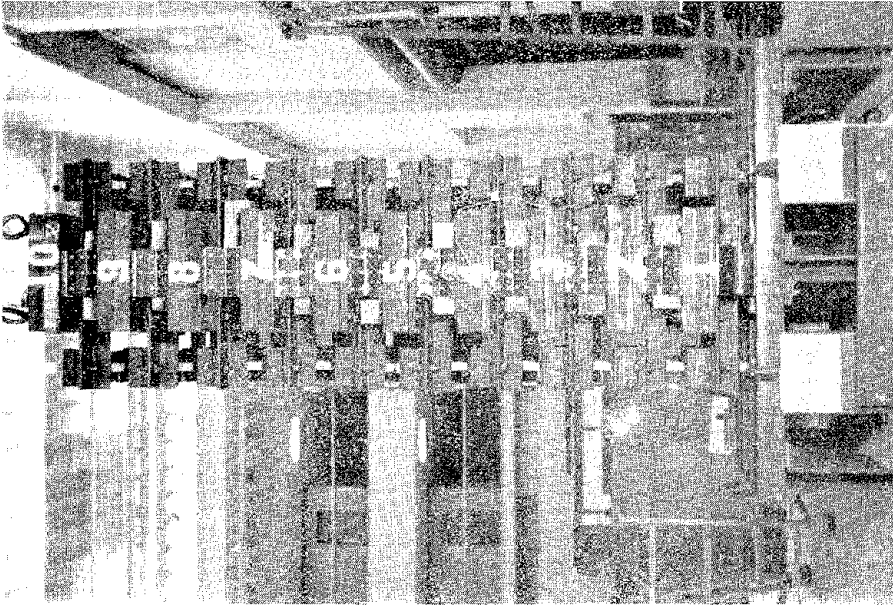
Fig. 3.1   Test Structure
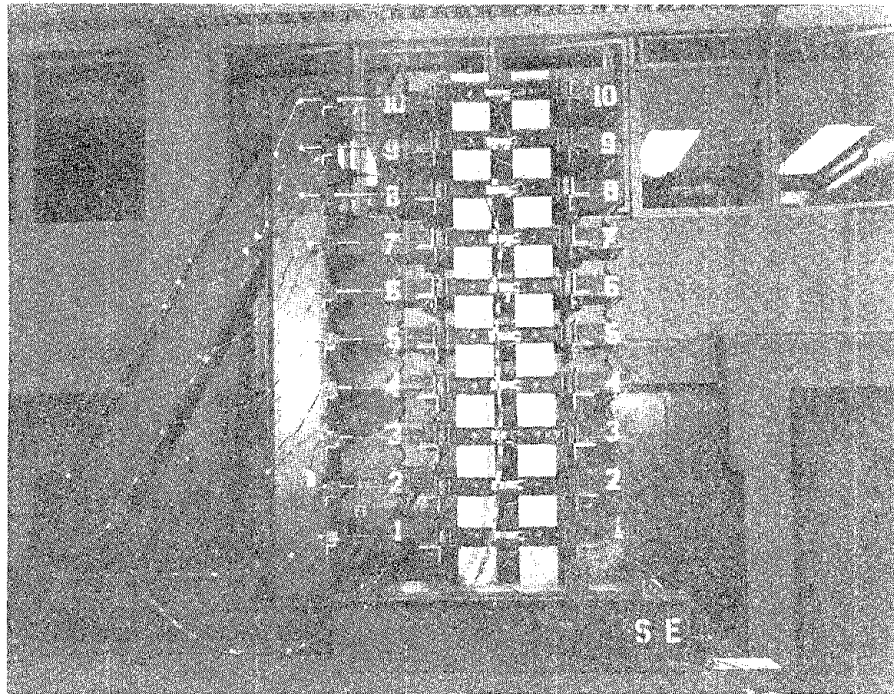
Fig. 3.2   Test Structure and A Frame
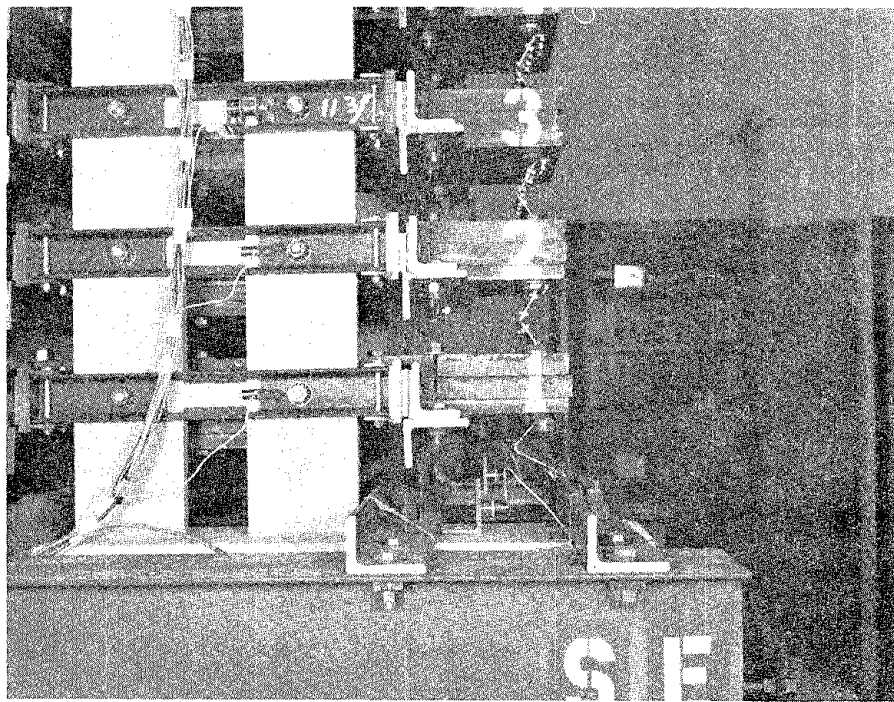
Fig. 3.3   Details of "Bellows" (Lateral View)
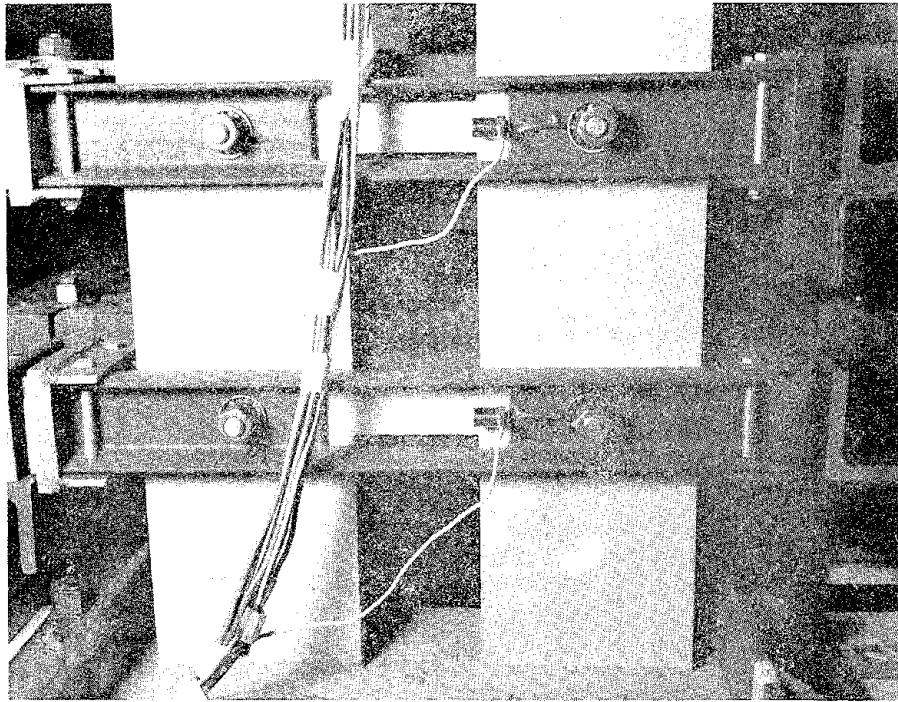
Fig. 3.4   Accelerometers and Connections
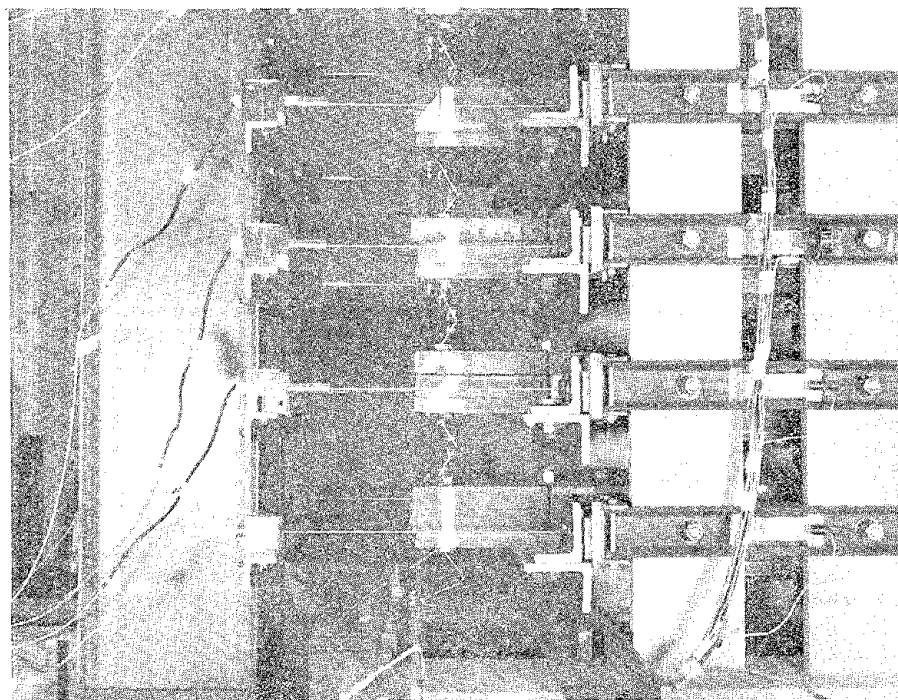
Fig. 3.5   LVDTs and Connections

Fig. 4.1 Test Run D1-1. Linear Response Spectra

162

Fig. 4.2 Test Run D1-1. Linear Response Spectra

Fig. 4.3 Observed Response, Test Run D1-1

164

Fig. 4.3 (Contd) Observed Response, Test Run D1-1

Fig. 4.3 (Contd) Observed Response, Test Run D1-1

BASE ACCELERATION,UNIT=G

FIRST-LEVEL ACCELERATION,UNIT=G

SECOND-LEVEL ACCELERATION,UNIT=G

THIRD-LEVEL ACCELERATION,UNIT=G

TIME, SEC.

DYN, TEST D1 - RUN 1 - ACC, 3S - (THREE SOUTH)
SCALE= 0.5000

DYN, TEST D1 - RUN 1 - ACC, 2S - (TWO SOUTH)
SCALE= 0.5000

DYN, TEST D1 - RUN 1 - ACC, 1S - (ONE SOUTH)
SCALE= 0.5000

DYN, TEST D1 - RUN 1 - ACC, BS - (BASE SOUTH)
SCALE= 0.5000

Fig. 4.4 Observed Response, Test Run D1-1

Fig. 4.4 (Contd) Observed Response, Test Run D1-1

EIGTH - LEVEL ACCELERATION,UNIT=G

NINTH - LEVEL ACCELERATION,UNIT=G

TENTH - LEVEL ACCELERATION,UNIT=G

INPUT ACCELERATION,UNIT=NONE

TIME, SEC.

DYN. TEST D1 - RUN 1 - ACC. 8S - (EIGTH SOUTH)   SCALE=   1.0000   G

DYN. TEST D1 - RUN 1 - ACC. 9S - (NINE SOUTH)   SCALE=   1.0000   G

DYN. TEST D1 - RUN 1 - ACC. 10S - (TEN SOUTH)   SCALE=   1.0000   G
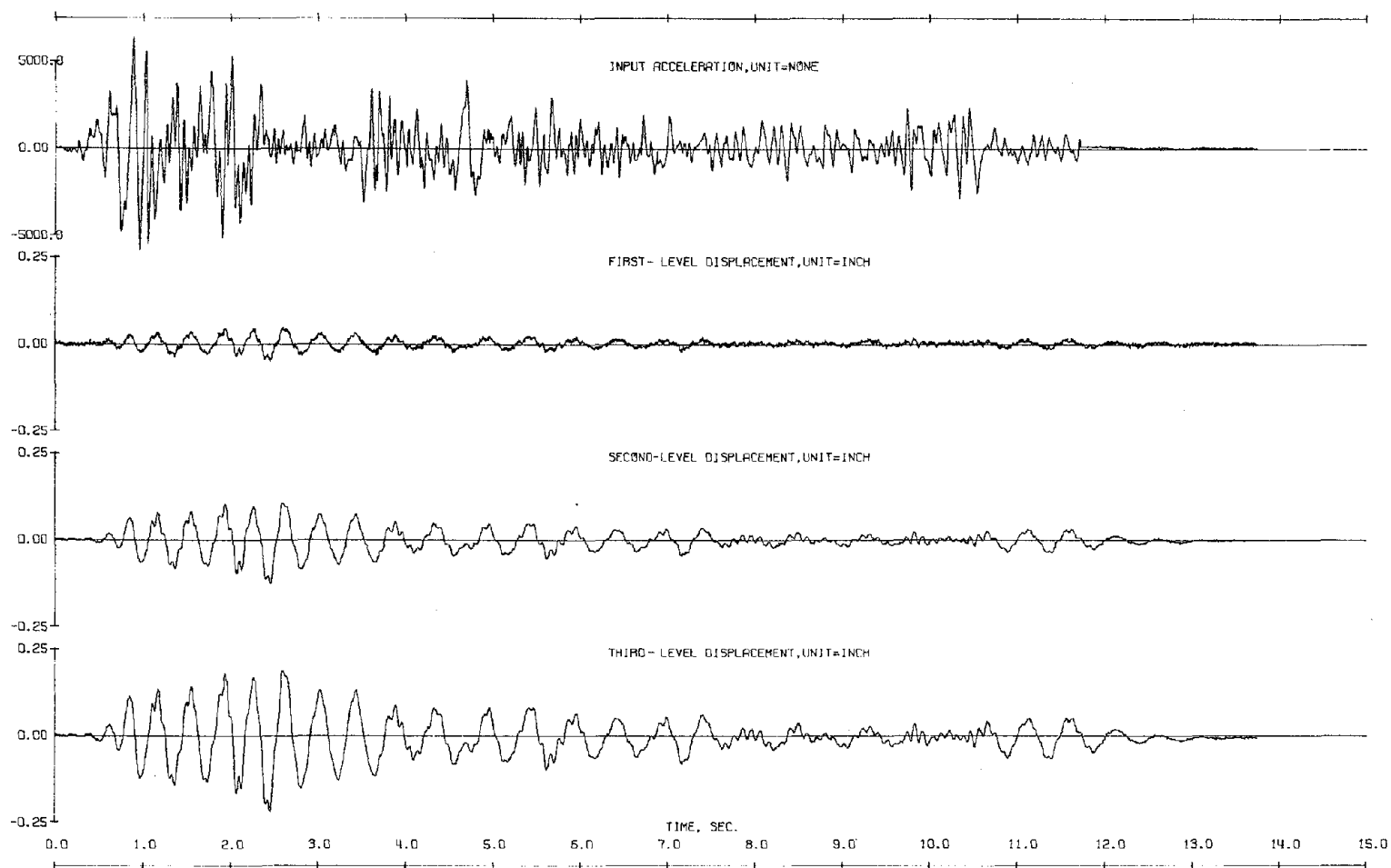
DYN. TEST D1 - RUN 1 - INPUT ACC.   SCALE=   NONE

169

Fig. 4.4 (Contd) Observed Response, Test Run D1-1

(a) Due to Test Run D1-1   (b) Due to Test Run D1-2

Fig. 4.5 Crack Patterns Observed in Test Structure D1
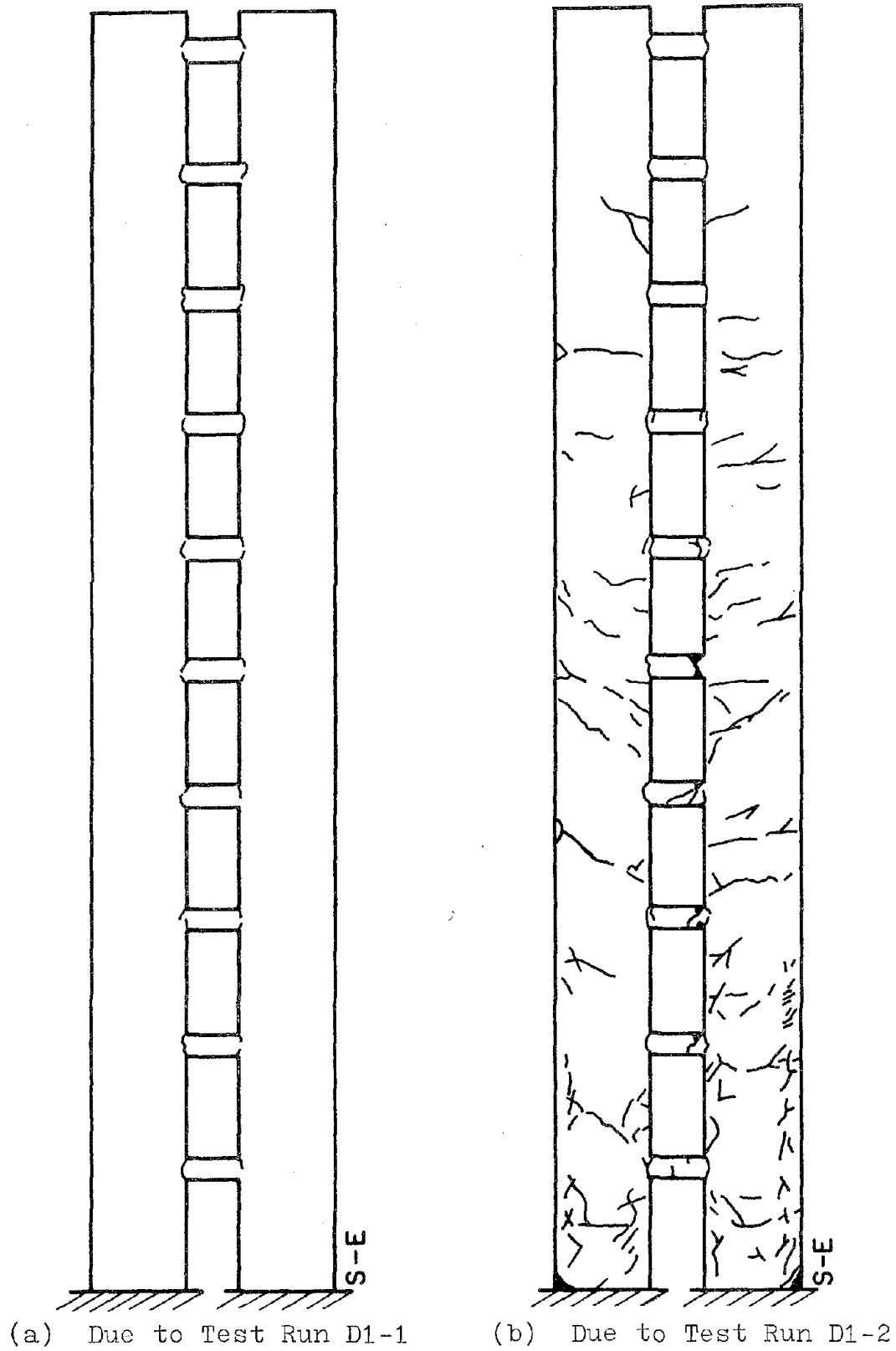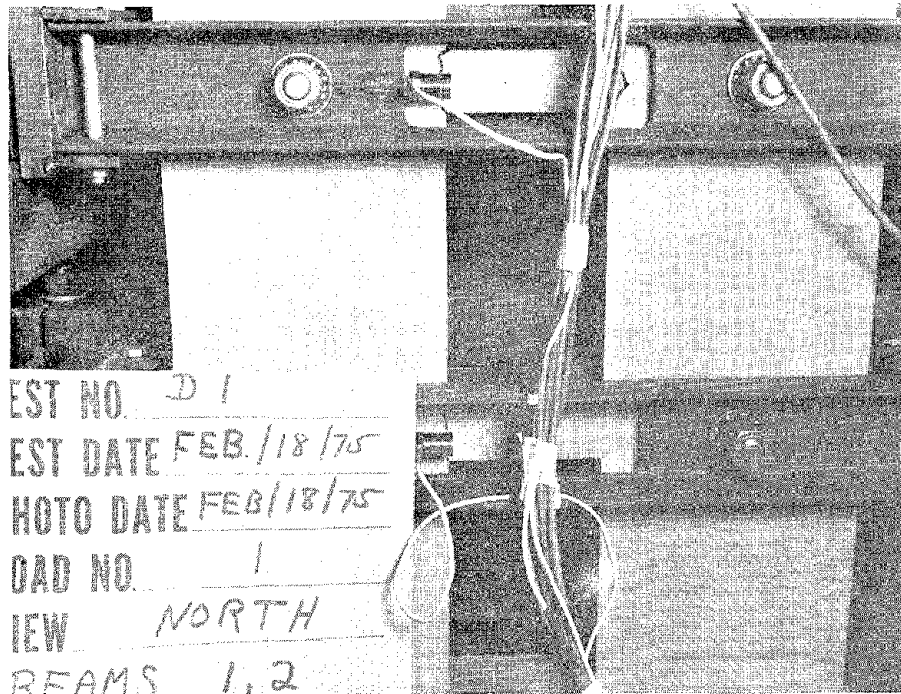
(a)   Damage in The First Two Levels
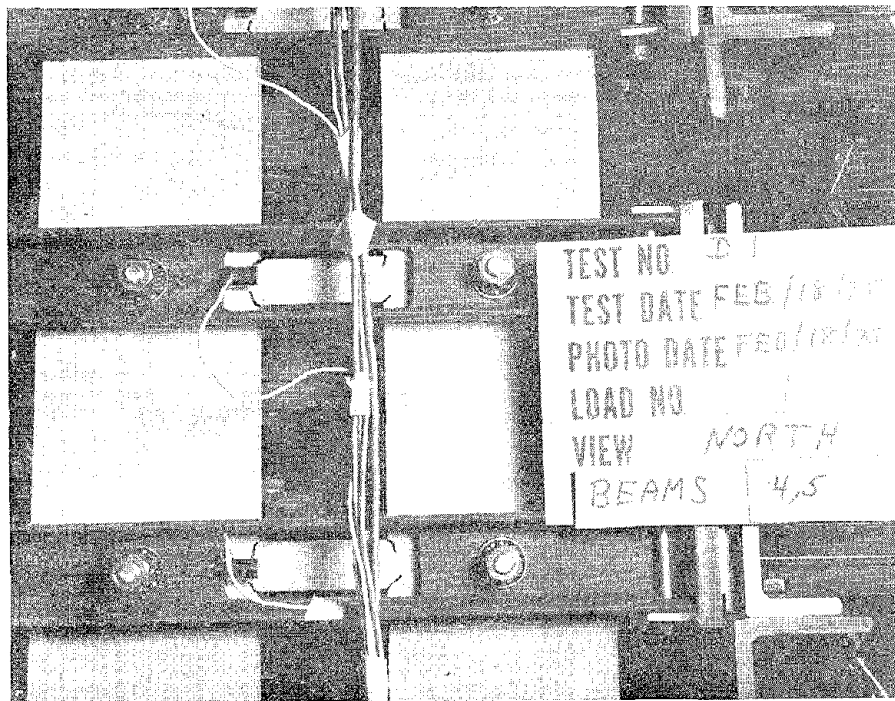
(b)   Damage in The Middle Floors (Fourth and Fifth)

Fig. 4.6   Damage in Test Structure D1(Test Run D1-1)
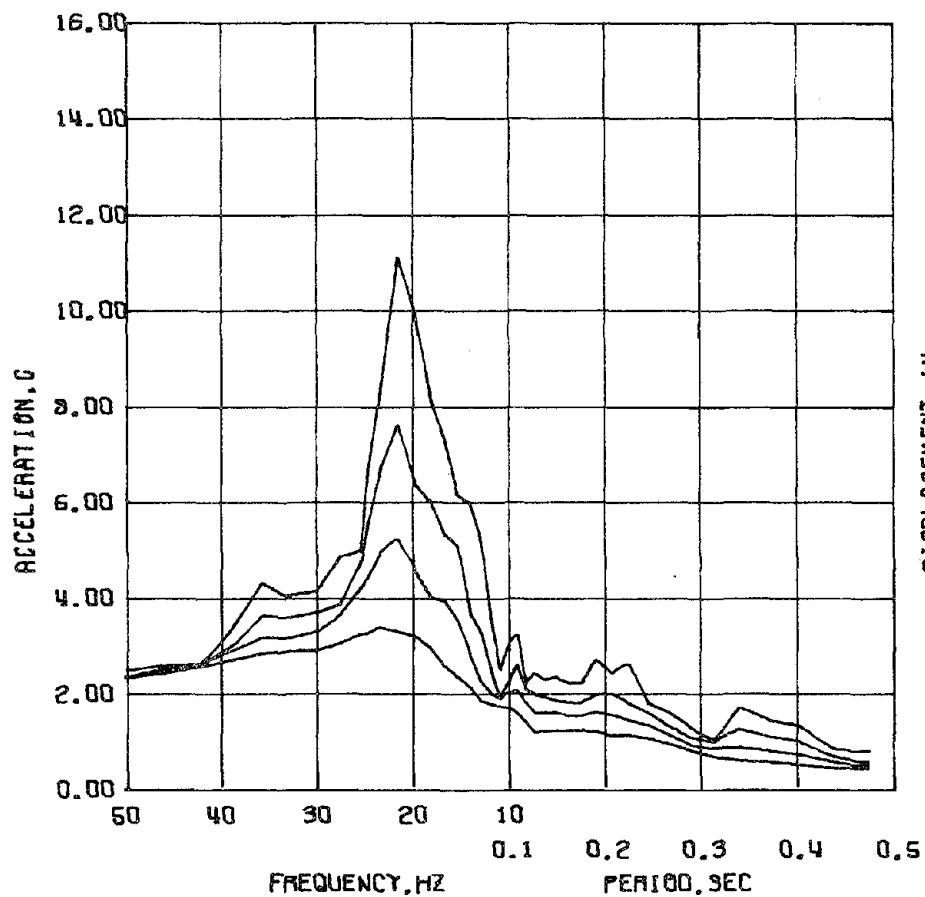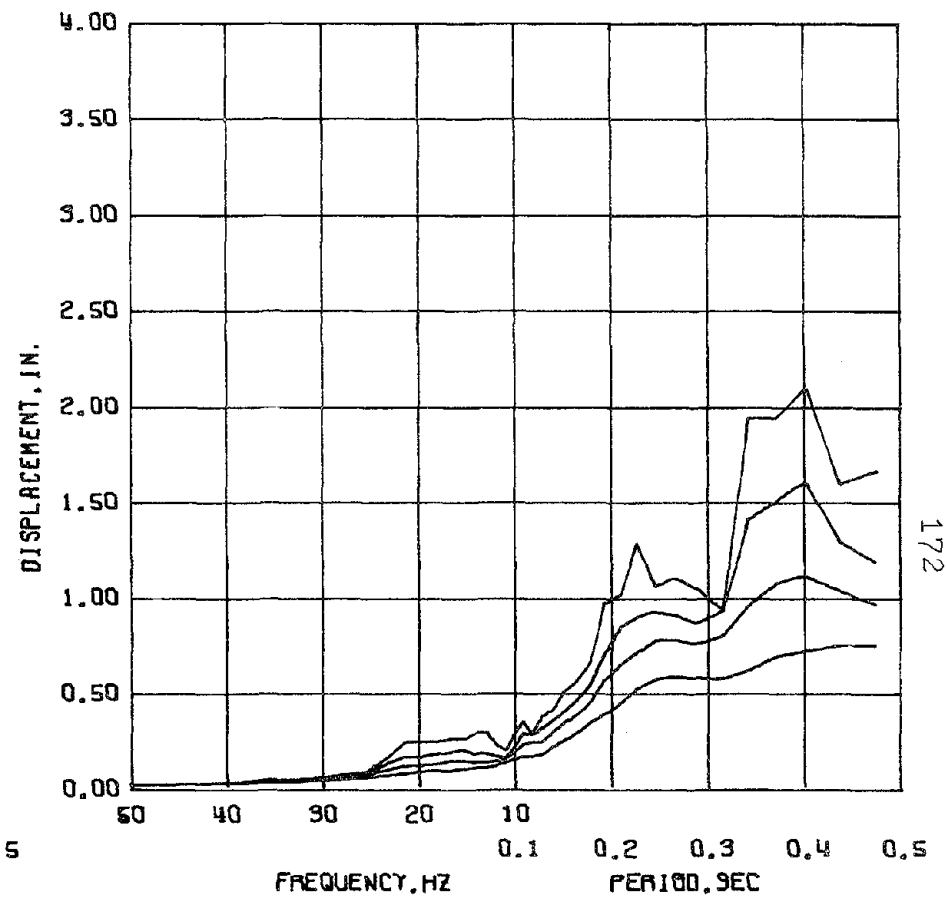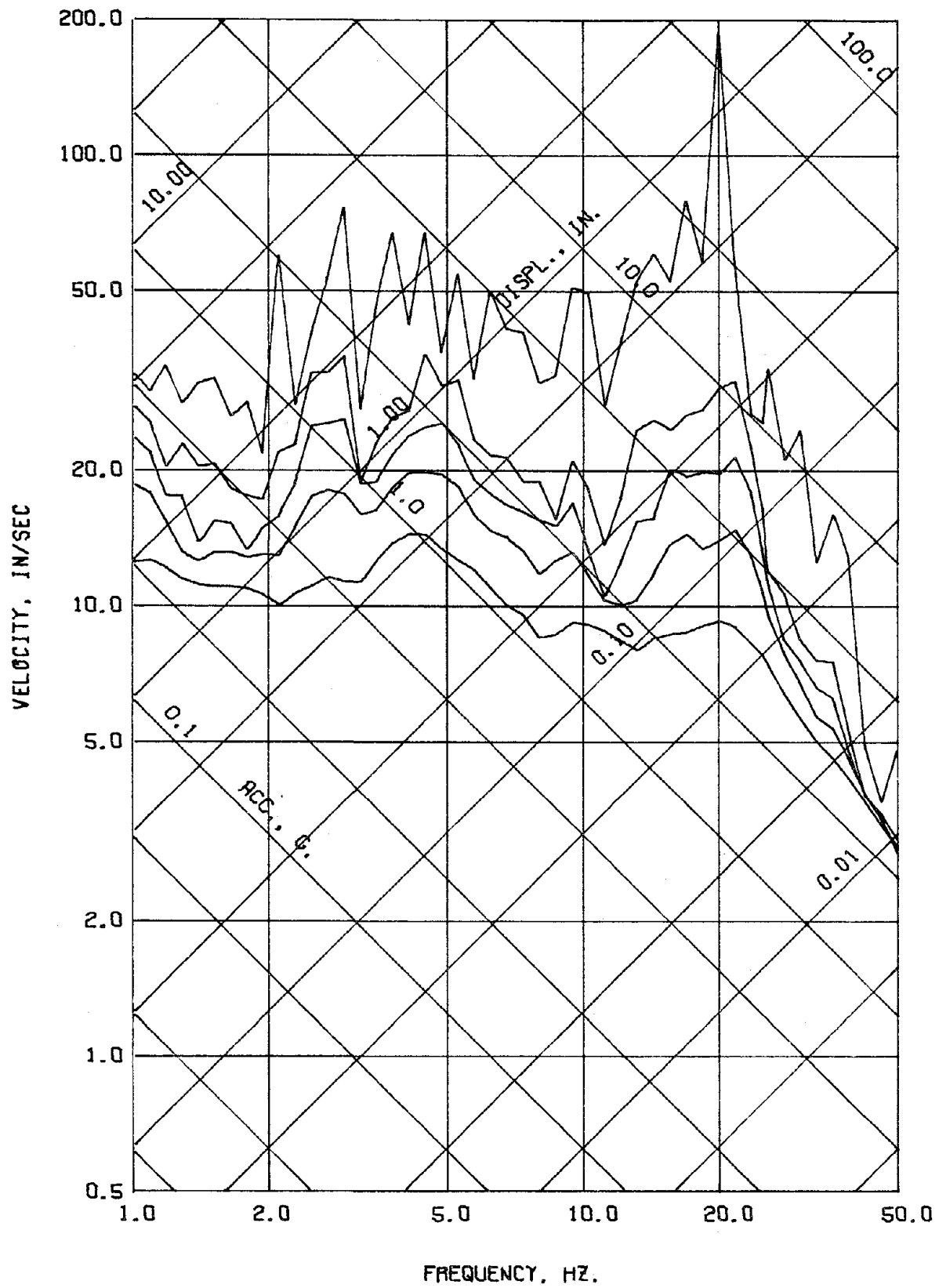
Fig. 4.7 Test Run D1-2. Linear Response Spectra

Fig. 4.8 Test Run D1-2. Linear Response Spectra

174

Fig. 4.9 Observed Response, Test Run D1-2

Fig. 4.9 (Contd) Observed Response, Test Run D1-2

Fig. 4.9 (Contd) Observed Response, Test Run D1-2

BASE ACCELERATION,UNIT=G

FIRST- LEVEL ACCELERATION,UNIT=G

SECOND-LEVEL ACCELERATION,UNIT=G

THIRD- LEVEL ACCELERATION,UNIT=G

TIME, SEC.

Fig. 4.10 Observed Response, Test Run D1-2

FOURTH-LEVEL ACCELERATION, UNIT=G

FIFTH-LEVEL ACCELERATION, UNIT=G

SIXTH-LEVEL ACCELERATION, UNIT=G

SEVENTH-LEVEL ACCELERATION, UNIT=G

TIME, SEC.

Fig. 4.10 (Contd) Observed Response, Test Run D1-2

Fig. 4.10 (Contd) Observed Response, Test Run D1-2
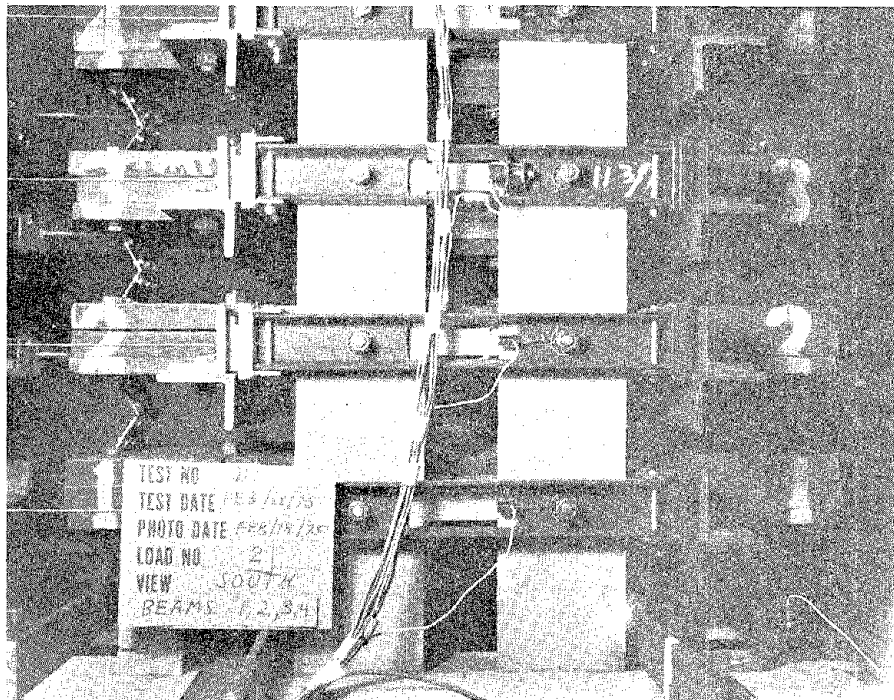
(a)   Damage in The First Four Levels
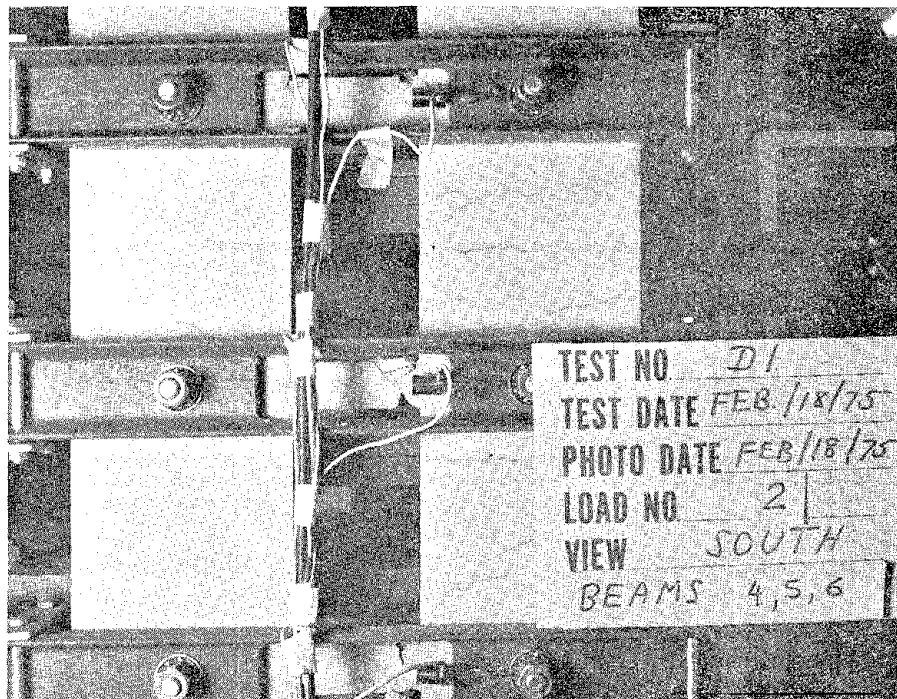
(b)   Damage in The Middle Floors (Fourth, Fifth and Sixth)

Fig. 4.11   Damage in Test Struture D (Test Run D1-2)
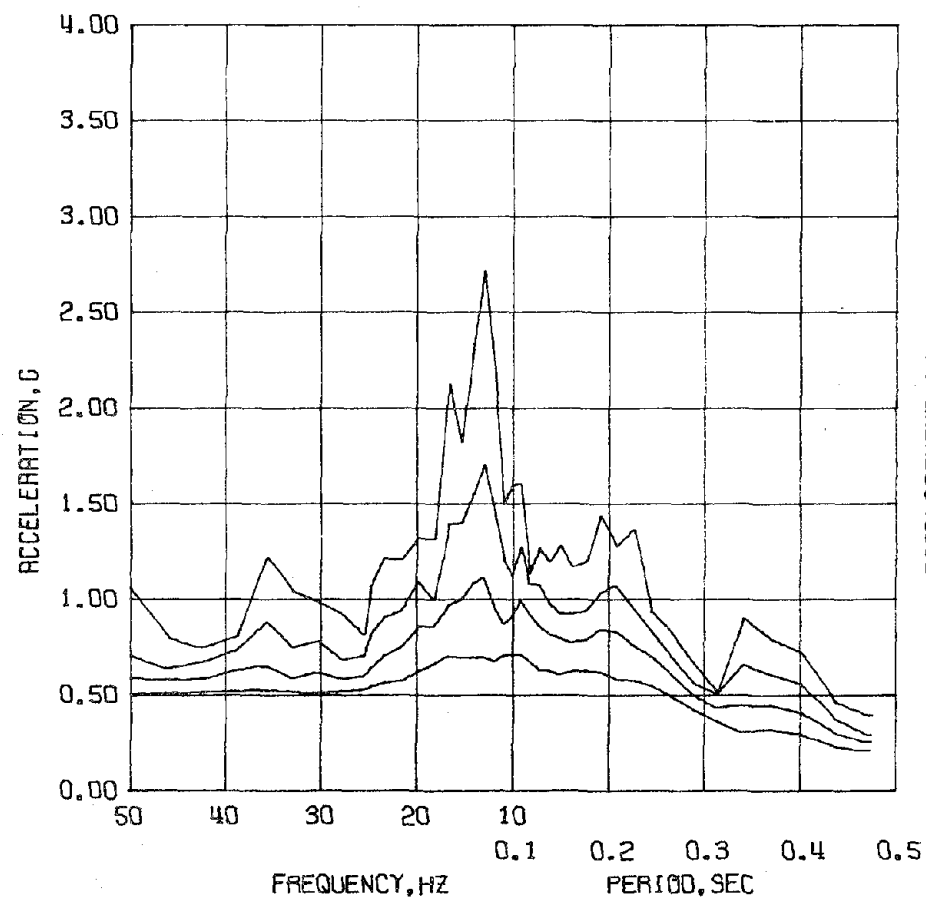
DYN. TEST D2 — RUN 1 — ACC. BS — (BASE SOUTH)
DAMPING FACTOR =   0.02 0.05 0.10 0.20
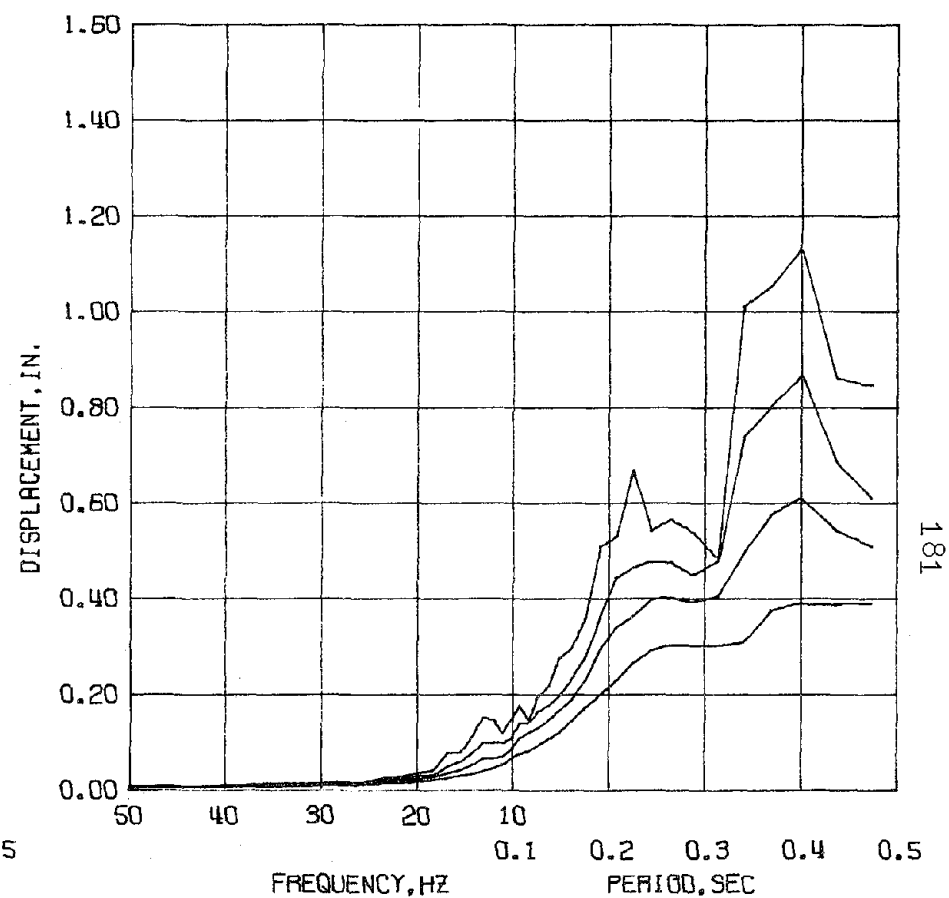
DYN. TEST D2 — RUN 1 — ACC. BS — (BASE SOUTH)
DAMPING FACTOR =   0.02 0.05 0.10 0.20

Fig. 4.12   Test Run D2-1. Linear Response Spectra
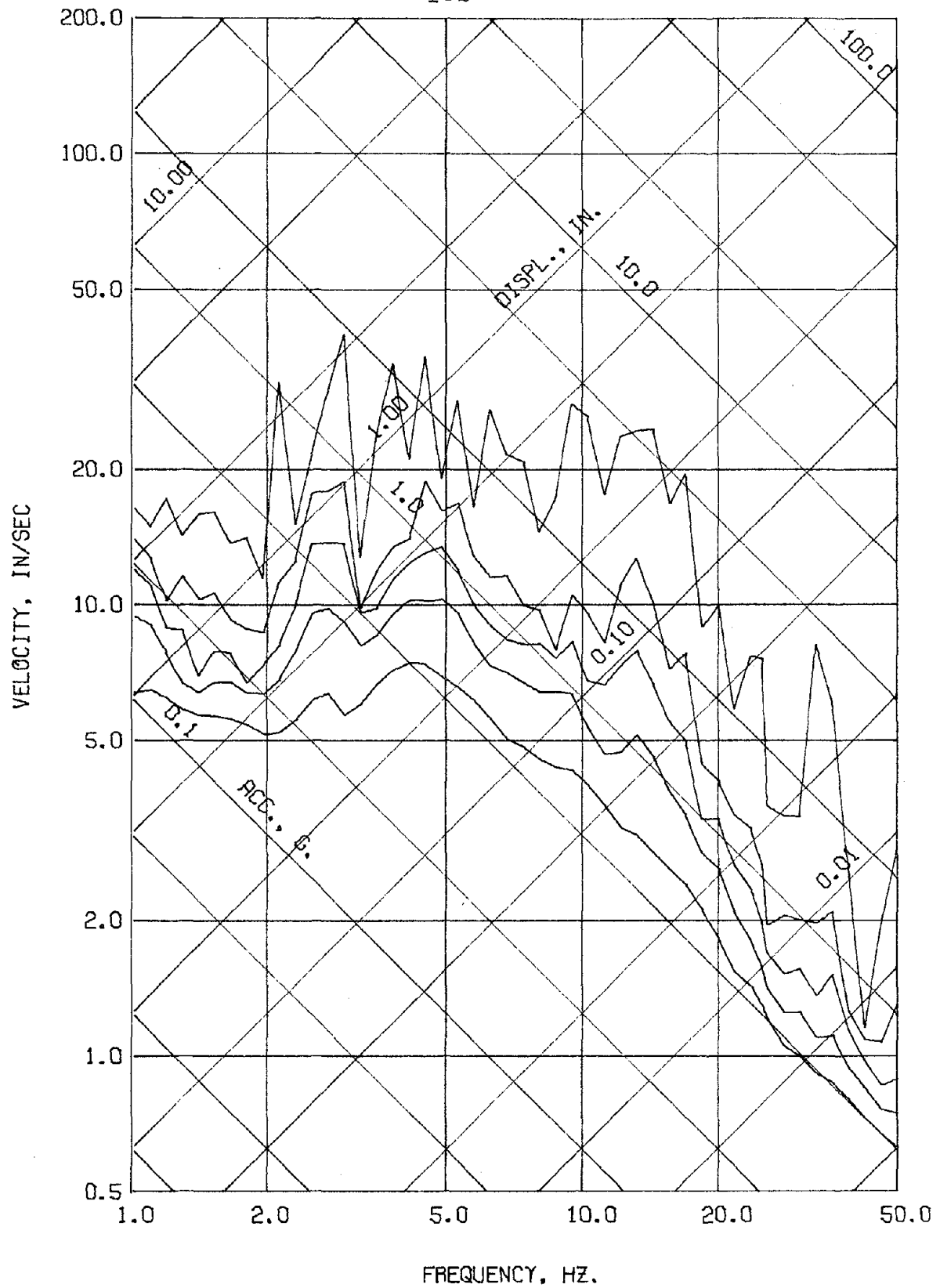
DYN. TEST D2 – RUN 1 – ACC. BS – (BASE SOUTH)

DAMPING FACTOR =   0.00   0.02   0.05   0.10   0.20

Fig. 4.13   Test Run D2-1. Linear Response Spectra

·Displacement signals for the first five levels are not reported
because of electronic noise
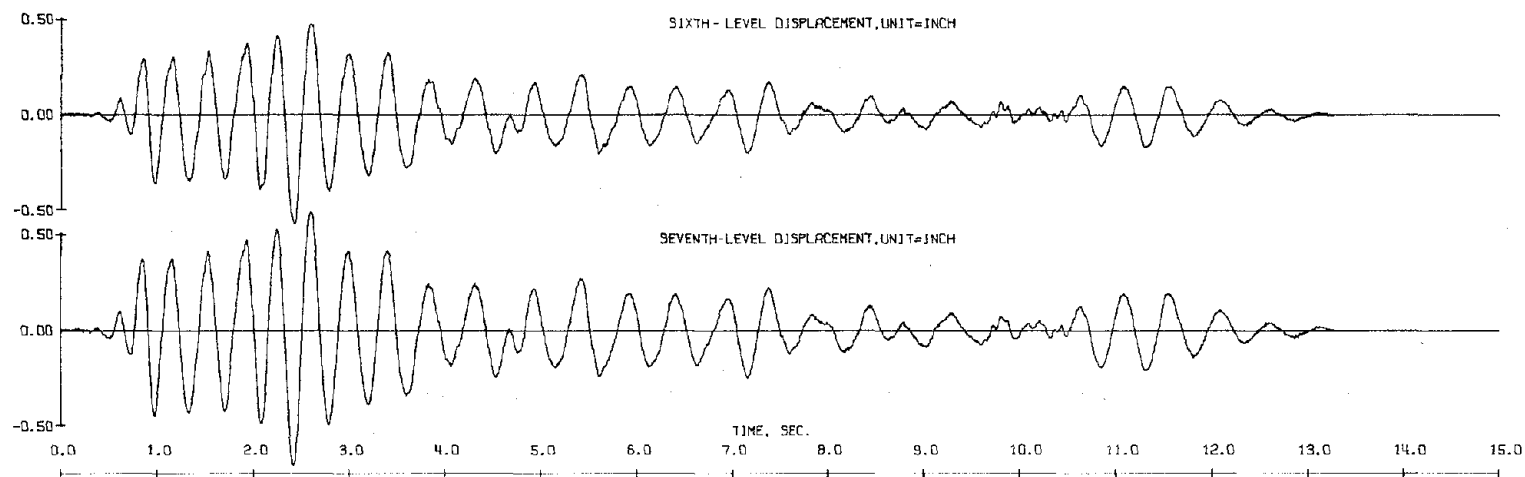
Fig. 4.14   Observed Response, Test Run D2-1

EIGTH - LEVEL DISPLACEMENT,UNIT=INCH

NINTH - LEVEL DISPLACEMENT,UNIT=INCH

TENTH - LEVEL DISPLACEMENT,UNIT=INCH

P-DELTA BASE MOMENT,UNIT=KIP-INCH

TIME, SEC.

DYN. TEST D2 - RUN 1 - LVDT 8S - (EIGTH SOUTH)
SCALE=   1.0000   INCH

DYN. TEST D2 - RUN 1 - LVDT 9S - (NINE SOUTH)
SCALE=   1.0000   INCH

DYN. TEST D2 - RUN 1 - LVDT 10S - (TEN SOUTH)
SCALE=   1.0000   INCH

DYN. TEST D2 - MARCH 14, 1975 - RUN 1 - P DELTA MOMENT - 0 LEVEL- SOUTH
KIP-INCH
SCALE=   2.0000

184
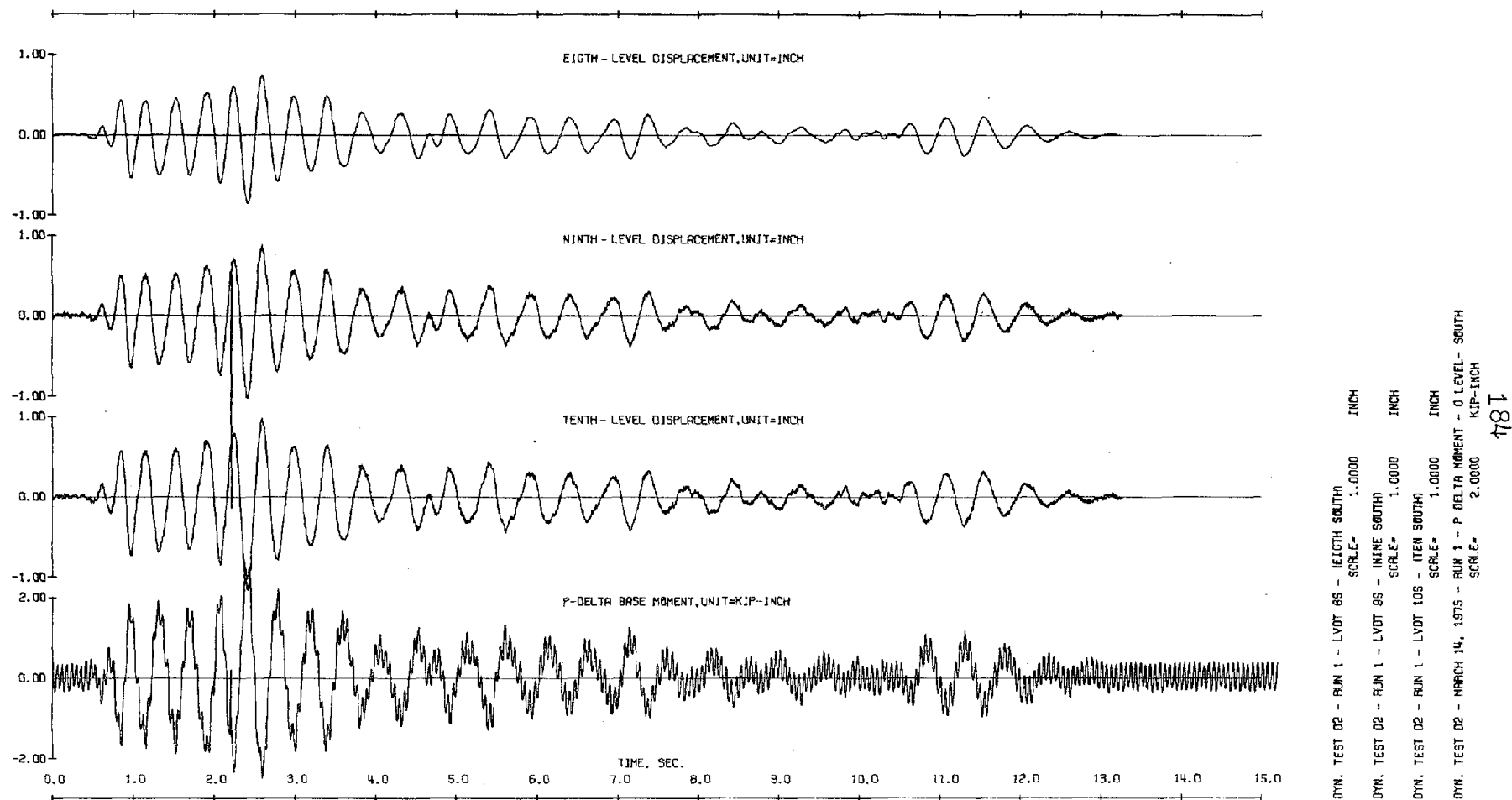
Fig. 4.14 (Contd) Observed Response, Test Run D2-1

Fig. 4.15 Observed Response, Test Run D2-1

FOURTH-LEVEL ACCELERATION,UNIT=G

FIFTH-LEVEL ACCELERATION,UNIT=G

SIXTH-LEVEL ACCELERATION,UNIT=G

SEVENTH-LEVEL ACCELERATION,UNIT=G

TIME, SEC.
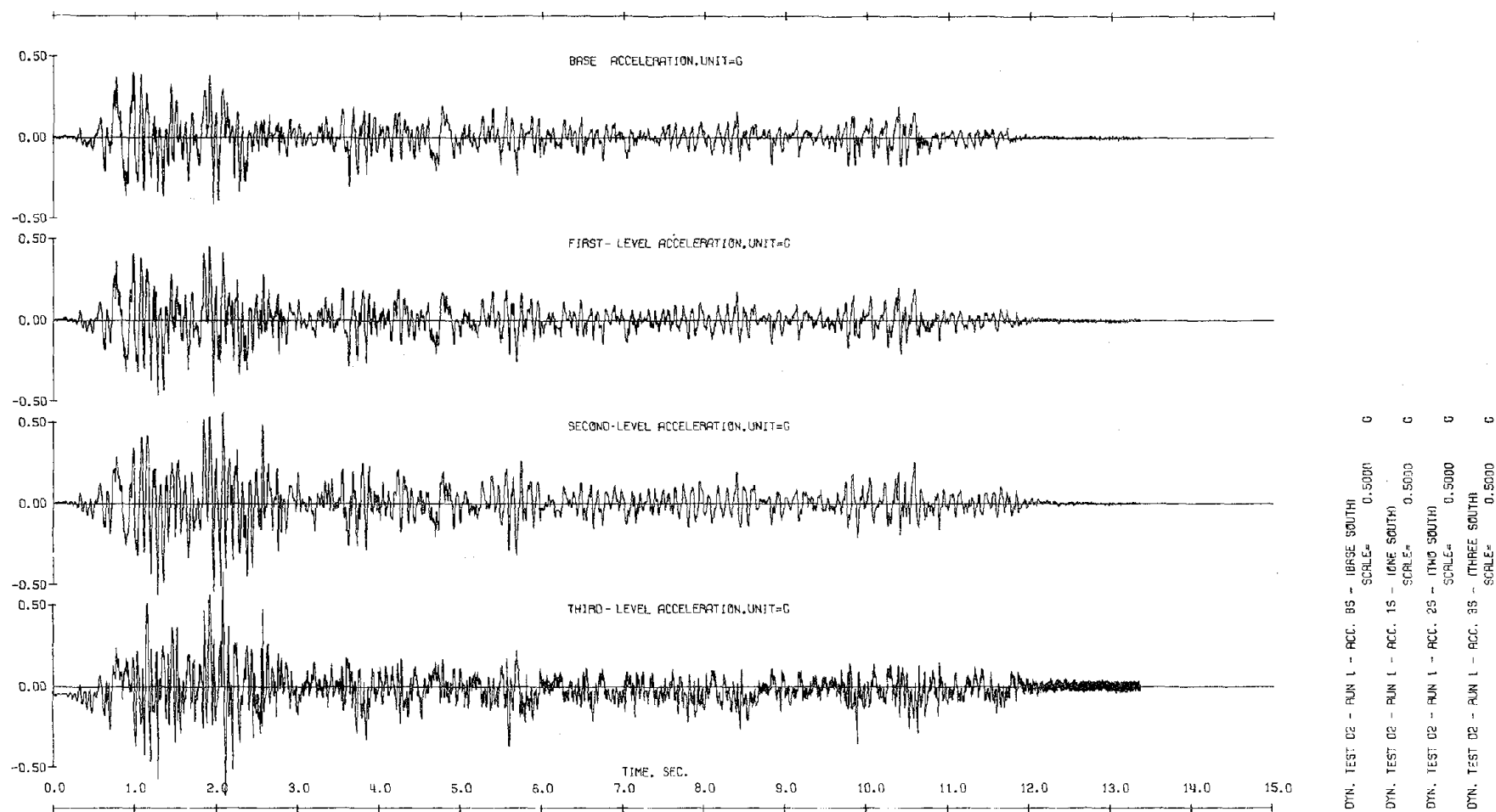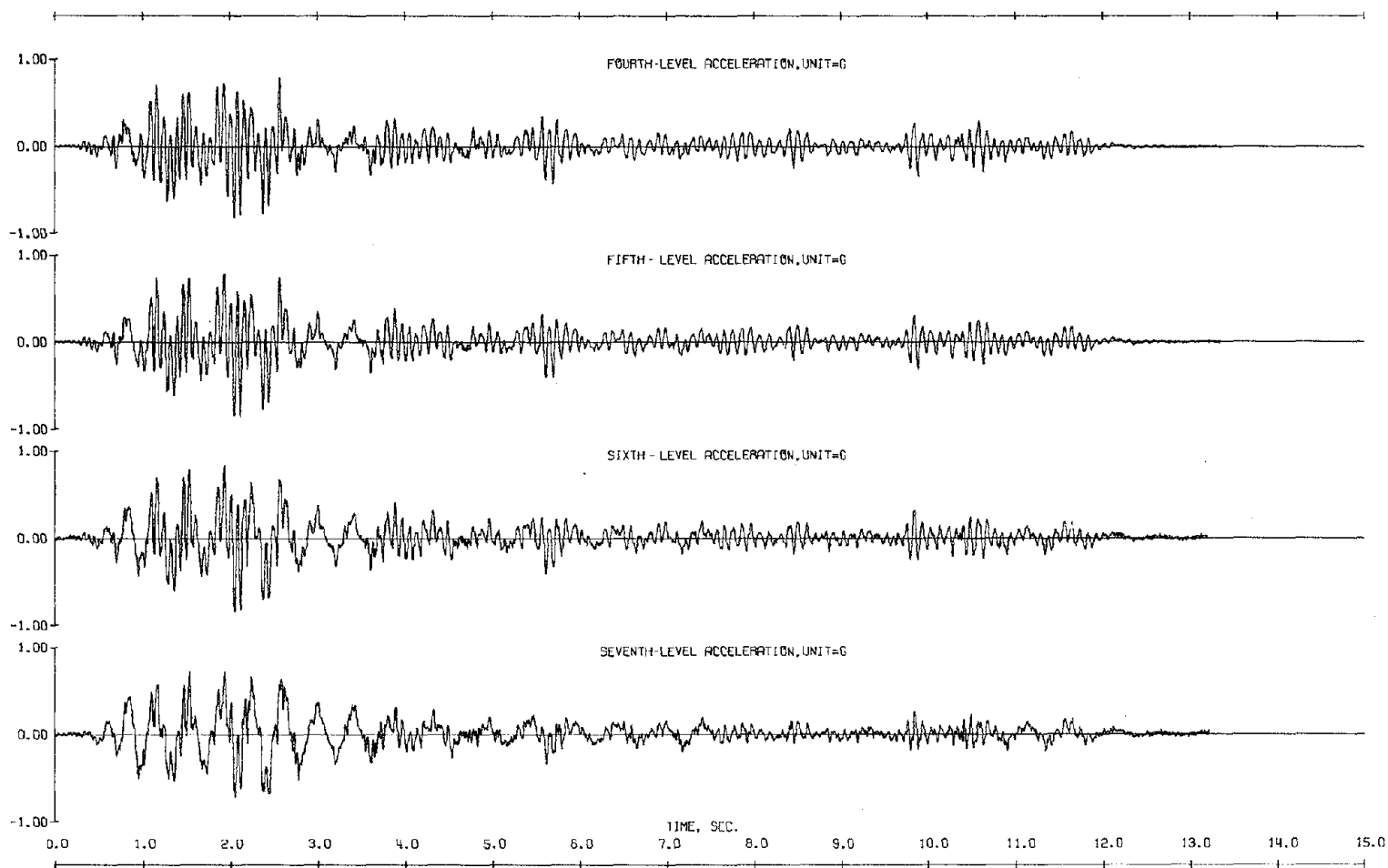
DYN. TEST D2 - RUN 1 - ACC. 4S - (FOUR SOUTH)   SCALE=   1.0000   G

DYN. TEST D2 - RUN 1 - ACC. 5S - (FIVE SOUTH)   SCALE=   1.0000   G

DYN. TEST D2 - RUN 1 - ACC. 6S - (SIX SOUTH)   SCALE=   1.0000   G

DYN. TEST D2 - RUN 1 - ACC. 7S - (SEVEN SOUTH)   SCALE=   1.0000   G

Fig. 4.15 (Contd) Observed Response, Test Run D2-1

EIGTH - LEVEL ACCELERATION, UNIT=G

NINTH - LEVEL ACCELERATION, UNIT=G

TENTH - LEVEL ACCELERATION, UNIT=G

INPUT ACCELERATION, UNIT=NONE

TIME. SEC.

Fig. 4.15 (Contd) Observed Response, Test Run D2-1

(a) Due to Shrinkage   (b) Due to Test Run D2-1
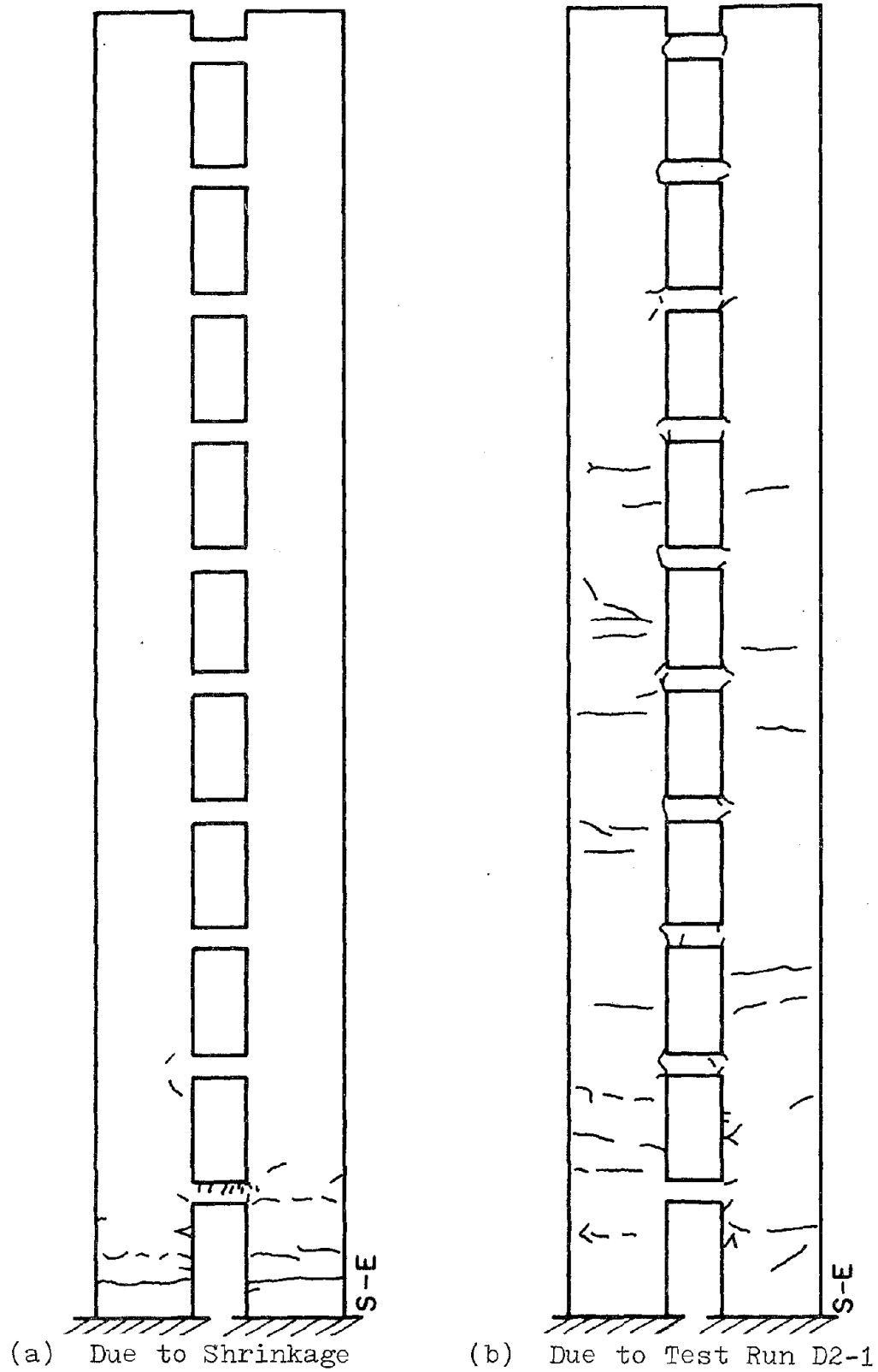
Fig. 4.16 Crack Patterns Observed in Test Structure D2

(c)   Due to Test Run D2-2   (d)   Due to Test Run D2-3
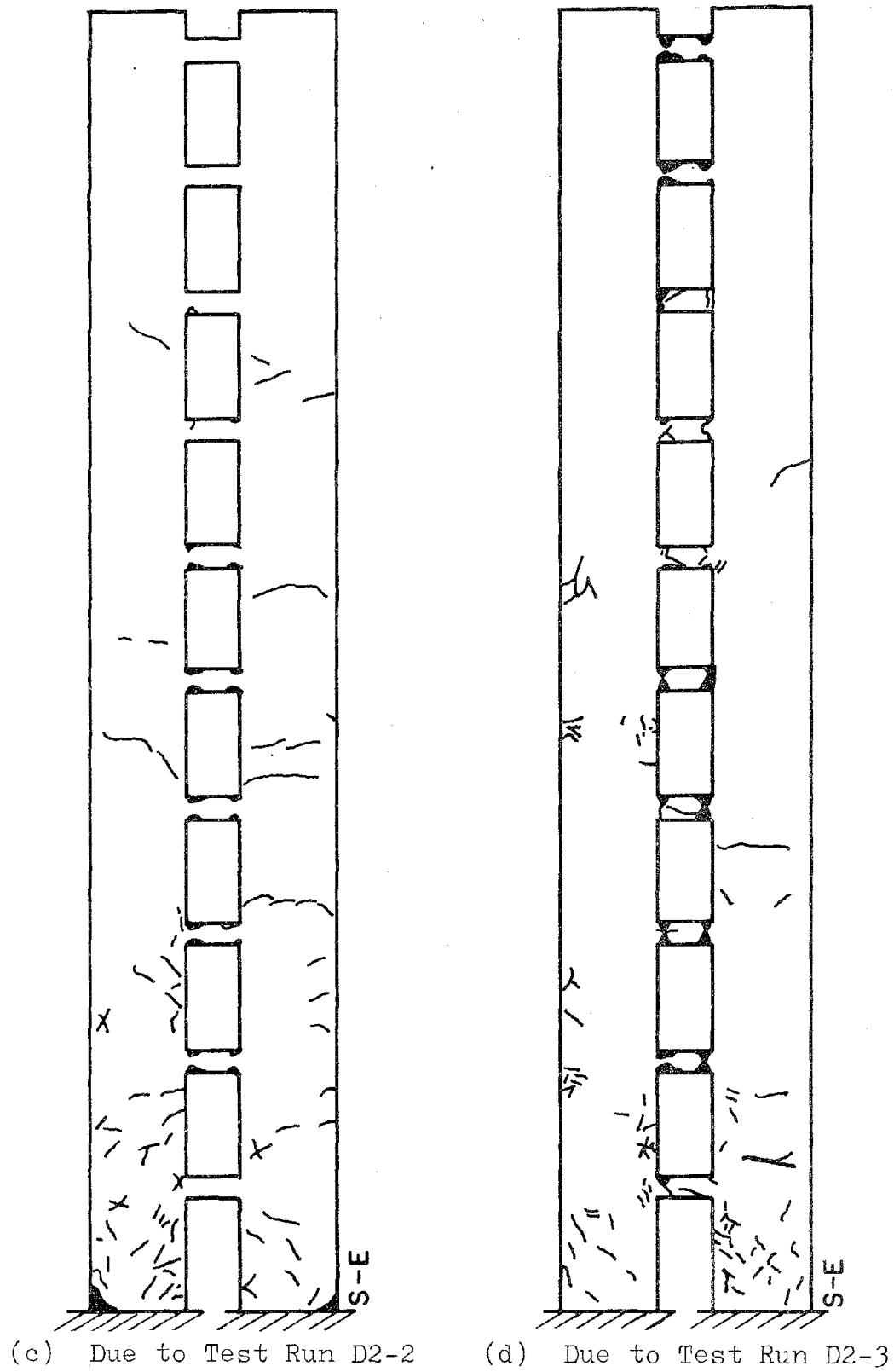
Fig. 4.16 (Contd) Crack Patterns Observed in Test Structure D2
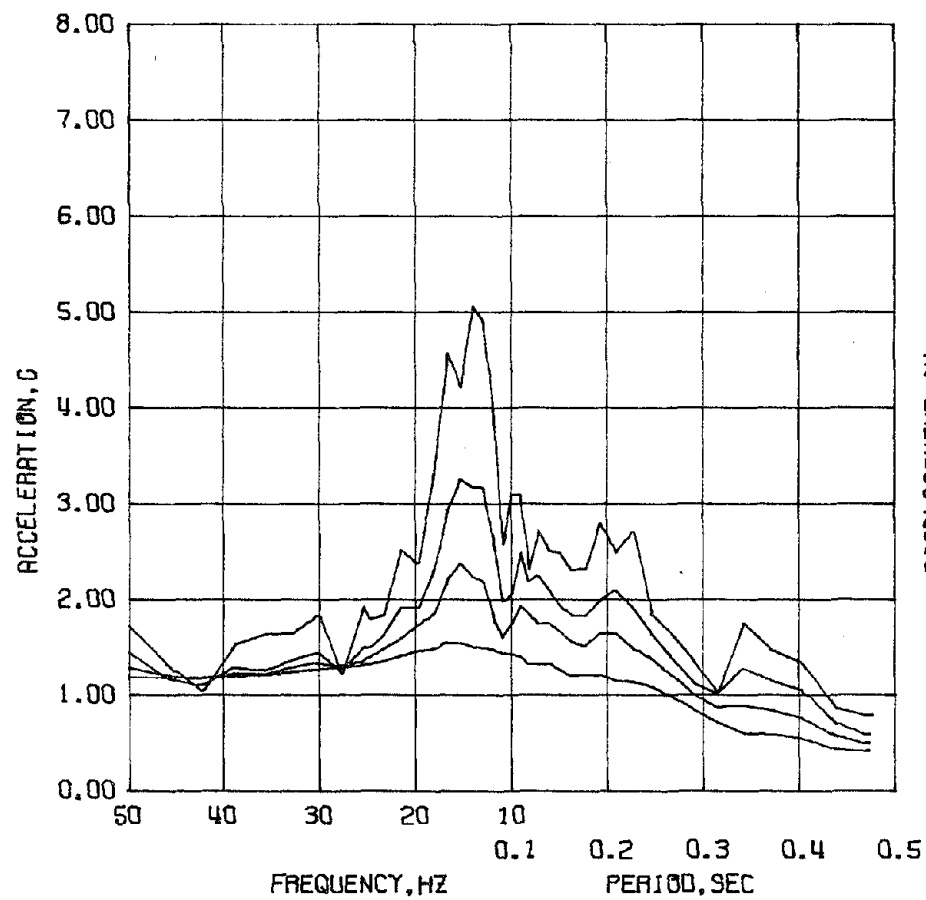
Fig. 4.17 Test Run D2-2. Linear Response Spectra
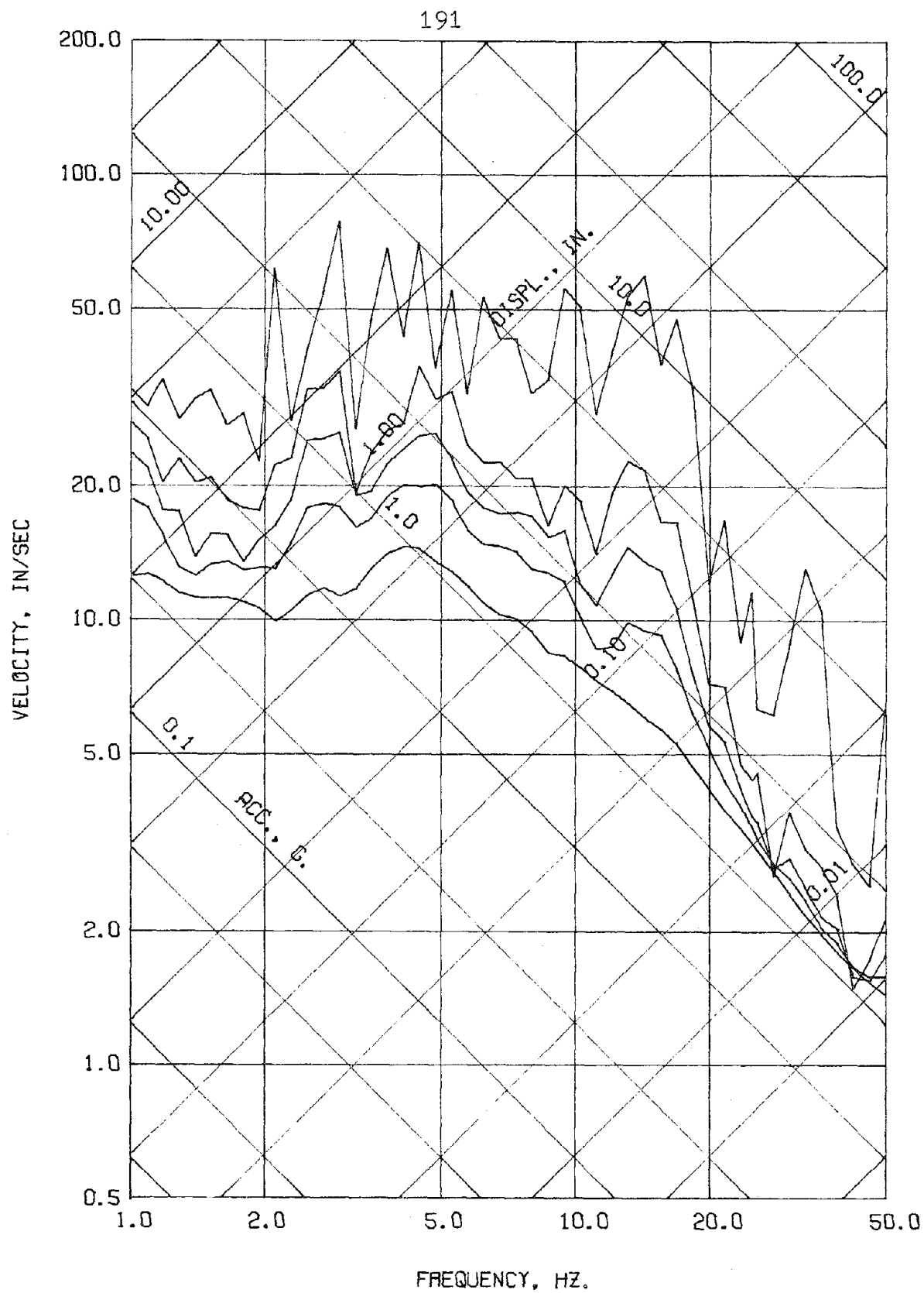
DYN. TEST D2 – RUN 2 – ACC. BS – (BASE SOUTH)

DAMPING FACTOR = 0.00 0.02 0.05 0.10 0.20

Fig. 4.18 Test Run D2-2. Linear Response Spectra

Fig. 4.19 Observed Response, Test Run D2-2

Fig. 4.19 (Contd) Observed Response, Test Run D2-2

Fig. 4.19 (Contd) Observed Response, Test Run D2-2

BASE ACCELERATION.UNIT=G

FIRST - LEVEL ACCELERATION.UNIT=G

SECOND-LEVEL ACCELERATION.UNIT=G

THIRD - LEVEL ACCELERATION.UNIT=G

TIME, SEC.

DYN. TEST D2 - RUN 2 - ACC. BS - (BASE SOUTH)   SCALE- 1.0000   G

DYN. TEST D2 - RUN 2 - ACC. 1S - (ONE SOUTH)   SCALE- 1.0000   G

DYN. TEST D2 - RUN 2 - ACC. 2S - (TWO SOUTH)   SCALE- 1.0000   G

DYN. TEST D2 - RUN 2 - ACC. 3S - (THREE SOUTH)   SCALE- 1.0000   G

Fig. 4.20   Observed Response, Test Run D2-2

196

Fig. 4.20 (Contd) Observed Response, Test Run D2-2

Fig. 4.20 (Contd) Observed Response, Test Run D2-2
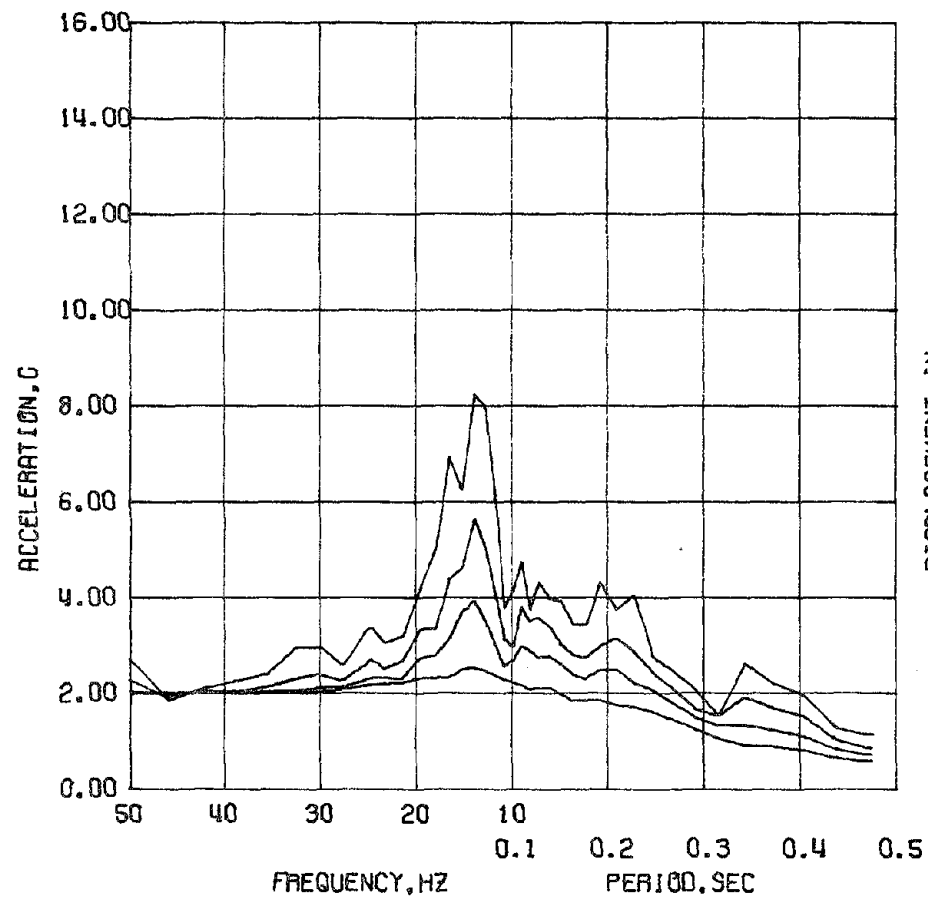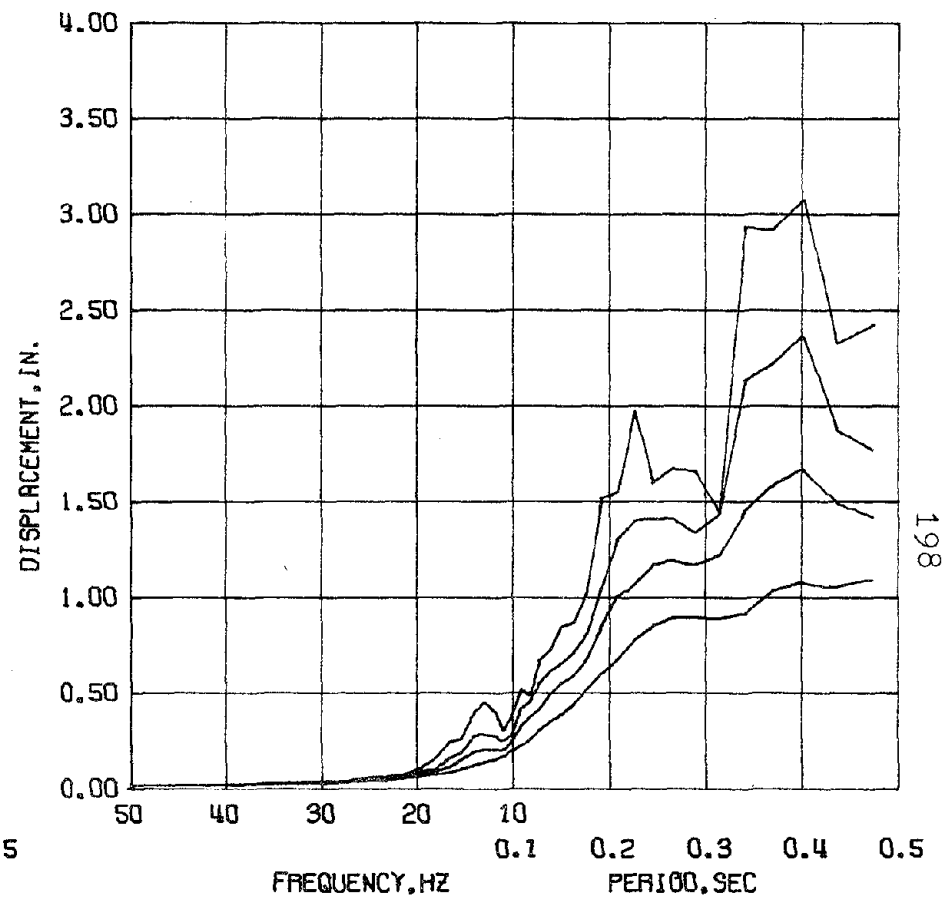
Fig. 4.21   Test Run D2-3. Linear Response Spectra
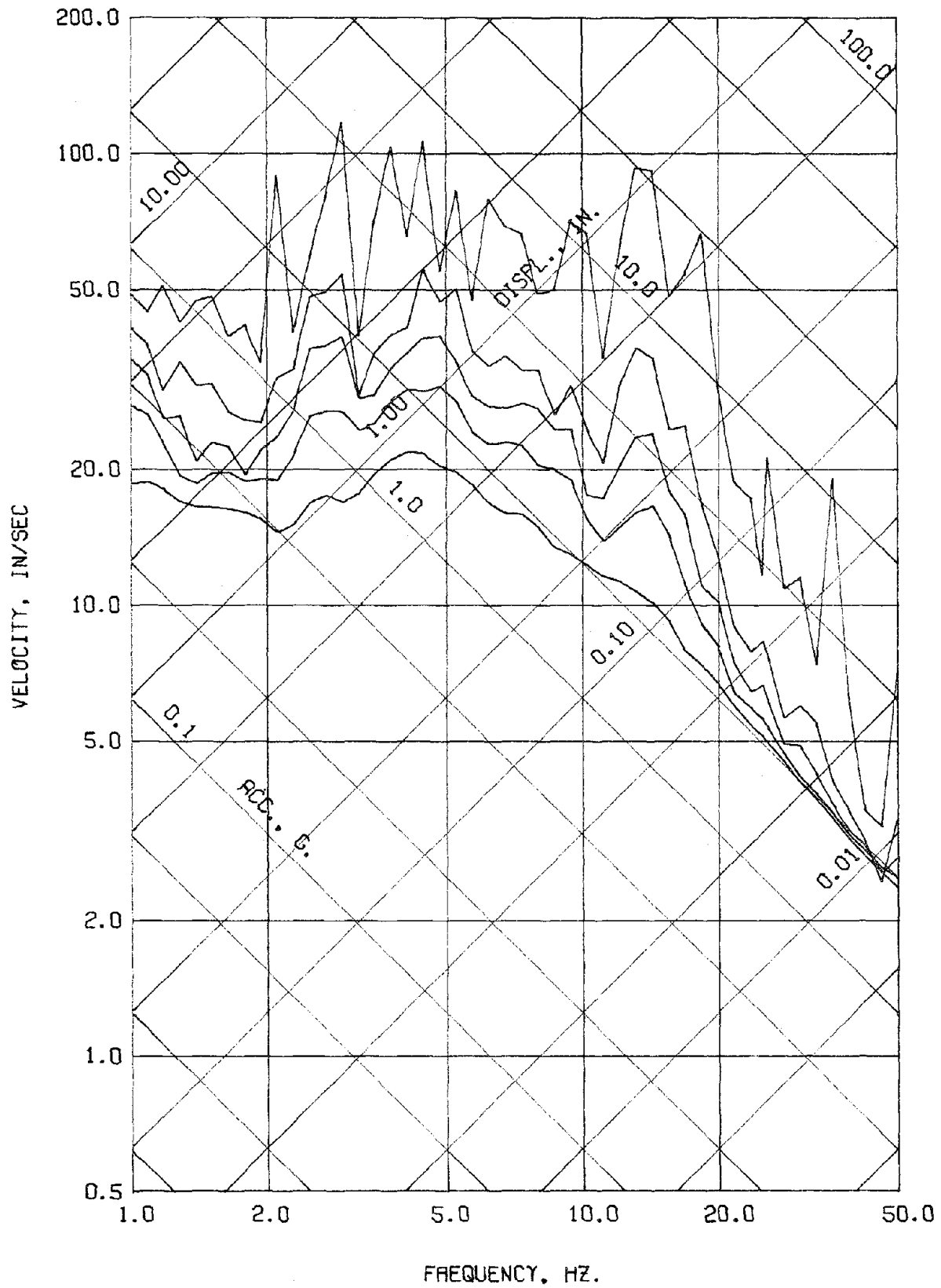
Fig. 4.22 Test Run D2-3. Linear Response Spectra

Fig. 4.23 Observed Response, Test Run D2-3

Fig. 4.23 (Contd) Observed Response, Test Run D2-3

Fig. 4.23 (Contd) Observed Response, Test Run D2-3

Fig. 4.24   Observed Response, Test Run D2-3

Fig. 4.24 (Contd) Observed Response, Test Run D2-3

Fig. 4.24 (Contd) Observed Response, Test Run D2-3

Fig. 4.25 Test Run M1-1. Linear Response Spectra
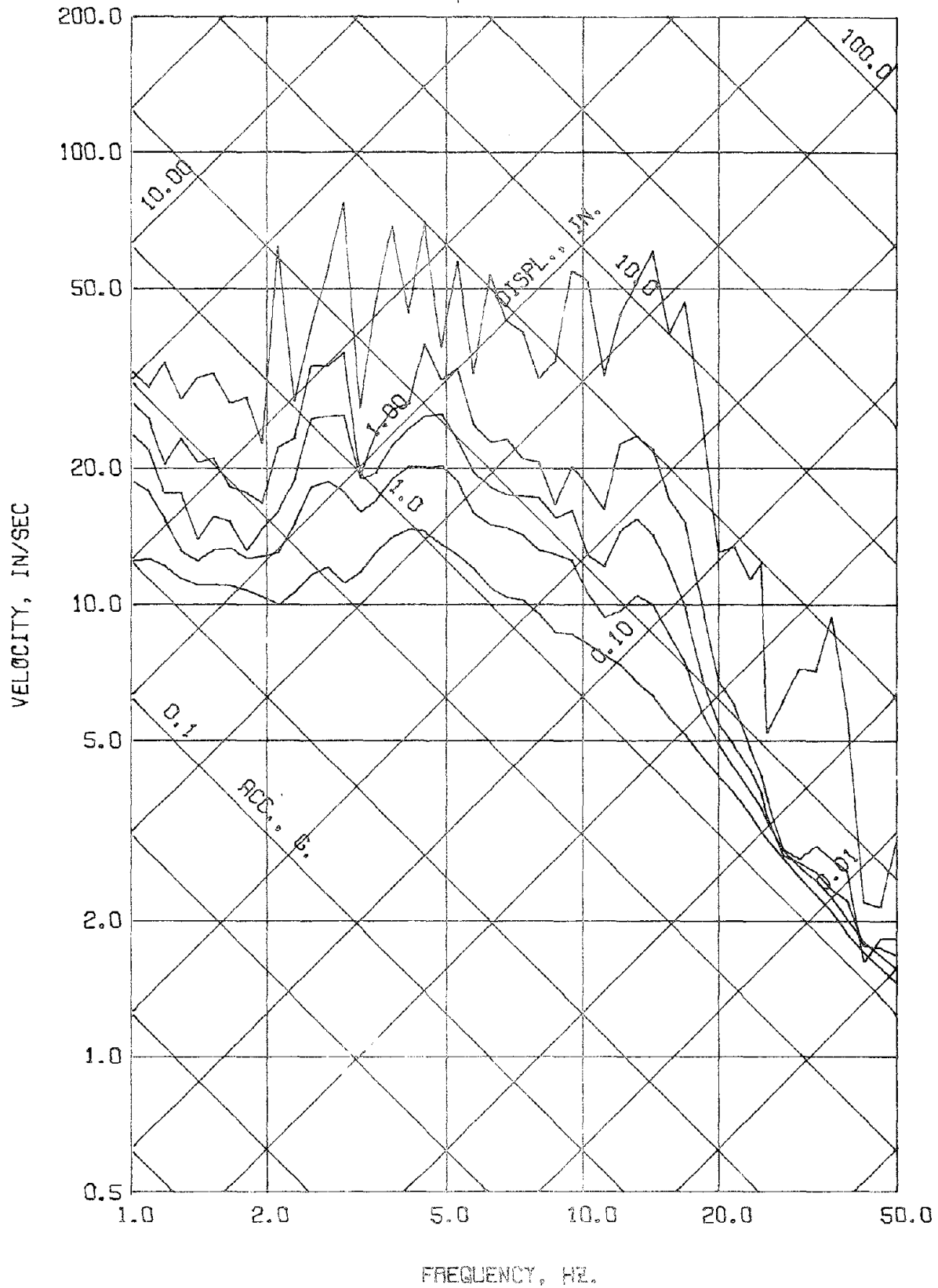
DYN. TEST M1 — RUN 1 — ACC. BS — (BASE SOUTH)

DAMPING FACTOR =   0.00 0.02 0.05 0.10 0.20

Fig. 4.26 Test Run M1-1. Linear Response Spectra

Fig. 4.27 Observed Response, Test Run M1-1 (North)

Fig. 4.27 (Contd) Observed Response, Test Run M1-1 (South)

Fig. 4.27 (Contd) Observed Response, Test Run M1-1 (South)

Fig. 4.27 (Contd) Observed Response, Test Run M1-1 (North)

Fig. 4.27 (Contd) Observed Response, Test Run M1-1 (North)

EIGHTH- LEVEL DISPLACEMENT,UNIT=INCH

NINTH- LEVEL DISPLACEMENT,UNIT=INCH

TENTH- LEVEL DISPLACEMENT,UNIT=INCH

P-DELTA BASE MOMENT,UNIT=KIP-INCH

TIME, SEC.

Fig. 4.27 (Contd) Observed Response, Test Run M1-1 (South)

BASE ACCELERATION,UNIT=G

FIRST- LEVEL ACCELERATION,UNIT=G

SECOND-LEVEL ACCELERATION,UNIT=G

THIRD- LEVEL ACCELERATION,UNIT=G

TIME, SEC.

DYN. TEST M1 - RUN 1 - ACC. BN - (BASE NORTH)
                                    SCALE=   1.0000

DYN. TEST M1 - RUN 1 - ACC. 1N - (ONE NORTH)
                                    SCALE=   1.0000

DYN. TEST M1 - RUN 1 - ACC. 2N - (TWO NORTH)
                                    SCALE=   1.0000

DYN. TEST M1 - RUN 1 - ACC. 3N - (THREE NORTH)
                                    SCALE=   1.0000

Fig. 4.28 Observed Response, Test Run M1-1 (North)

Fig. 4.28 (Contd) Observed Response, Test Run M1-1 (South)

Fig. 4.28 (Contd) Observed Response, Test Run M1-1 (North)

216

FOURTH-LEVEL ACCELERATION,UNIT=G

FIFTH-LEVEL ACCELERATION,UNIT=G

SIXTH-LEVEL ACCELERATION,UNIT=G

SEVENTH-LEVEL ACCELERATION,UNIT=G

TIME, SEC.

Fig. 4.28 (Contd) Observed Response, Test Run M1-1 (South)

Fig. 4.28 (Contd) Observed Response, Test Run M1-1 (North)

Fig. 4.28 (Contd) Observed Response, Test Run M1-1 (South)

(a) Due to Shrinkage   (b) Due to Test Run M1-1

Fig. 4.29 Crack Patterns Observed in Test Structure M1

Fig. 4.30 Damage in Lower Piers of Test Structure M
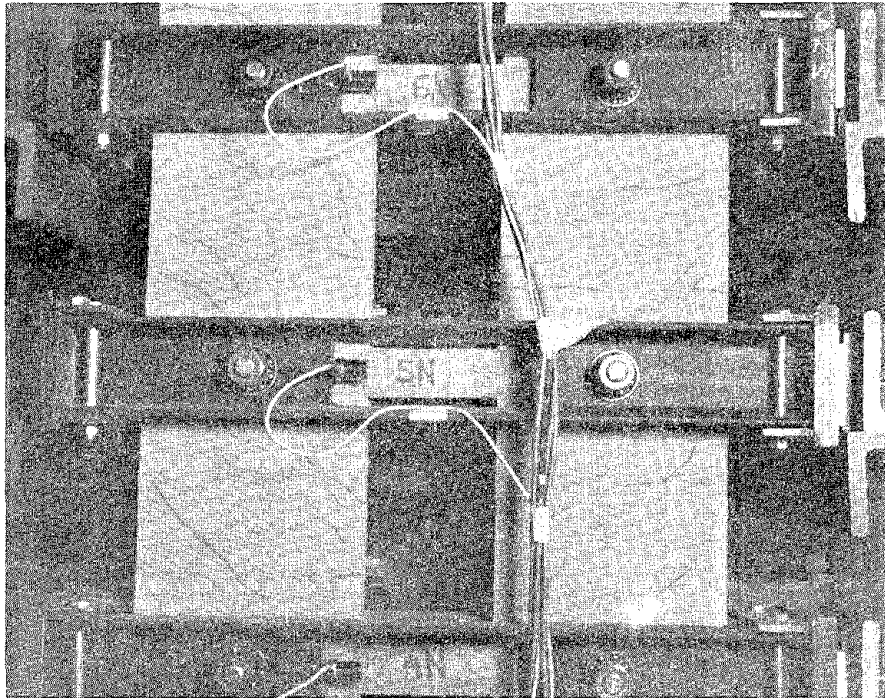
(b)   Damage in The Fourth and Fifth Levels
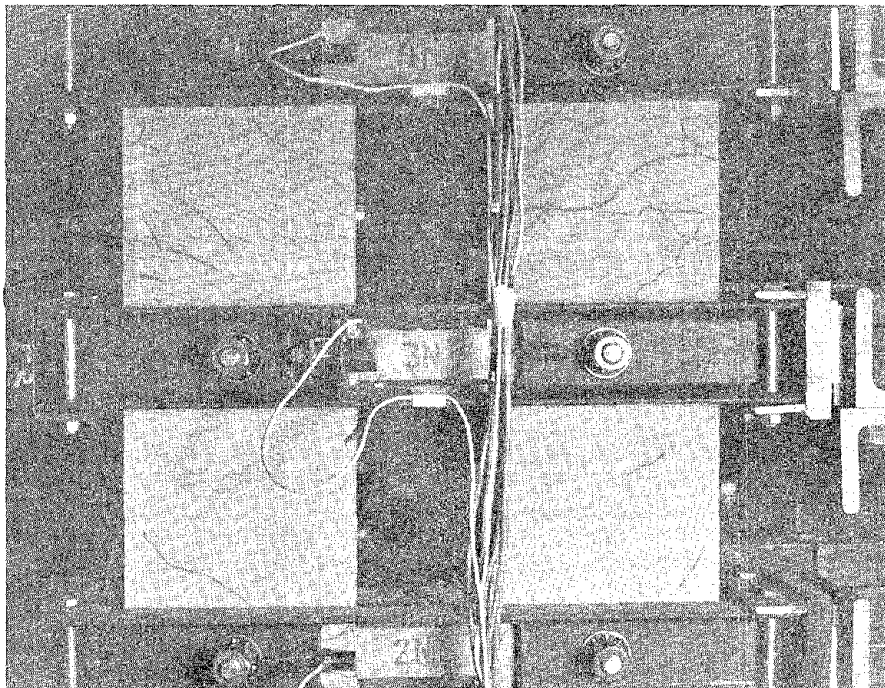
(a)   Damage in The Second and Third Levels

Fig. 4.31   Damage in Test Structure M (Test Run M1-1)
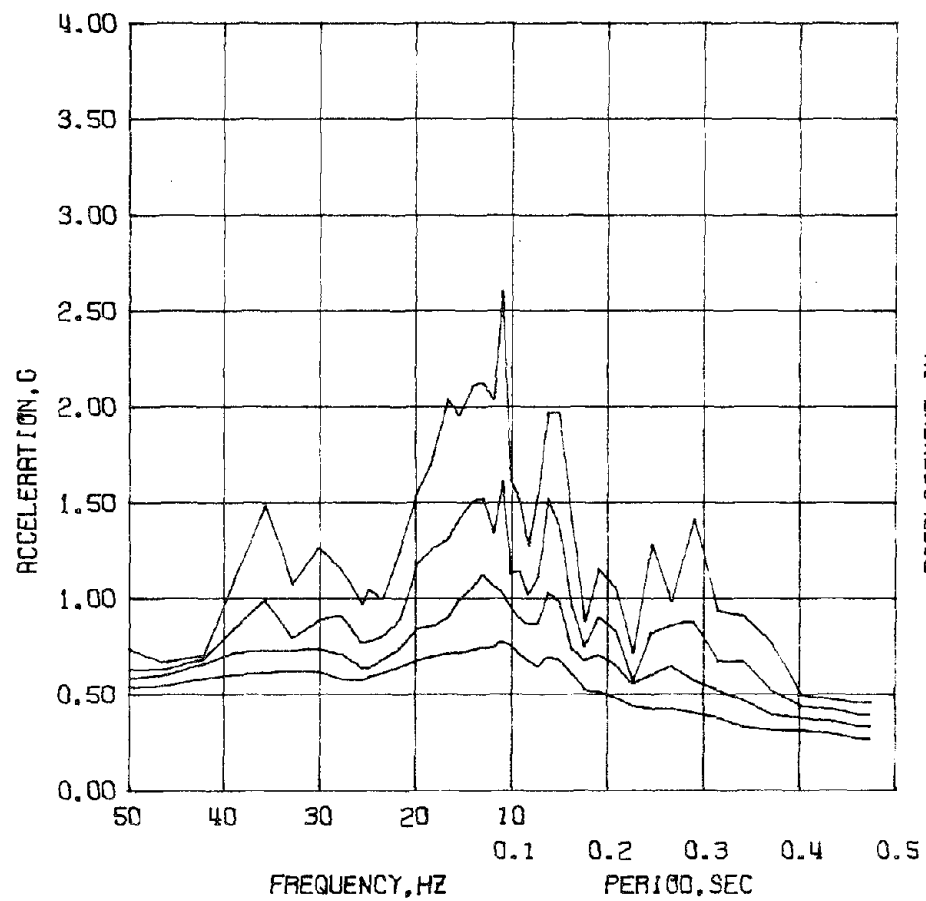
DYN. TEST D3 - RUN 1 - ACC. BS - (BASE SOUTH)
DAMPING FACTOR =   0.02 0.05 0.10 0.20
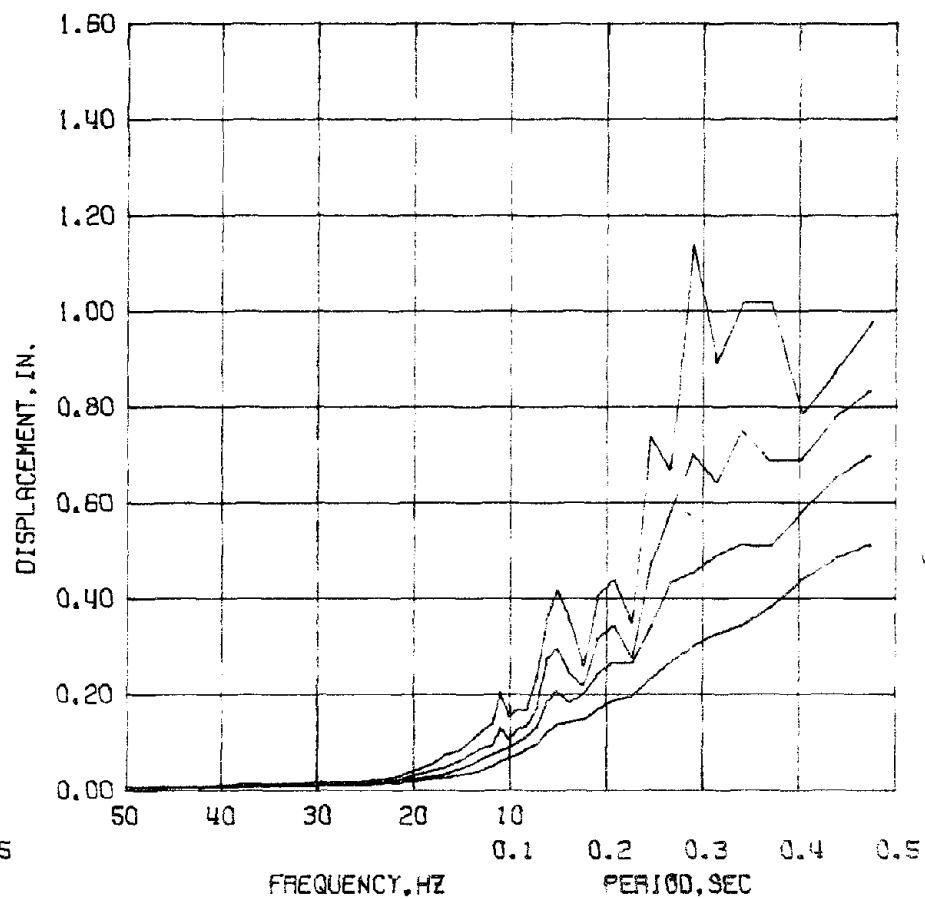
DYN. TEST D3 - RUN 1 - ACC. BS - (BASE SOUTH)
DAMPING FACTOR =   0.02 0.05 0.10 0.20

Fig. 4.32   Test Run D3-1. Linear Response Spectra
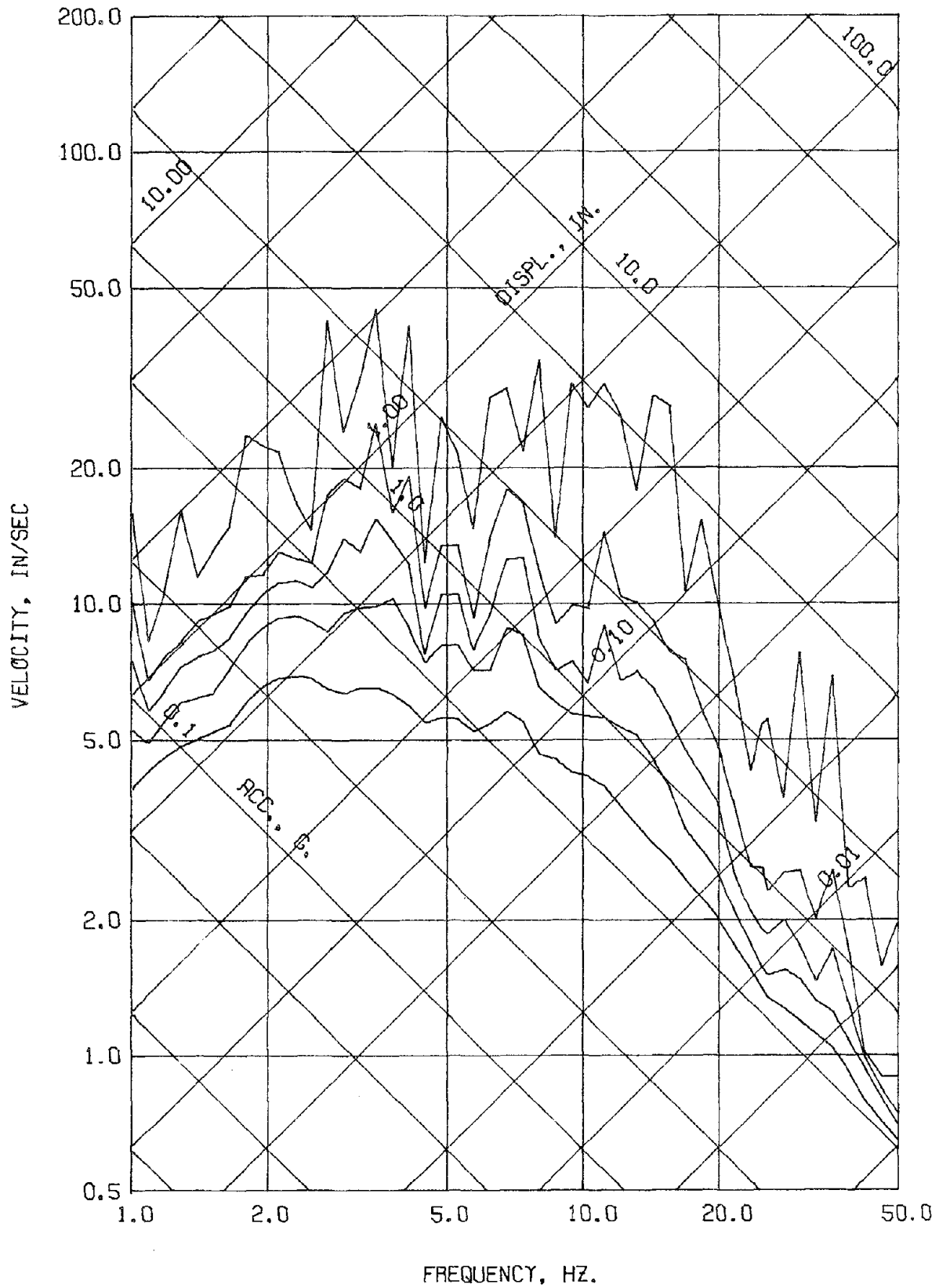
DYN. TEST D3 — RUN 1 — ACC. BS — (BASE SOUTH)

DAMPING FACTOR =   0.00 0.02 0.05 0.10 0.20

Fig. 4.33 Test Run D3-1. Linear Response Spectra

Fig. 4.34   Observed Response, Test Run D3-1

Fig. 4.34 (Contd) Observed Response, Test Run D3-1

Fig. 4.34 (Contd) Observed Response, Test Run D3-1

Fig. 4.35 Observed Response, Test Run D3-1

Fig. 4.35 (Contd) Observed Response, Test Run D3-1

Fig. 4.35 (Contd) Observed Response, Test Run D3-1

(a)   Due to Shrinkage   (b)   Due to Test Run D3-1

Fig. 4.36   Crack Patterns Observed in Test Structure D3
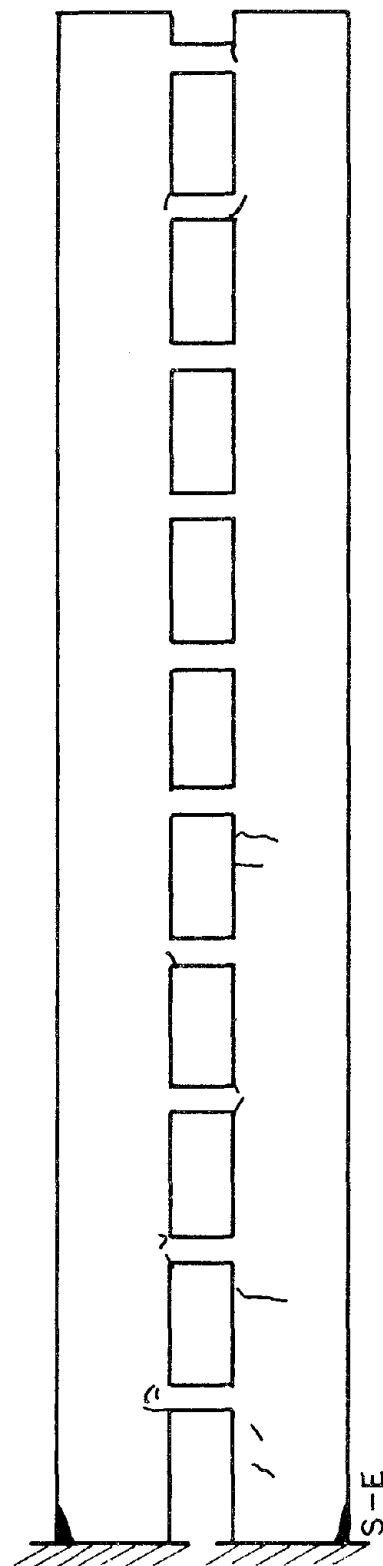
(c)   Due to Test Run D3-2

Fig. 4.36 (Contd) Crack Patterns Observed in Test Structure D3
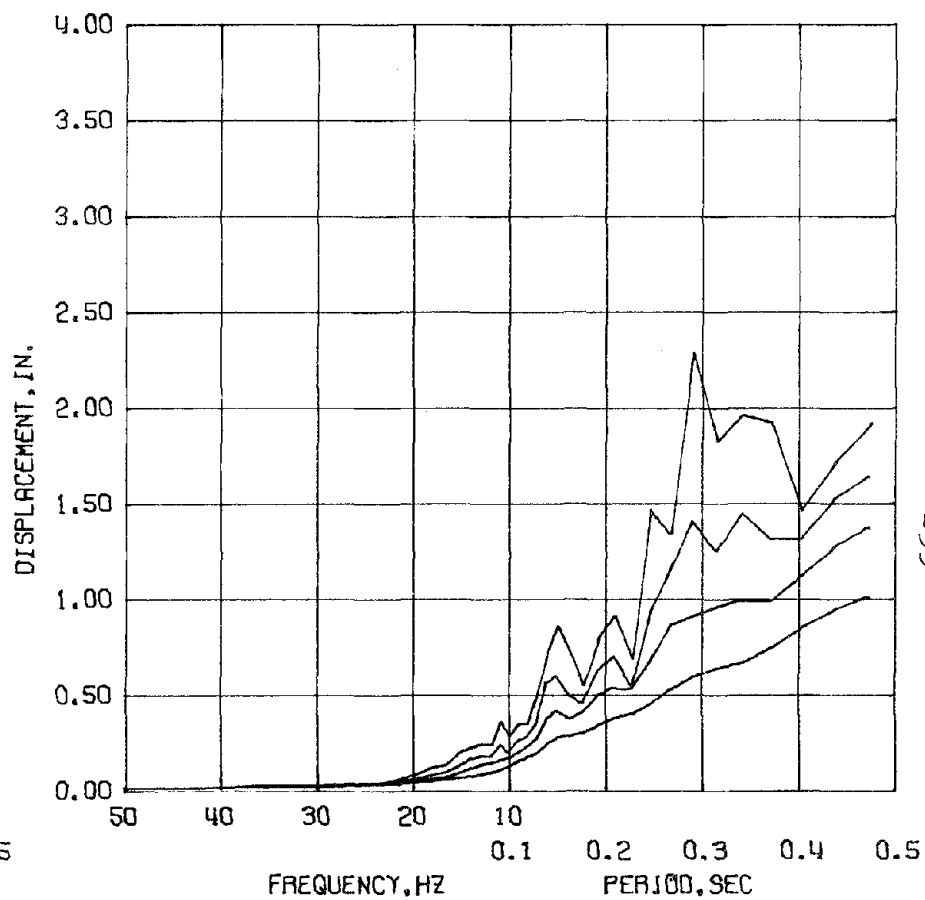
Fig. 4.37   Test Run D3-2. Linear Response Spectra
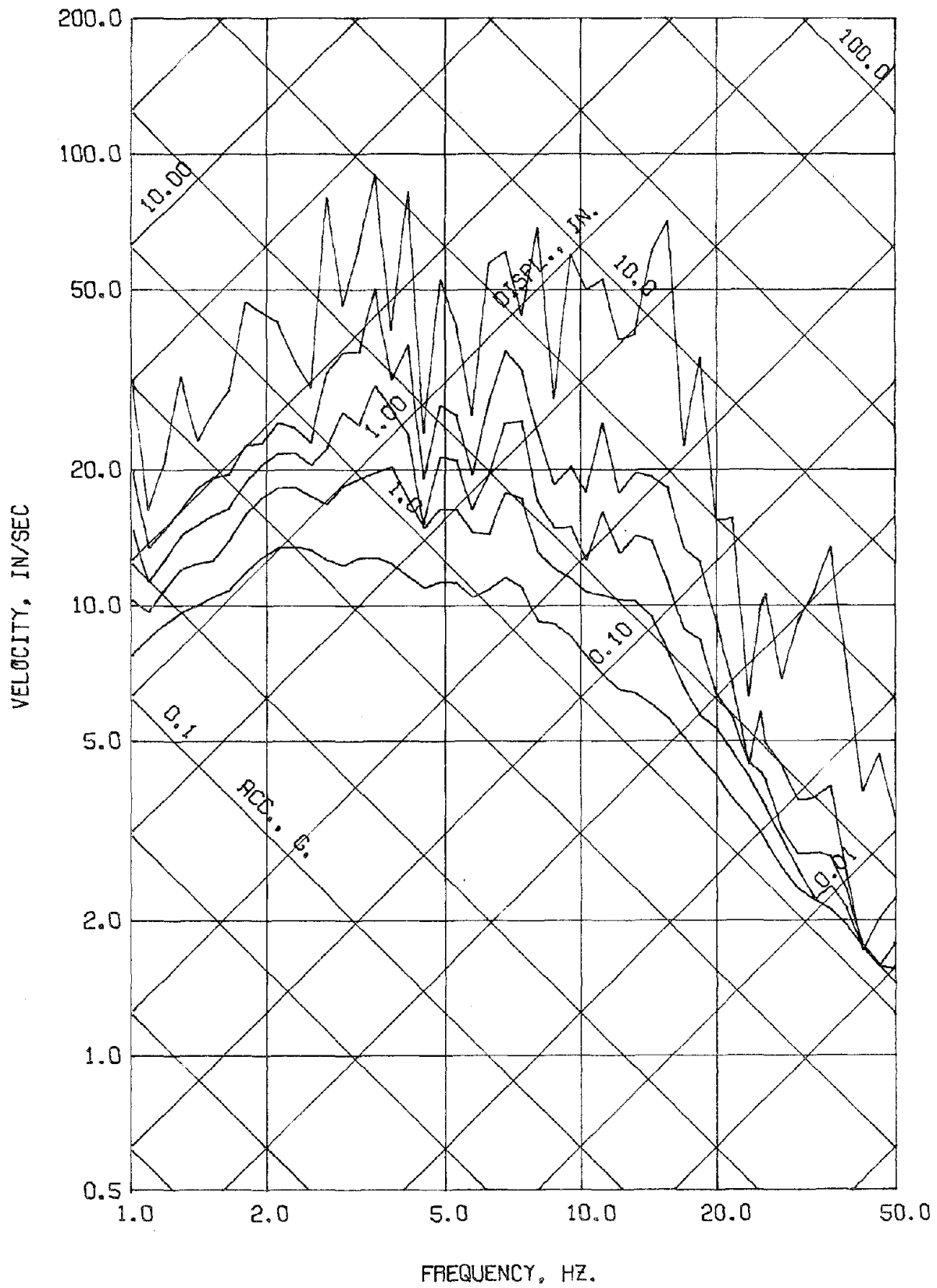
Fig. 4.38 Test Run D3-2. Linear Response Spectra
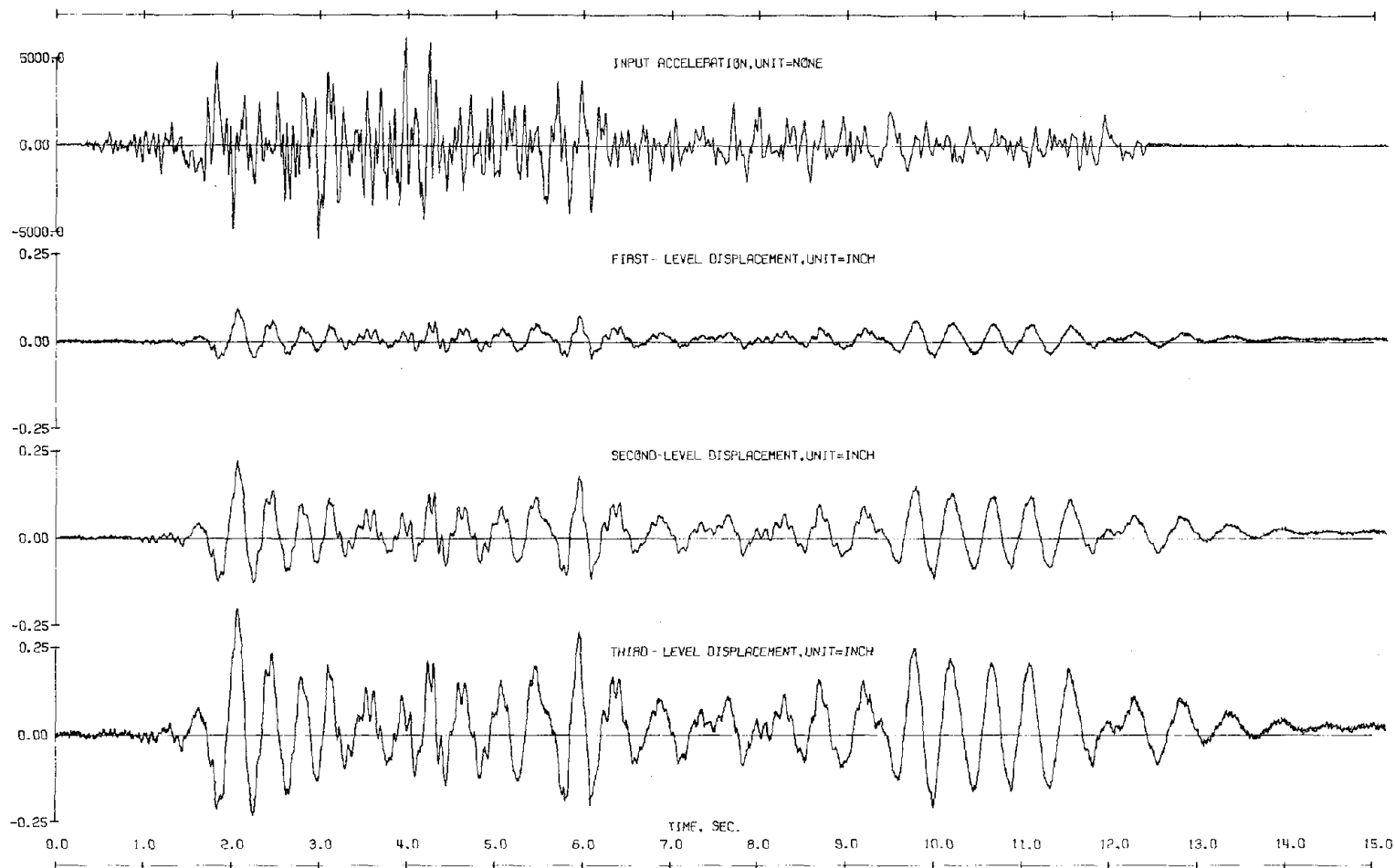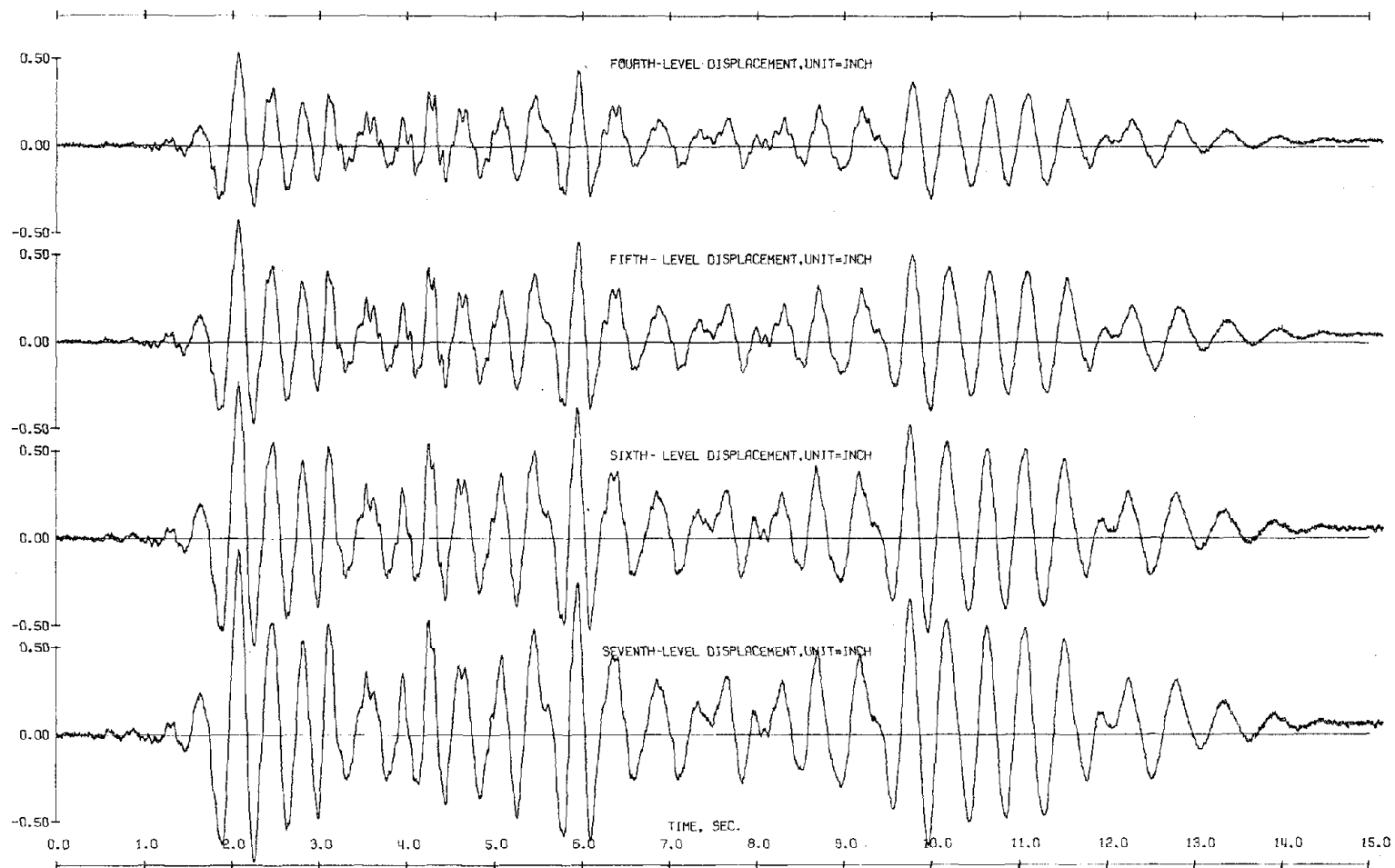
Fig. 4.39 Observed Response, Test Run D3-2

Fig. 4.39 (Contd) Observed Response, Test Run D3-2

Fig. 4.39 (Contd) Observed Response, Test Run D3-2

Fig. 4.40   Observed Response, Test Run D3-2

Fig. 4.40 (Contd) Observed Response, Test Run D3-2

Fig. 4.40 (Contd) Observed Response, Test Run D3-2

DYN. TEST D1 - RUN 1 - LVOT 1S - (ONE SOUTH)

DYN. TEST D1 - RUN 1 - LVOT 2S - (TWO SOUTH)

DYN. TEST D1 - RUN 1 - LVOT 3S - (THREE SOUTH)

DYN. TEST D1 - RUN 1 - LVOT 4S - (FOUR SOUTH)

DYN. TEST D1 - RUN 1 - LVOT 5S - (FIVE SOUTH)

DYN. TEST D1 - RUN 1 - LVOT 6S - (SIX SOUTH)

DYN. TEST D1 - RUN 1 - LVOT 7S - (SEVEN SOUTH)

DYN. TEST D1 - RUN 1 - LVOT 8S - (EIGTH SOUTH)

DYN. TEST D1 - RUN 1 - LVOT 9S - (NINE SOUTH)

DYN. TEST D1 - RUN 1 - LVOT 10S - (TEN SOUTH)

Fig. 5.1a Amplitude Fourier Spectra of Displacements, Test Run D1-1

241

DYN. TEST D1 - RUN 1 - ACC. 1S - (ONE SOUTH)

DYN. TEST D1 - RUN 1 - ACC. 6S - (SIX SOUTH)

DYN. TEST D1 - RUN 1 - ACC. 2S - (TWO SOUTH)

DYN. TEST D1 - RUN 1 - ACC. 7S - (SEVEN SOUTH)

DYN. TEST D1 - RUN 1 - ACC. 3S - (THREE SOUTH)

DYN. TEST D1 - RUN 1 - ACC. 8S - (EIGTH SOUTH)

DYN. TEST D1 - RUN 1 - ACC. 4S - (FOUR SOUTH)

DYN. TEST D1 - RUN 1 - ACC. 9S - (NINE SOUTH)

DYN. TEST D1 - RUN 1 - ACC. 5S - (FIVE SOUTH)

DYN. TEST D1 - RUN 1 - ACC. 10S - (TEN SOUTH)

Fig. 5.1b Amplitude Fourier Spectra of Accelerations, Test Run D1-1

Fig. 5.2a Amplitude Fourier Spectra of Displacements, Test Run D1-2

243

Fig. 5.2b Amplitude Fourier Spectra of Accelerations, Test Run D1-2

244

Fig. 5.3   Comparison of Spectrum Intensities of Different Dampings
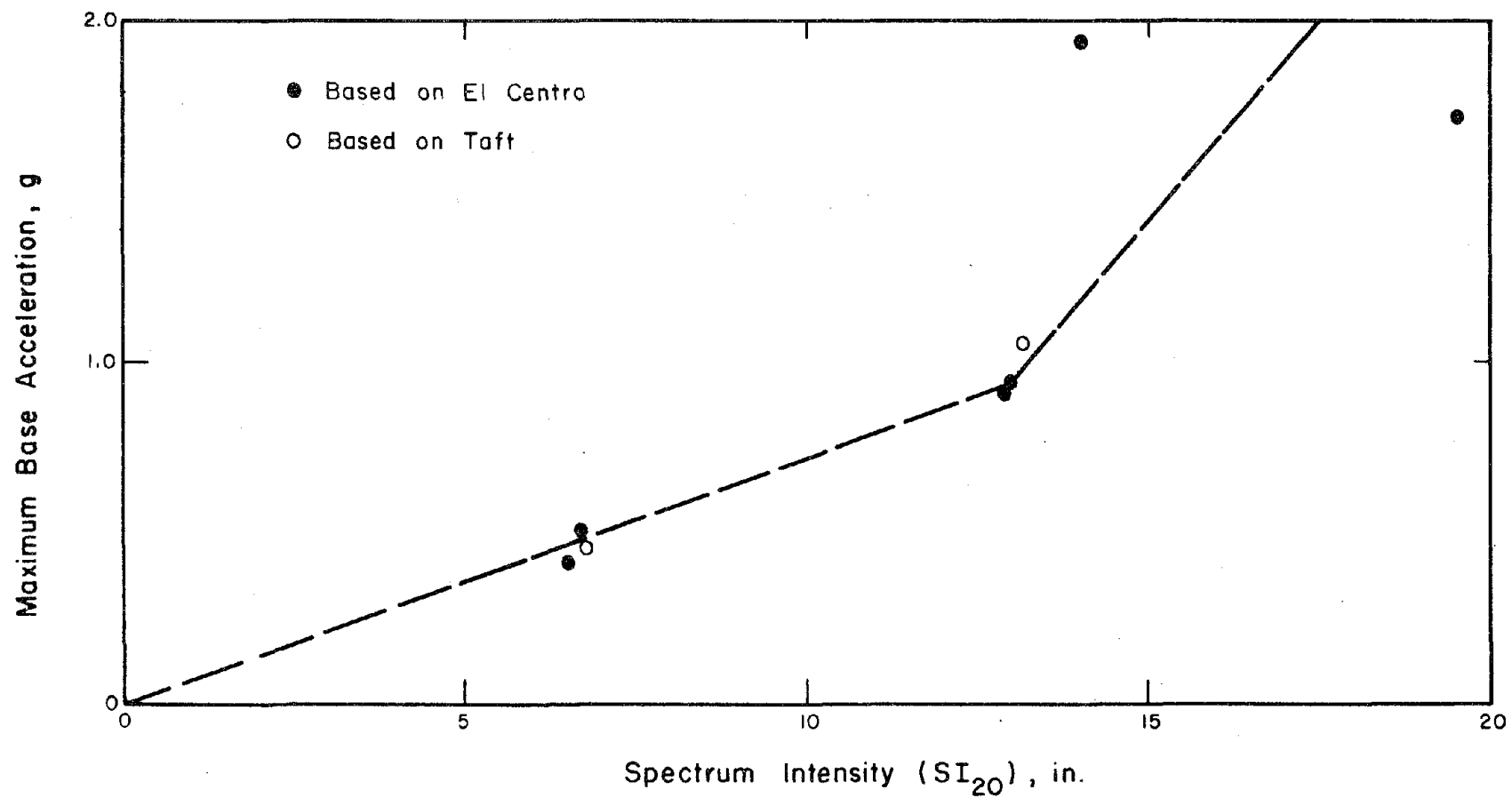
Fig. 5.4   Comparison of Maximum Base Acceleration with Spectrum Intensity
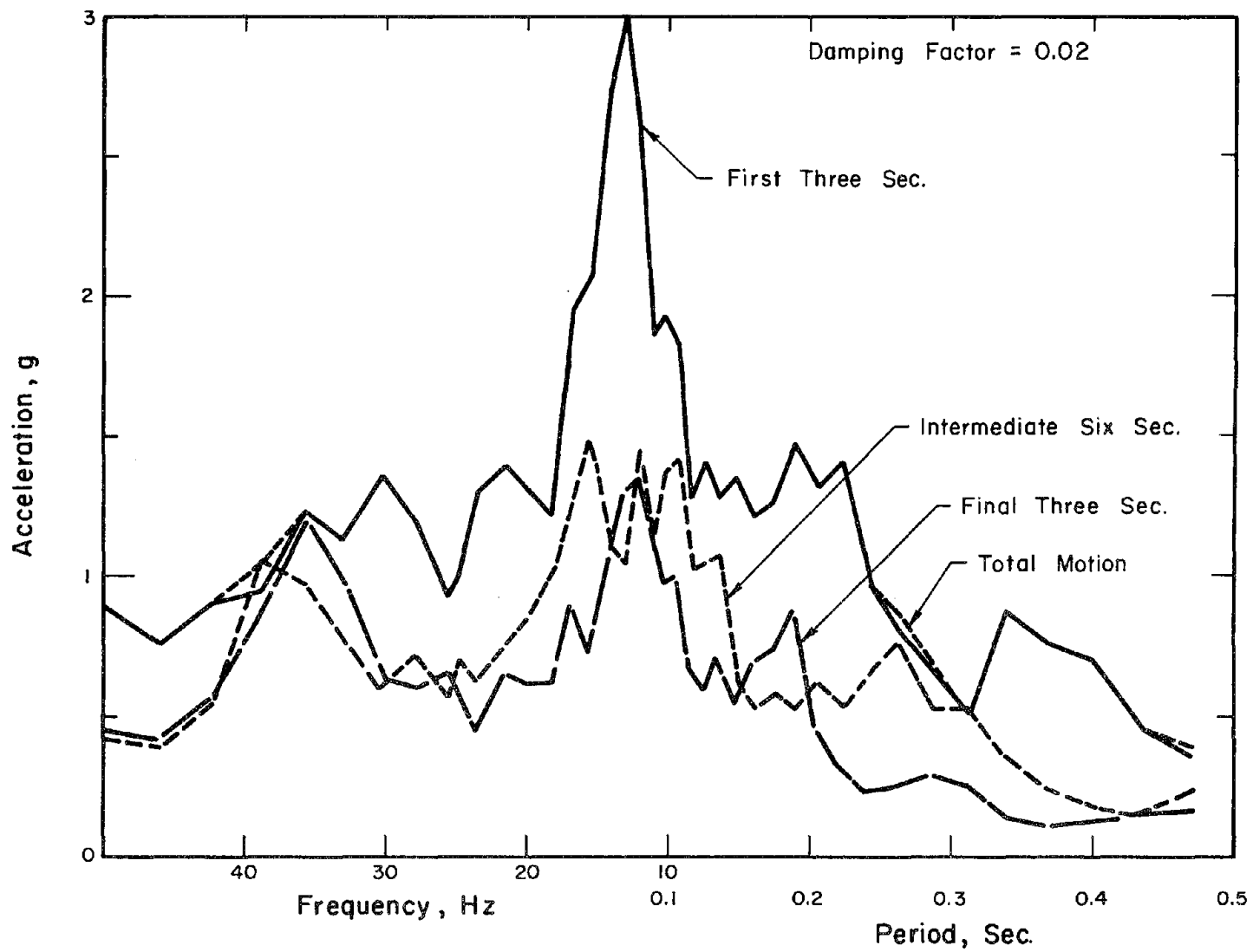
Fig. 5.5a   Response Spectra for Different Time Intervals of
Base Motion of Test Run D1-1
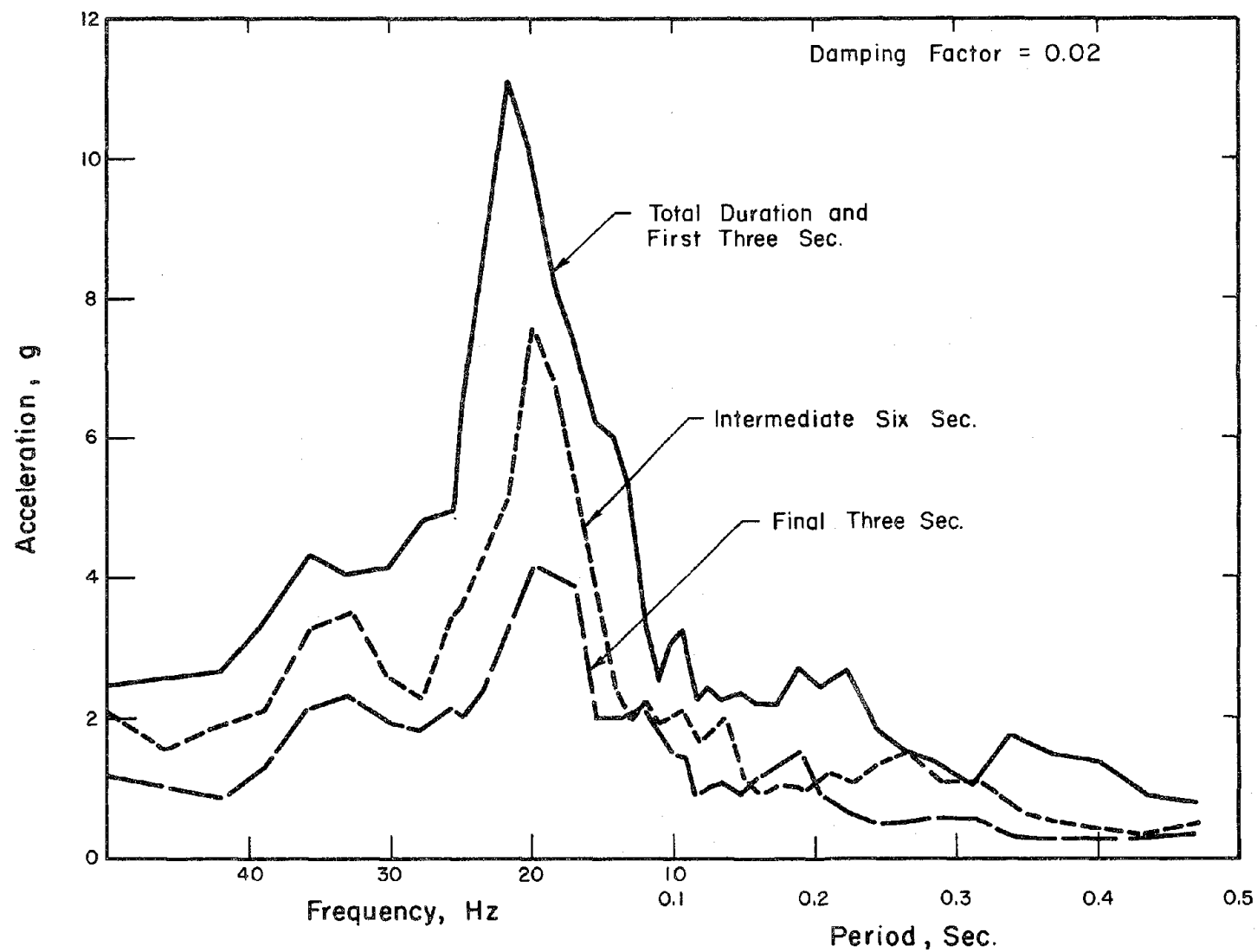
Fig. 5.5b   Response Spectra for Different Time Intrevals of
Base Motion of Test Run D1-2

248
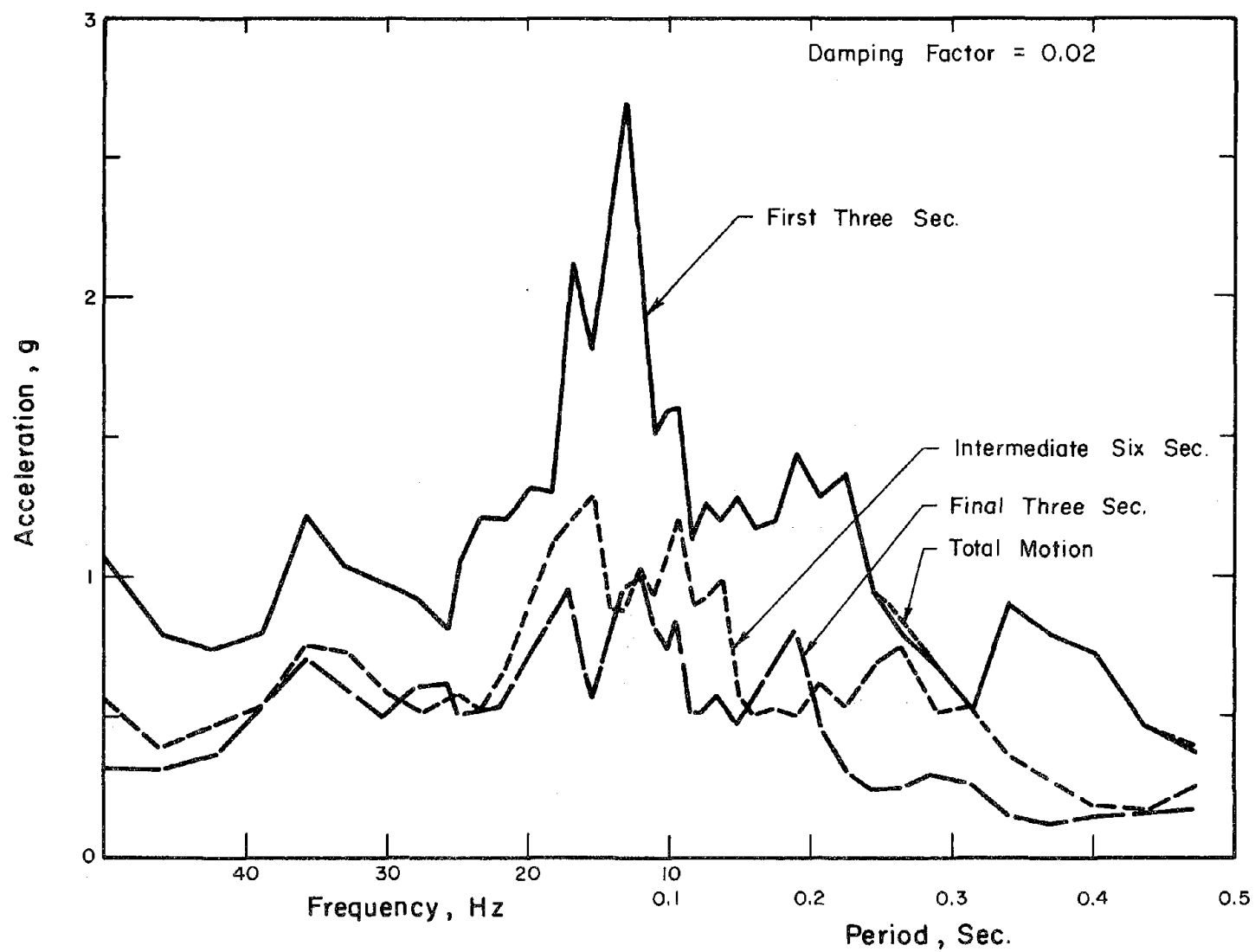
Fig. 5.5c Response Spectra for Different Time Intervals of
Base Motion of Test Run D2-1
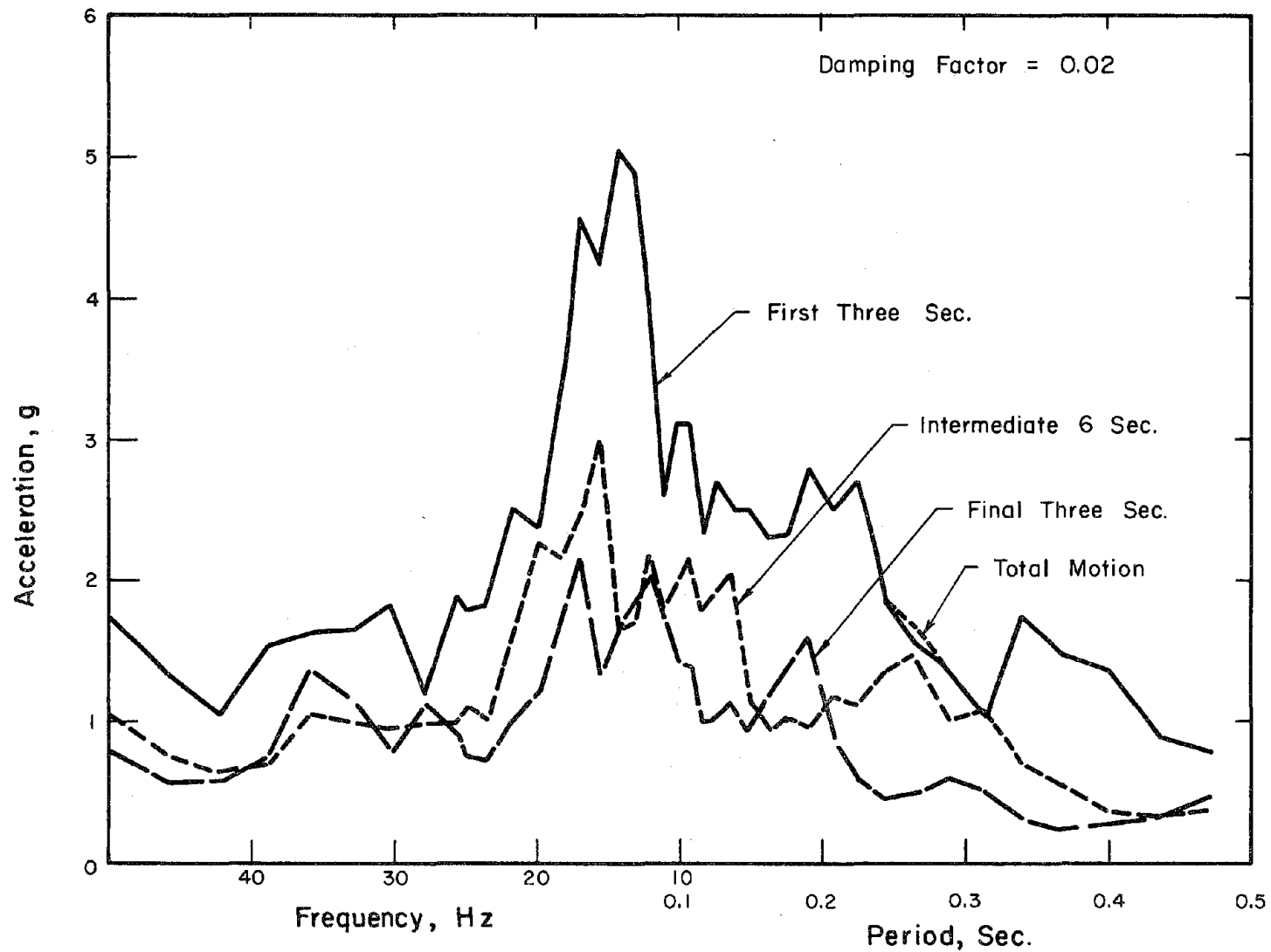
Fig. 5.5d   Response Spectra for Different Time Intervals of
Base Motion of Test Run D2-2
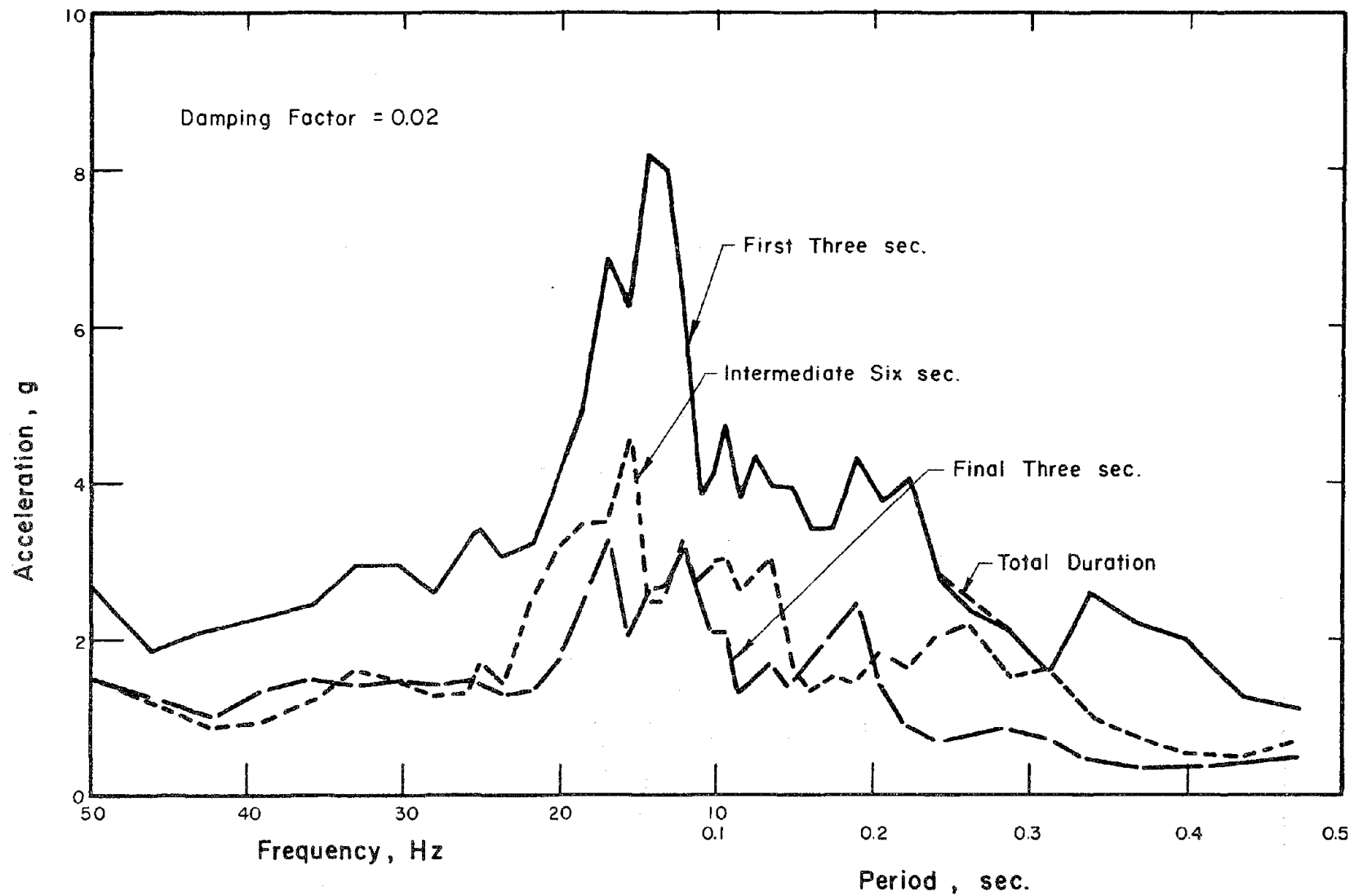
Fig. 5.5e   Response Spectra for Different Time Intervals of
Base Motion of Test Run D2-3

251
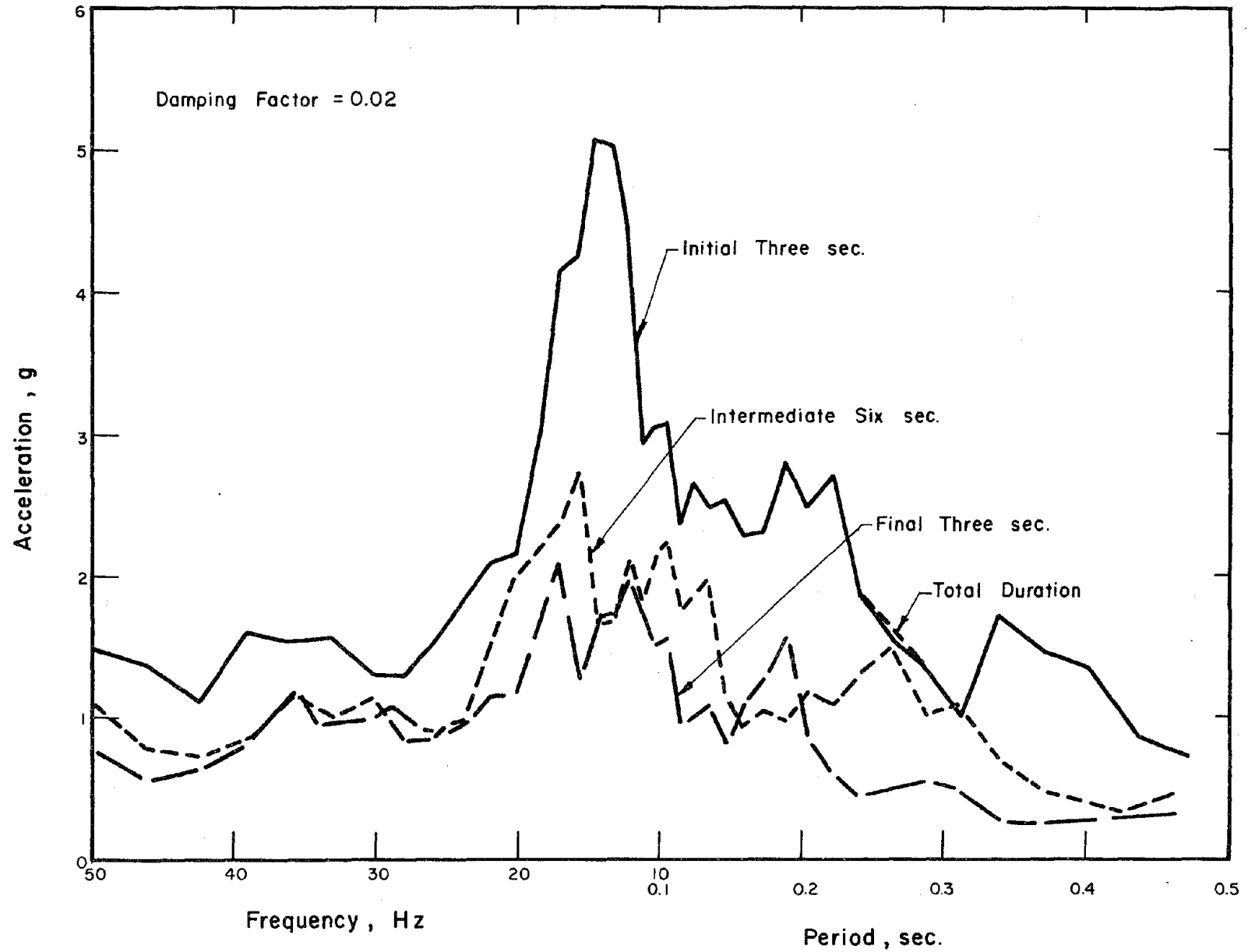
Fig. 5.5f Response Spectra for Different Time Intervals of
Base Motion of Test Run M1-1
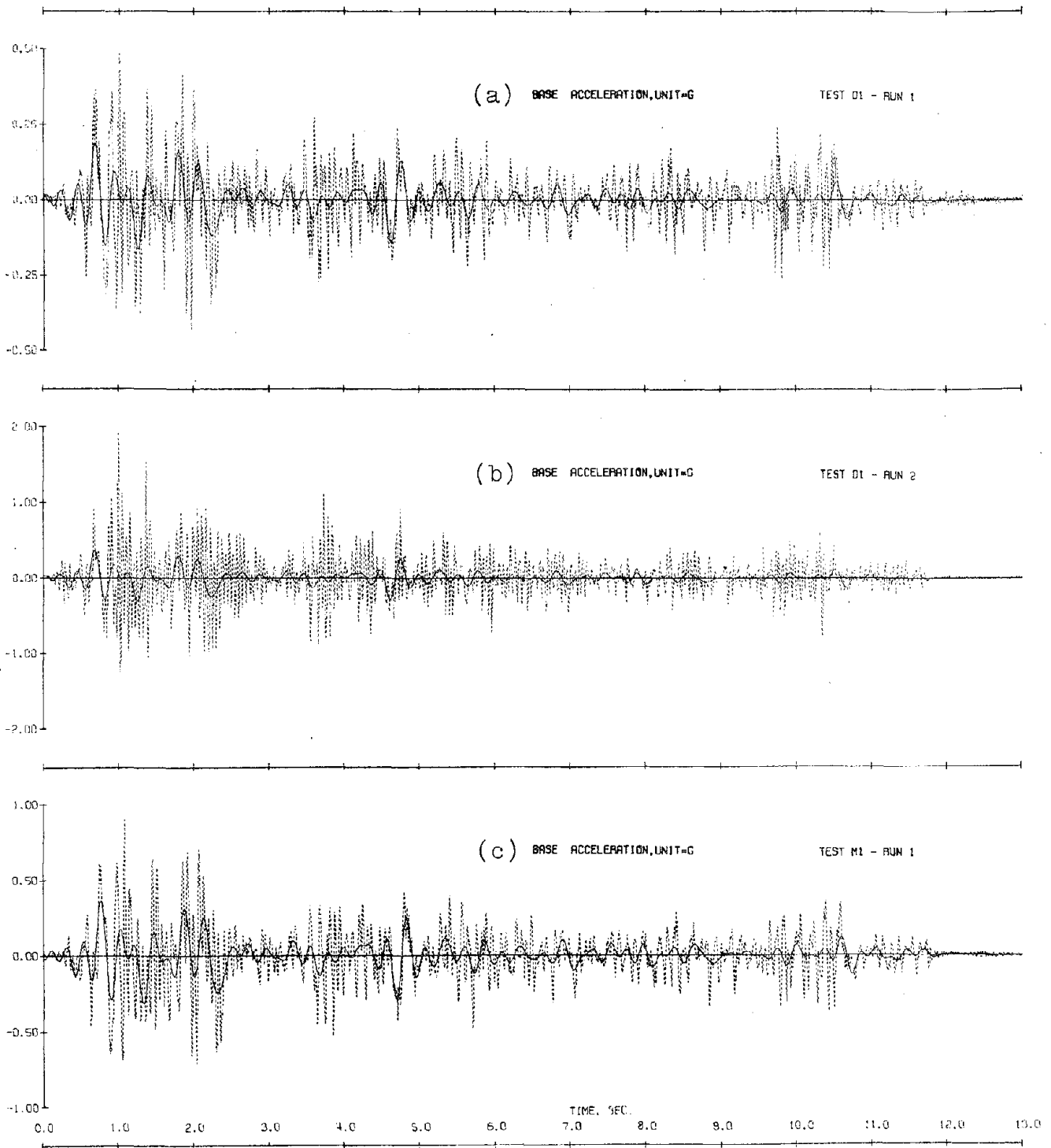
Fig. 5.6   Base Acceleration Wavefoms (Broken Line) and Filtered
Components Below 5.0 Hz (Solid Line)
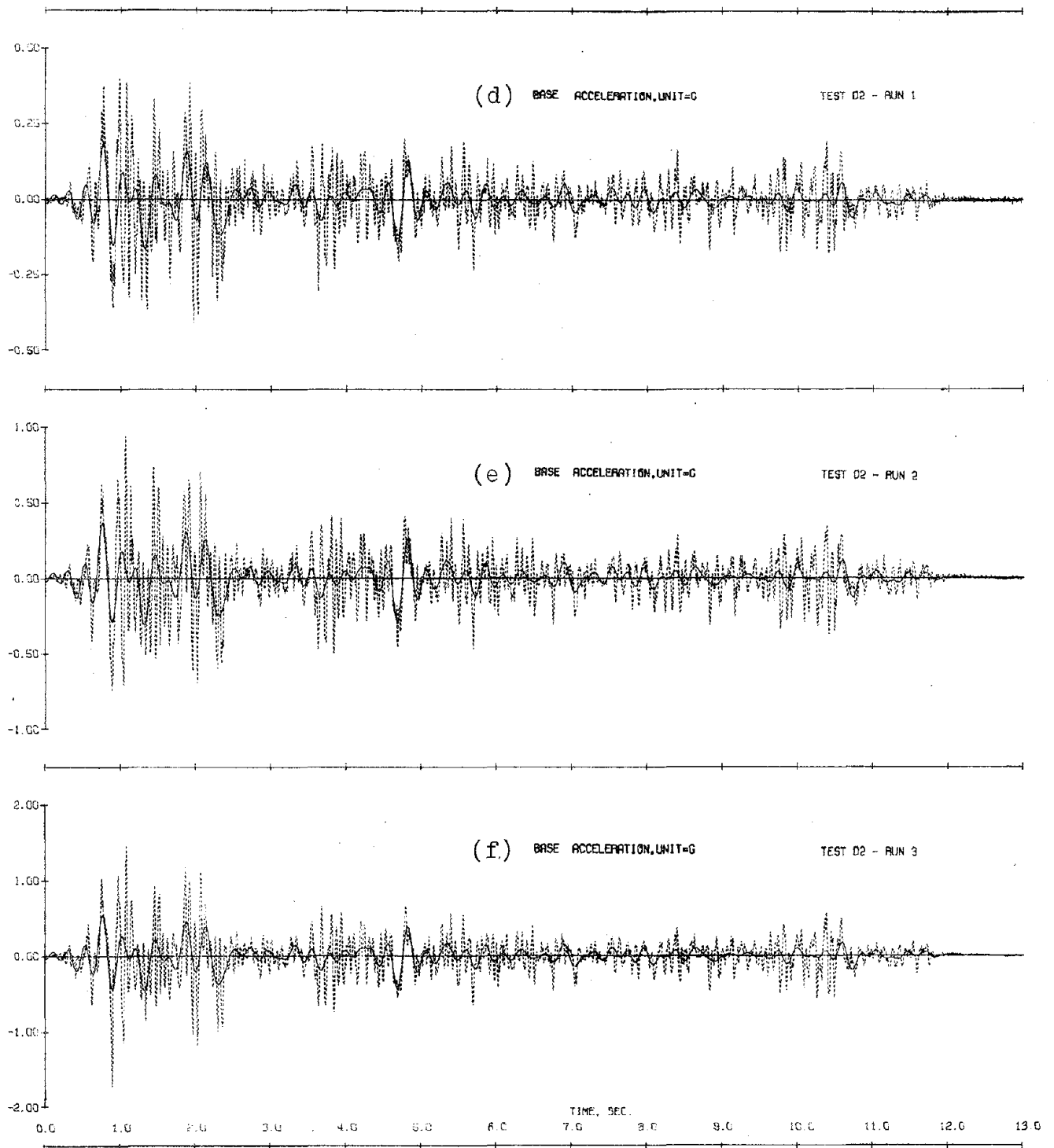
Fig. 5.6 (Contd) Base Acceleration Waveforms (Broken Line) and Filtered Components Below 5.0 Hz (Solid Line)
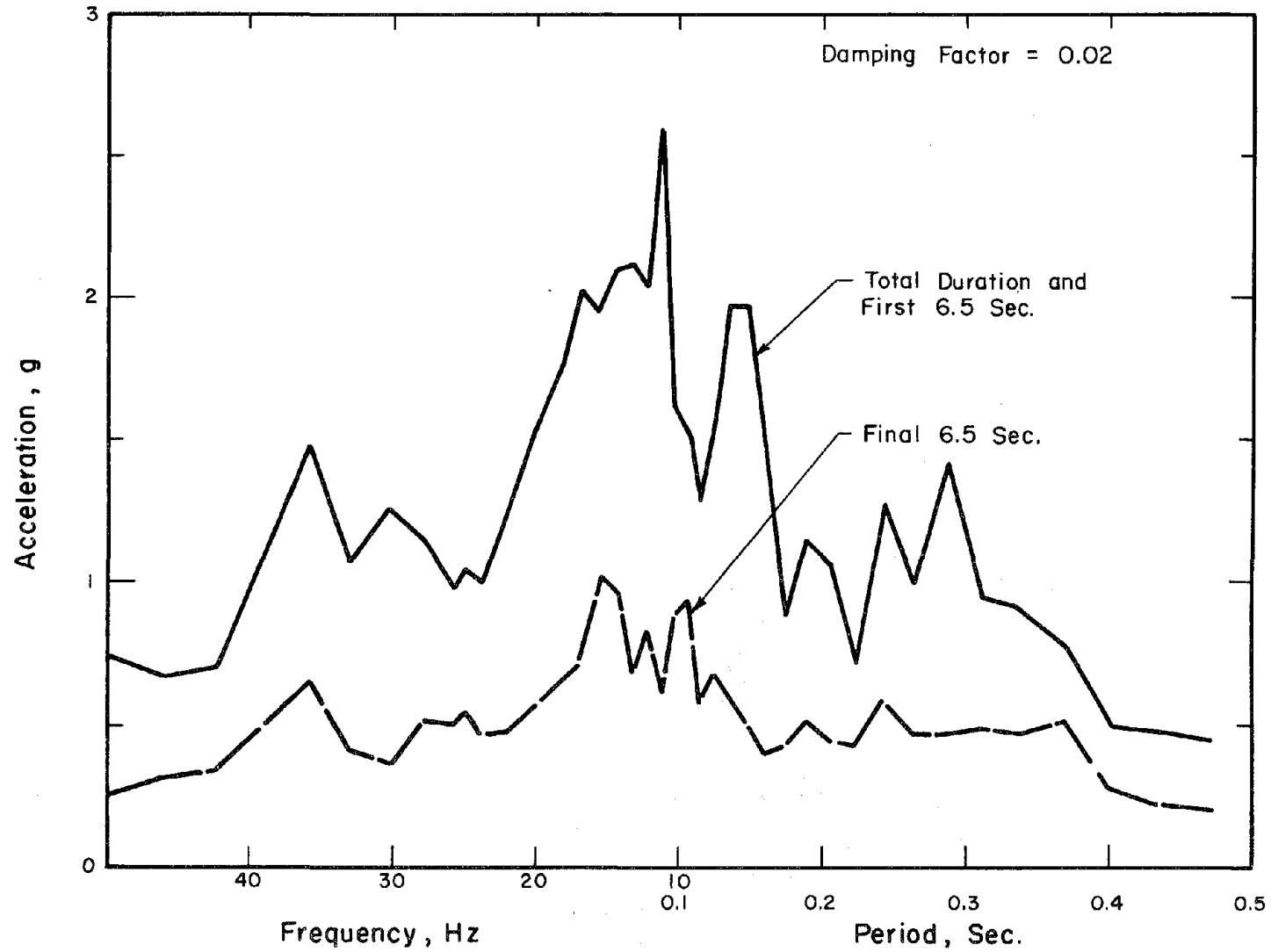
Fig. 5.7a   Response Spectra for Different Time Intervals
of Base Motion of Test Run D3-1

255
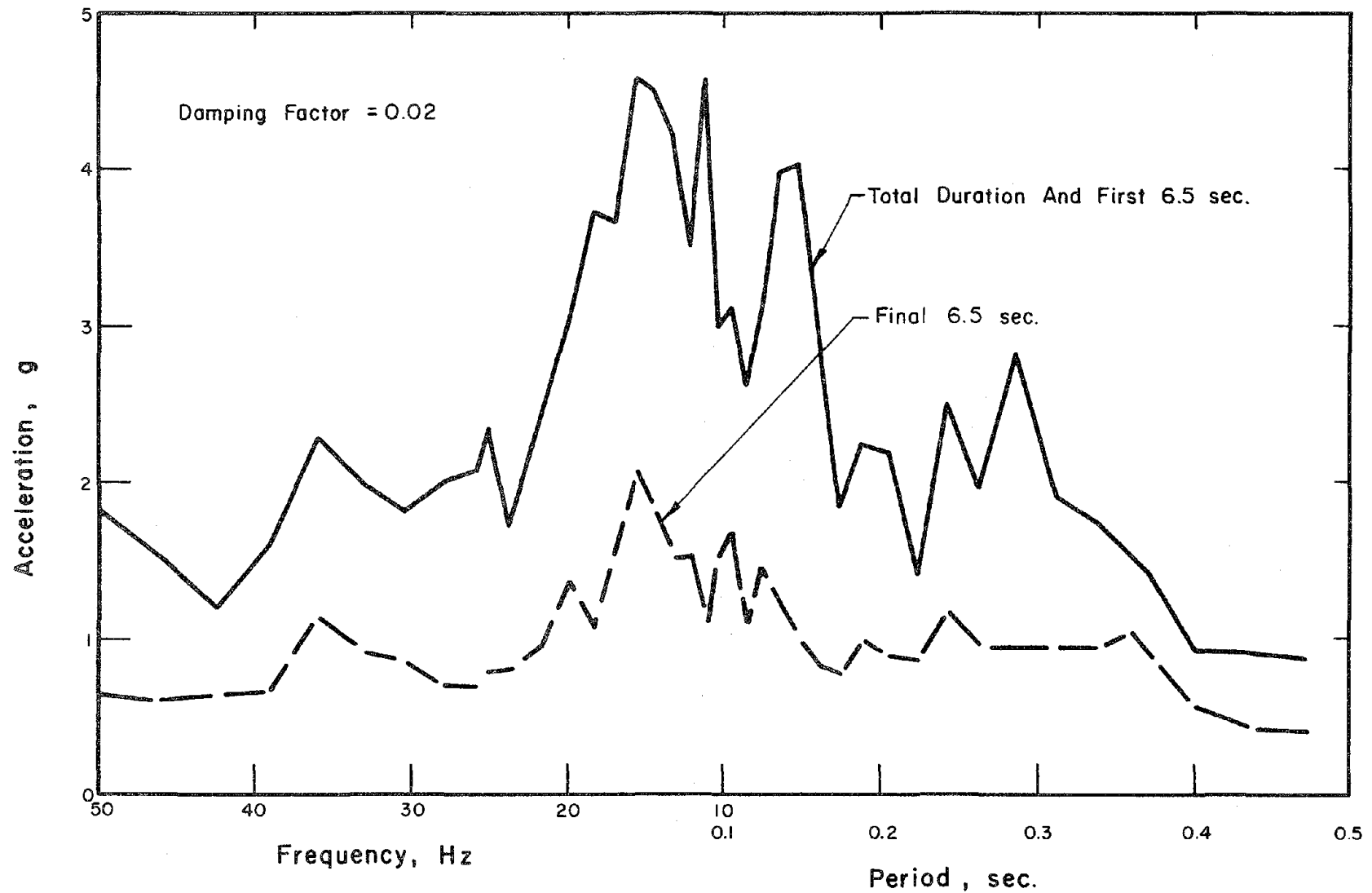
Fig. 5.7b   Response Spectra for Different Time Intervals
of Base Motion of Test Run D3-2
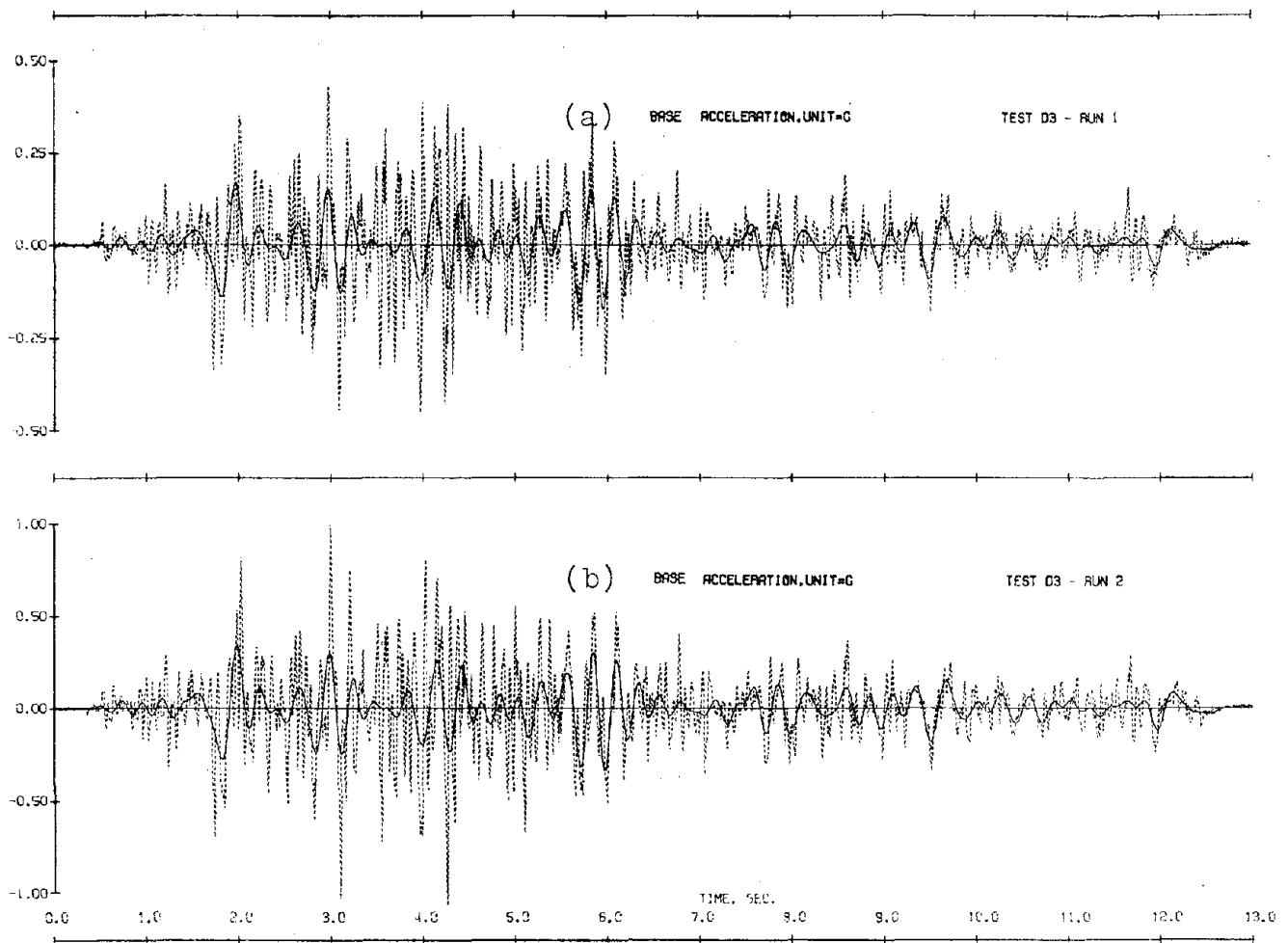
256

Fig. 5.8   Base Acceleration Waveforms (Broken Line) and Filtered
Components Below 5.0 Hz (Solid Line)

Symmetrical About Axis

Test Platform

Base Girder

12" 12" 12" 12"

9"

12"

(a) Base Girder

H

L = 24"
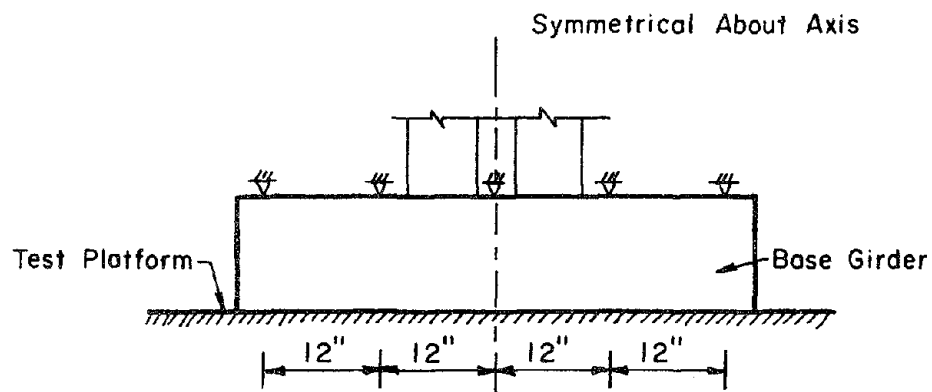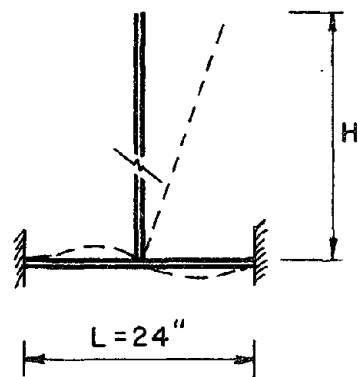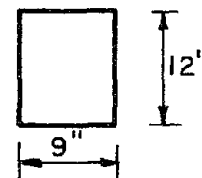
(b) Assumed Model Of Structure
And Base Girder

$L = 24"$, $b = 9"$, $h = 12"$, $H = 90"$
$W = 10^4$ lbs

$I = \dfrac{bh^3}{12} = 1300$ in.^{4}

$K = 8\,\dfrac{EI}{L} = 13 \times 10^8$ lb-in.

$J = \dfrac{1}{3}\,\dfrac{W}{g} \times H^2 = 7 \times 10^4$ lb-in.-sec^2

Frequency Of $\qquad f_2 = \dfrac{1}{2\pi}\sqrt{\dfrac{K}{J}} = \dfrac{137}{6.28} = 22$ Hz
Model (b)

$T^2 = \left(\dfrac{1}{f}\right)^2 \approx \underbrace{\left(\dfrac{1}{5.4}\right)^2}_{\text{Uncracked}} + \left(\dfrac{1}{22}\right)^2 = (0.034 + 0.002)$ sec^2

$\qquad\qquad\qquad\qquad = 0.036$ sec^2

$T \approx 0.19$ sec

$\dfrac{T}{T_{calculated}} = 1.02$

Fig. 5.9 Effect of Base Fixity on the Fundamental Frequency of
The Test Structure

258
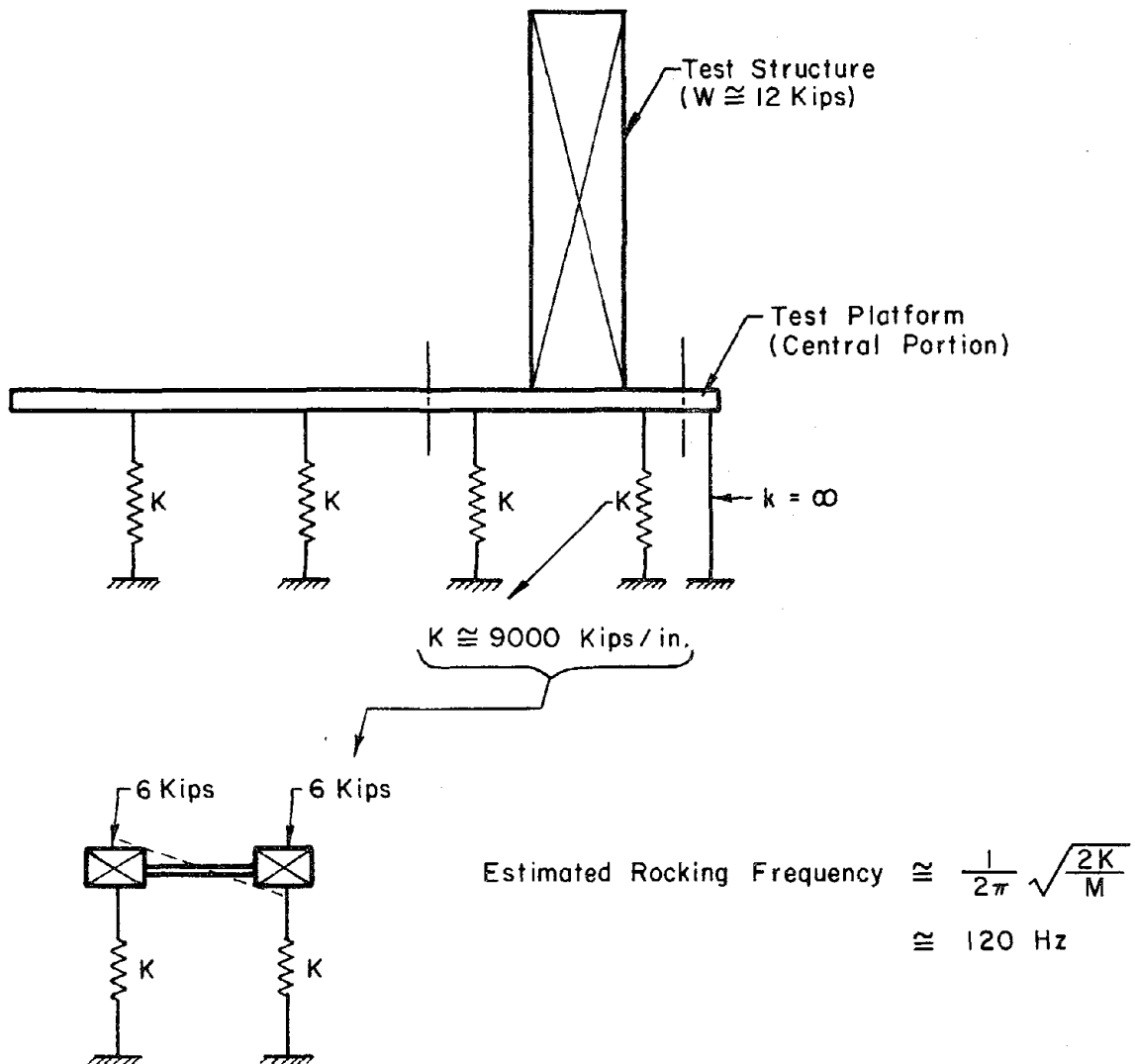
Fig. 5.10   Rocking Frequency of the Test Structure
Plus the Platform
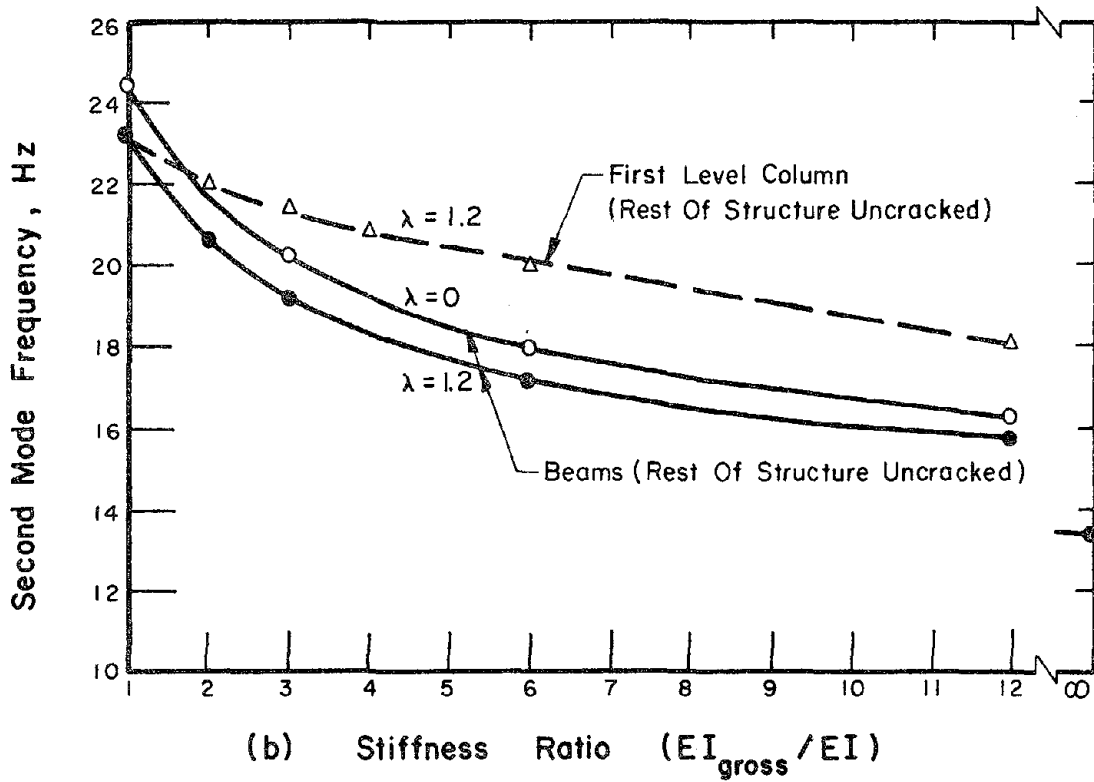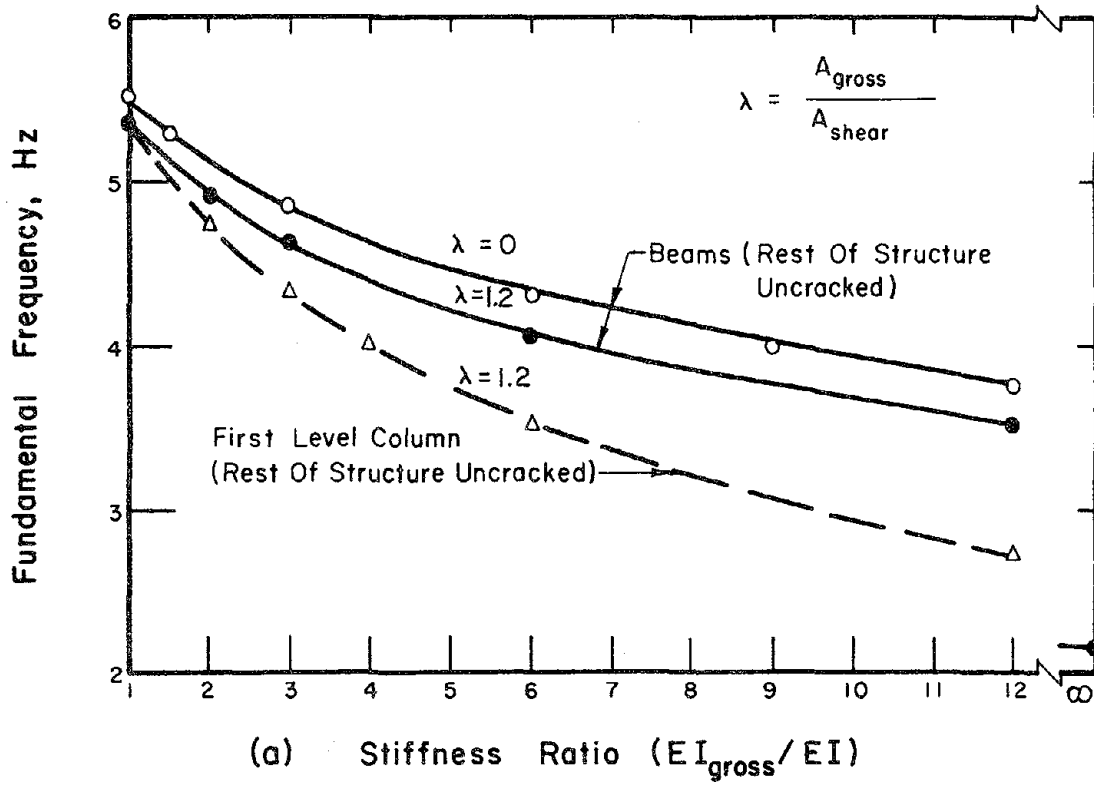
Fig. 5.11 Variation in Frequency with Beam Stiffness (Solid Line) and with Base Column Stiffness (Broken Line)
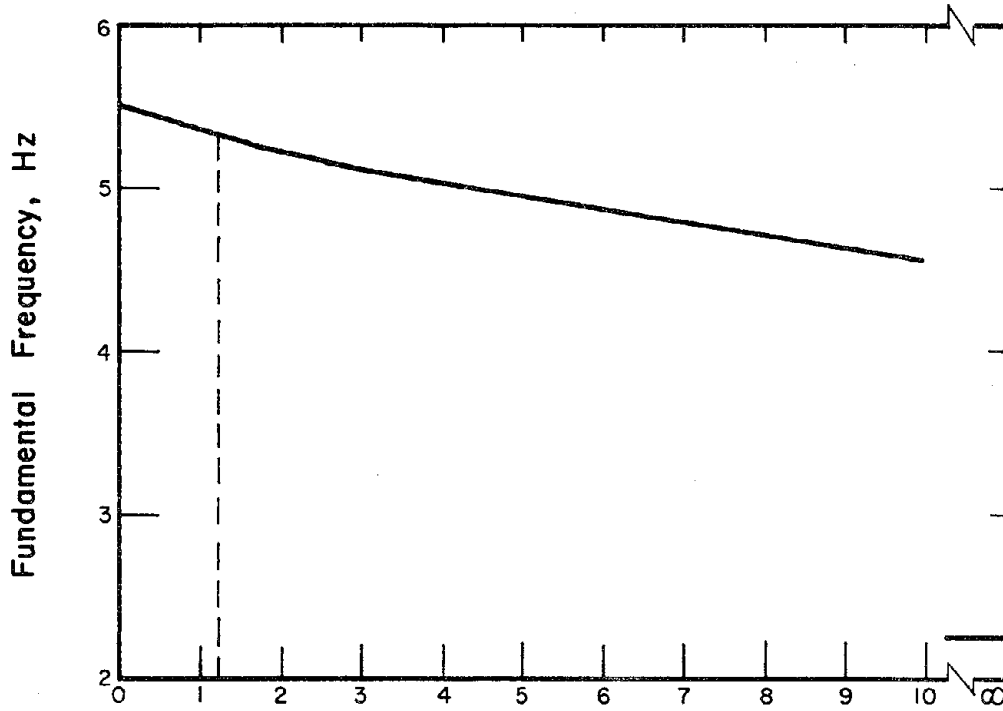
(a)   Beam Shear Area Ratio (A_{gross}/A_{shear})
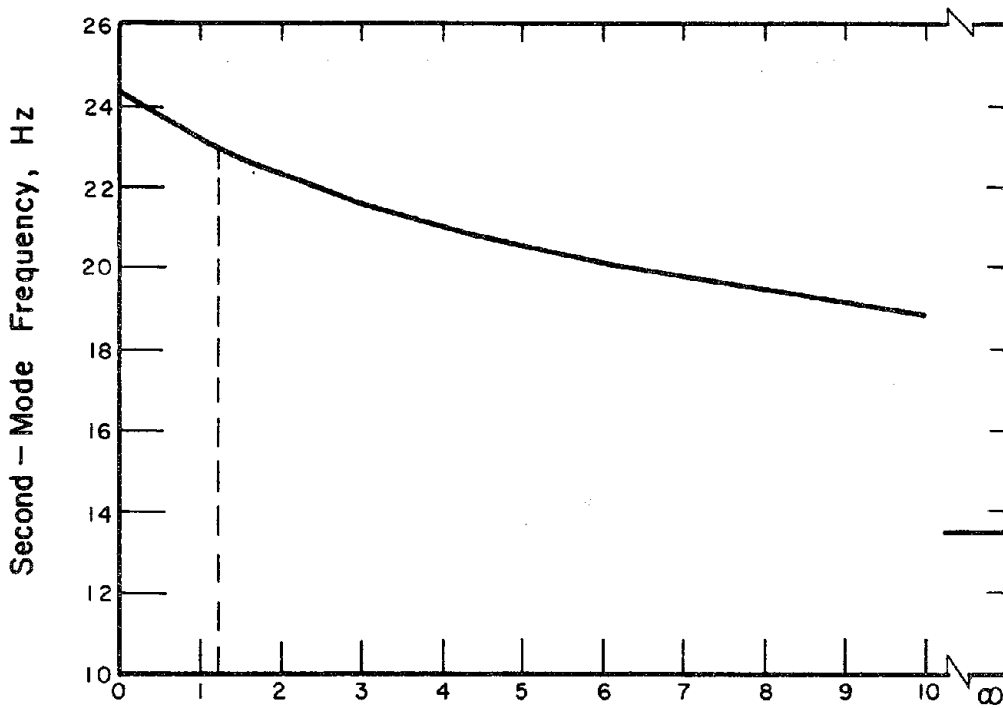
(b)   Beam Shear Area Ratio (A_{gross}/A_{shear})

Fig. 5.12   Effect of Beam Shear Stiffness on Frequency
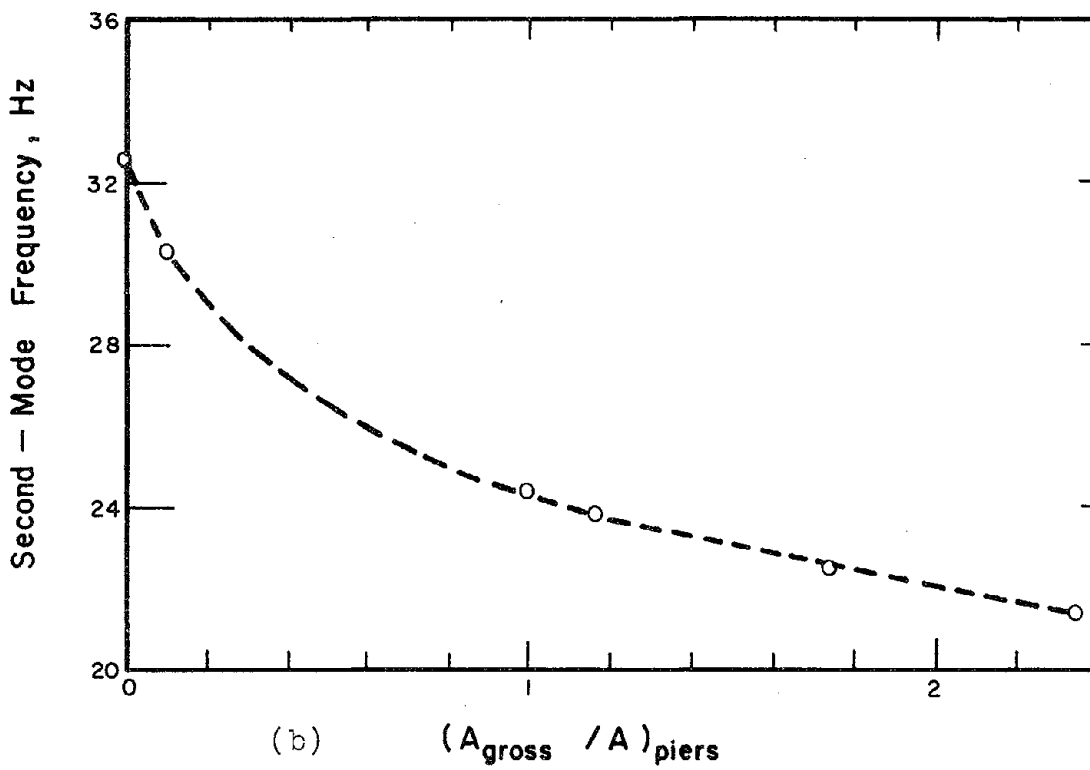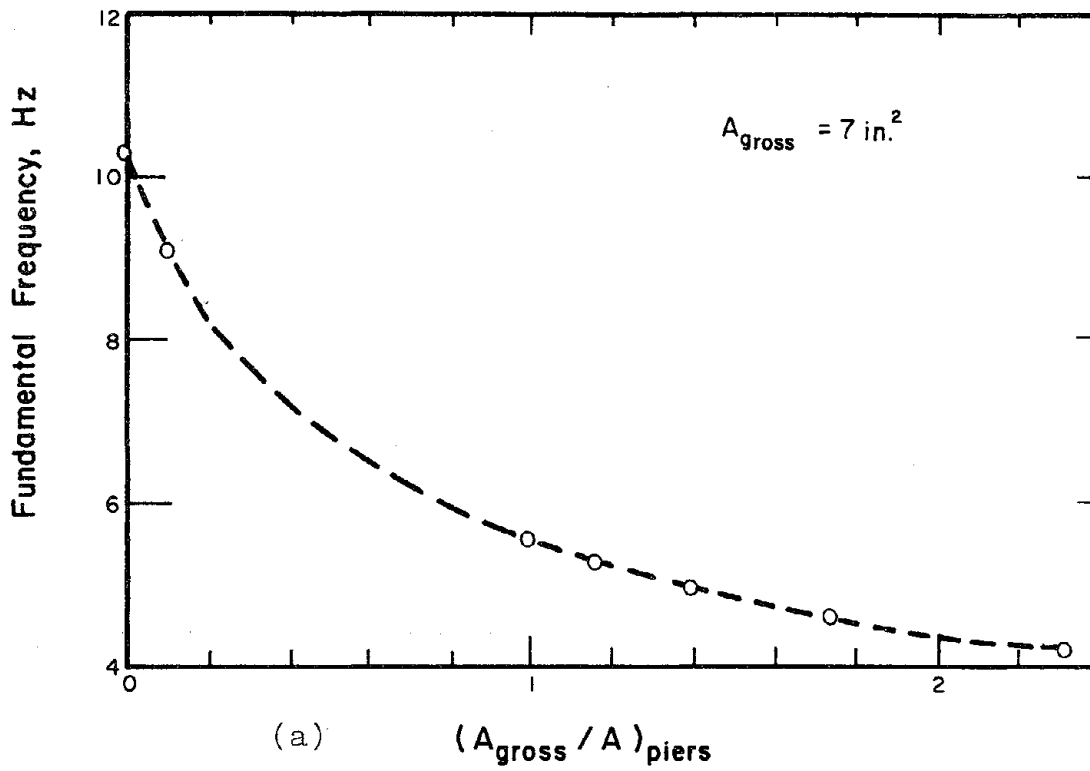
Fig. 5.13 Variation of Frequency with Axial Stiffness of the Piers
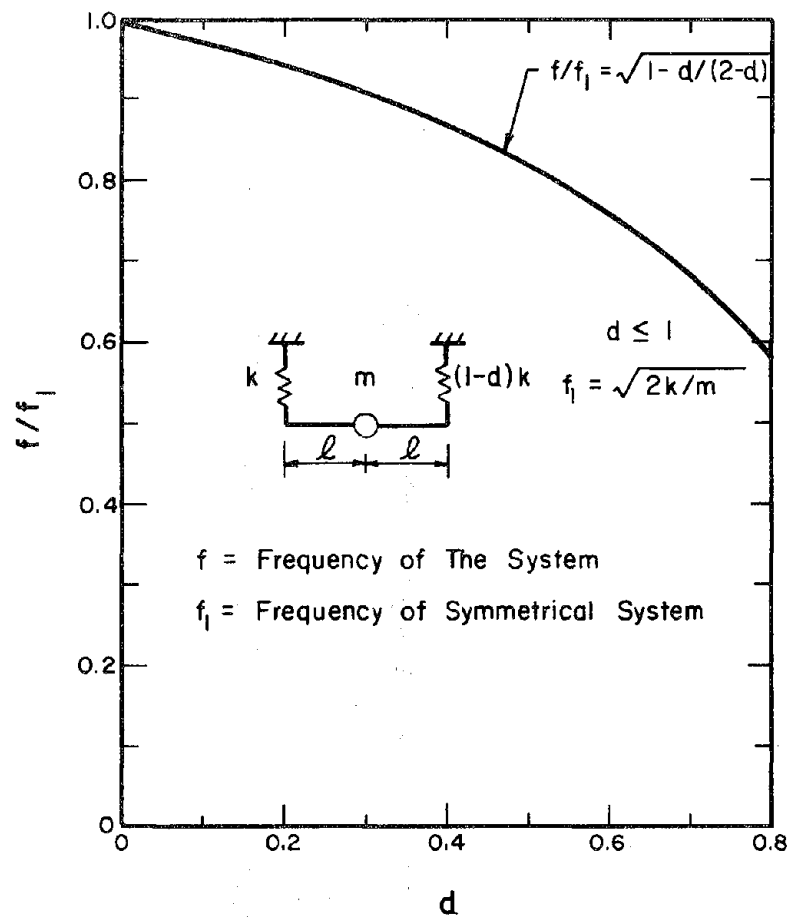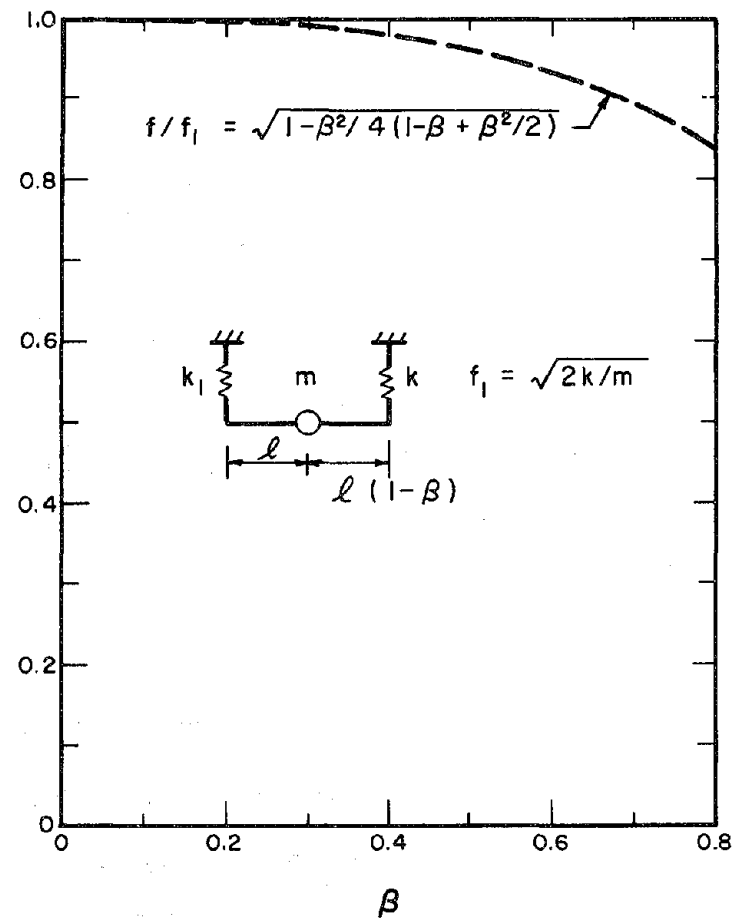
Fig. 5.14   Effects of Stiffness and Mass Eccentricity on
Natural Frequency
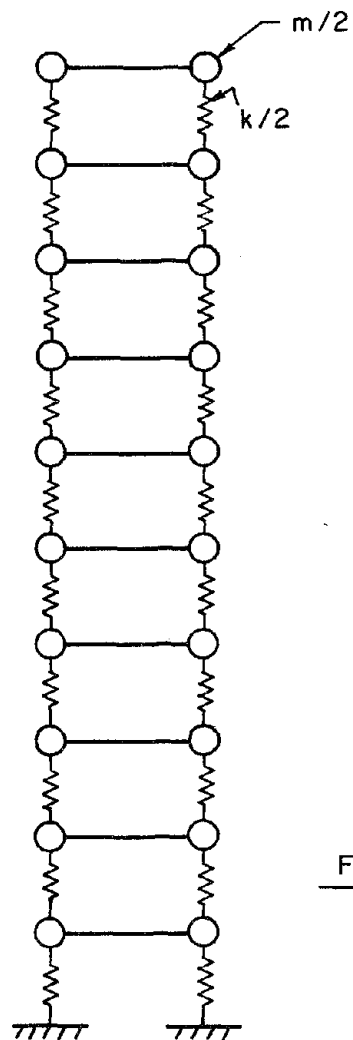
Vertical Natural Frequencies (Thompson, 1972, Page 245)

$$f_1 = \frac{1}{\pi} \sqrt{\frac{k}{m}} \ Sin \ \frac{(2i-1)\pi}{2(2N+1)}$$

N = Number of Stories (N = 10)

i = Mode Number

$$\frac{k}{2} = \frac{AE}{L} = \frac{7 \times 3 \times 10^6}{9} = 2.33 \times 10^6 \ lb/in$$

$$\frac{m}{2} = \frac{250}{386} = 0.648 \ lb - sec^2/in$$

Fundamental Frequency = $f_i \cong$ 45 Hz

Fig. 5.15 Vertical Frequency of Test Structure
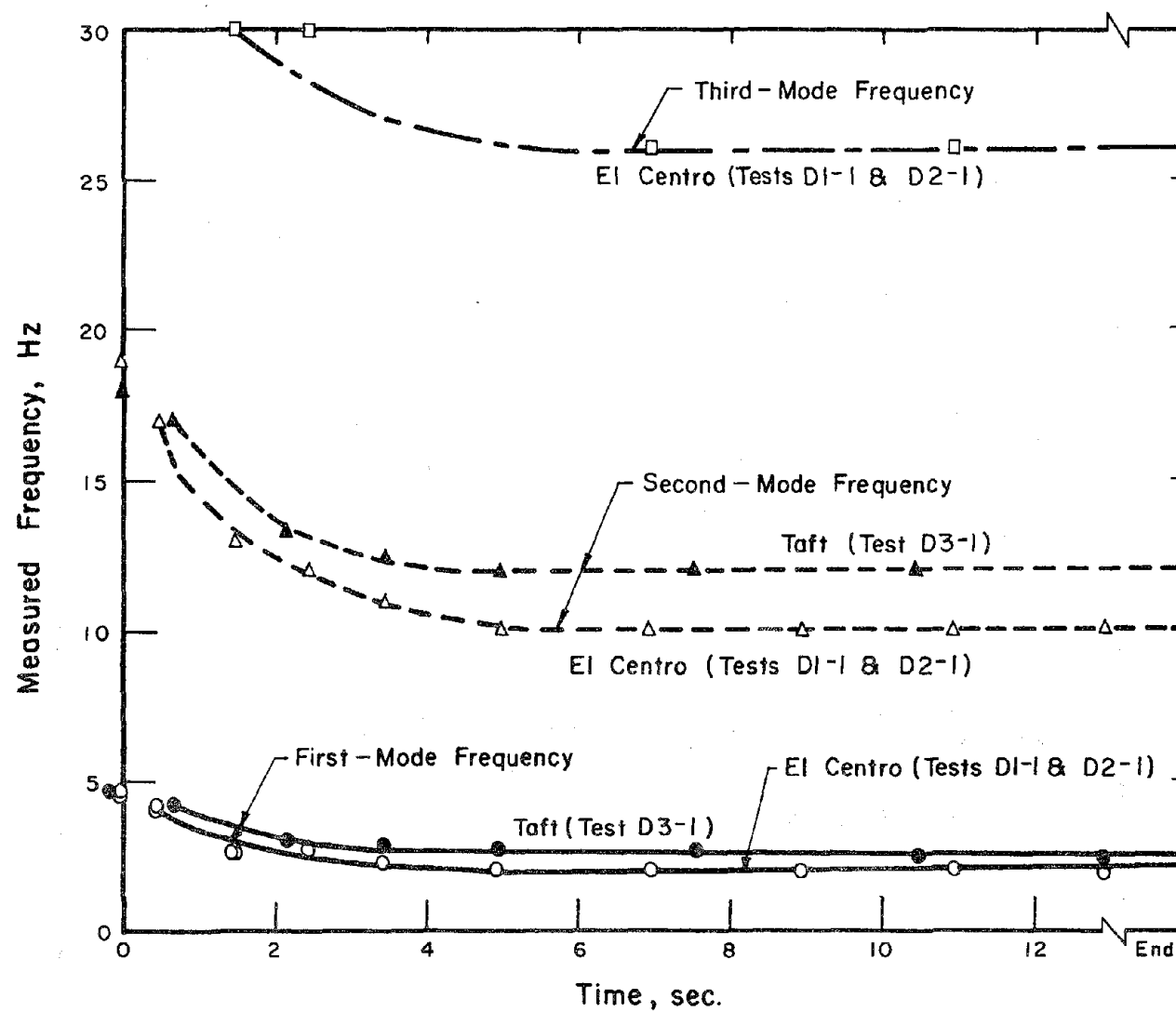
Fig. 5.16 Changes in Apparent Frequency During First Test Runs
(Test Structure D)
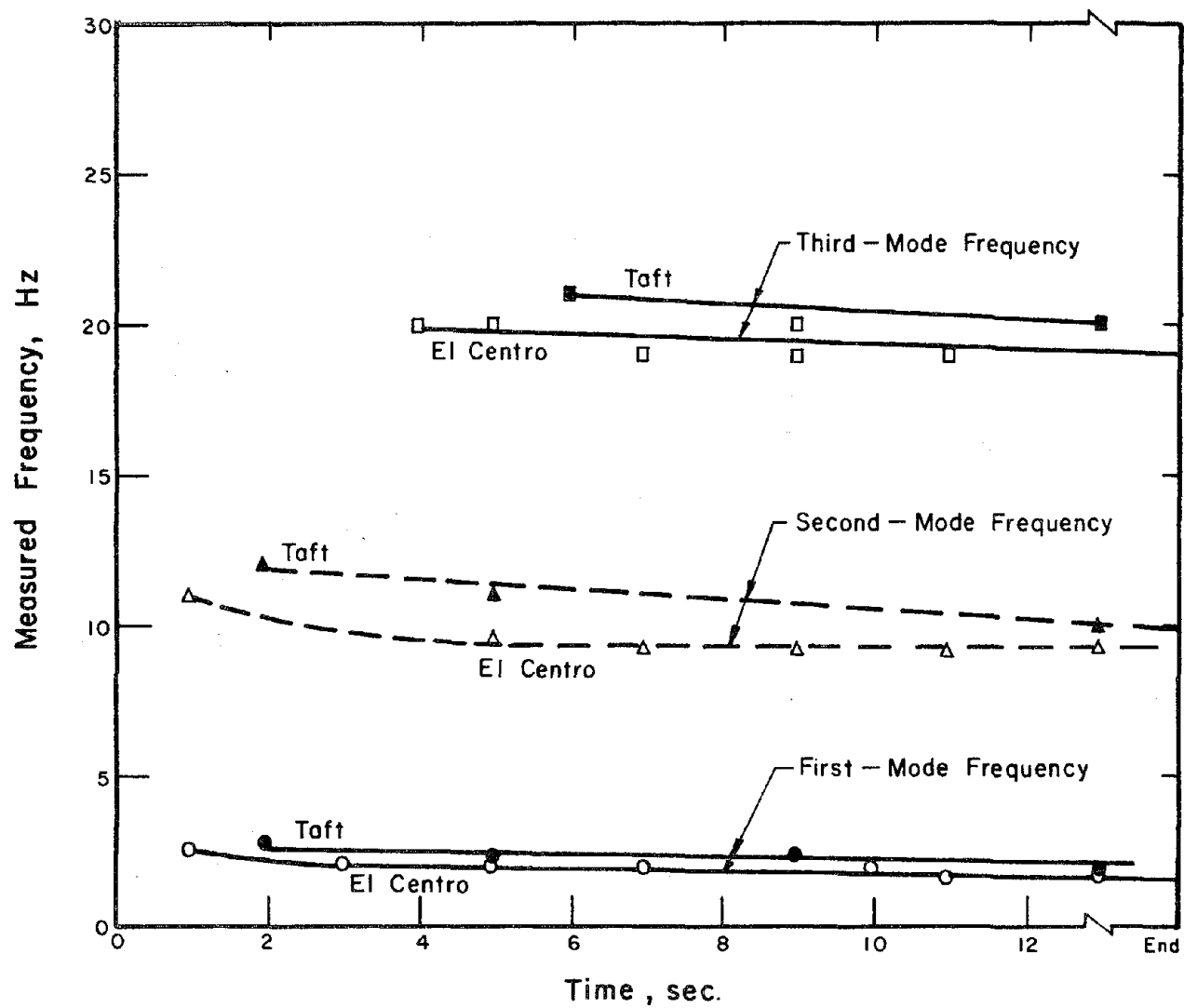
Fig. 5.17 Changes in Apparent Frequency During Second Test Runs (Test Structure D)

266
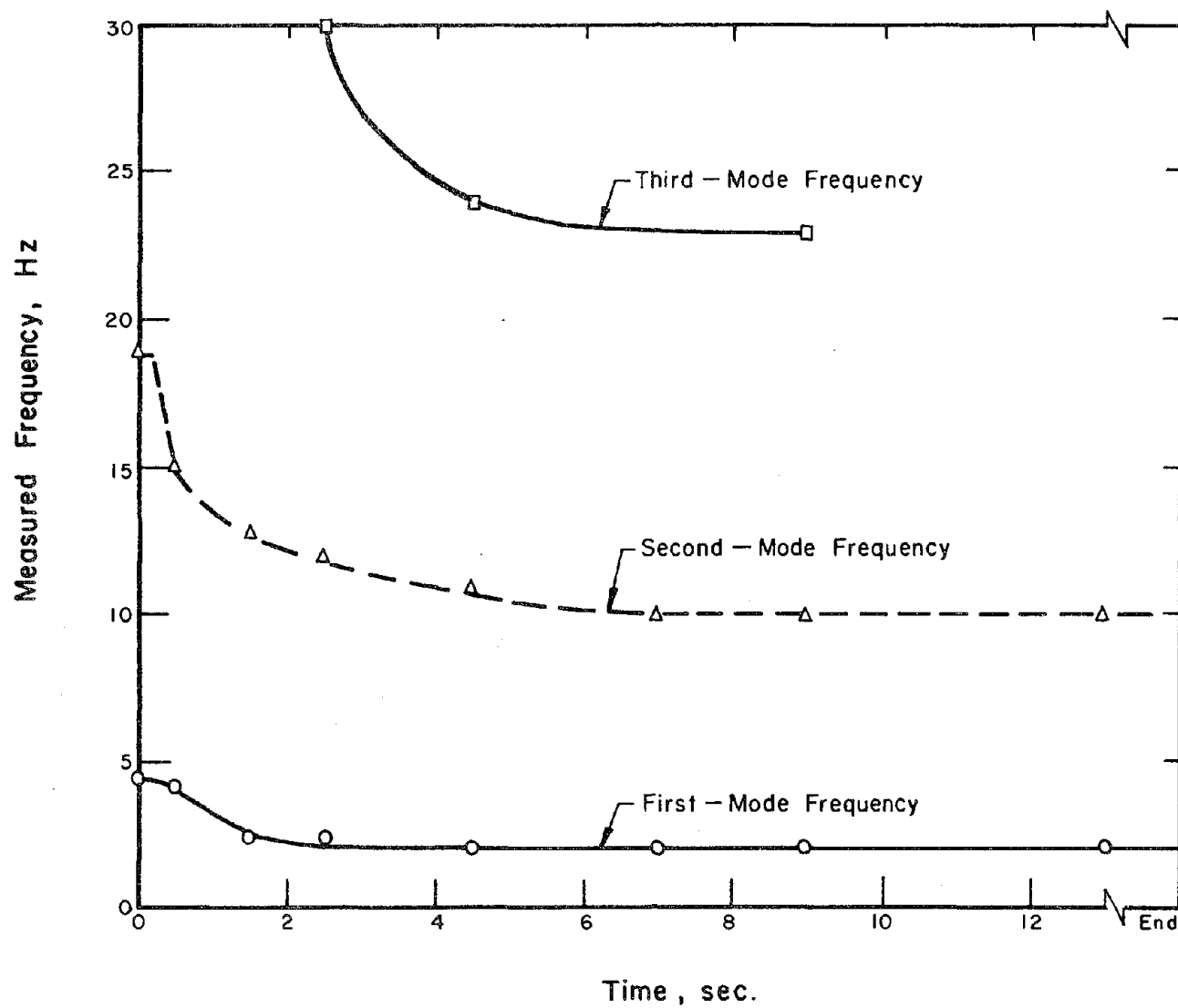
Fig. 5.18 Changes in Apparent Frequency During First Test Run
(Test Structure M)
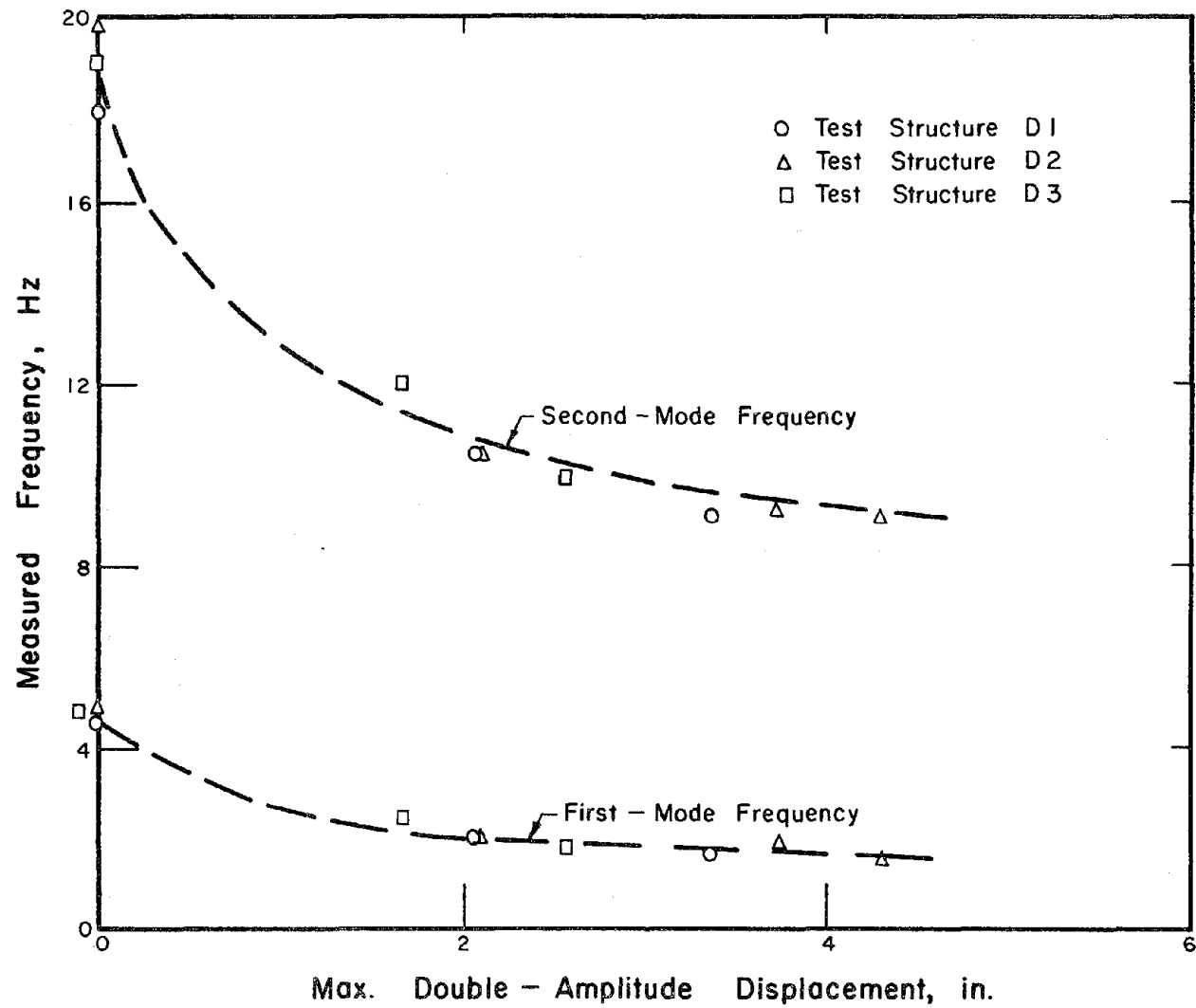
Fig. 5.19 Variation of Frequency with Maximum Double-Amplitude
Top-Level Displacement (Test Structure D)
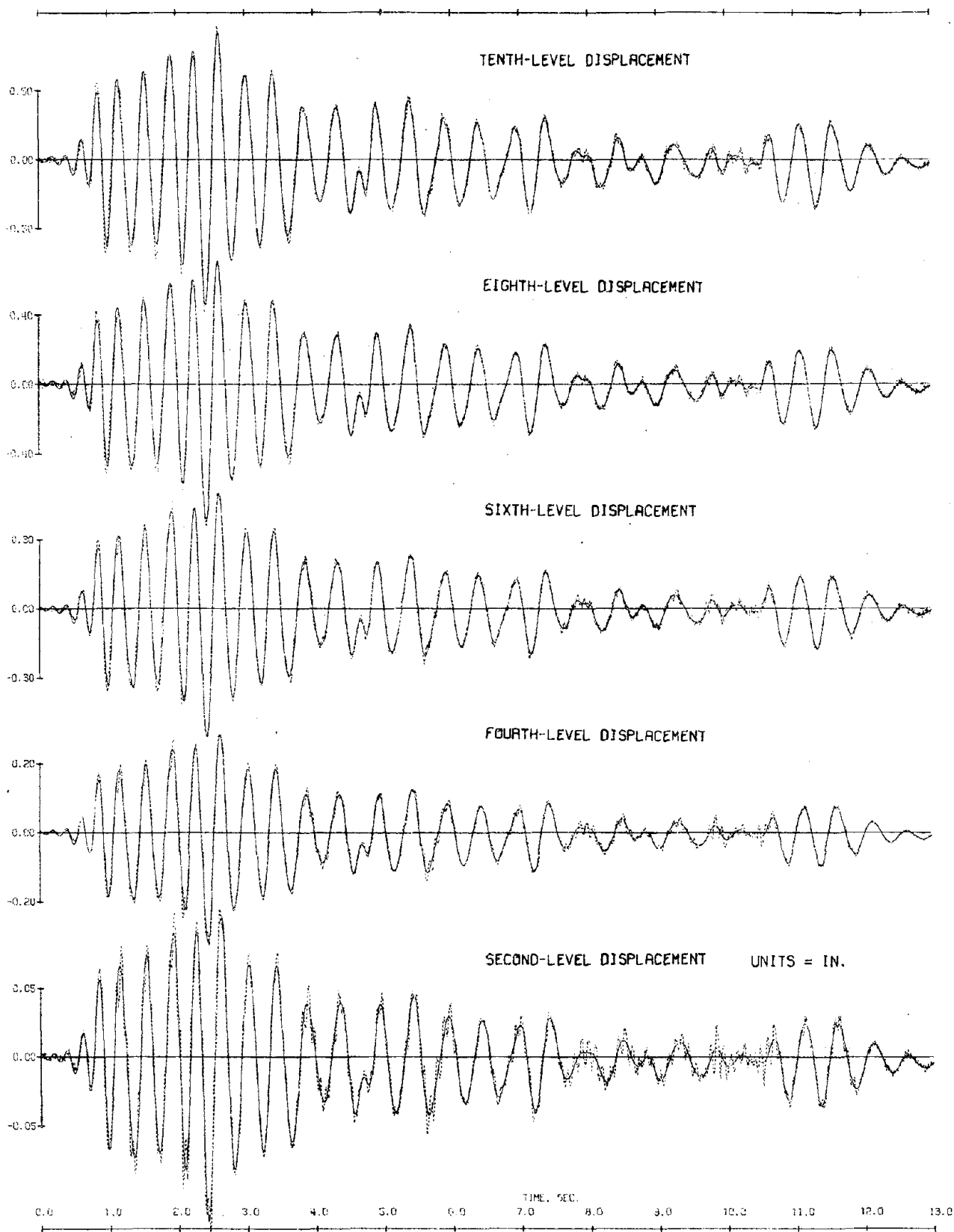
Fig. 5.20   Test Run D1-1.   Displacement Waveforms (Broken Line)
and Filtered Components Below 5.0 Hz (Solid Line)
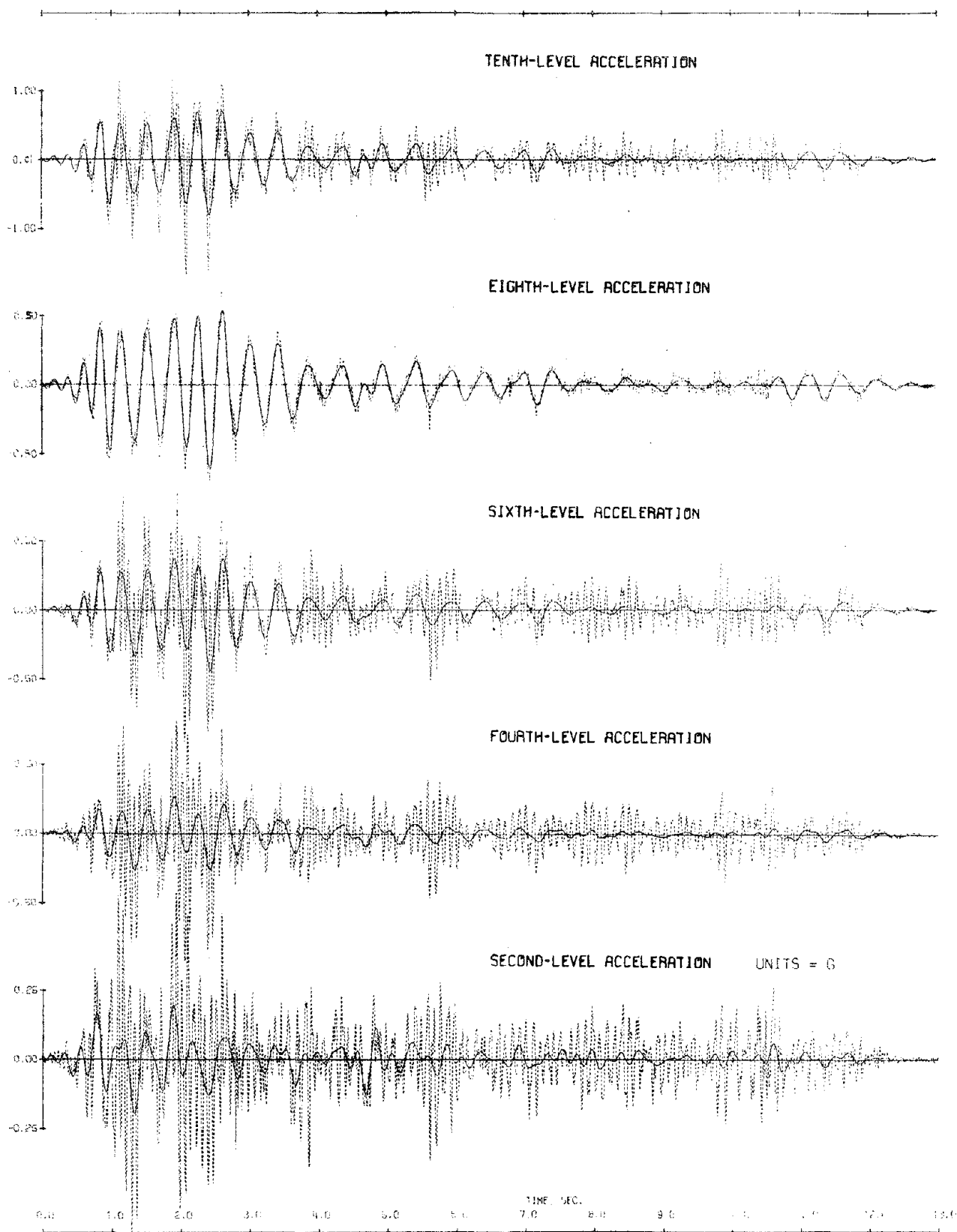
Fig. 5.21 Test Run D1-1. Acceleration Waveforms (Broken Line)
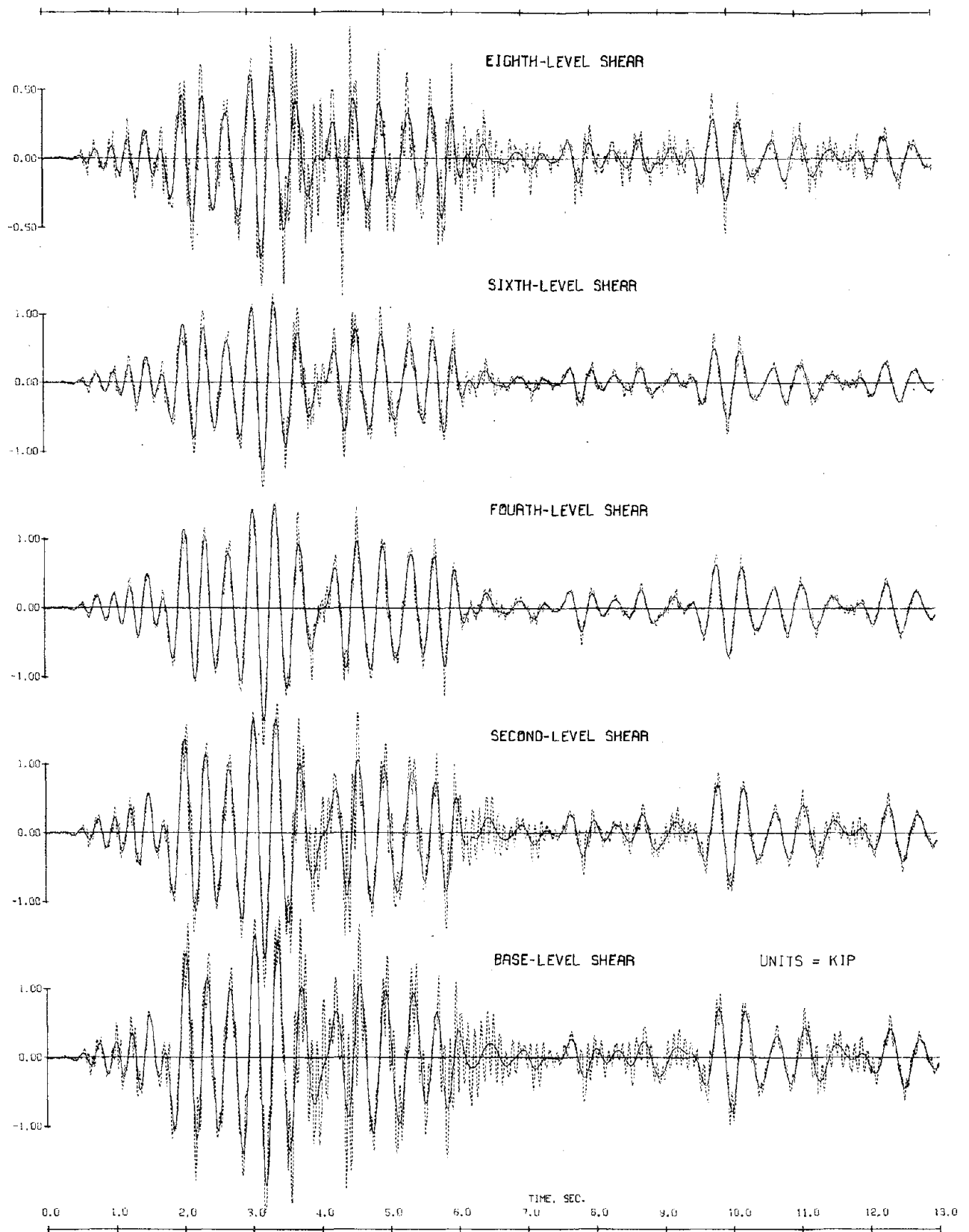and Filtered Components Below 5.0 Hz (Solid Line)
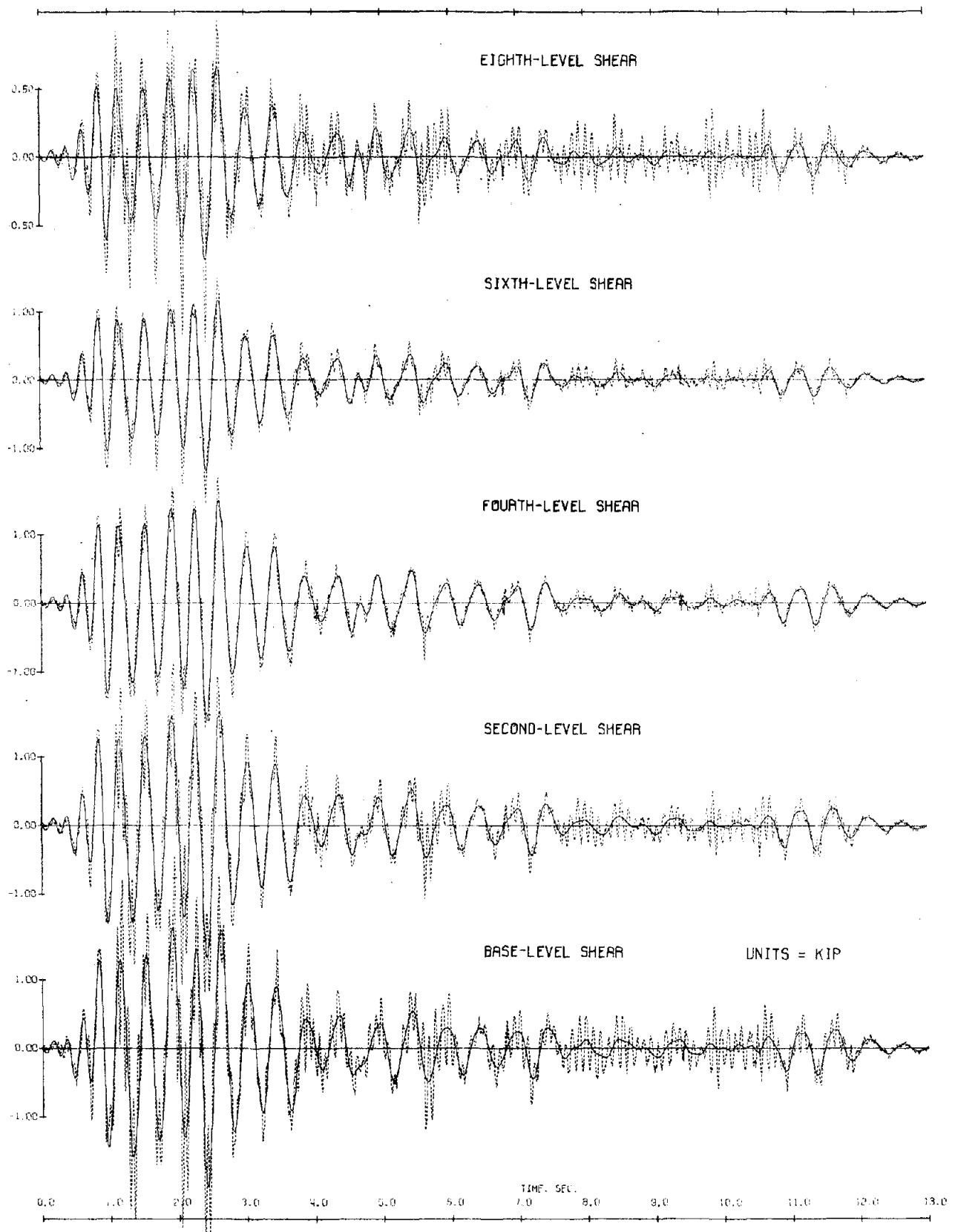
Fig. 5.22   Test Run D1-1.   Shear Waveforms (Broken Line) and
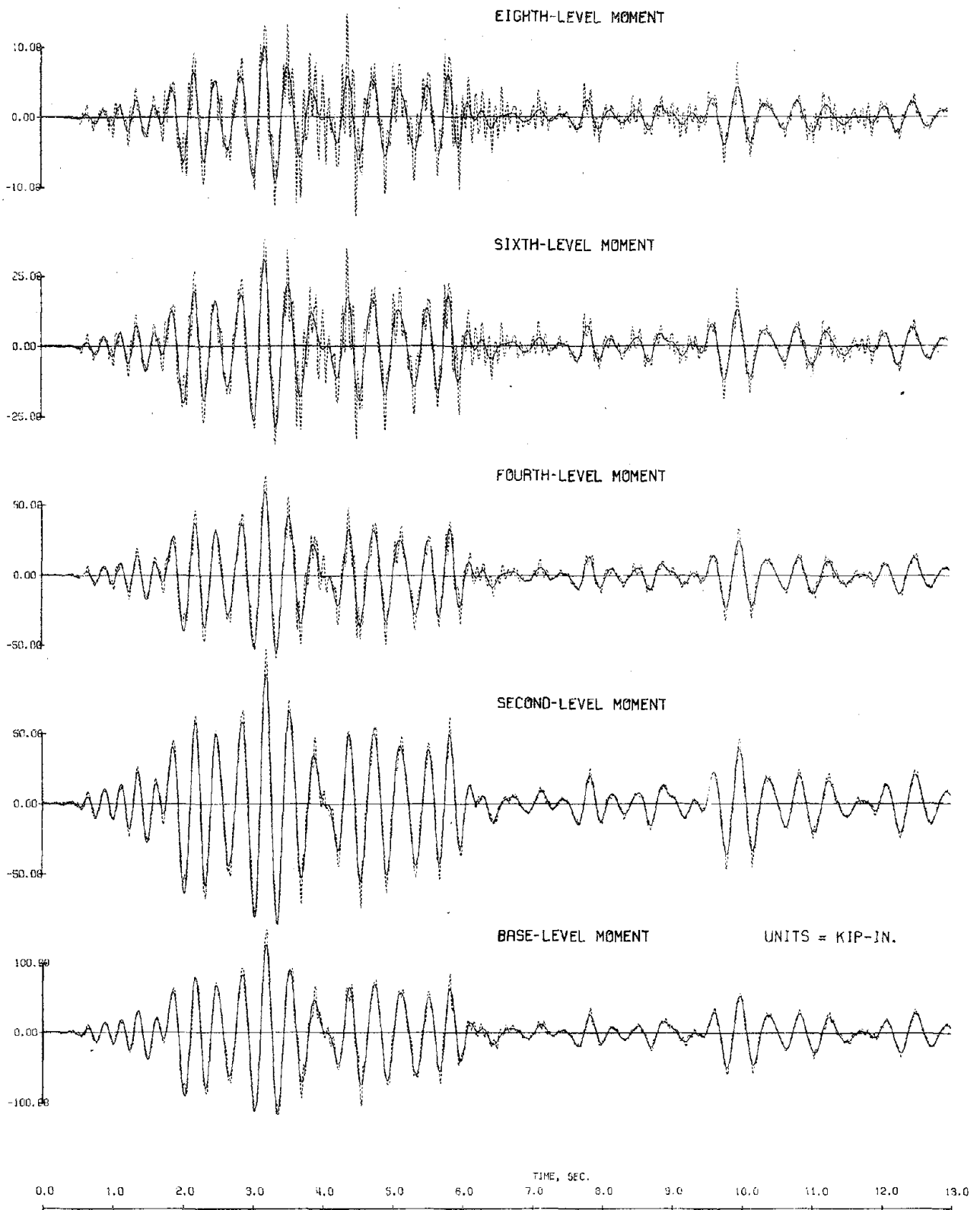Filtered Components Below 5.0 Hz (Solid Line)
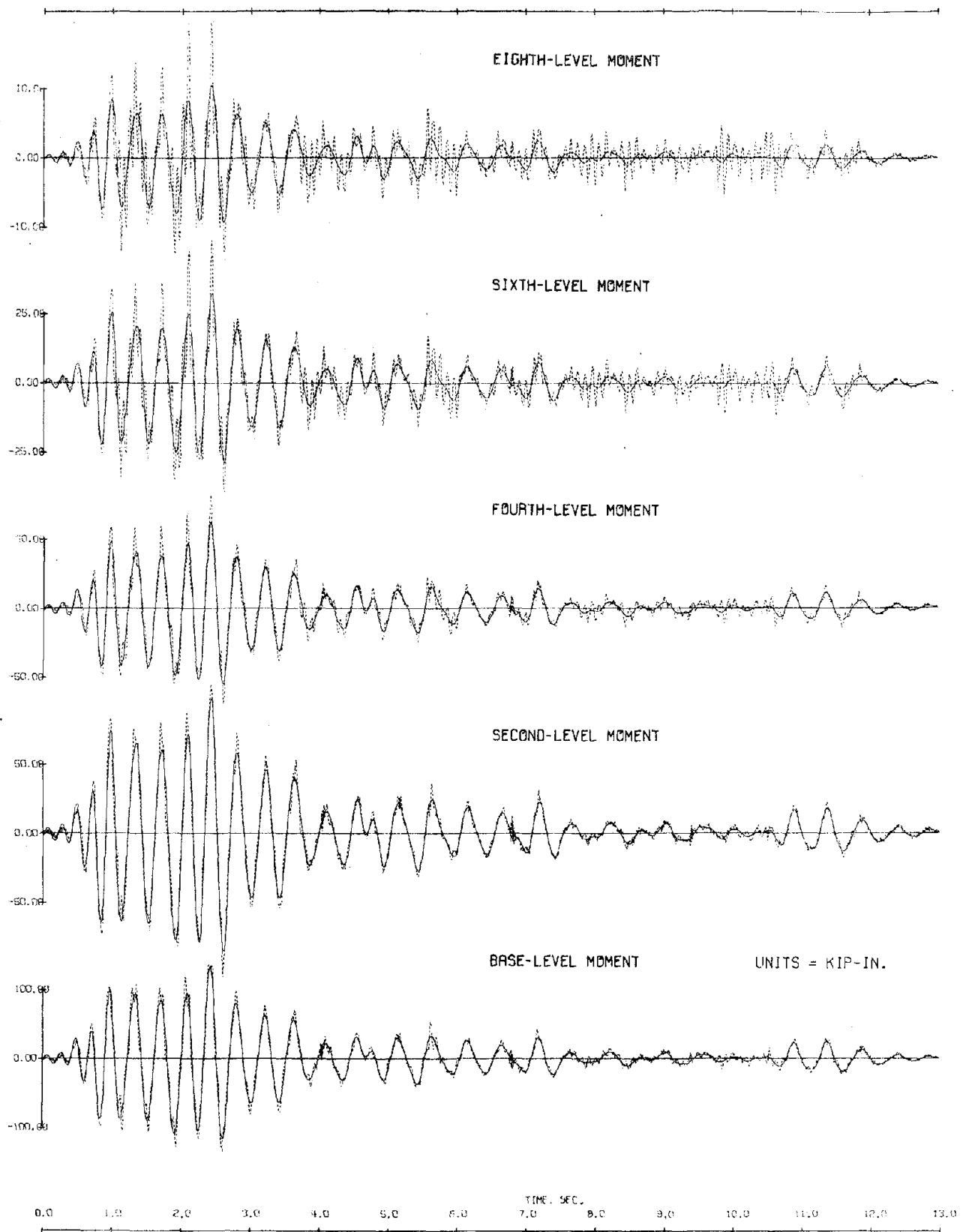
Fig. 5.23 Test Run D1-1. Moment Waveforms (Broken Line) and
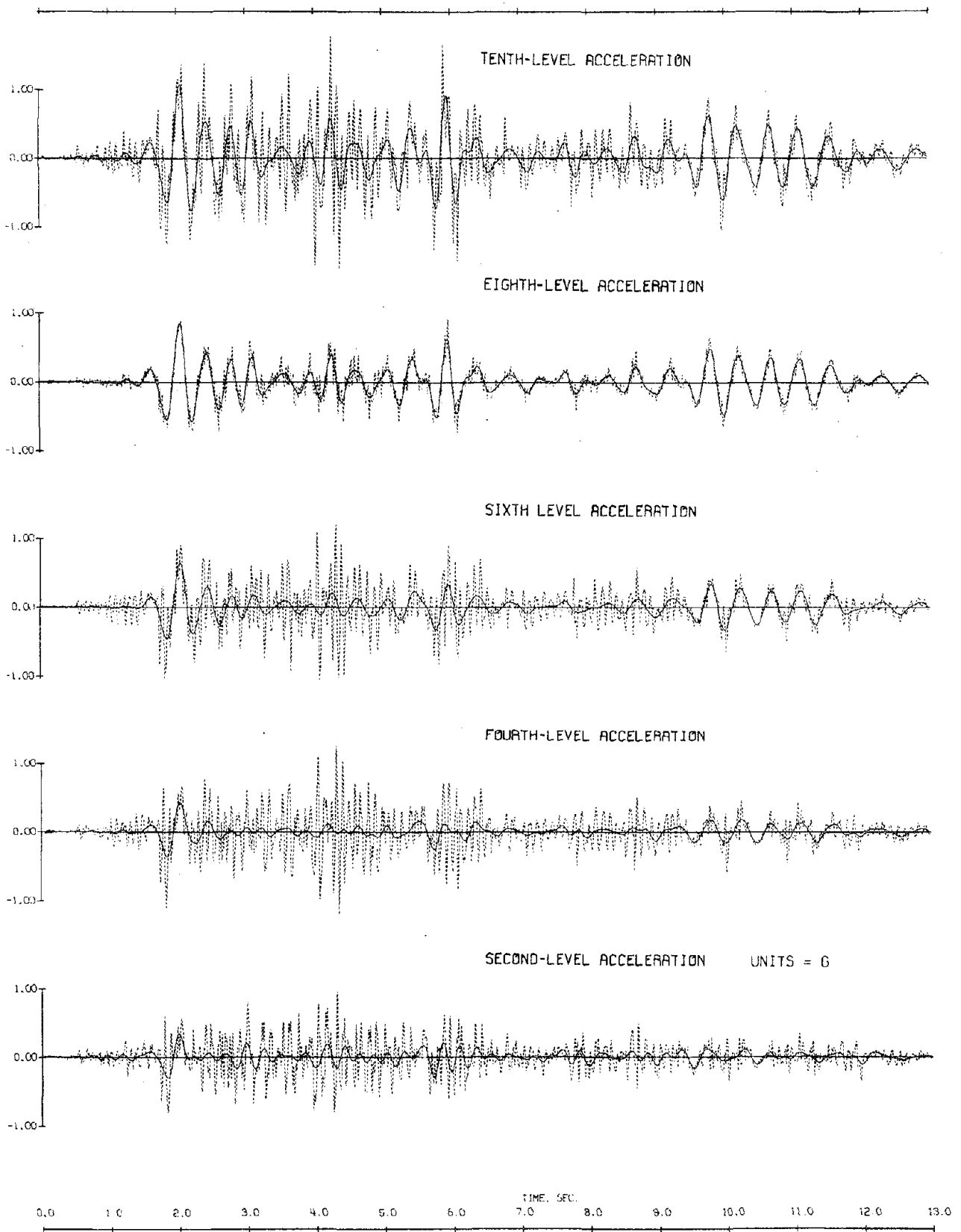Filtered Components Below 5.0 Hz (Solid Line)
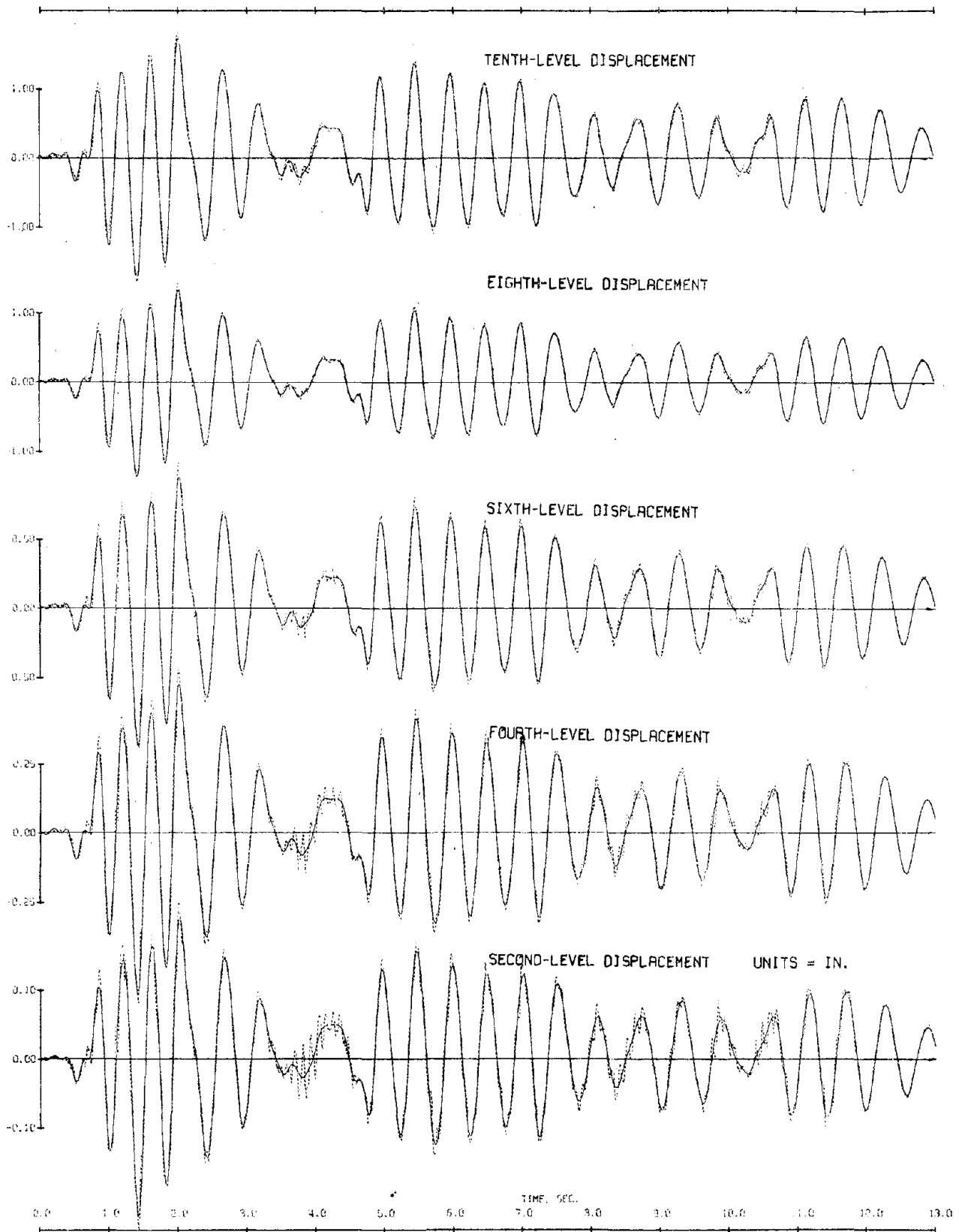
Fig. 5.24 Test Run D1-2. Displacement Waveforms (Broken Line) and Filtered Components Below 5.0 Hz (Solid Line)
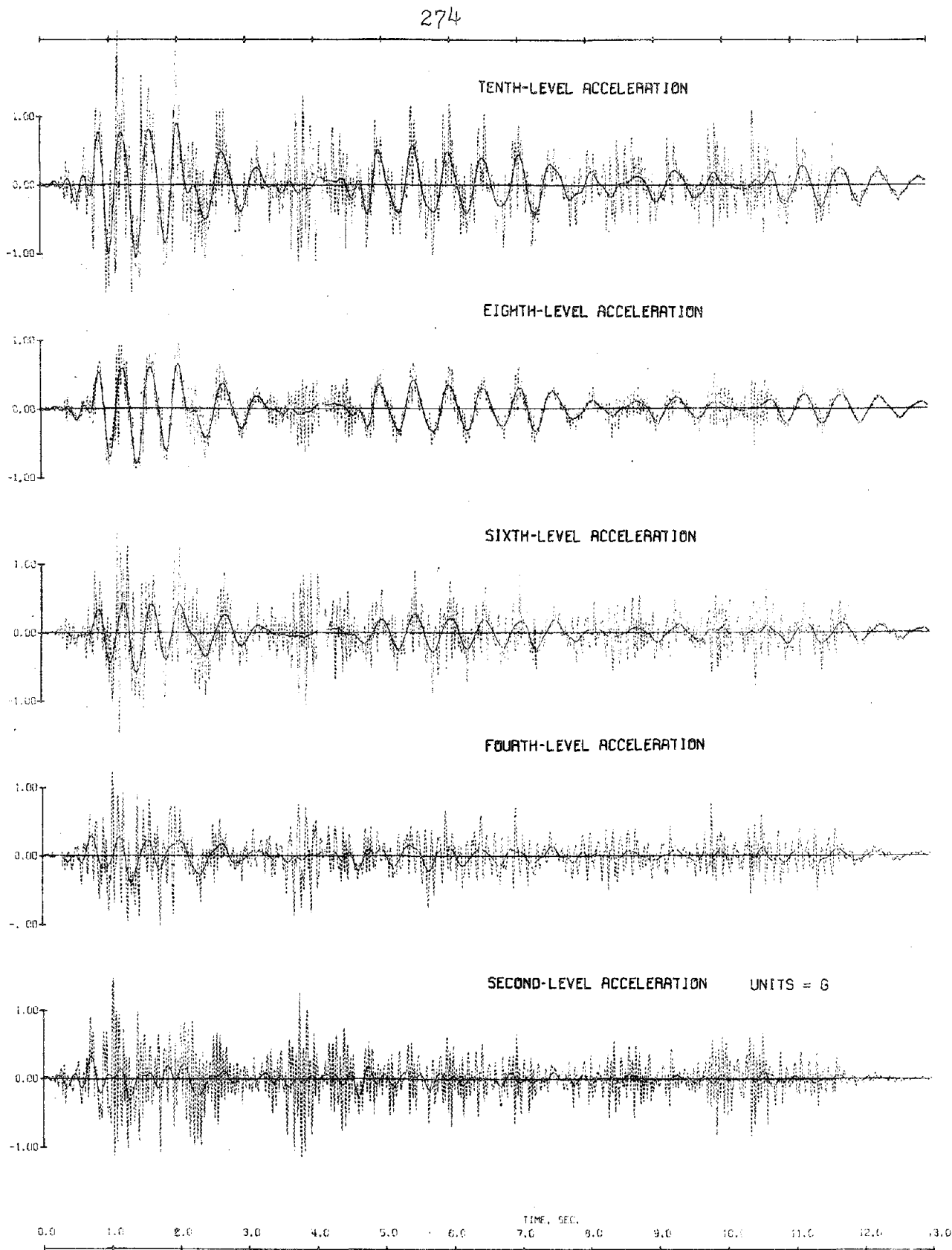
Fig. 5.25   Test Run D1-2.   Acceleration Waveforms (Broken Line)
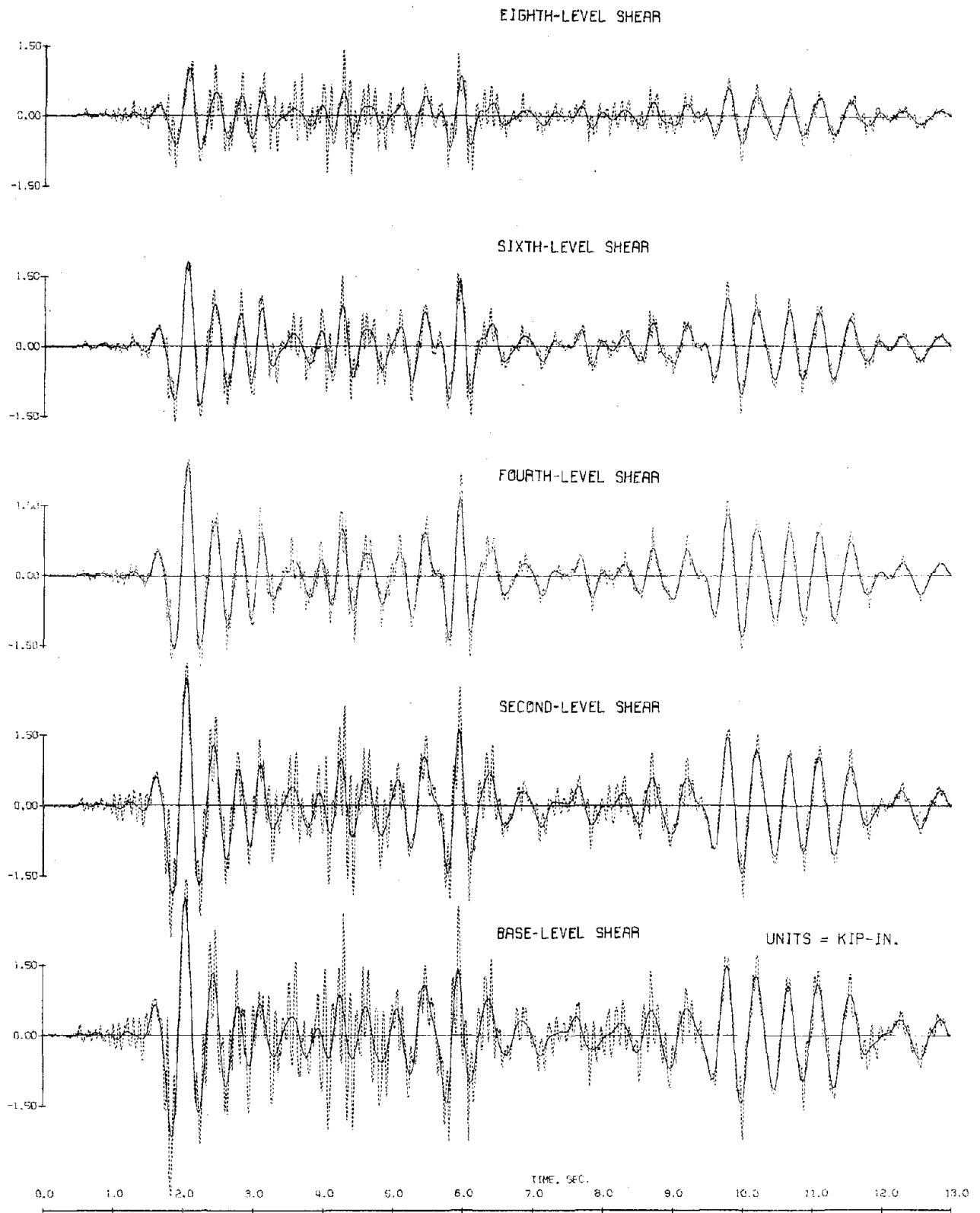and Filtered Components Below 5.0 Hz (Solid Line)
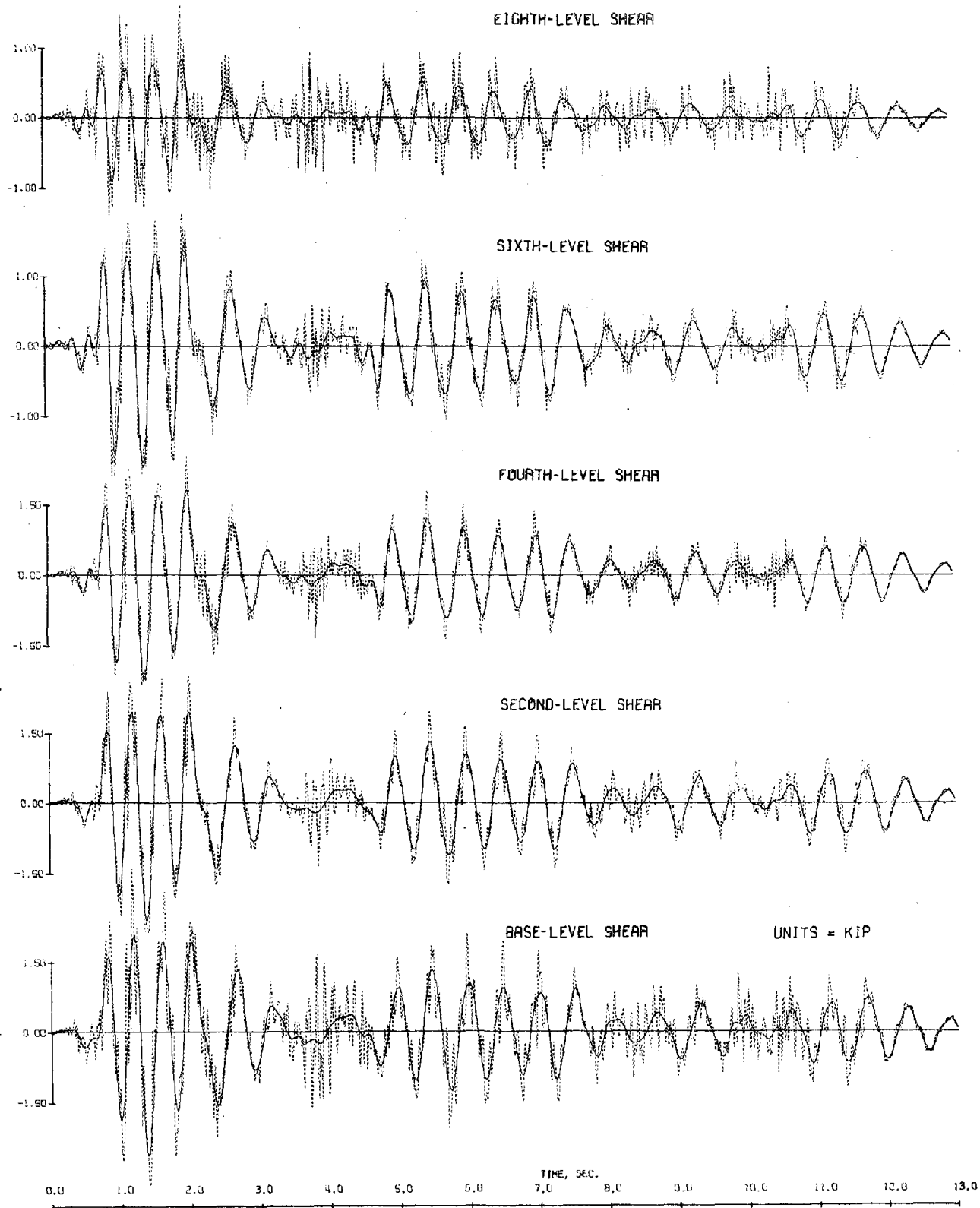
Fig. 5.26   Test Run D1-2.   Shear Waveforms (Broken Line) and
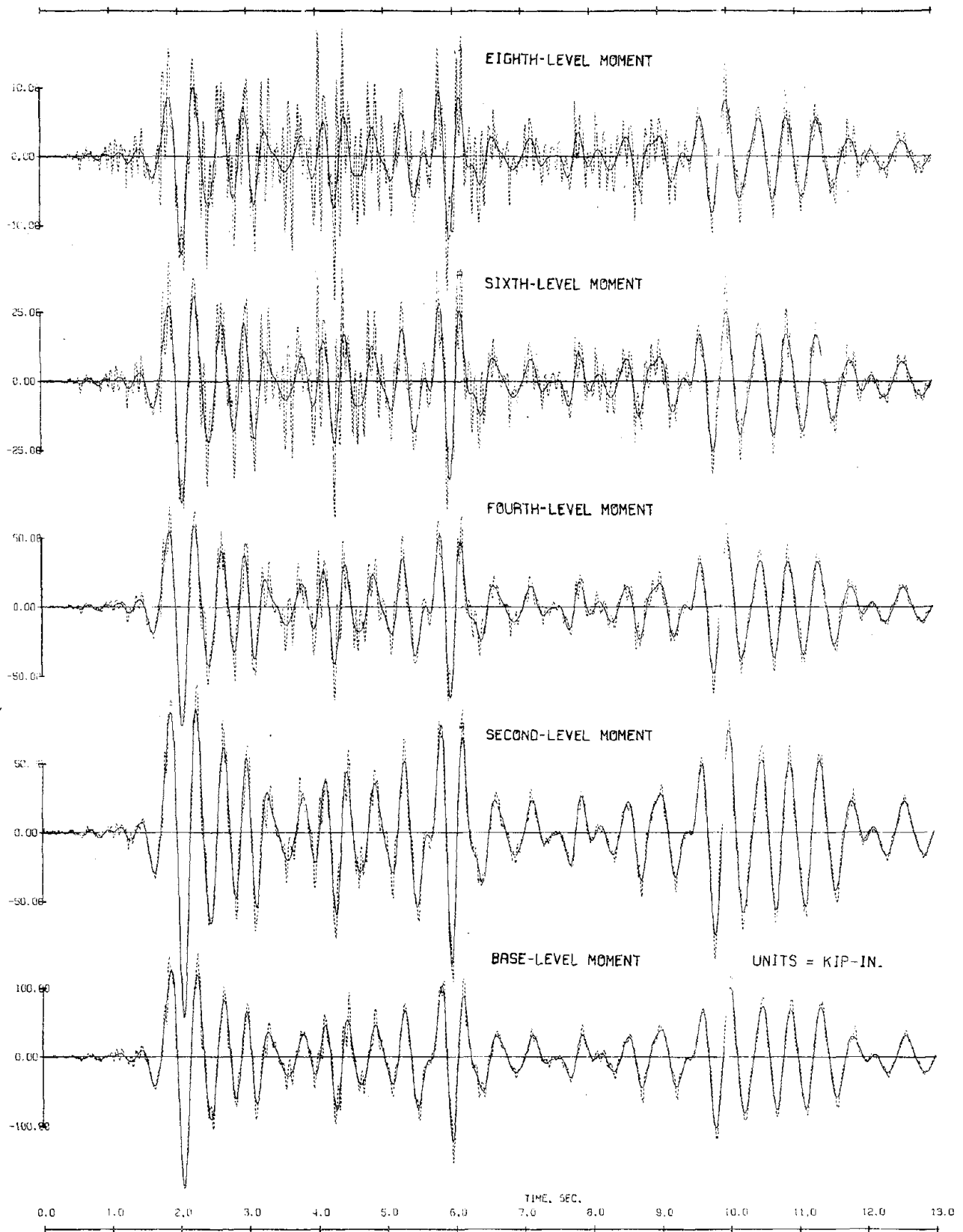   Filtered Components Below 5.0 Hz (Solid Line)
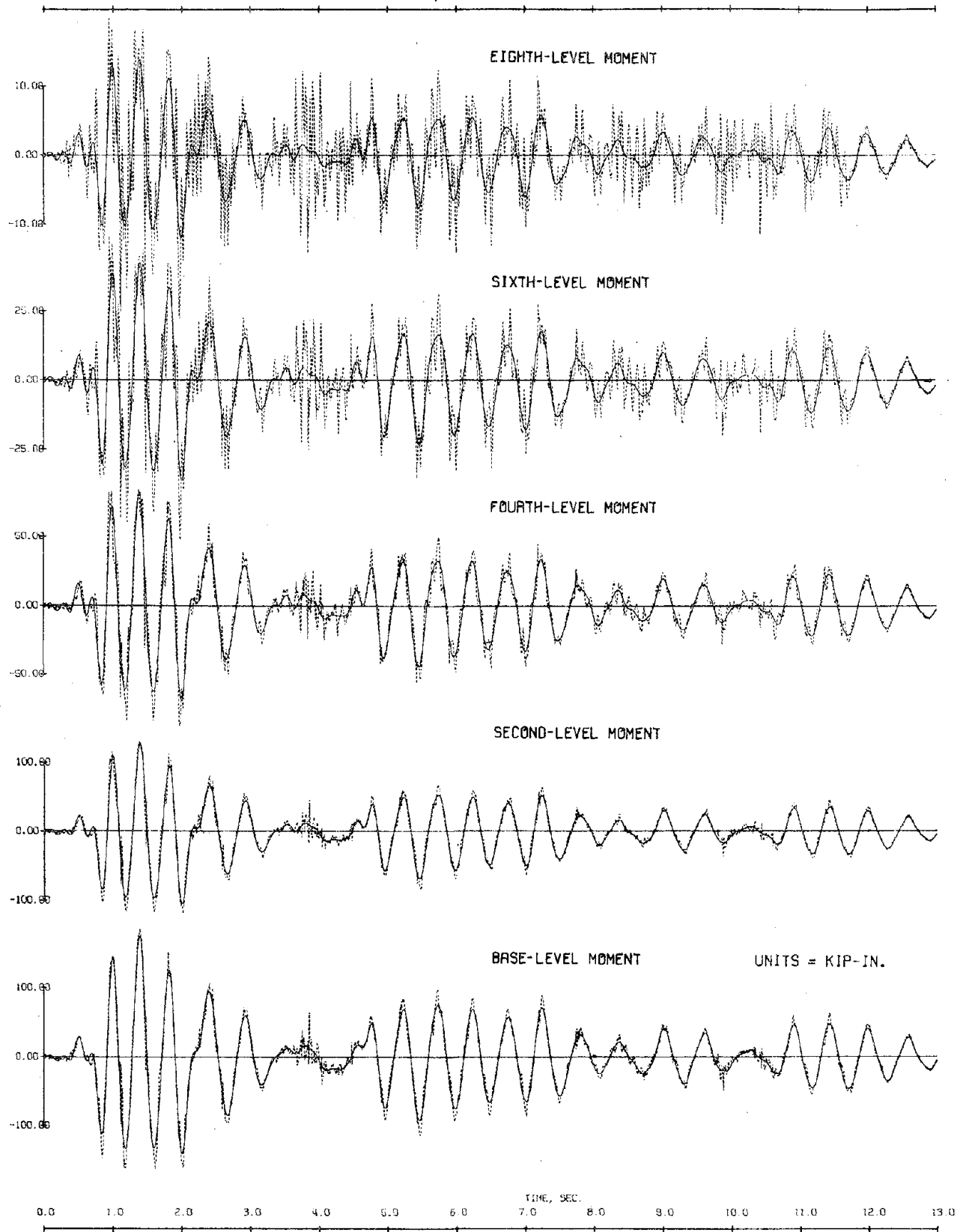
Fig. 5.27   Test Run D1-2.   Moment Waveforms (Broken Line) and
Filtered Components Below 5.0 Hz (Solid Line)
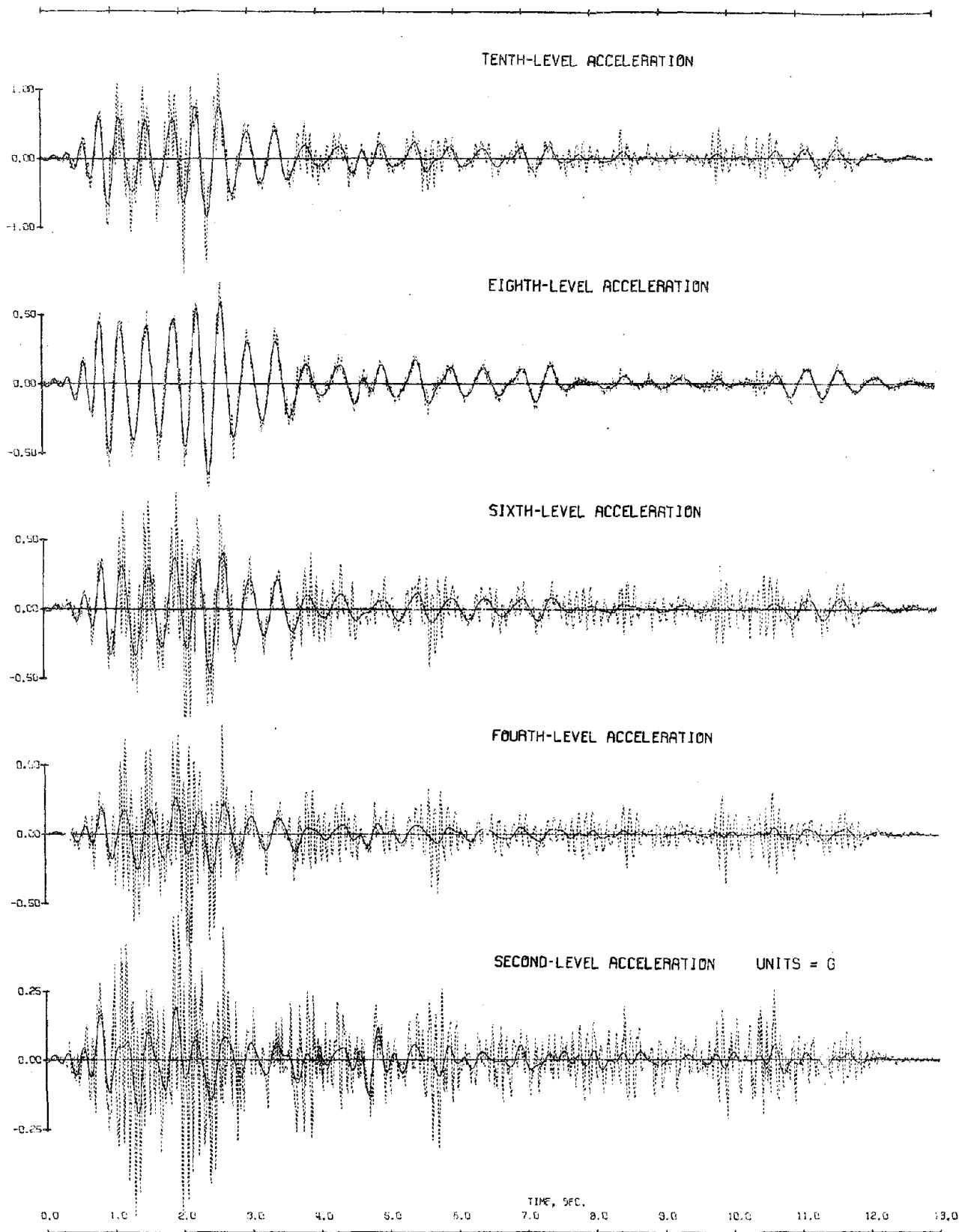
Fig. 5.28 Test Run D2-1. Acceleration Waveforms (Broken Line)
and Filtered Components Below 5.0 Hz (Solid Line)
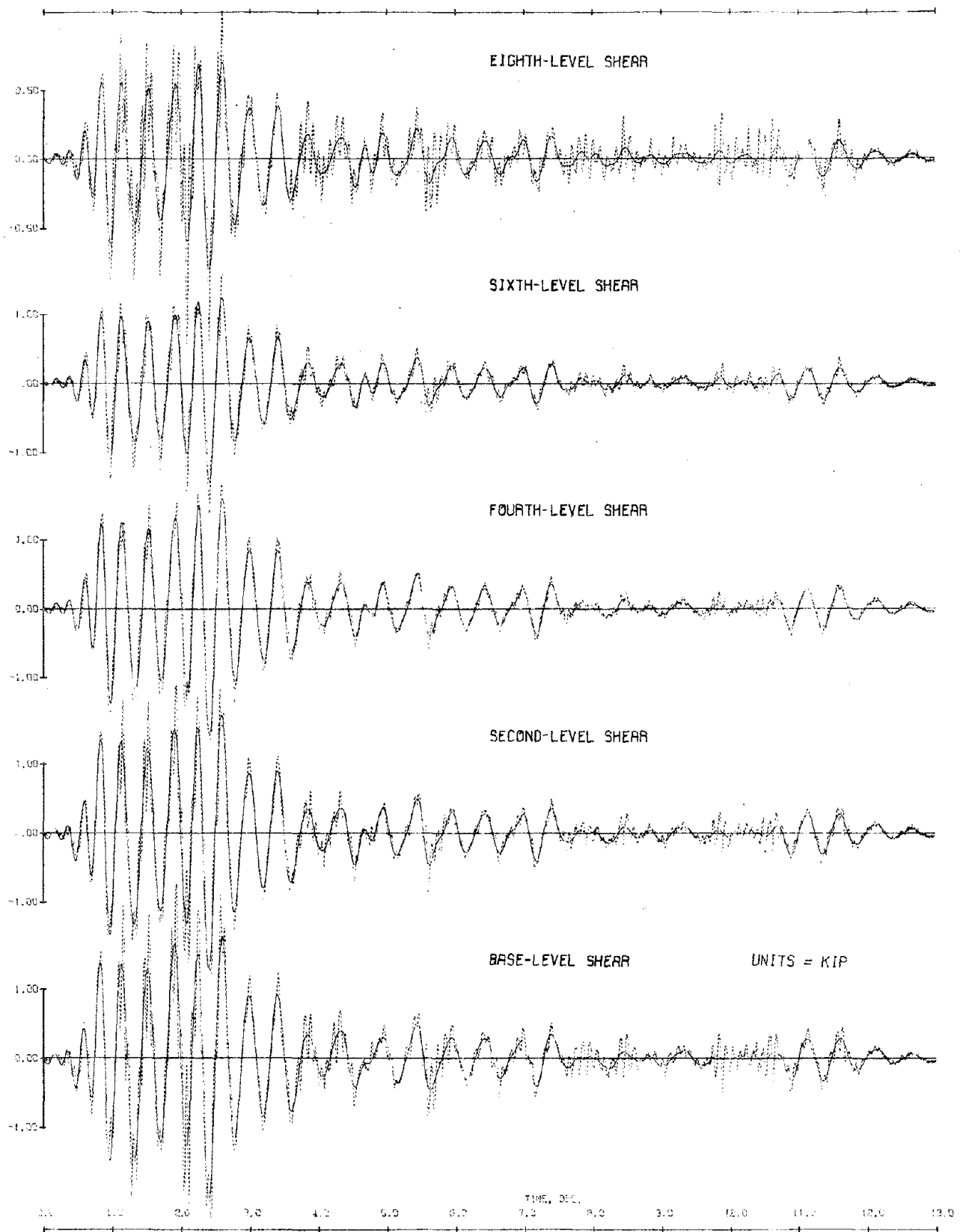
Fig. 5.29 Test Run D2-1. Shear Waveforms (Broken Line) and
Filtered Components Below 5.0 Hz (Solid Line)
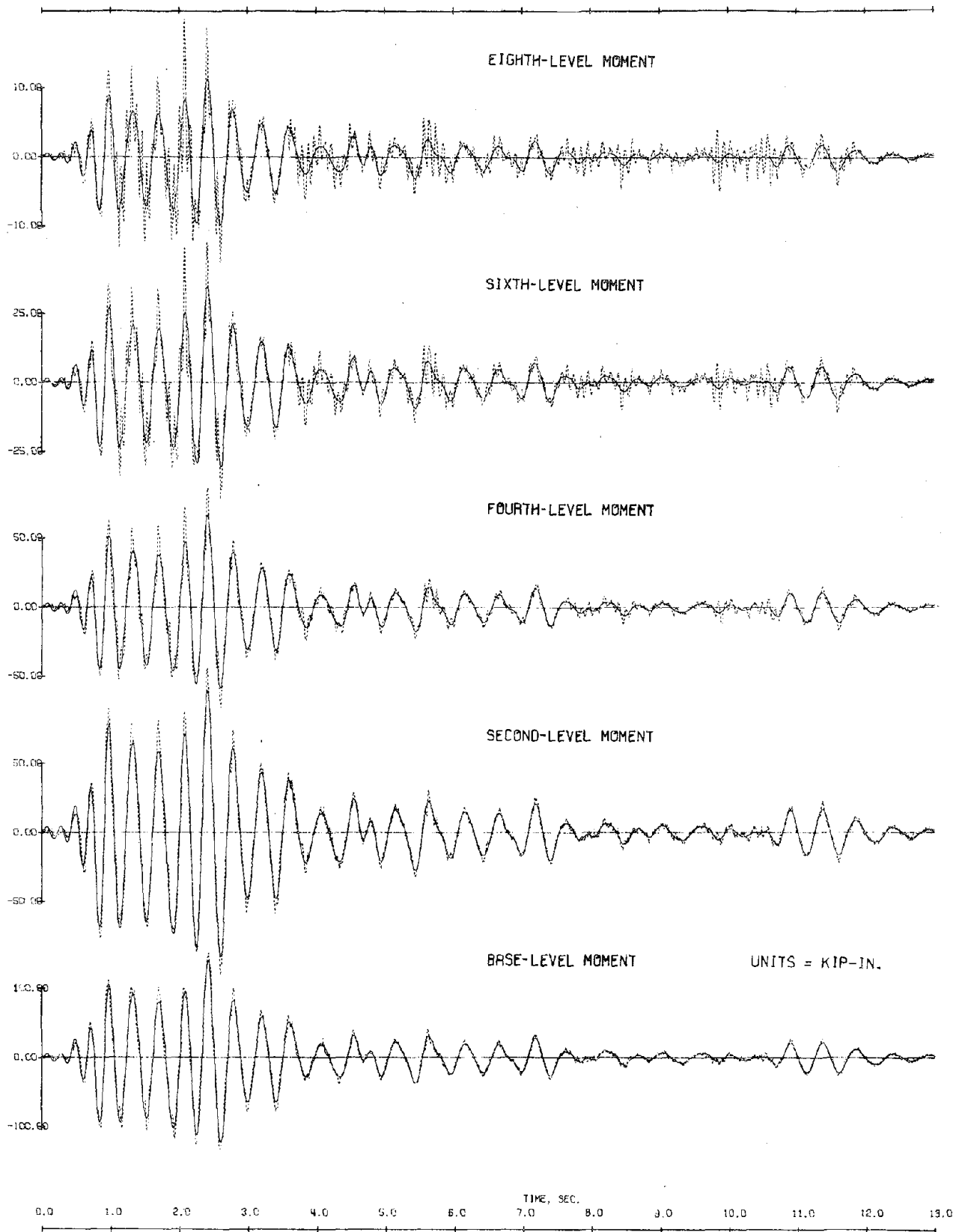
Fig. 5.30   Test Run D2-1.   Moment Waveforms (Broken Line) and
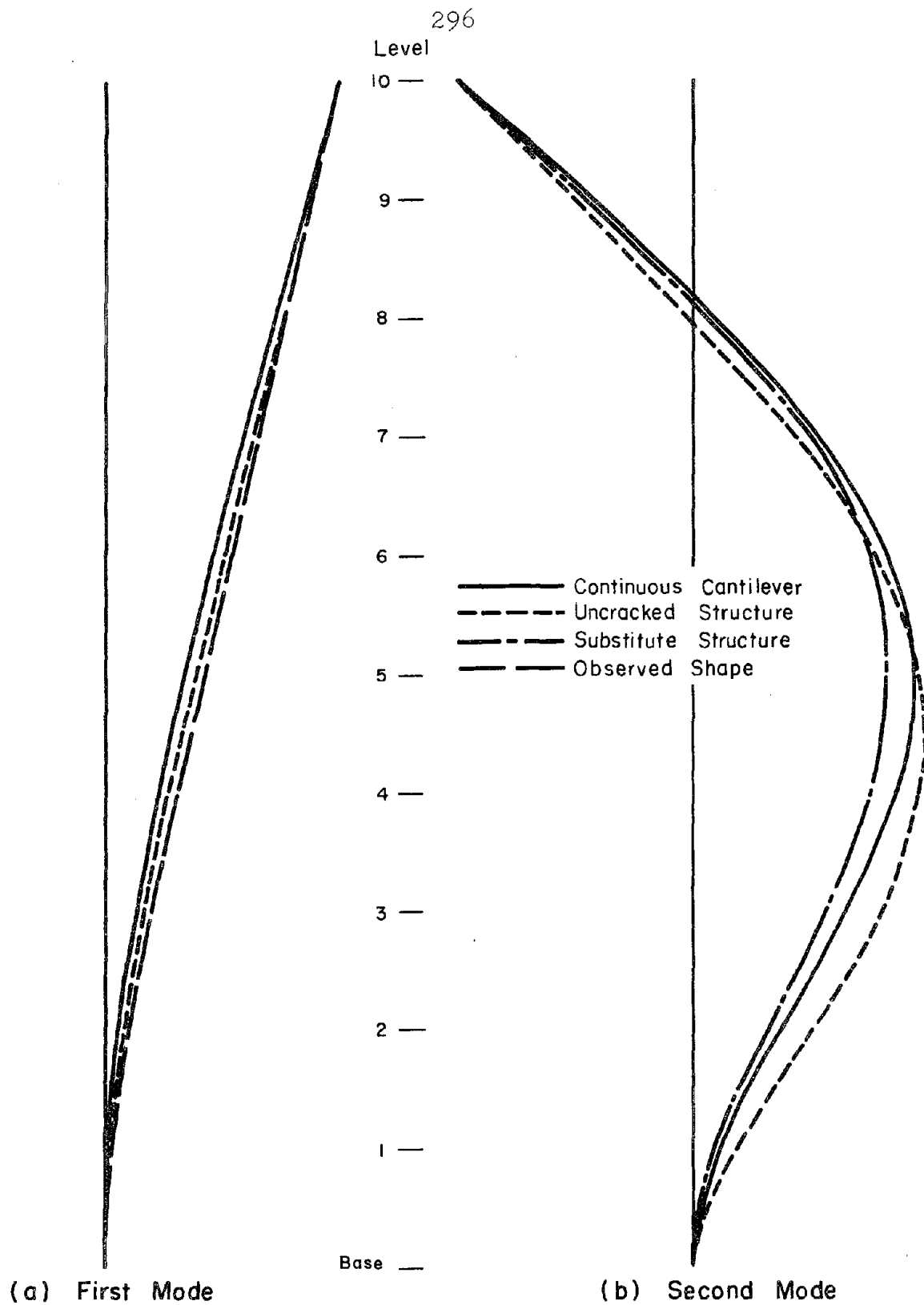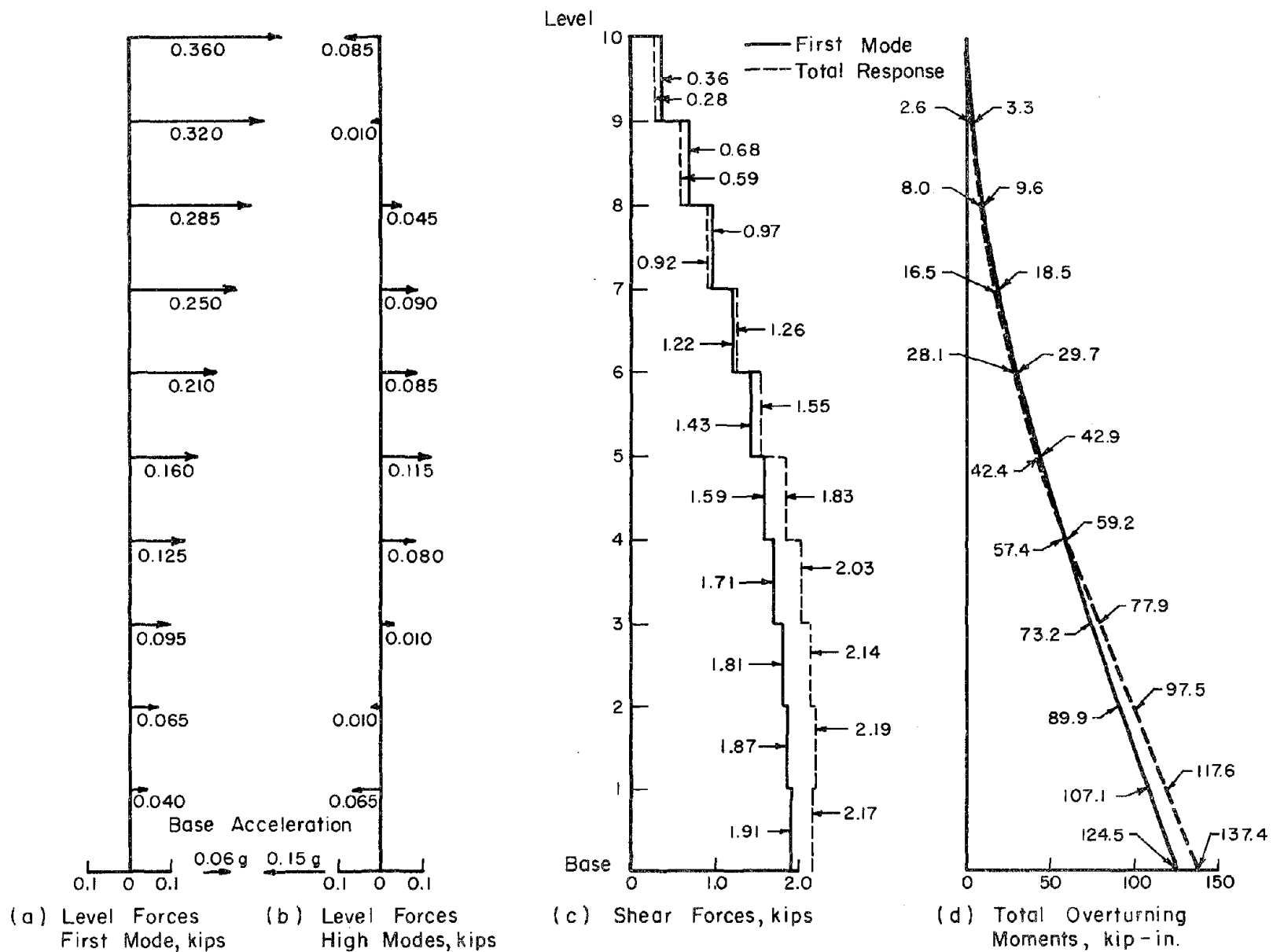Filtered Components Below 5.0 Hz (Solid Line)
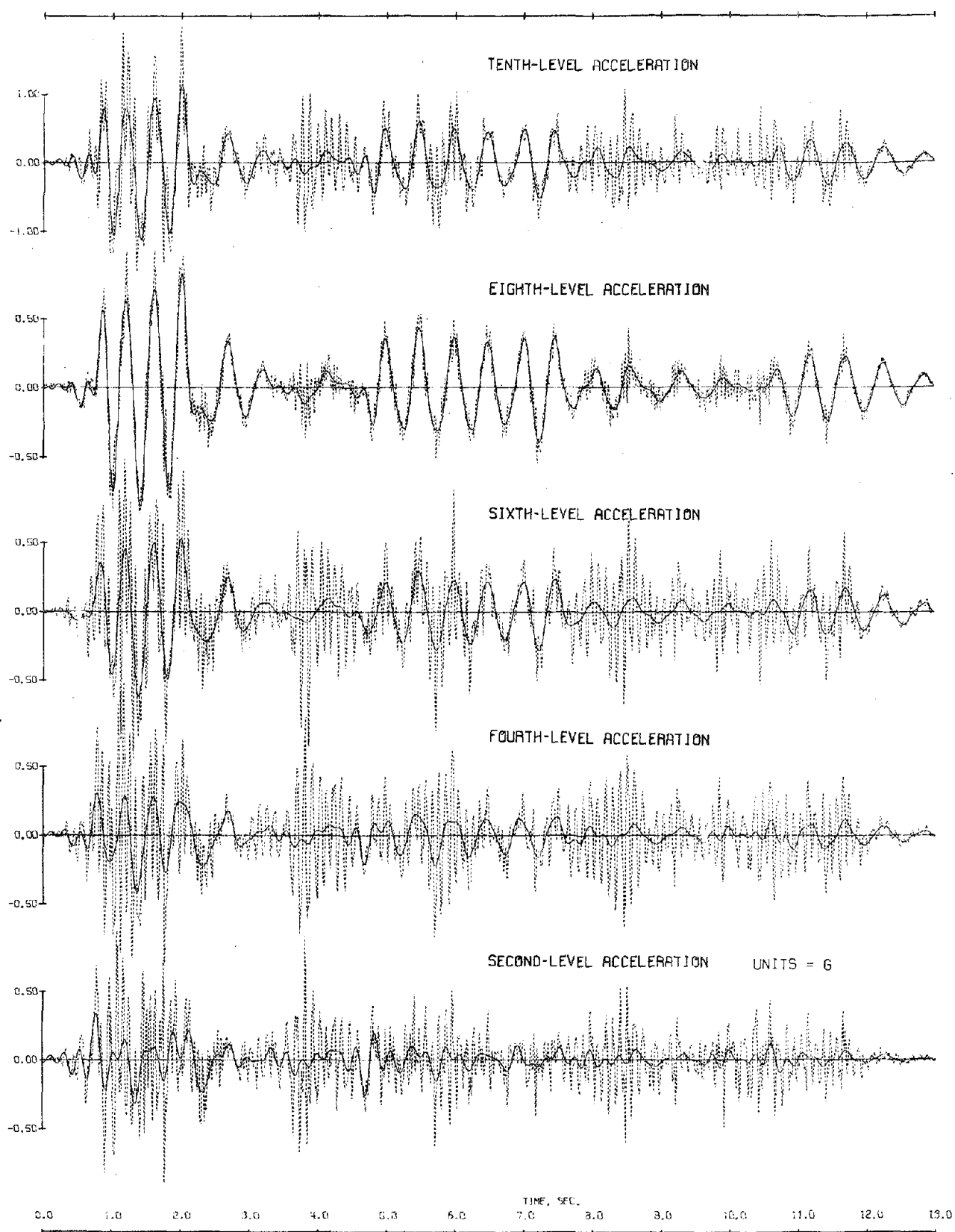
Fig. 5.31 Test Run D2-2. Acceleration Waveforms (Broken Line)
and Filtered Components Below 5.0 Hz (Solid Line)
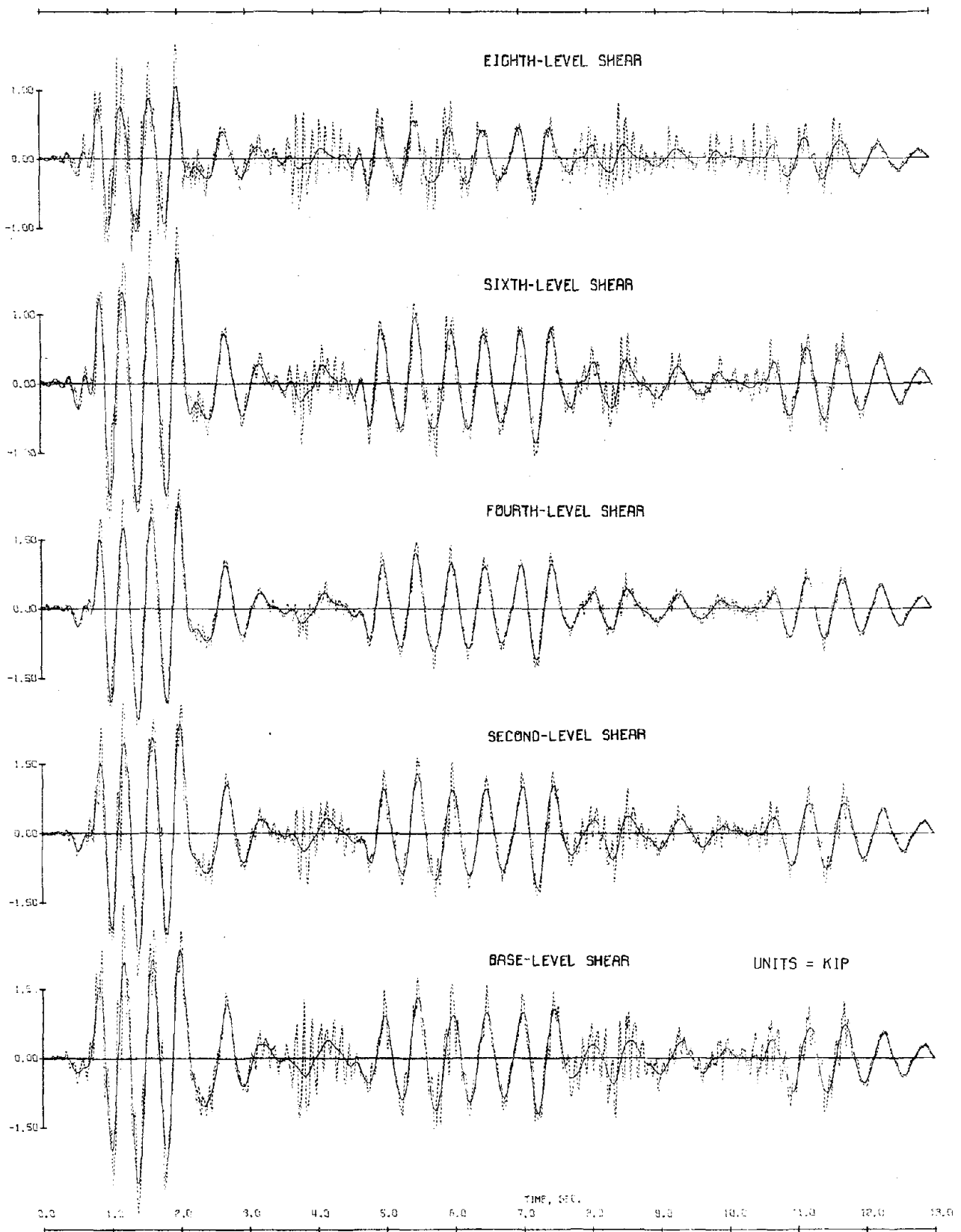
Fig. 5.32 Test Run D2-2. Shear Waveforms (Broken Line) and
Filtered Components Below 5.0 Hz (Solid Line)
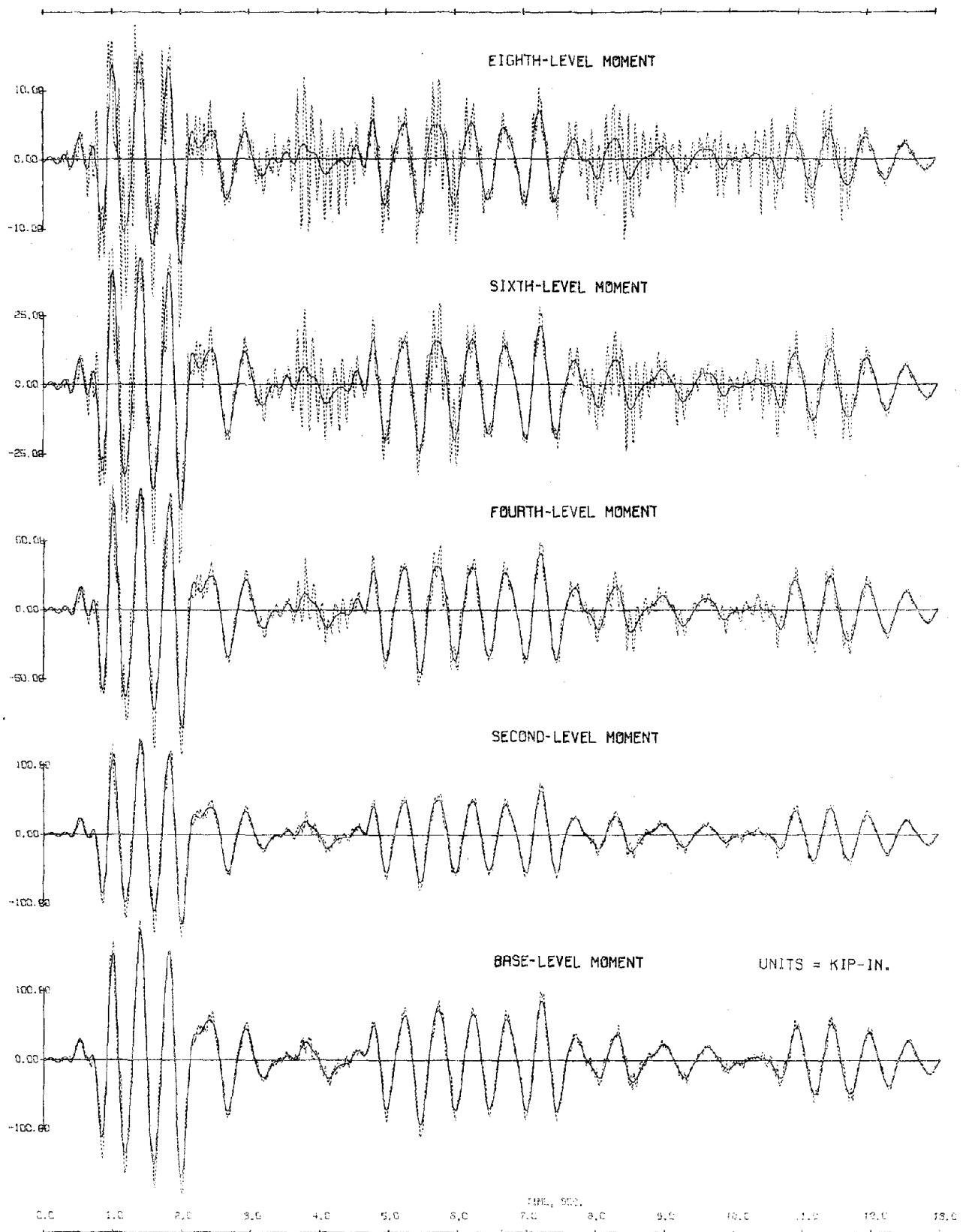
Fig. 5.33   Test Run D2-2.   Moment Waveforms (Broken Line) and
Filtered Components Below 5.0 Hz (Solid Line)
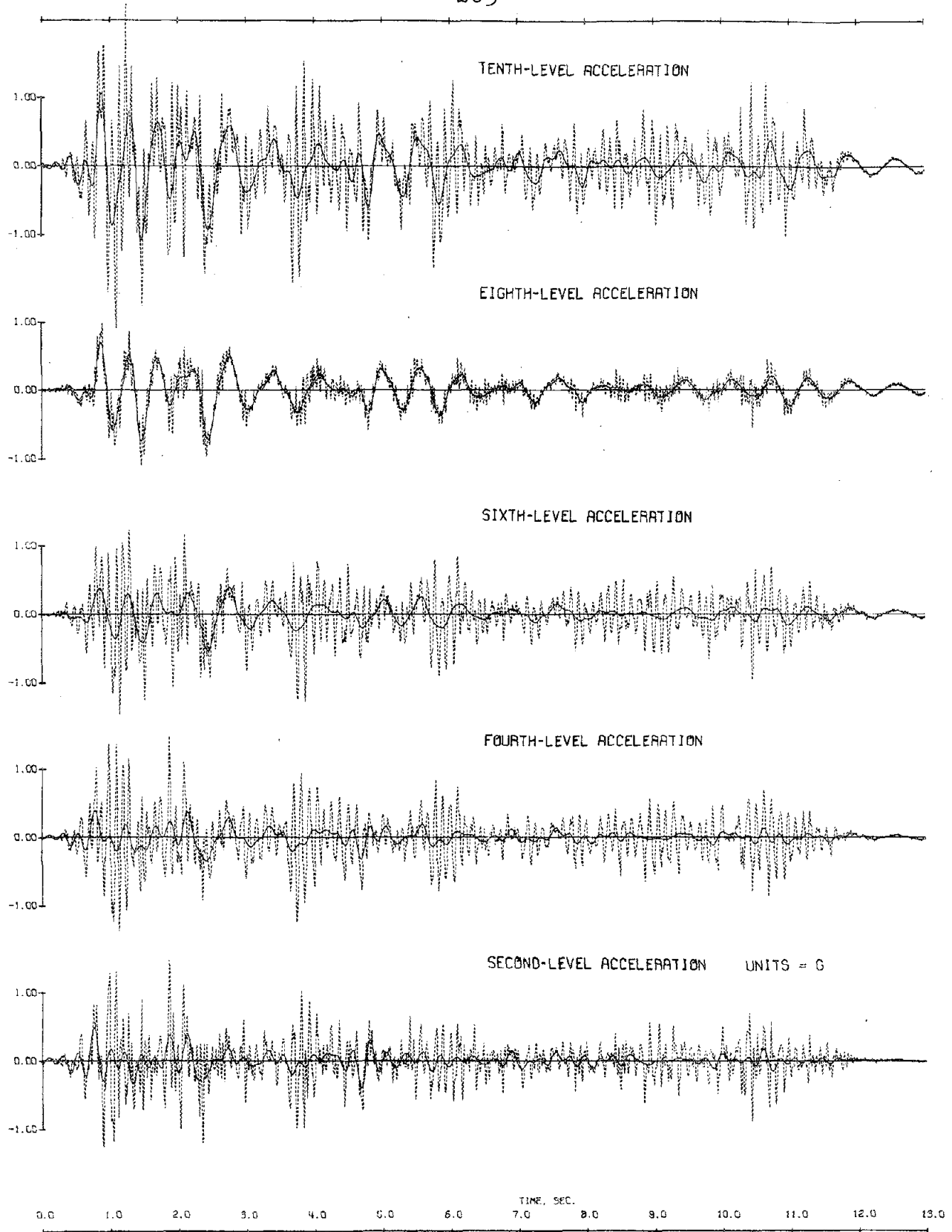
Fig. 5.34 Test Run D2-3. Acceleration Waveforms (Broken Line)
and Filtered Components Below 5.0 Hz (Solid Line)
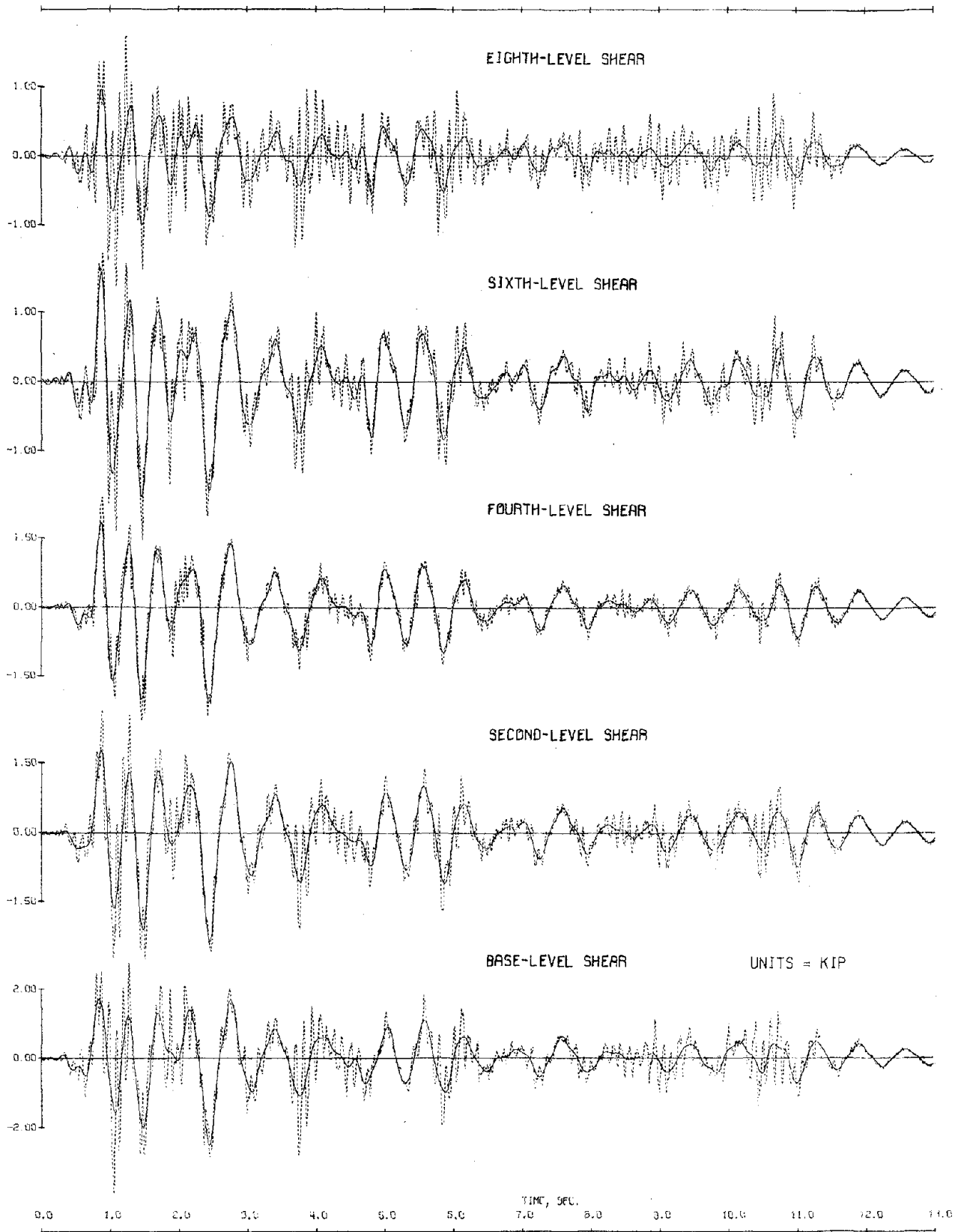
Fig. 5.35 Test Run D2-3. Shear Waveforms (Broken Line) and
Filtered Components Below 5.0 Hz (Solid Line)
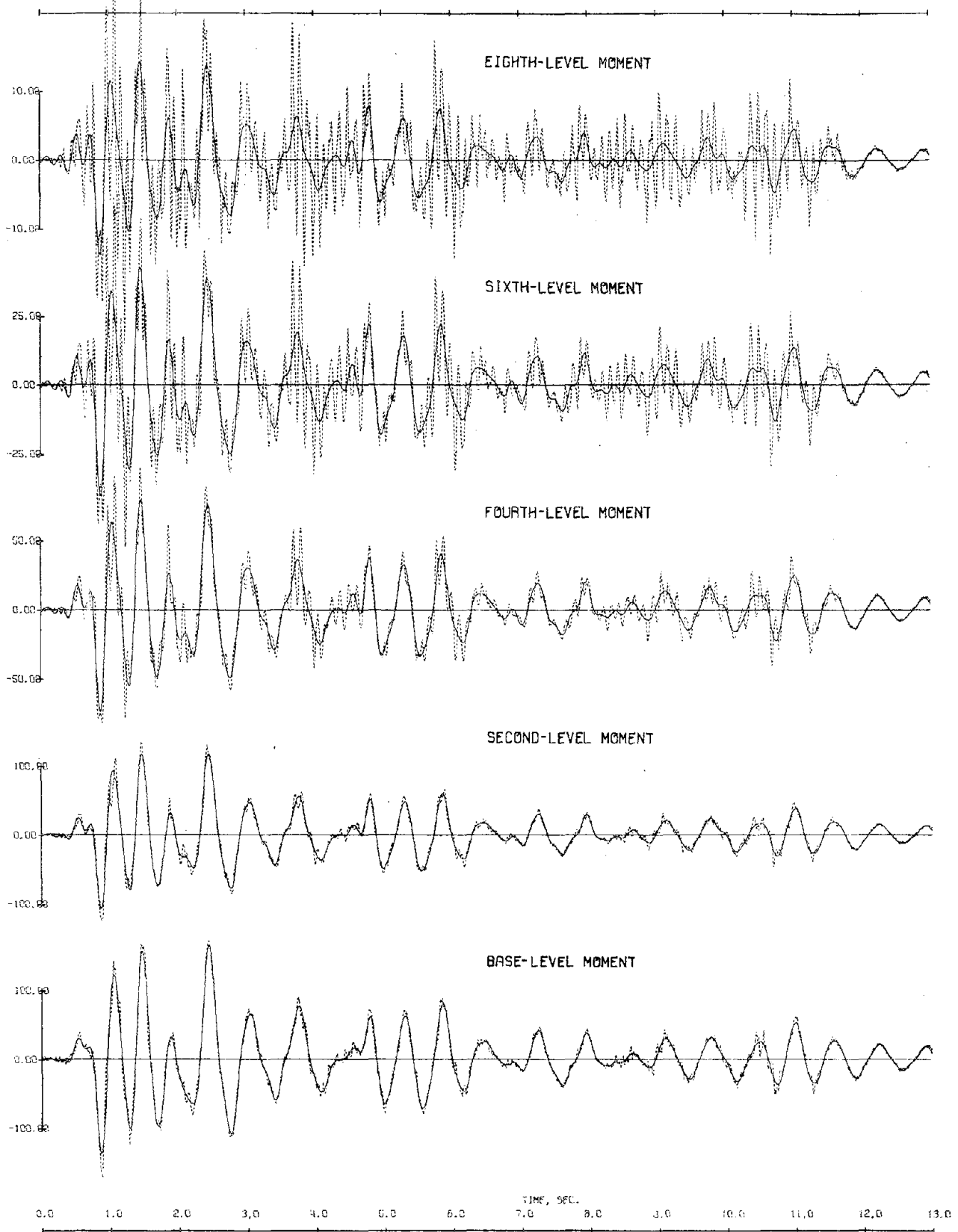
Fig. 5.36   Test Run D2-3.   Moment Waveforms (Broken Line) and
Filtered Components Below 5.0 Hz (Solid Line)
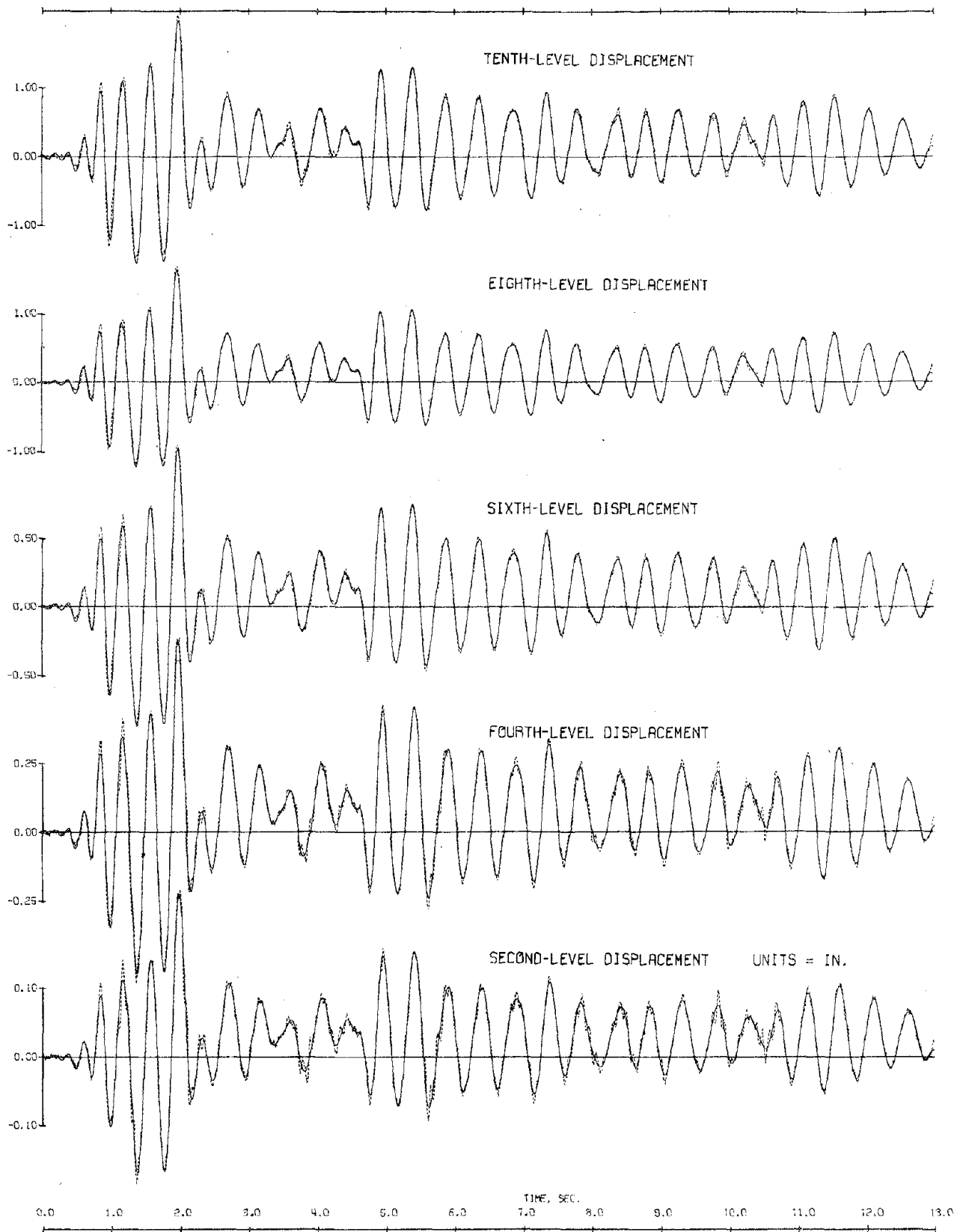
Fig. 5.37   Test Run M1-1.   Displacements Waveforms (Broken Line)
and Filtered Components Below 5.0 Hz (Solid Line)
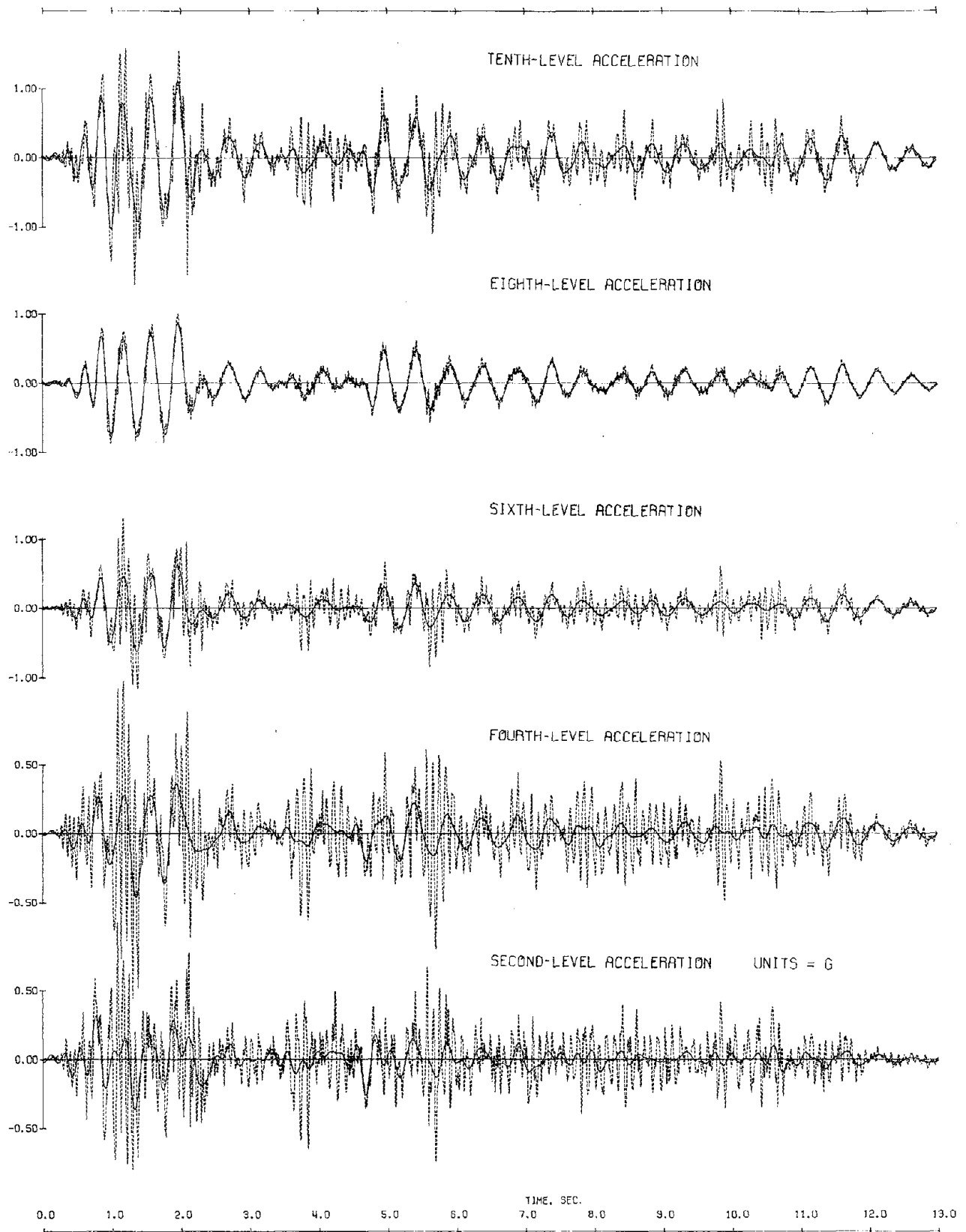
Fig. 5.38   Test Run M1-1.   Acceleration Waveforms (Broken Line)
and Filtered Components Below 5.0 Hz (Solid Line)
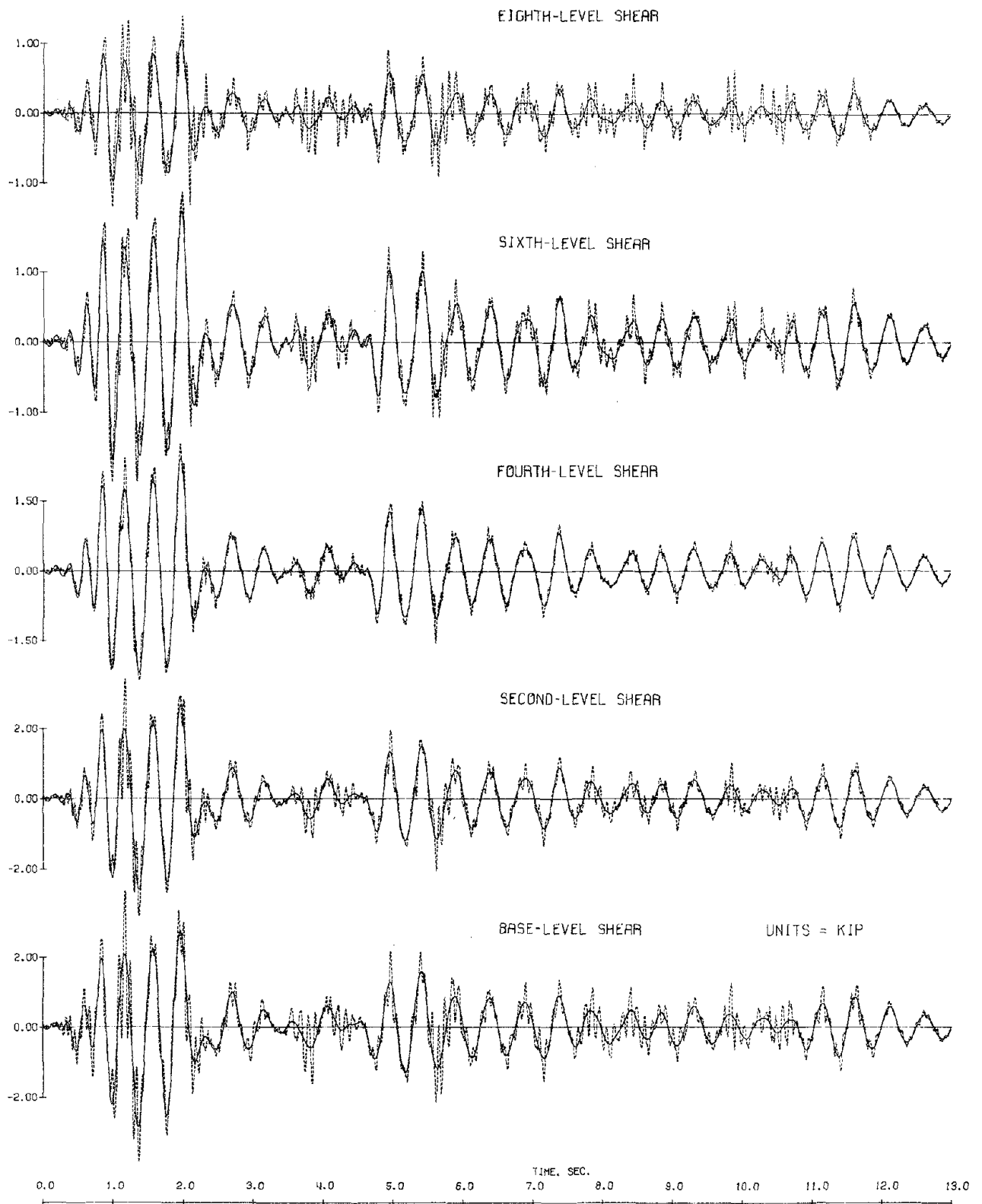
Fig. 5.39   Test Run M1-1.   Shear Waveforms (Broken Line) and
Filtered Components Below 5.0 Hz (Solid Line)
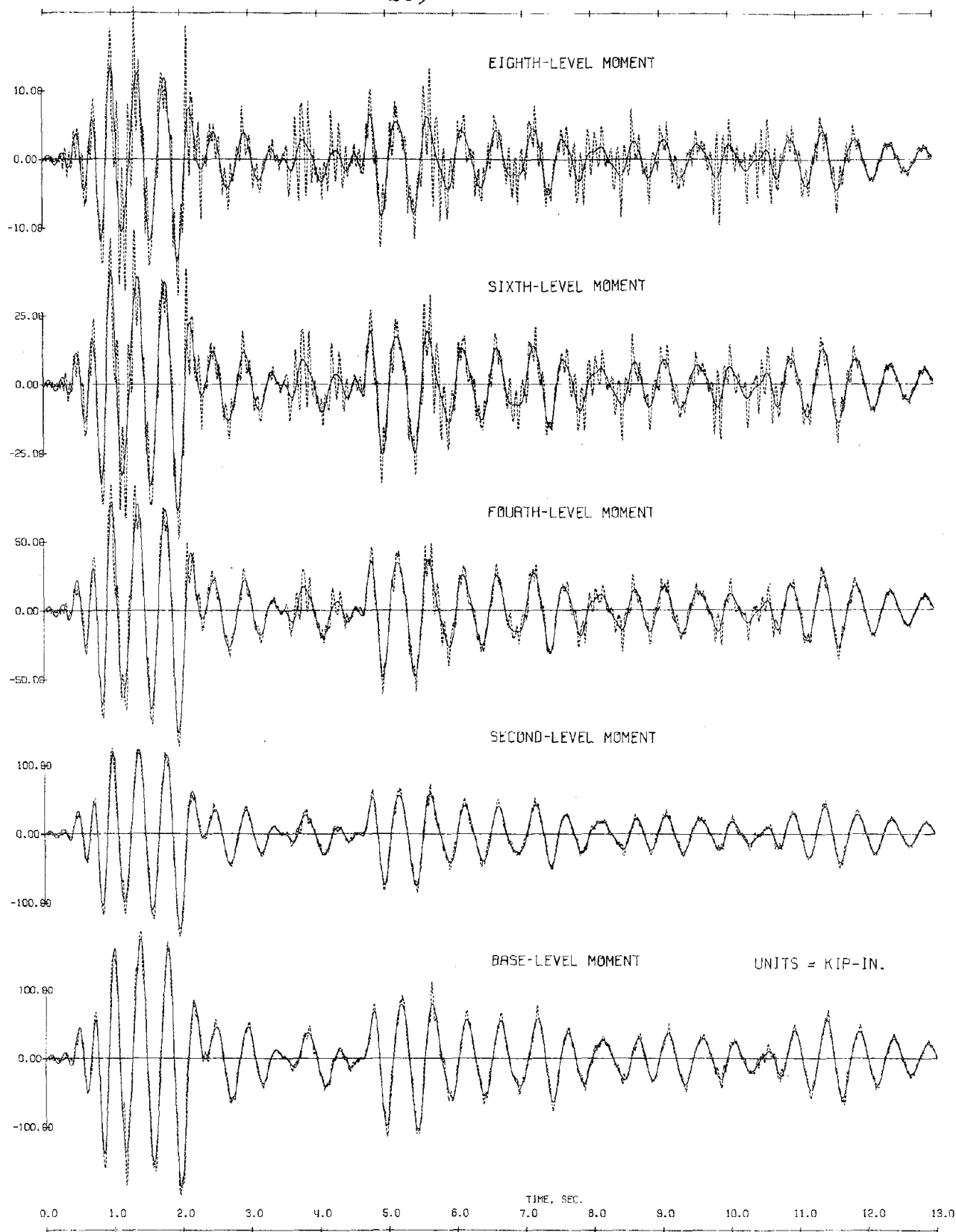
Fig. 5.40   Test Run M1-1.   Moment Waveforms (Broken Line) and
Filtered Components Below 5.0 Hz (Solid Line)
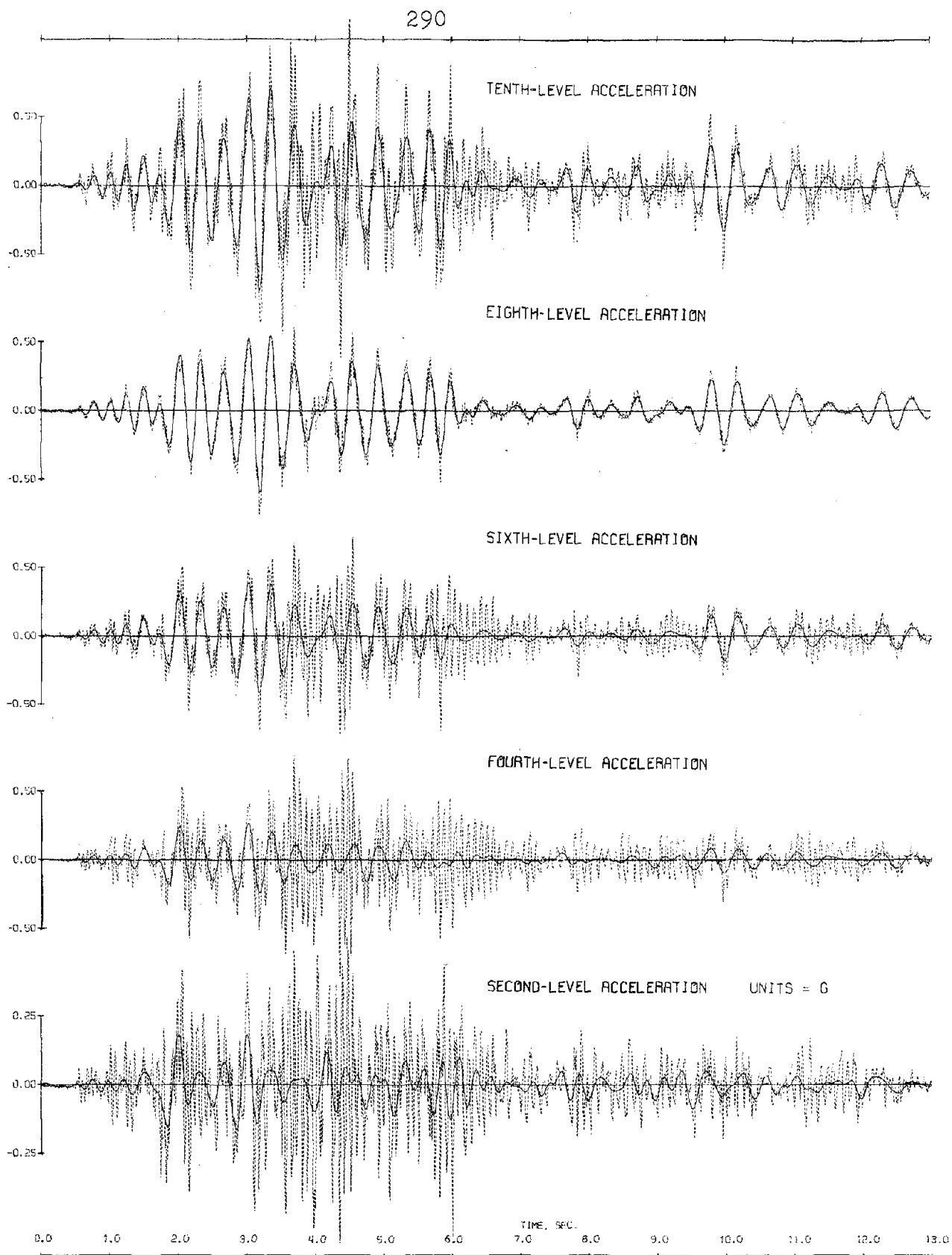
Fig. 5.41   Test Run D3-1.   Acceleration Waveforms (Broken Line)
and Filtered Components Below 5.0 Hz (Solid Line)

Fig. 5.42   Test Run D3-1.   Shear Waveforms (Broken Line) and
Filtered Components Below 5.0 Hz (Solid Line)

Fig. 5.43 Test Run D3-1. Moment Waveforms (Broken Line) and
Filtered Components Below 5.0 Hz (Solid Line)

Fig. 5.44   Test Run D3-2.   Acceleration Waveforms (Broken Line)
and Filtered Components Below 5.0 Hz (Solid Line)

Fig. 5.45   Test Run D3-2.   Shear Waveforms (Broken Line) and
Filtered Components Below 5.0 Hz (Solid Line)

Fig. 5.46   Test Run D3-2.   Moment Waveforms (Broken Line) and
Filtered Components Below 5.0 Hz (Solid Line)

Fig. 5.47 Modal Shapes of Test Structure D

297

(a) Level Forces
First Mode, kips

(b) Level Forces
High Modes, kips

(c) Shear Forces, kips

(d) Total Overturning
Moments, kip-in.

Fig. 5.48 Test Run D1-1. Forces at the Instant of Max. Base Moment

298

(a) Level Forces First Mode, kips

(b) Level Forces High Modes, kips

(c) Shear Forces, kips

(d) Total Overturning Moments, kip-in.
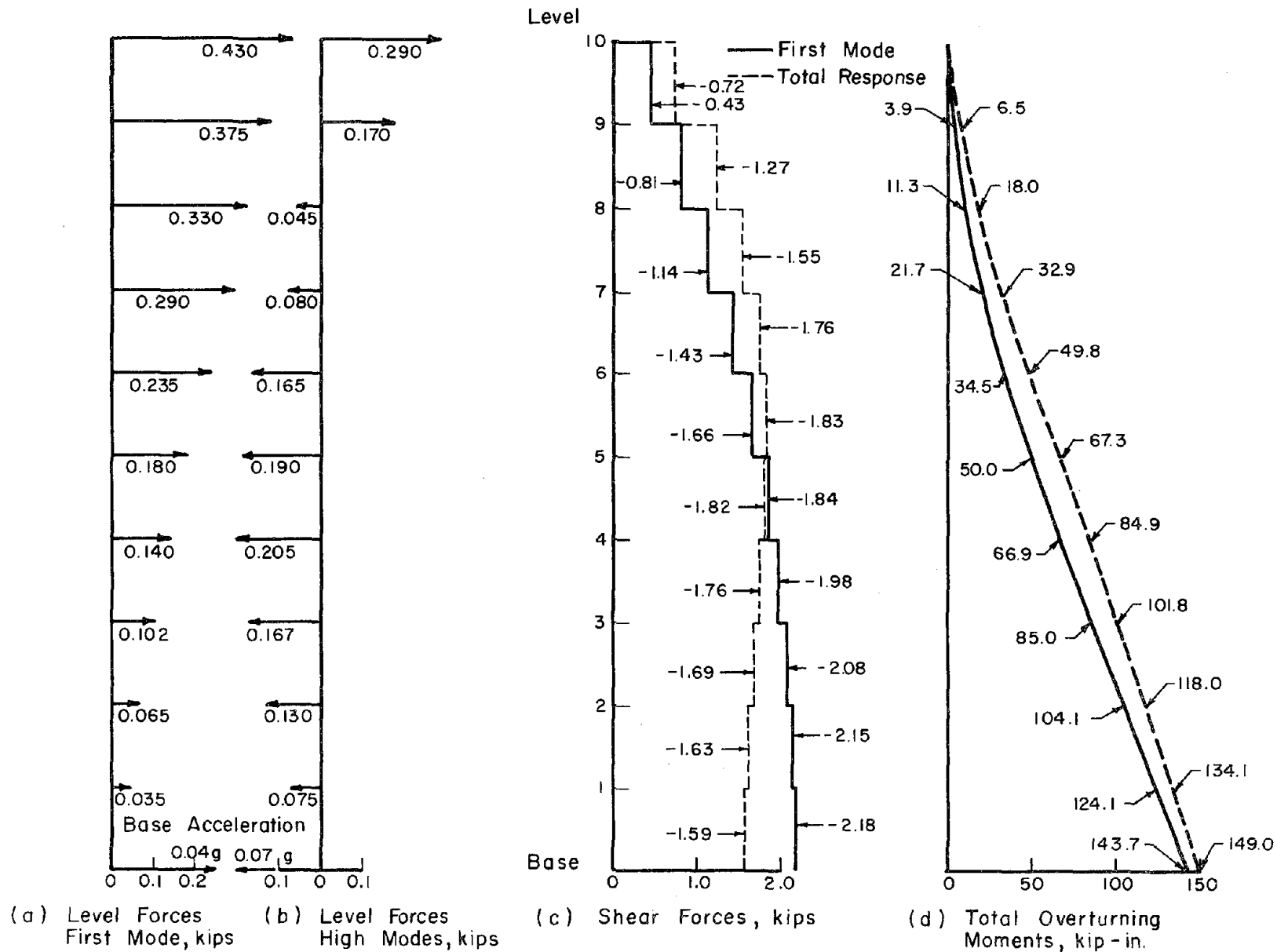
Fig. 5.49 Test Run D2-1. Forces at the Instant of Max. Base Moment
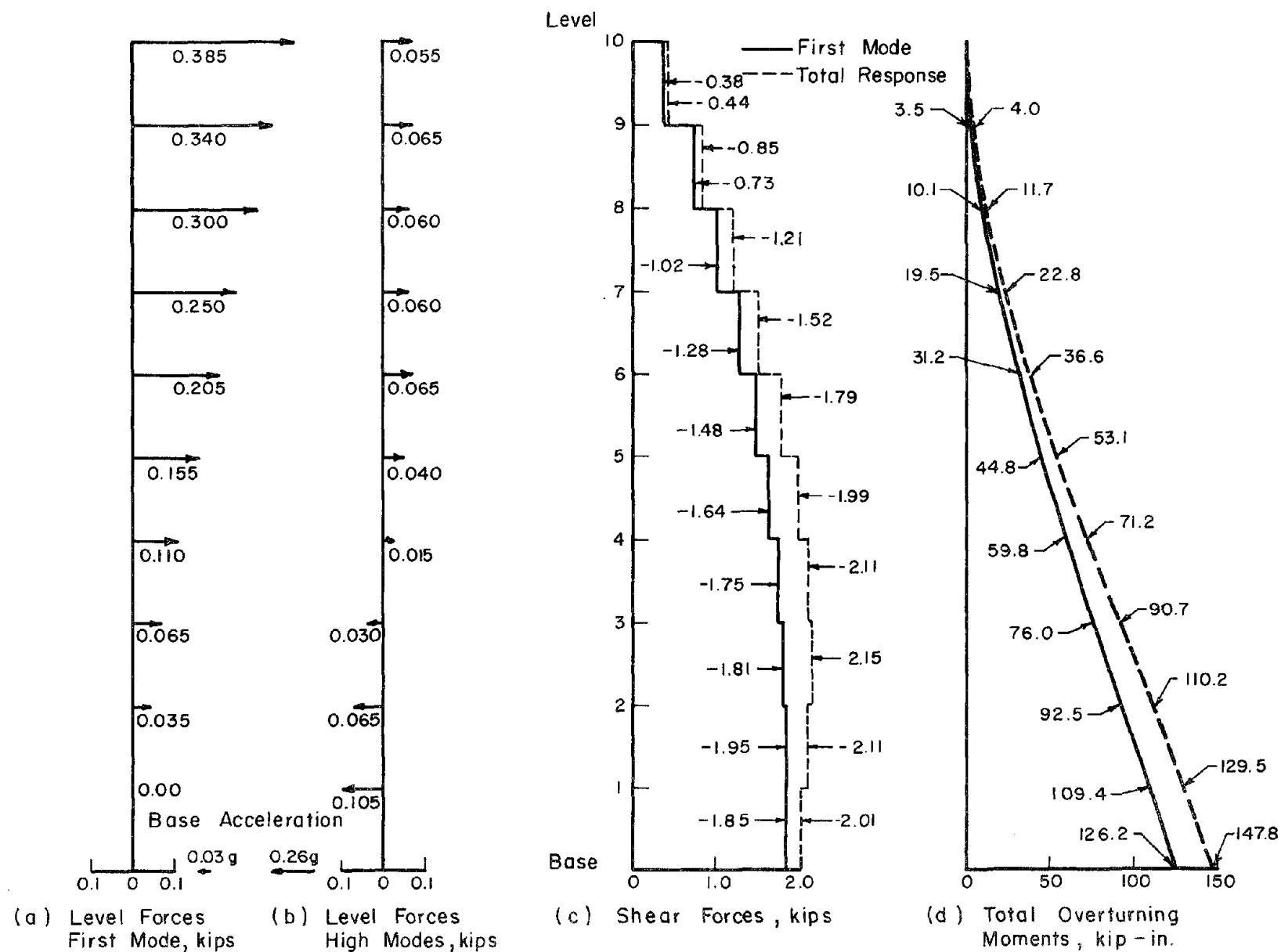
Fig. 5.50   Test Run D3-1.   Forces at the Instant of Max. Base Moment

Level

(a) Level Forces First Mode, kips

0.550   0.035
0.500   0.020
0.440   0.065
0.375   0.105
0.310   0.100
0.240   0.060
0.170   0.000
0.110   0.080
0.060   0.155
0.010   0.225

Base Acceleration

0.05g   0.16g

0   0.1

(b) Level Forces High Modes, kips

0.1   0   0.1

—— First Mode
---- Total Response

← 0.55
← 0.51
1.05 →   ← 1.04
1.49 →   ← 1.54
1.86 →   ← 2.02
2.18 →   ← 2.43
2.41 →   ← 2.72
2.58 →   ← 2.89
2.69 →   ← 2.93
2.75 →   ← 2.83
← 2.76
2.61 →

Base

0   1.0   2.0   3.0

(c) Shear Forces, kips

−4.7   −5.0
−14.3   −14.7
−28.4   −28.5
−45.7   −47.2
−65.9   −69.7
−88.2   −94.9
−112.2 −121.7
−137.4 −149.0
−162.6 −174.9
−188.1 −199.1

0   50   100   150   200

(d) Total Overturning Moments, kip-in.

300

Fig. 5.51   Test Run M1-1.   Forces at the Instant of Max. Base Moment
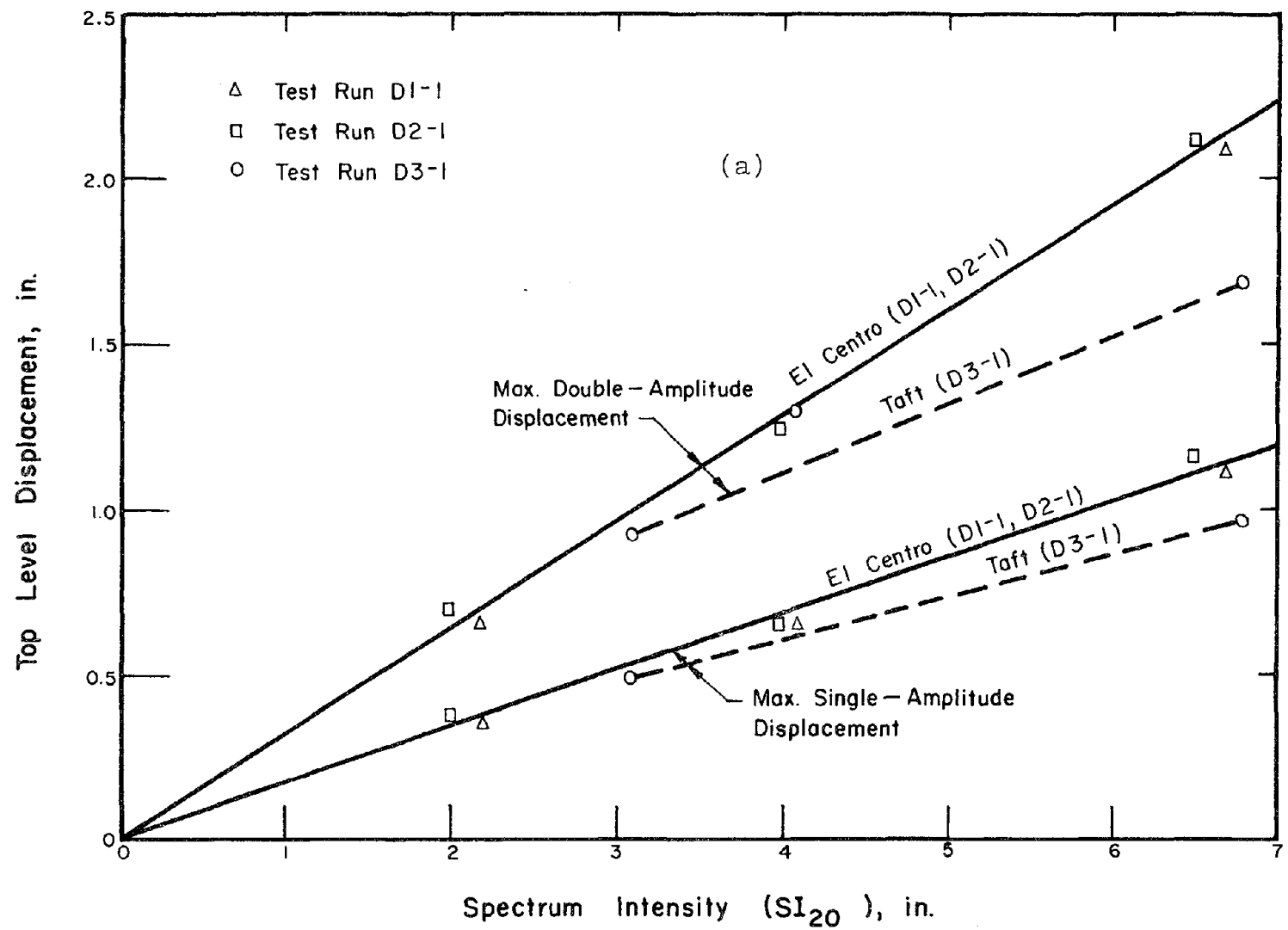
Fig. 5.52   Comparison of Maximum Top-Level Displacement   with Spectrum
Intensity at 20% Damping
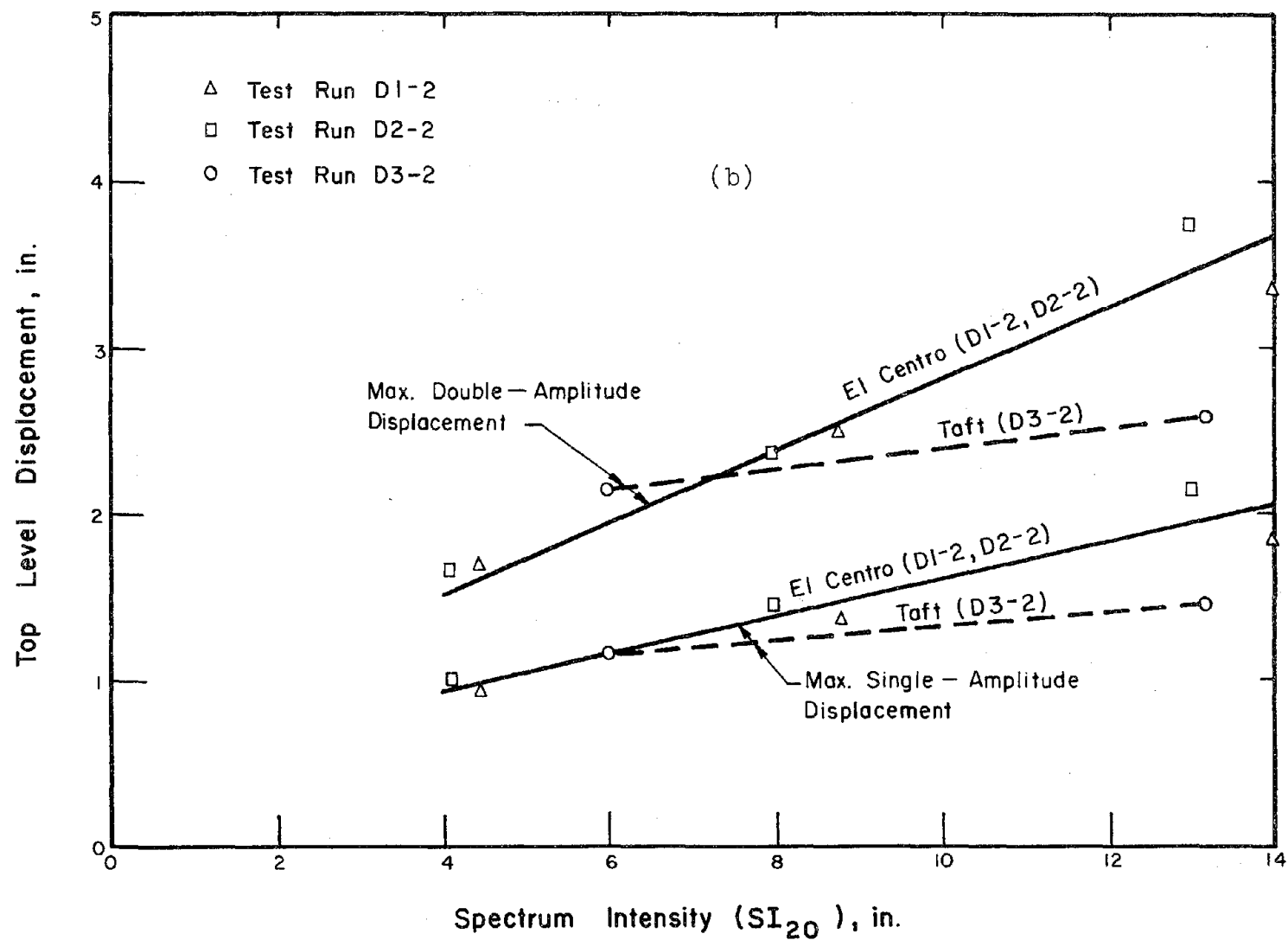
Fig. 5.52 (Contd)   Comparison of Maximum Top-Level Displacement with Spectrum
Intensity at 20% Damping
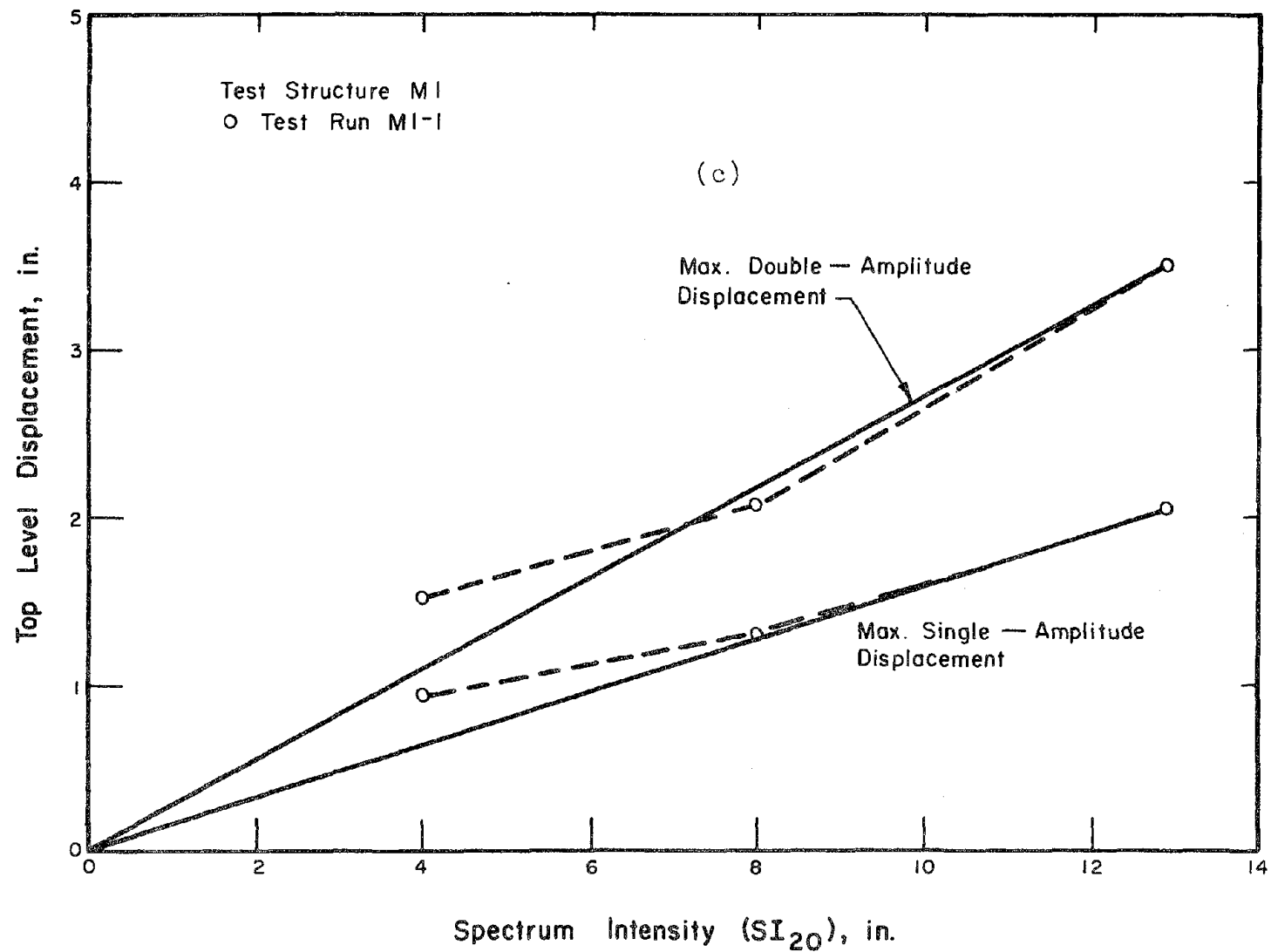
Fig. 5.52 (Contd) Comparison of Maximum Top-Level Displacement with Spectrum Intensity at 20% Damping
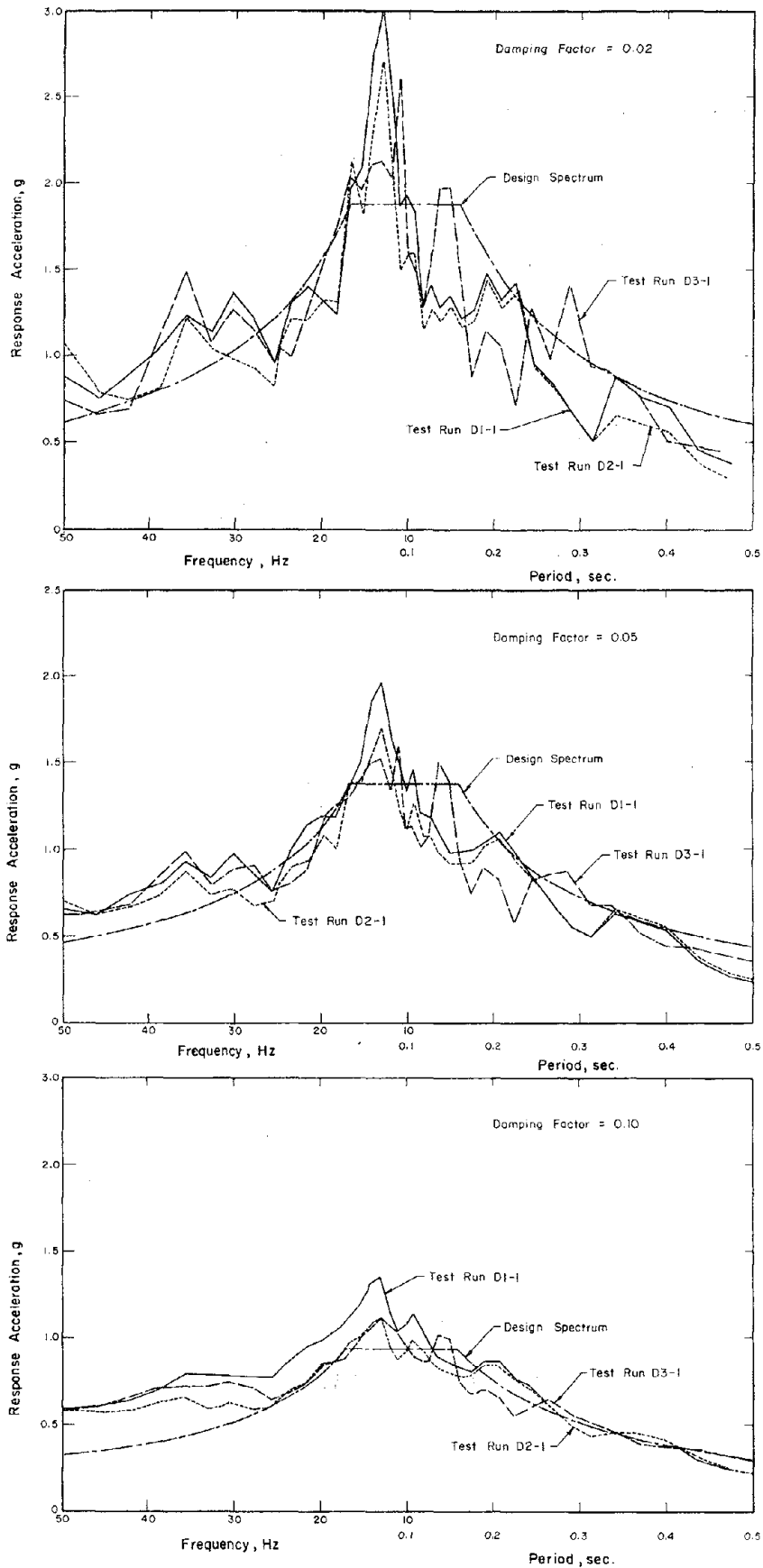
Fig. 6.1 Comparison of Design and Obtained Spectra
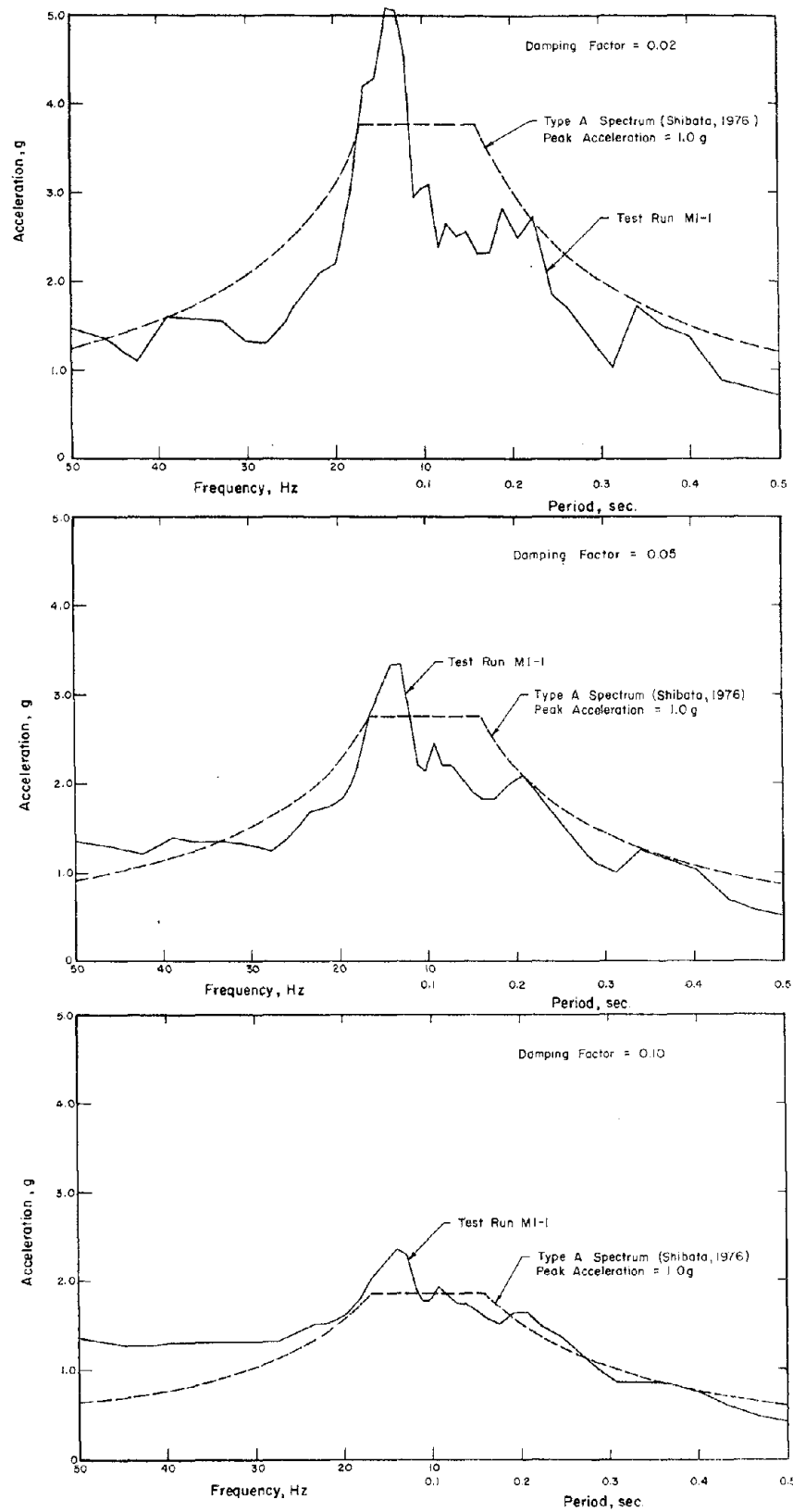
Fig. 6.2 Comparison of Design and Obtained Spectra
(Test Structure M)
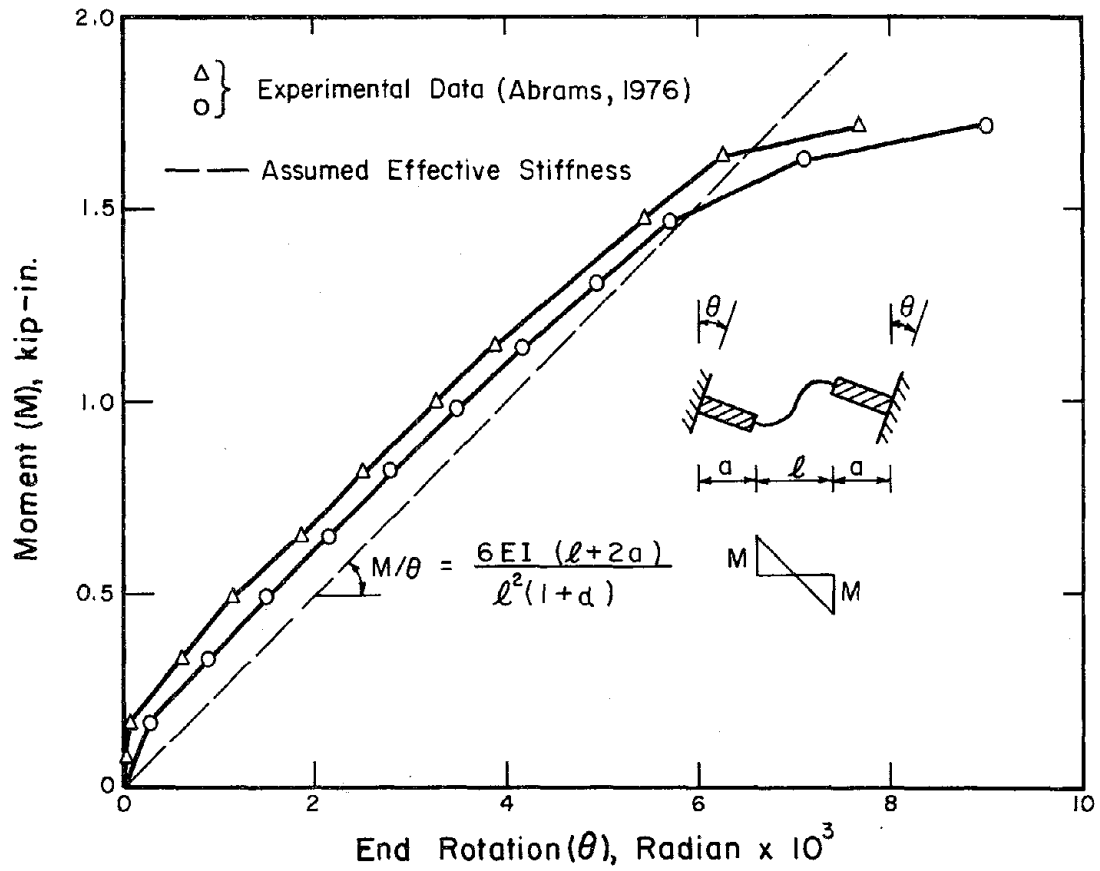
Fig. 6.3a   Moment-Rotation Relationship for Connecting Beam
(Test Structure D)
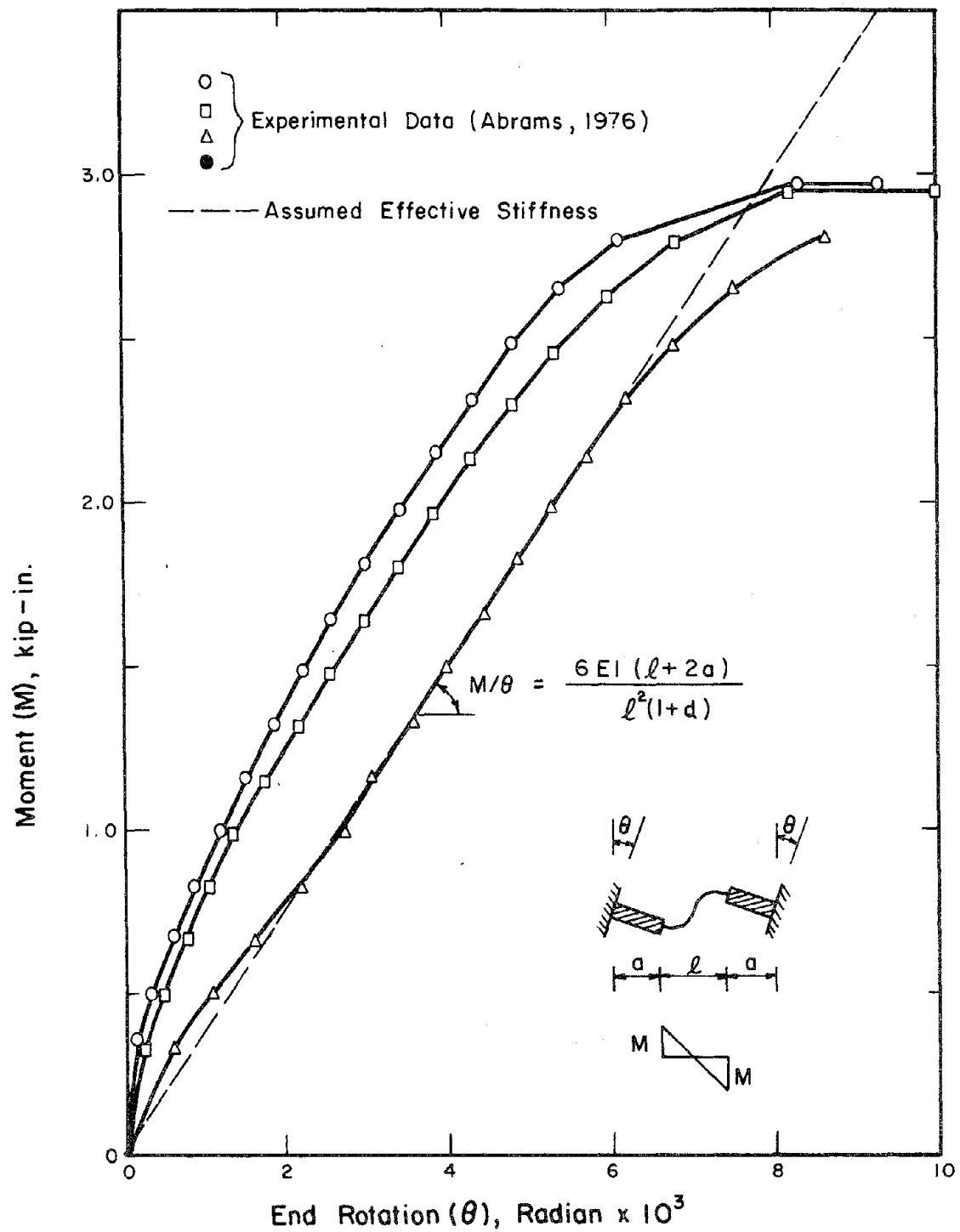
Fig. 6.3b   Moment-Rotation Relationship for Connecting Beam
(Test Structure M)
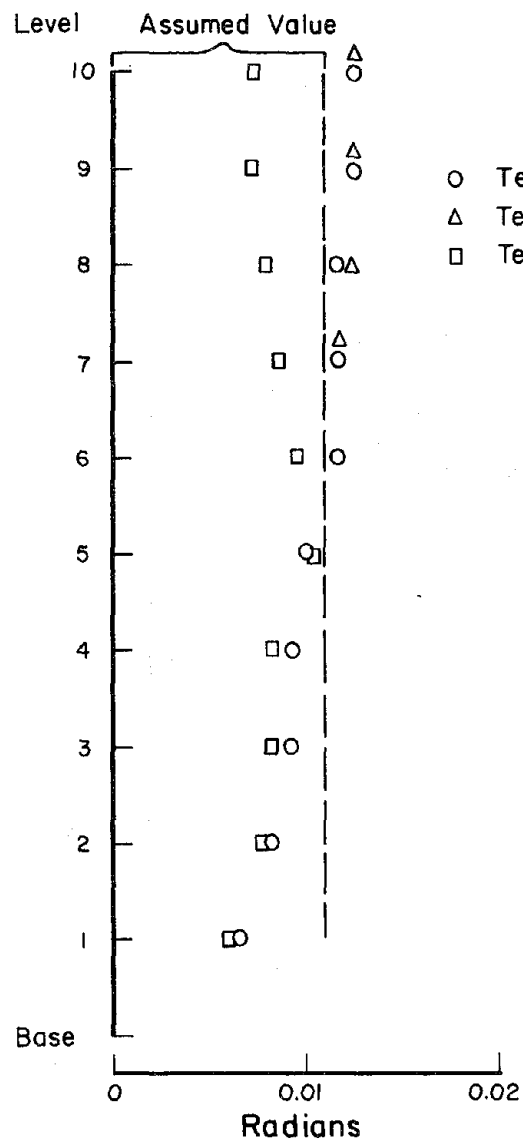
(a) Test Structures D
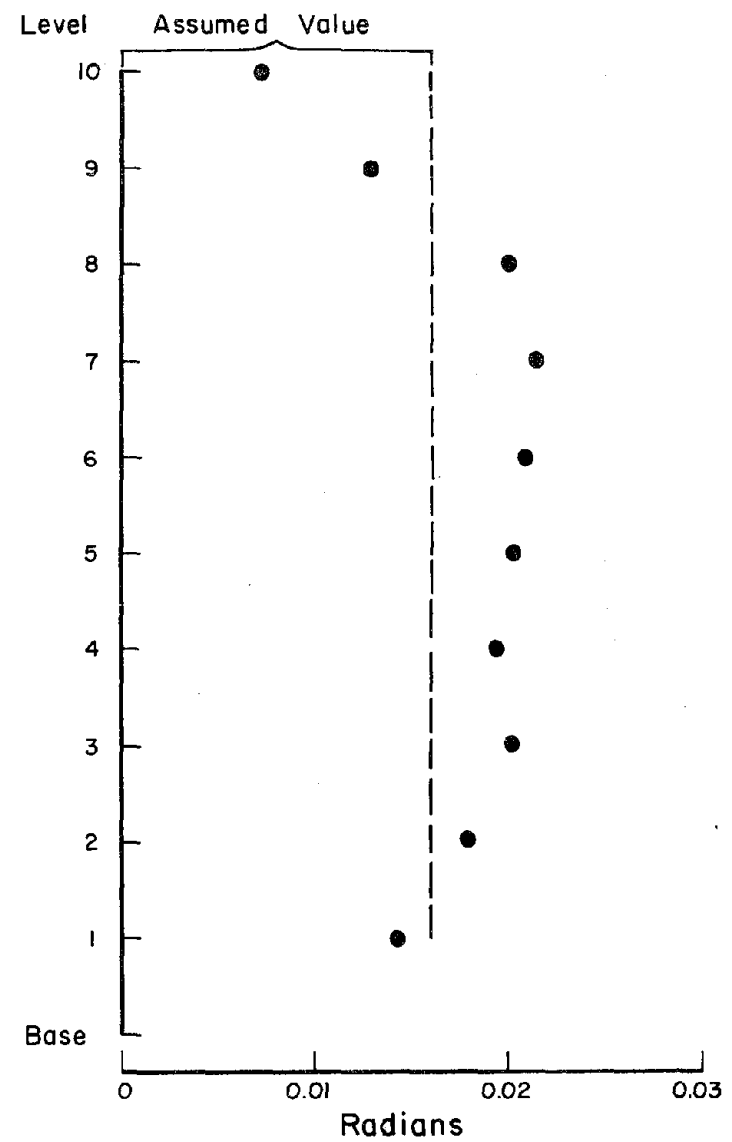
(b) Test Structure M

Fig. 6.4 Calculated End Rotations of Connecting Beams
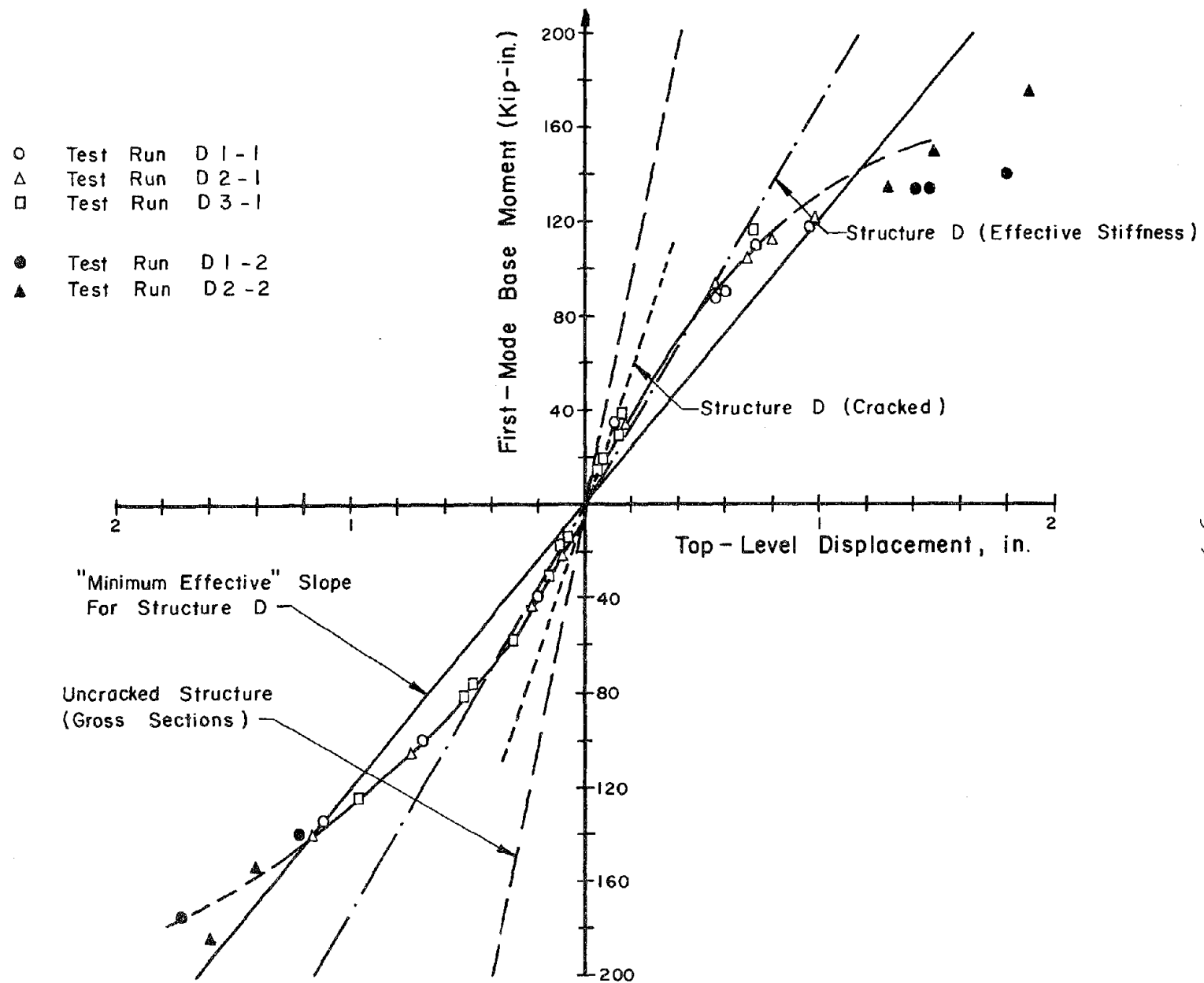
Fig. 6.5a   Relationship of First-Mode Base Moment and Top-Level Displacement
of Test Structures D
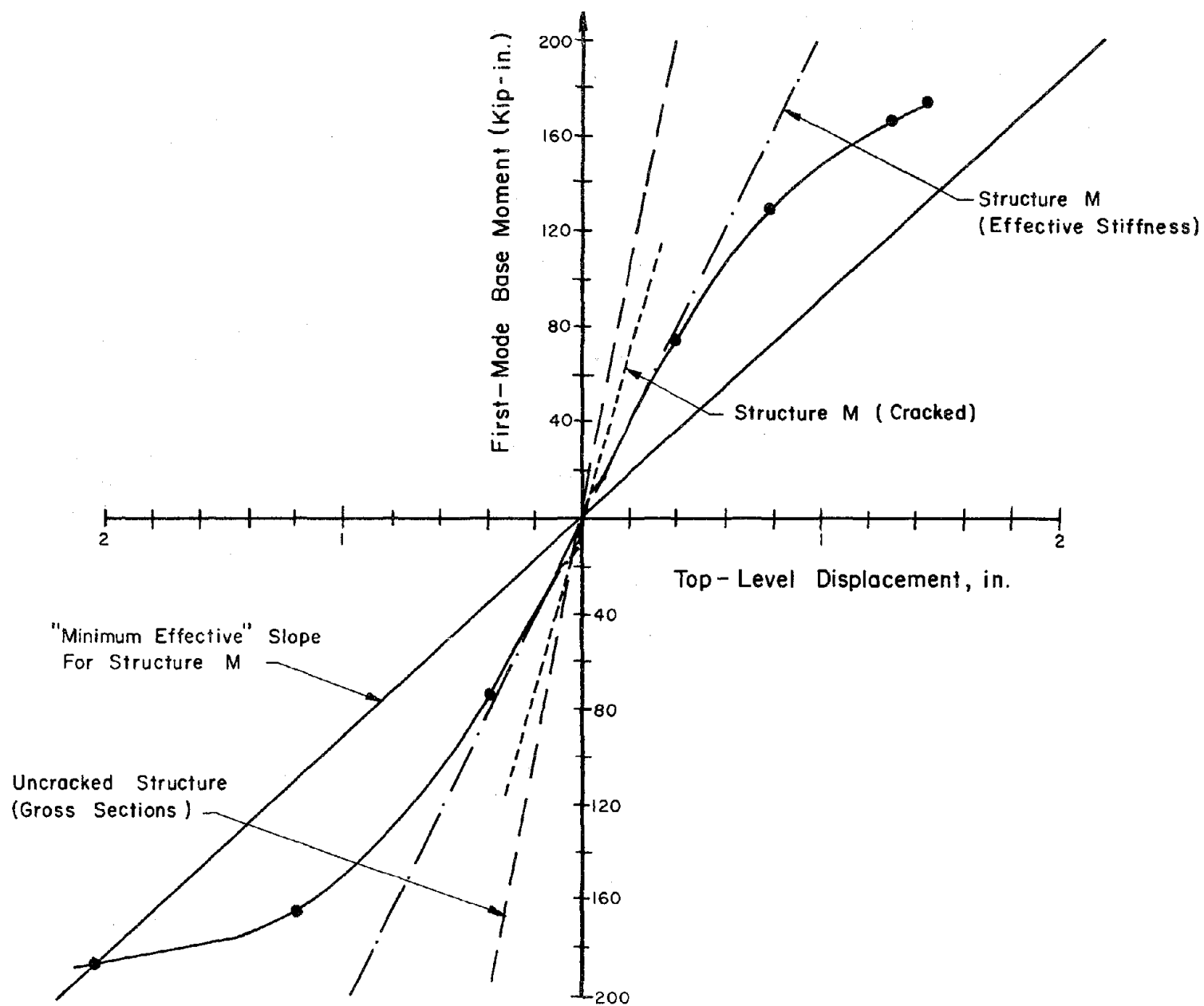
Fig. 6.5b Relationship of First-Mode Base Moment and Top-Level Displacement of Test Structure M

310
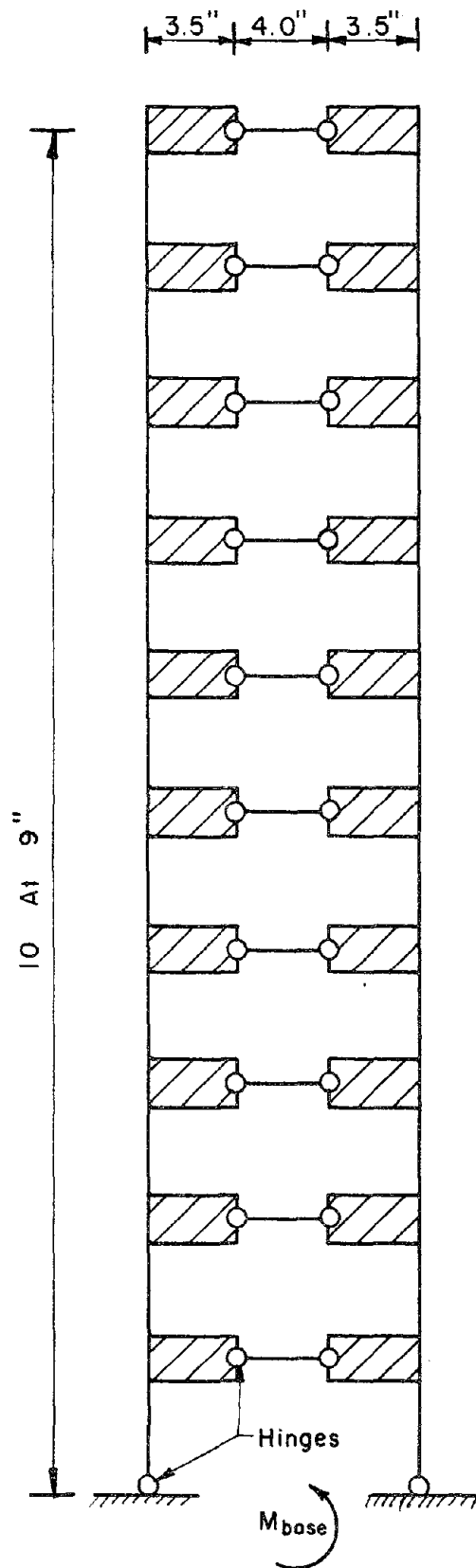
Yield Base Moment Of

(1)   Test Structure D

$$M_{base} = \underbrace{8 \text{ kips} \times 11 \text{ in.}}_{\substack{\text{Axial Load x} \\ \text{Level Arm}}} + \underbrace{(56 + 22) \text{ kip-in.}}_{\substack{\text{Moment Capacities} \\ \text{(At 10.5 kips And} \\ \text{-5.5 kips) See} \\ \text{Figure 2.26}}}$$

$$= 166 \text{ kip-in.}$$

(2)   Test Structure M

$$M_{base} = \underbrace{15 \text{ kips} \times 11 \text{ in.}}_{\substack{\text{Axial Load x} \\ \text{Level Arm}}} + \underbrace{(50 + 0) \text{ kip-in.}}_{\substack{\text{Moment Capacities} \\ \text{(At 17.5 And -12.5 kips)}}}$$

$$= 215 \text{ kip-in.}$$

(a)   Failure Mechanism

Fig. 6.6   Yield and Ultimate Forces at the Base of
a Single Frame

Symmetrical About Axis

1"

"Confined Flange"

5.5"

(b) Assumed Cross Section Of Base Pier At Ultimate
(Test Structure D)

6.5

f_{su} = 83 ksi

0.250   0.250

6.84 (=$A_s f_{su}$)   0.84

(c) Ultimate Forces On Base Pier Under Tension Force
(Test Structure D)

11.5

(Forces In Kips)

0.250   0.250

12

6.84   6.84

(d) Ultimate Forces On Base Pier Under Compressive
Force (Test Structure D)
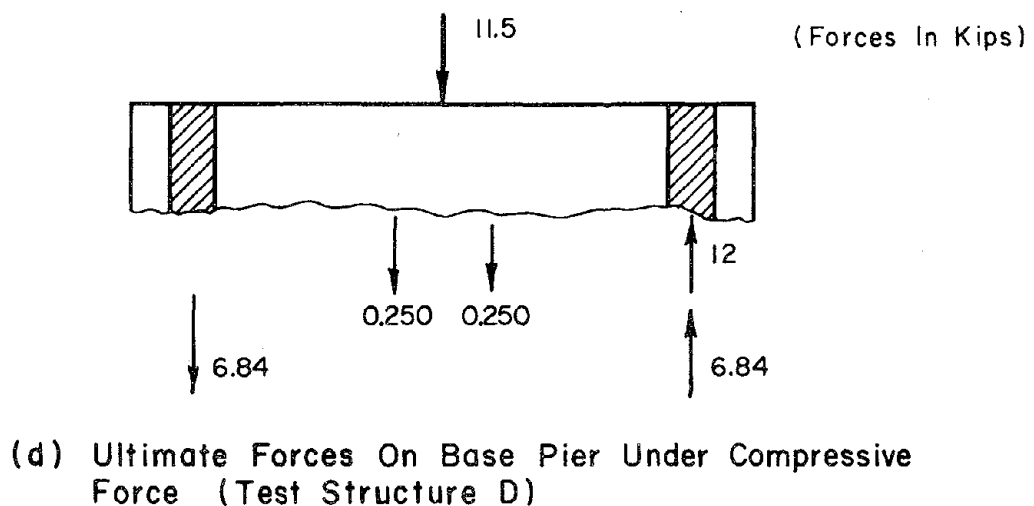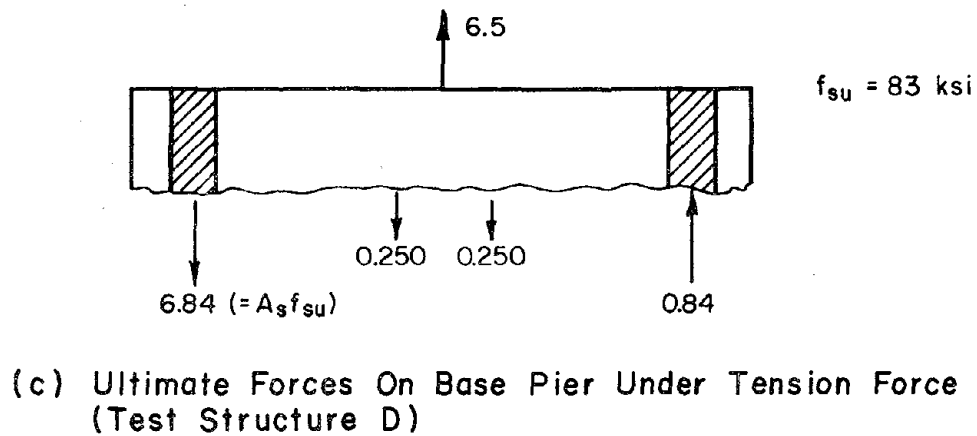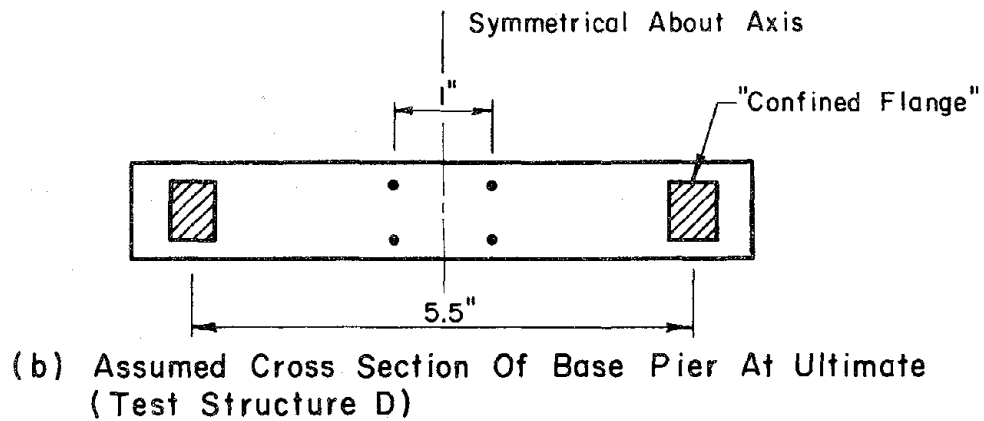
Fig. 6.6 (Contd) Yield and Ultimate Forces at the Base of
a Single Frame
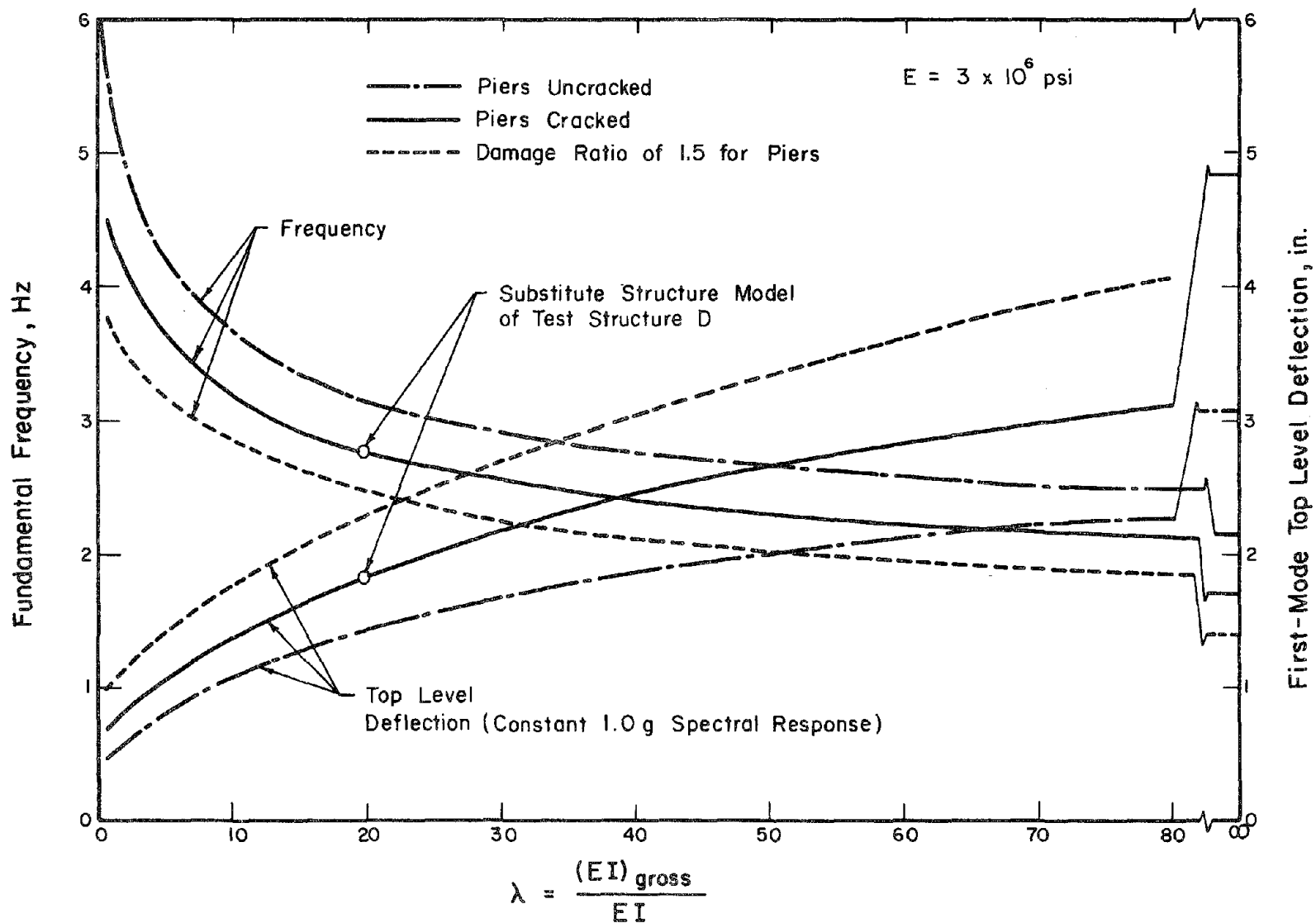
Fig. 6.7a   Variation of Fundamental Frequency and Top-Level Displacement
with Increase in Beam Flexibility
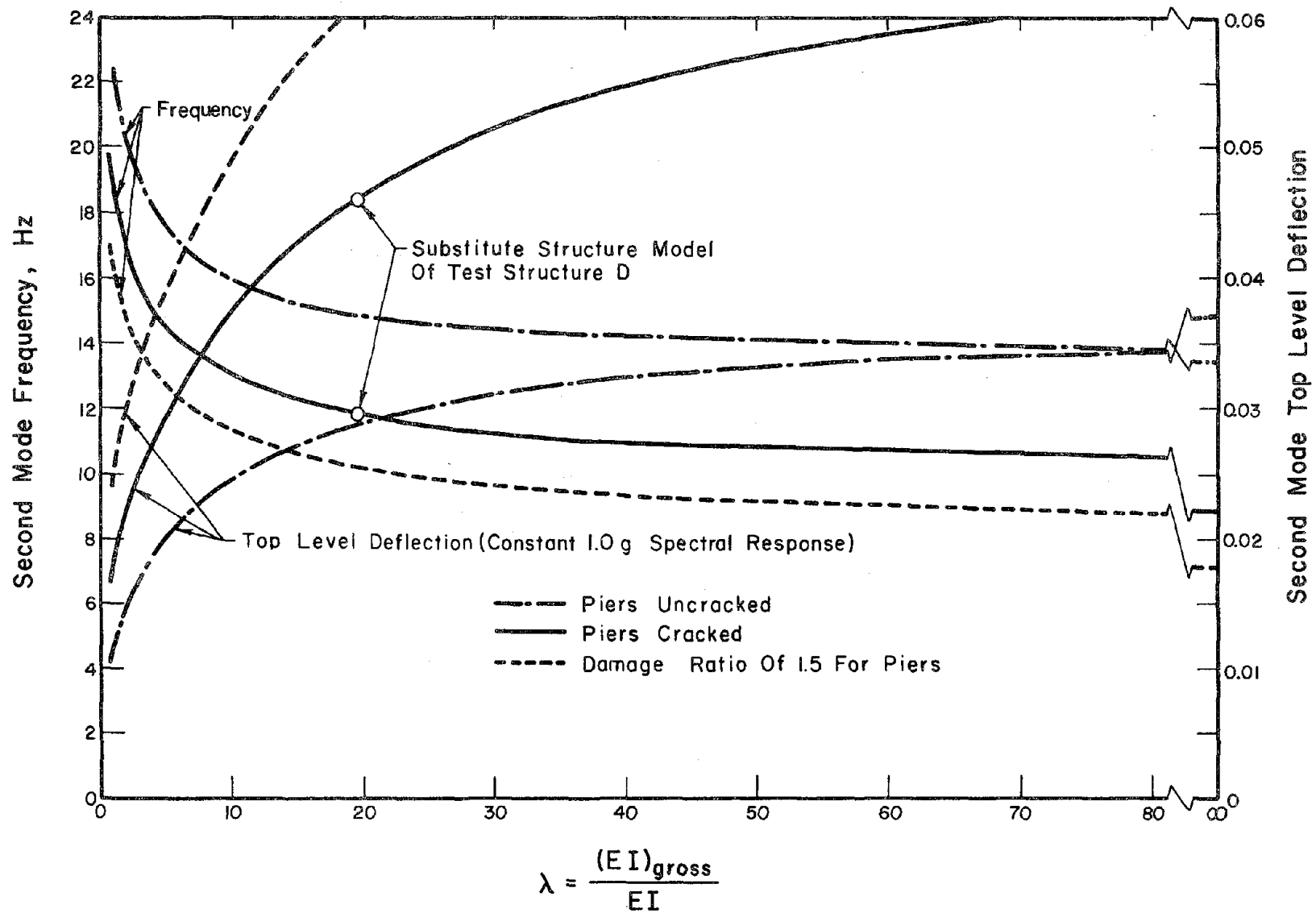
Fig. 6.7b   Variation of Second-Mode Frequency and Top-Level Displacement with
            Increase in Beam Flexibility
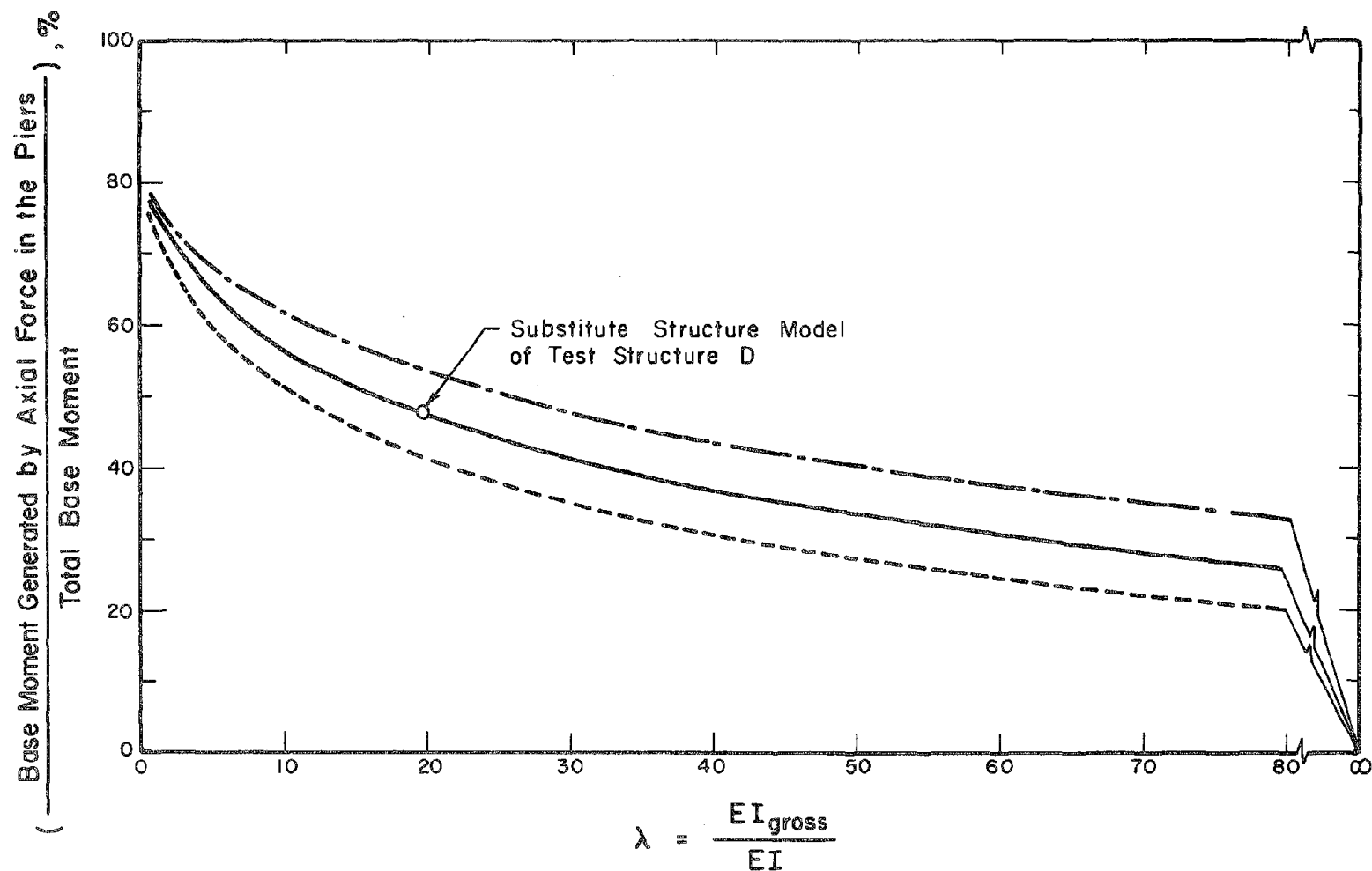
Fig. 6.8   Variation of "Coupling Factor" with Beam Flexibility
(Coupling Factor is defined by the legend on the y-axis)
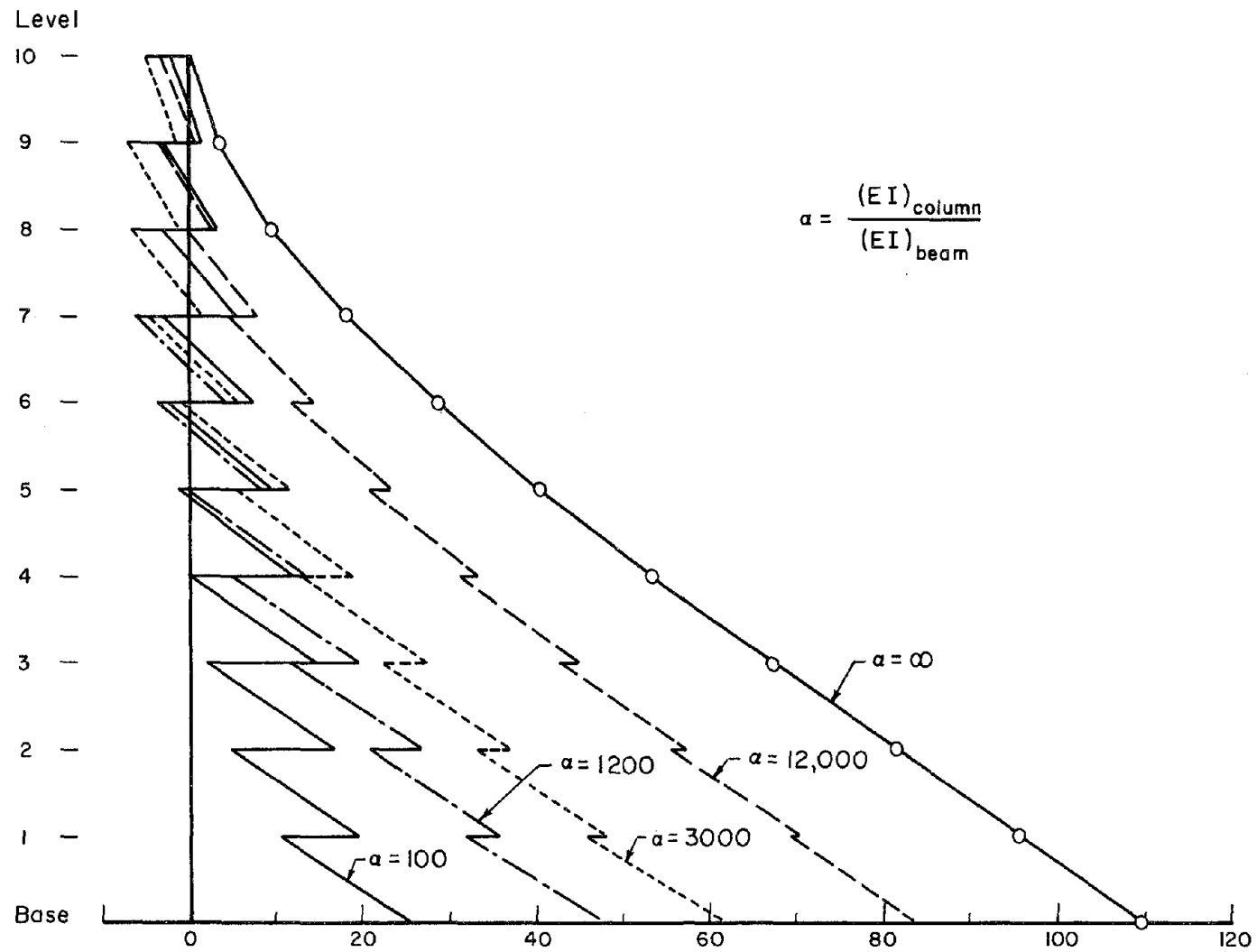
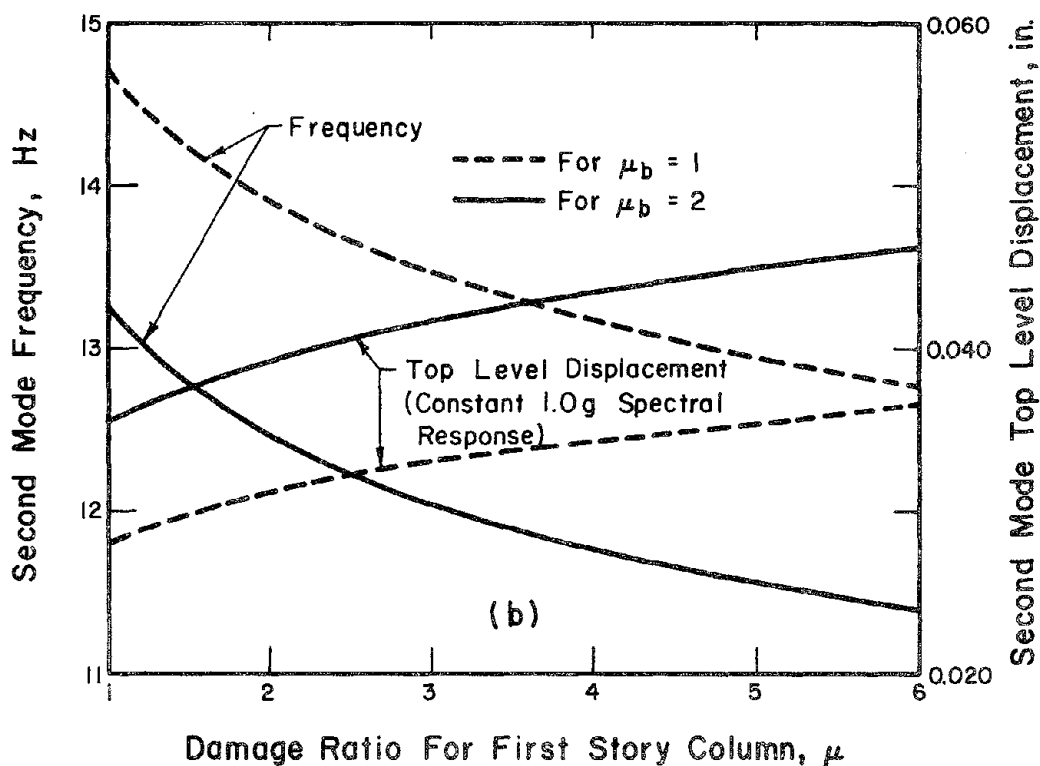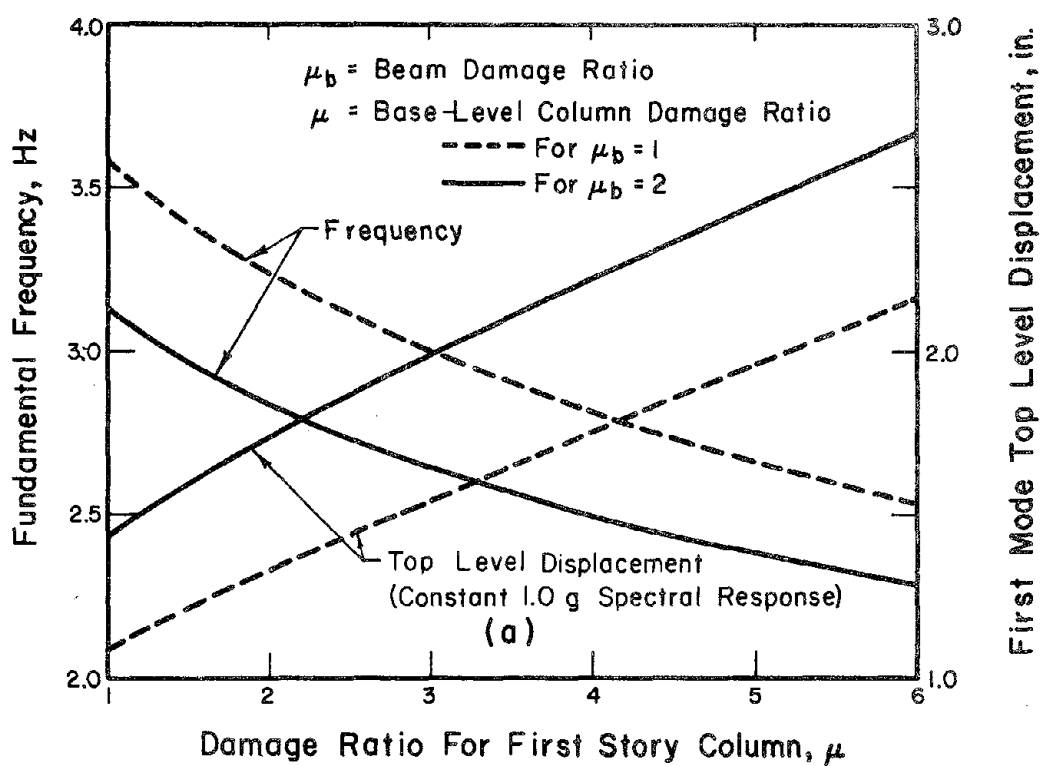Fig. 6.9 Variation of Flexural Moments Along a Single Pier of Test Structure D with Relative Beam Stiffness. First Mode. (piers cracked)

316

Fig. 6.10   Variation of Frequency and Top-Level Displacement
with First-Story Column Damage Ratio
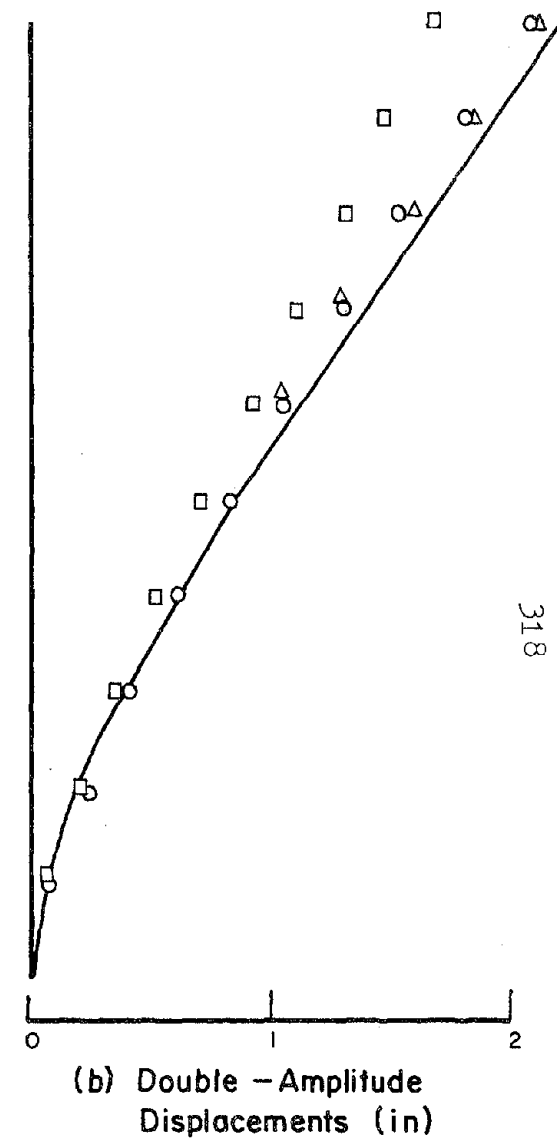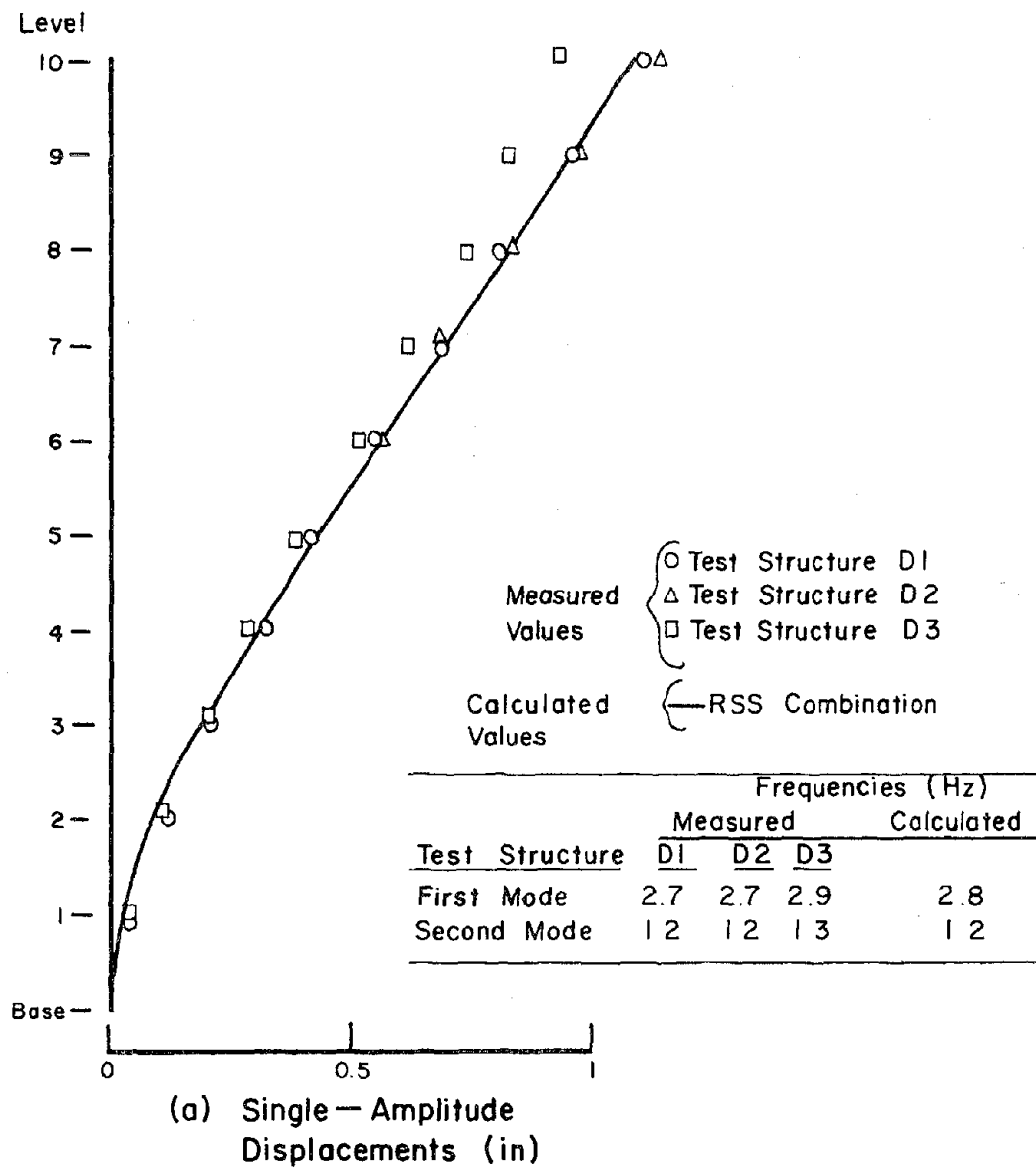
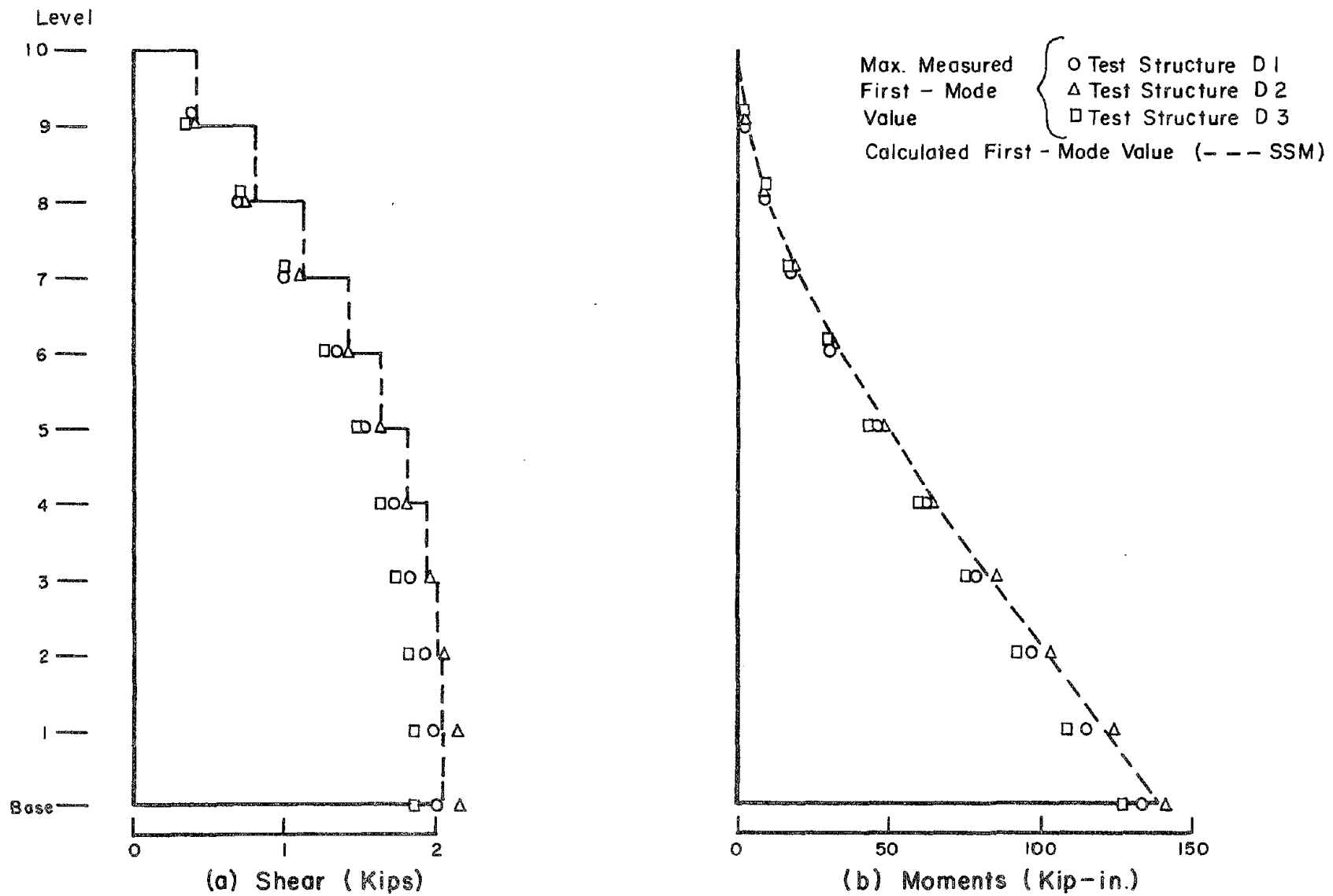Fig. 6.11 Comparison of Maximum Obtained Displacements with the Design Values

Level

10
9
8
7
6
5
4
3
2
1
Base

Measured Values
○ Test Structure D1
△ Test Structure D2
□ Test Structure D3

Calculated Values
—RSS Combination

Test Structure	Frequencies (Hz)			
	Measured			Calculated
	D1	D2	D3	
First Mode	2.7	2.7	2.9	2.8
Second Mode	12	12	13	12

0   0.5   1

(a) Single — Amplitude
     Displacements (in)

0   1   2

(b) Double — Amplitude
     Displacements (in)

318

Fig. 6.12   Comparison of Maximum Obtained Forces with the Design Values.
First Mode.

Level

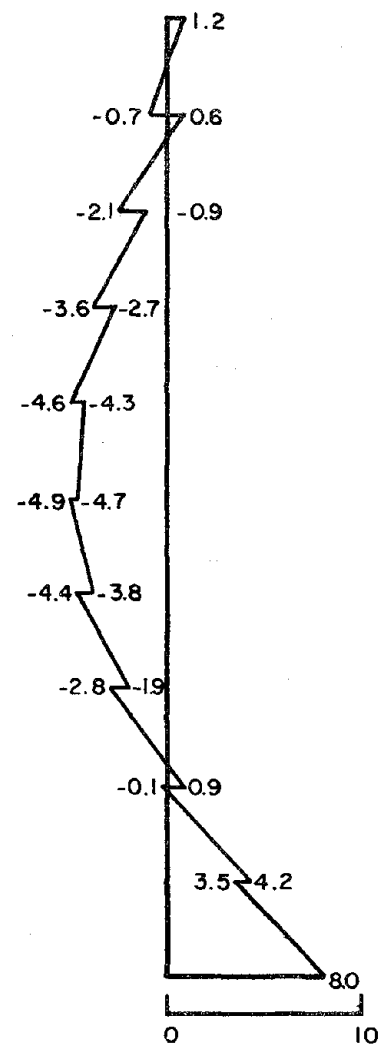Max. Measured Values $\left\{\begin{array}{l}\text{O Test Structure D I}\\\triangle\text{ Test Structure D 2}\\\square\text{ Test Structure D 3}\end{array}\right.$

Calculated (SSM) $\left\{\begin{array}{l}\text{--- RSS Combination}\\\left[\dfrac{RSS}{2}+\dfrac{|(1)|+|(2)|}{RSS}\right]\text{x RSS}_{\text{Base Shear}}\end{array}\right.$

(a) Shear (Kips)

(b) Moments (Kip-in.)
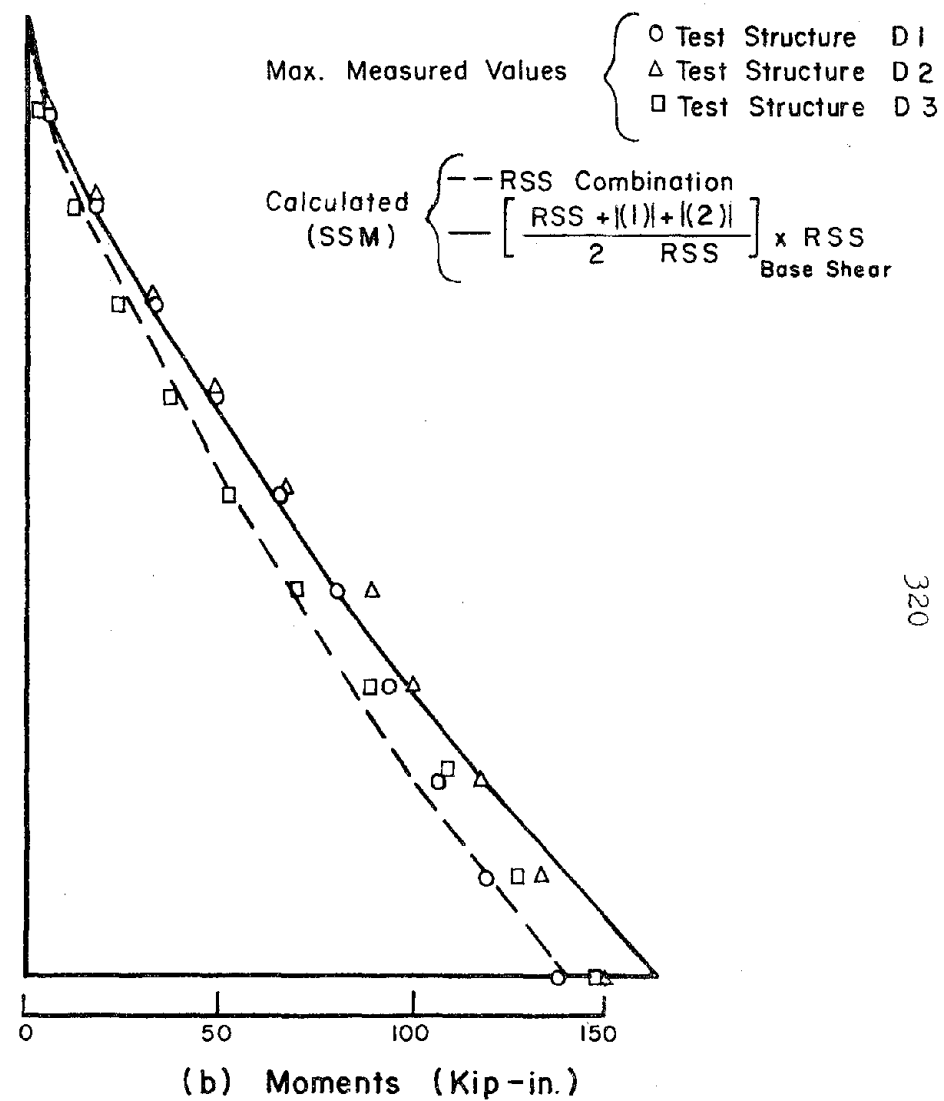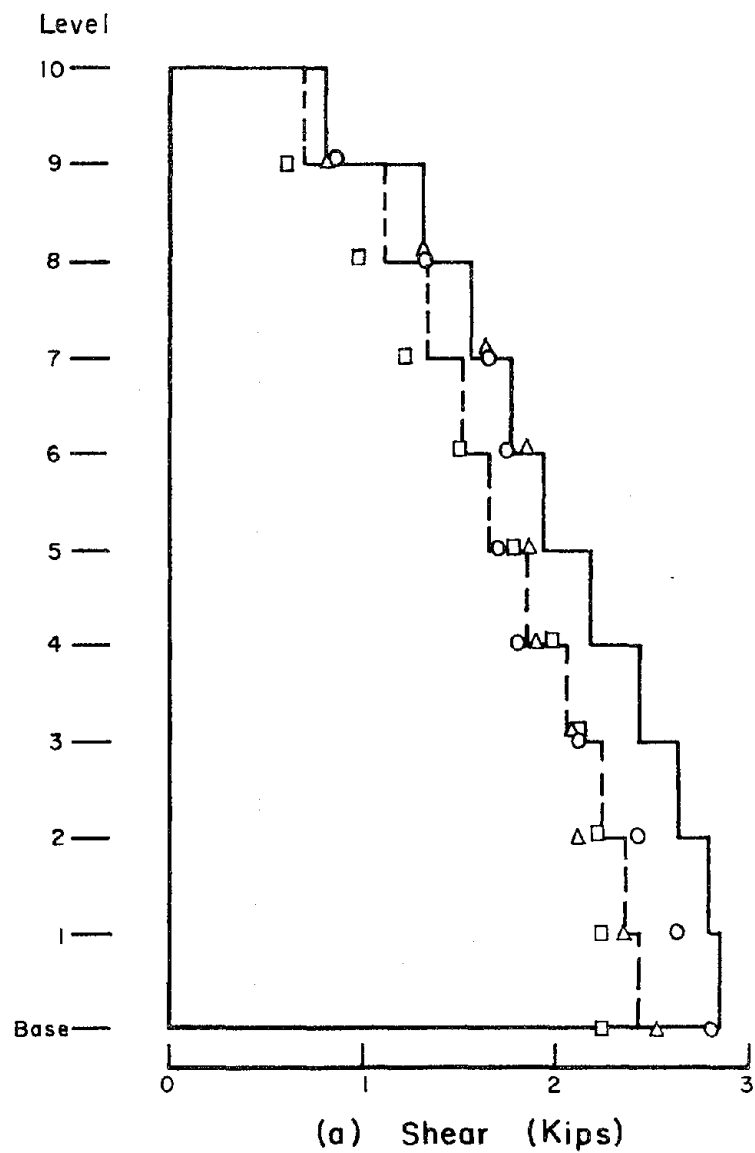
Fig. 6.13 Comparison of Maximum Obtained Forces with the Design Values
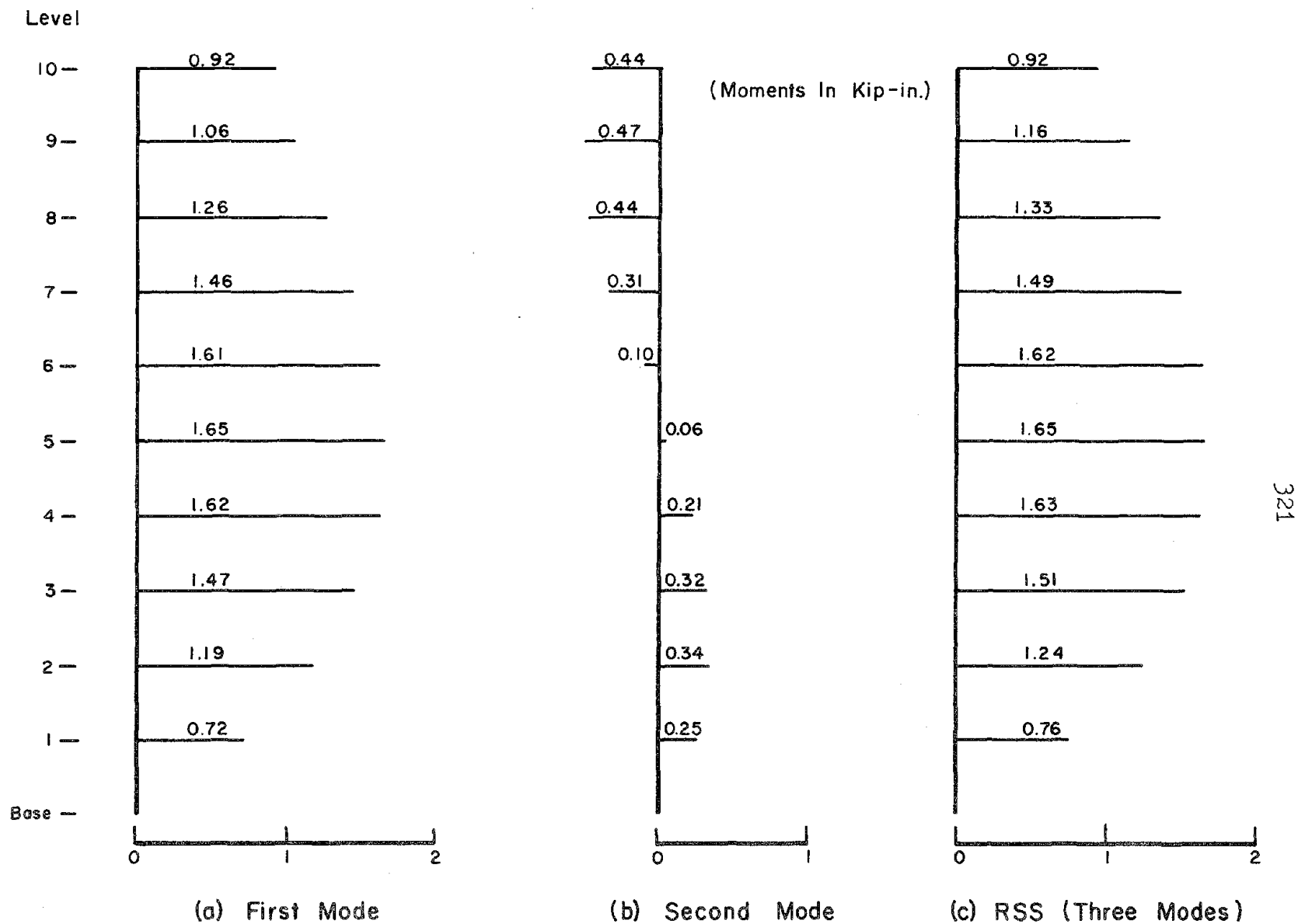
Fig. 6.14   Moments at Ends of Connecting Beams.   Model of Test Structure D
$(\mu_b = \mu_c = 1.5)$

321
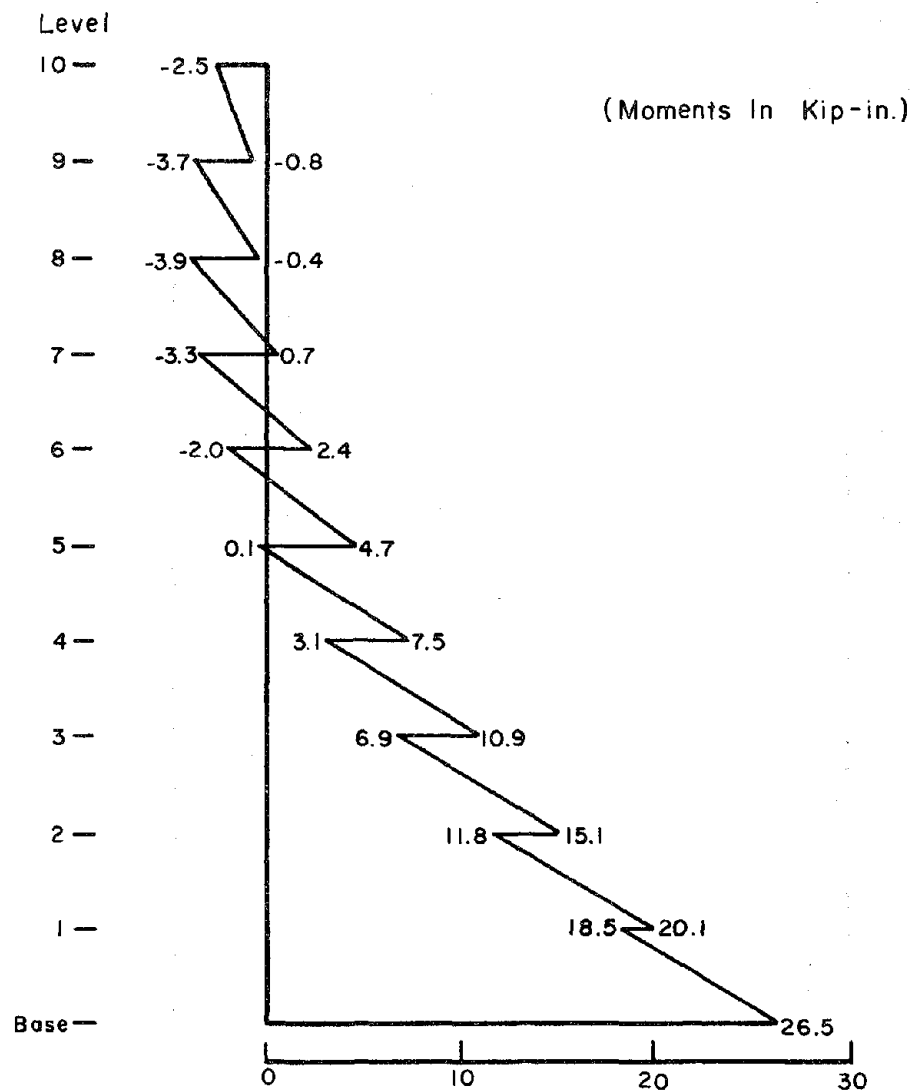
Fig. 6.15 Flexural Moments over a Single Pier. Model of Test Structure D

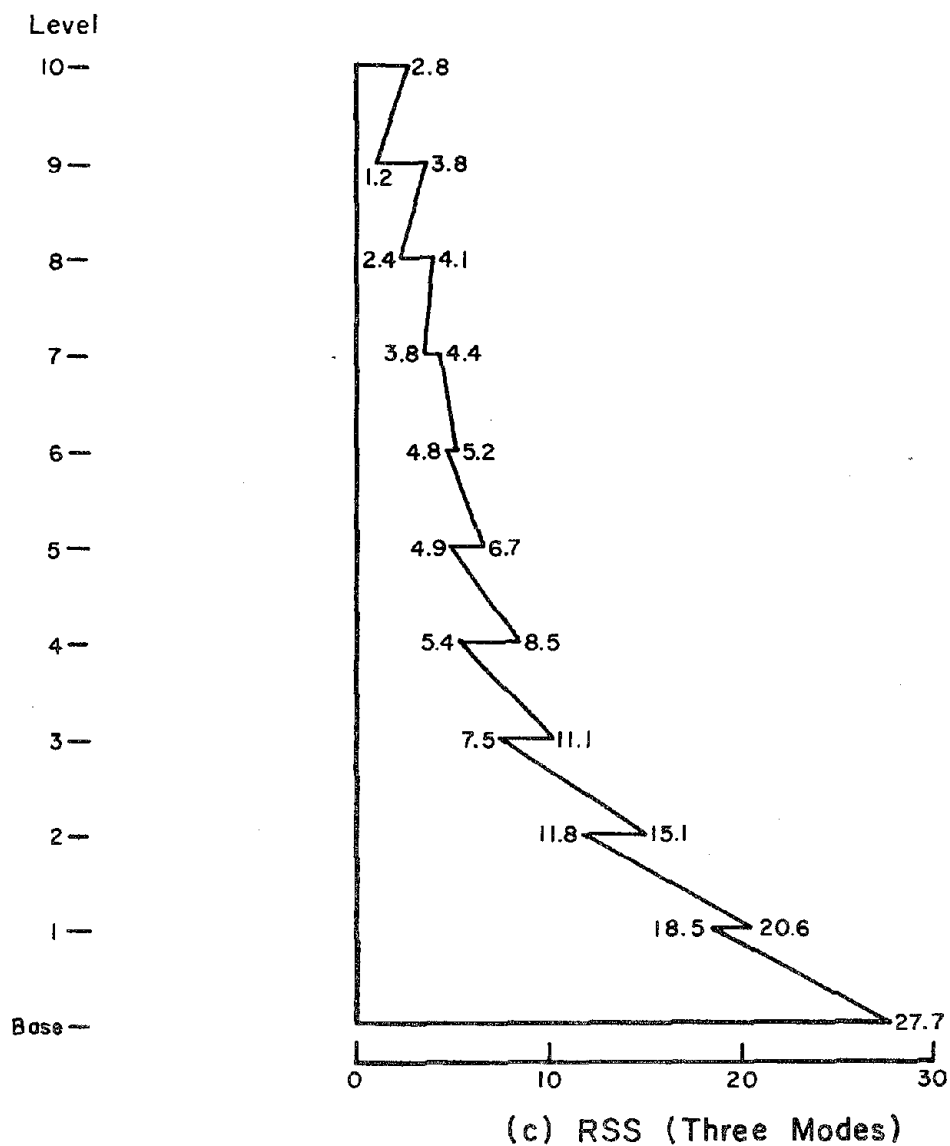$(\mu_b = \mu_c = 1.5)$

Fig. 6.15   (Contd) Flexural Moments over a Single Pier.   Model of Test Structure D
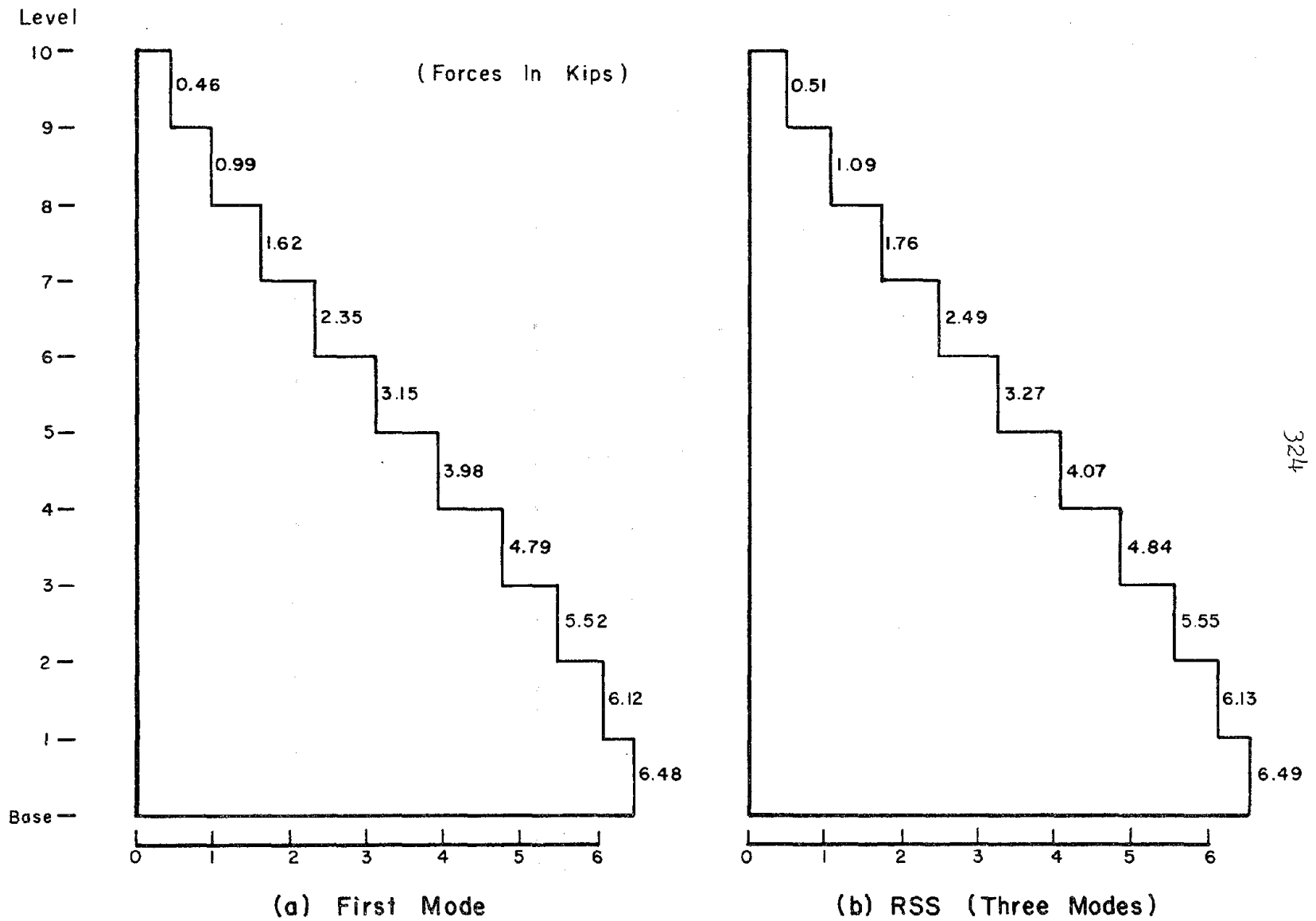
$$(\mu_b = \mu_c = 1.5)$$

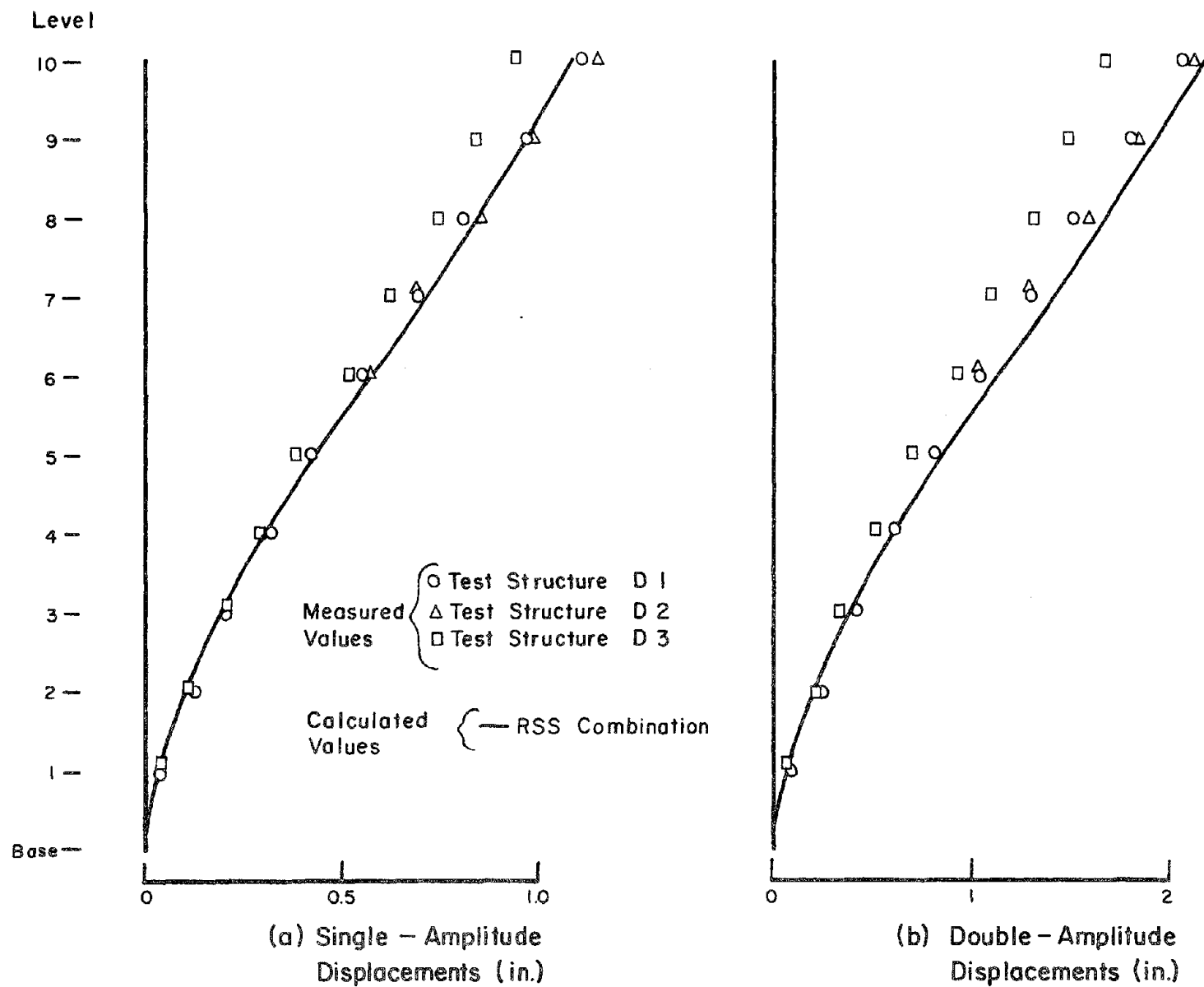Fig. 6.16 Axial Load in the Piers. Model of Test Structure D ($\mu_b = \mu_c = 1.5$)
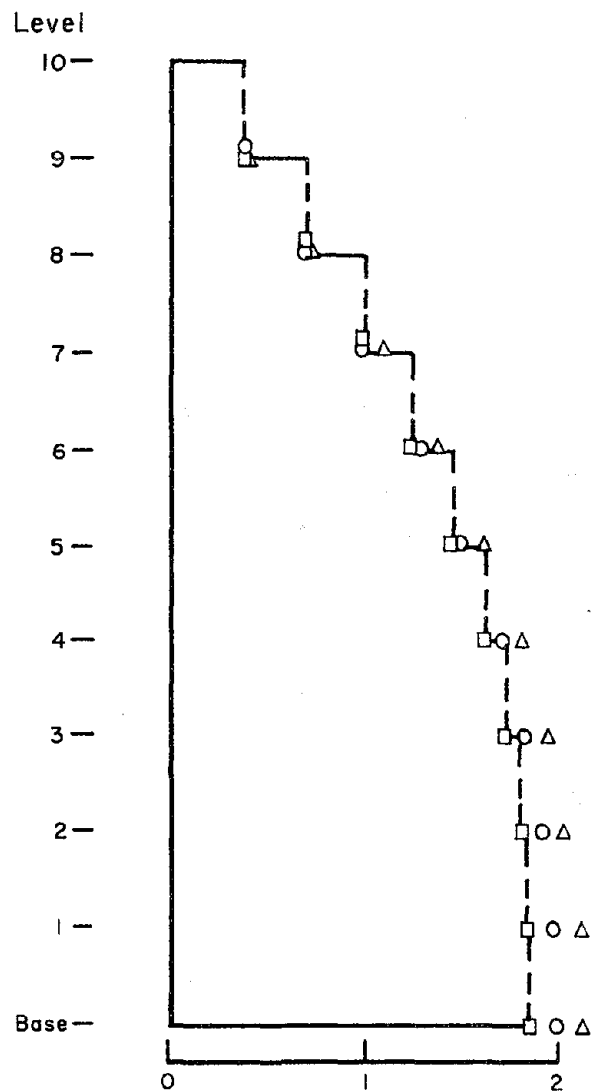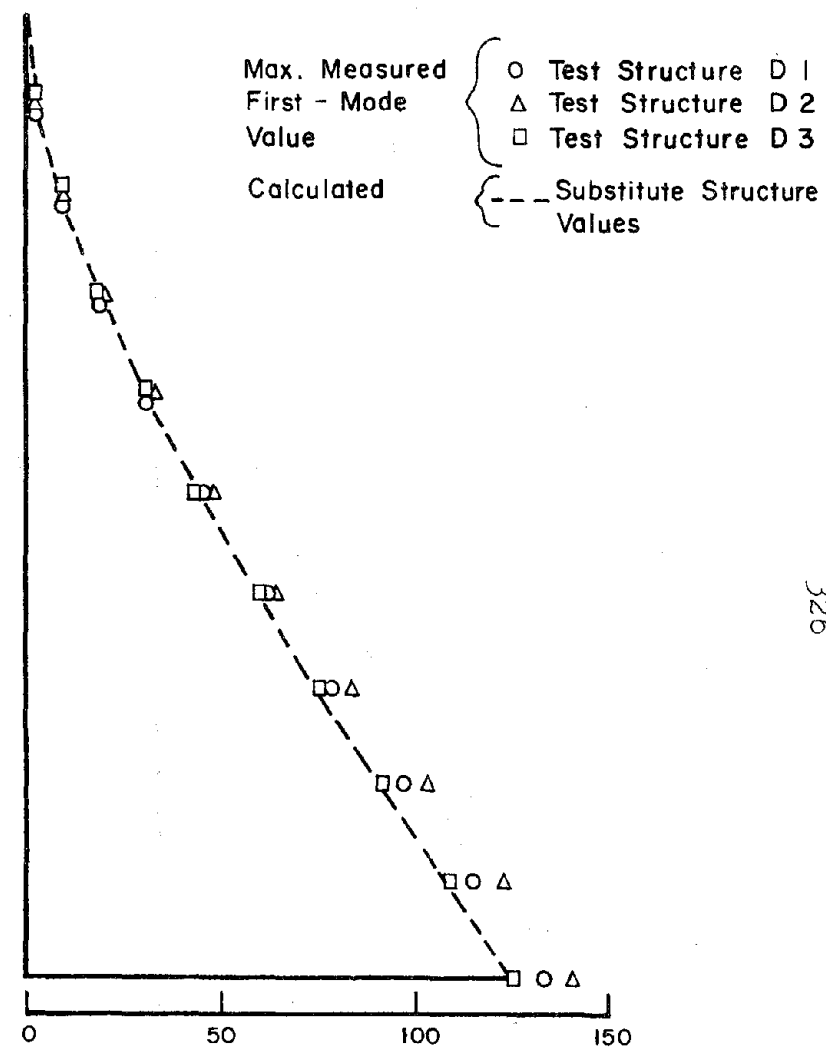
Fig. 6.17 Comparison of Maximum Obtained Displacements with Calculated Values. Model of Test Structure D ($\mu_b = \mu_c = 1.5$)

Fig. 6.18 Comparison of Maximum Obtained Forces with Calculated Values. First Mode.
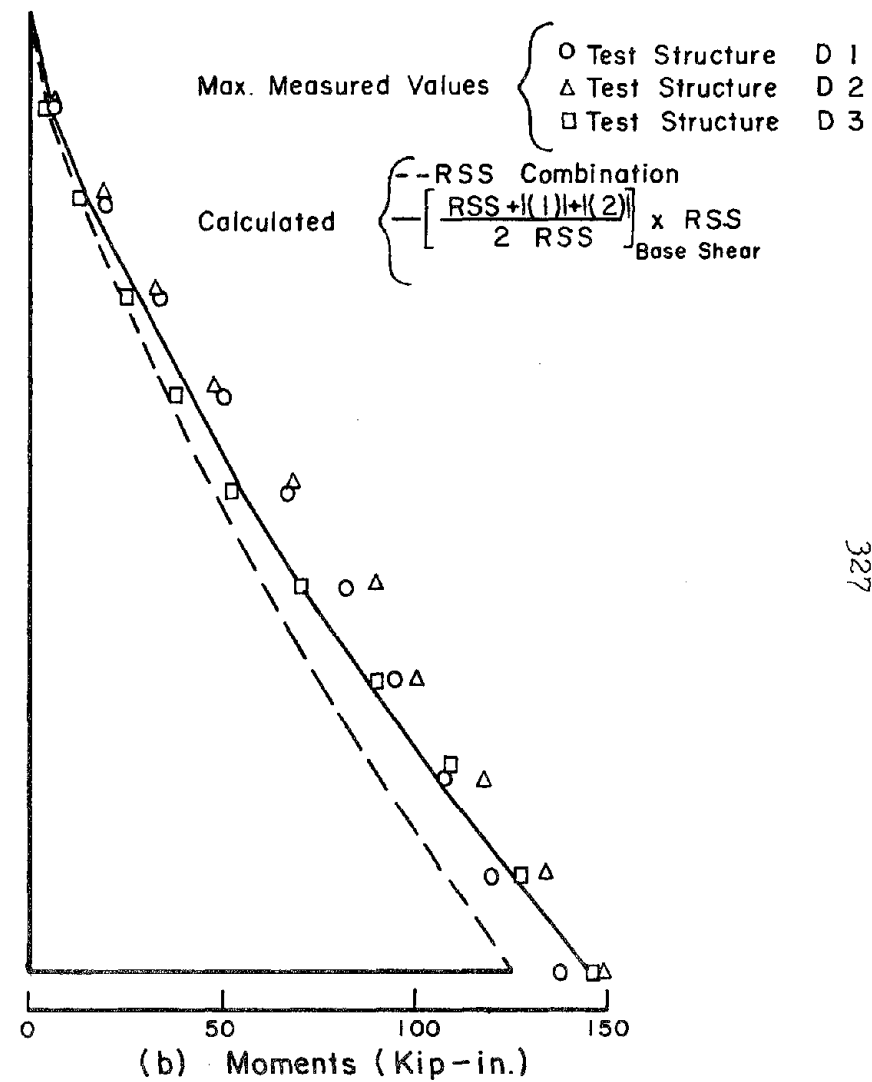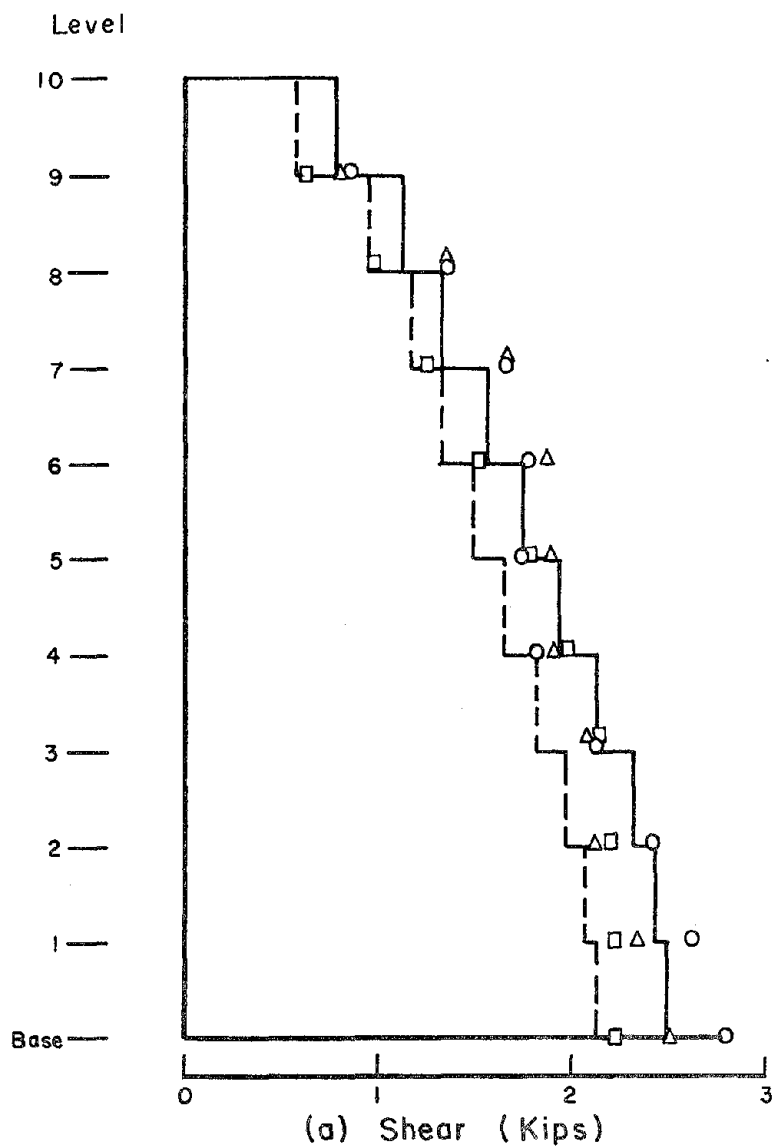Model of Test Structure D ($\mu_b = \mu_c = 1.5$)

326
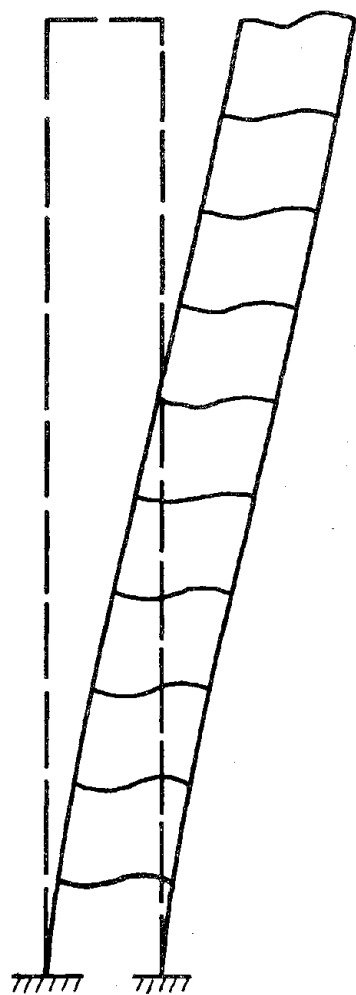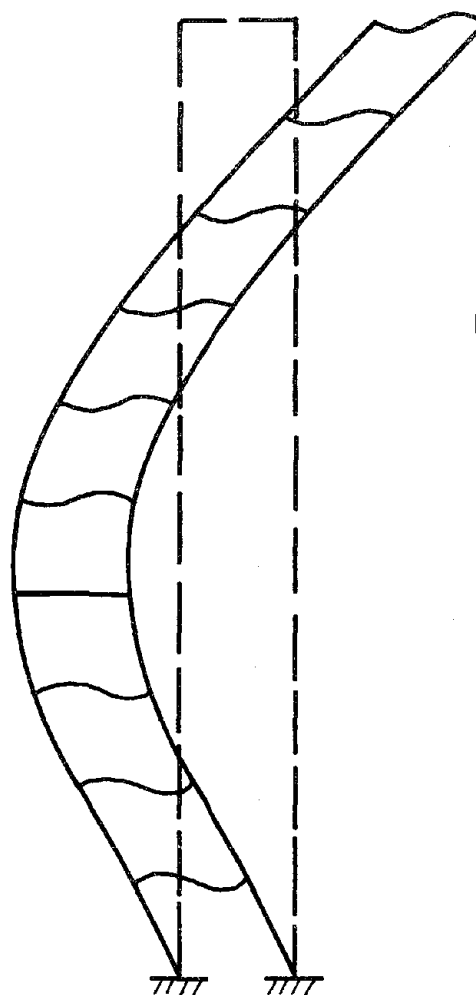
Fig. 6.19 Comparison of Maximum Obtained Forces with Calculated Values.
Model of Test Structure D ($\mu_b = \mu_c = 1.5$)

Level

10

9
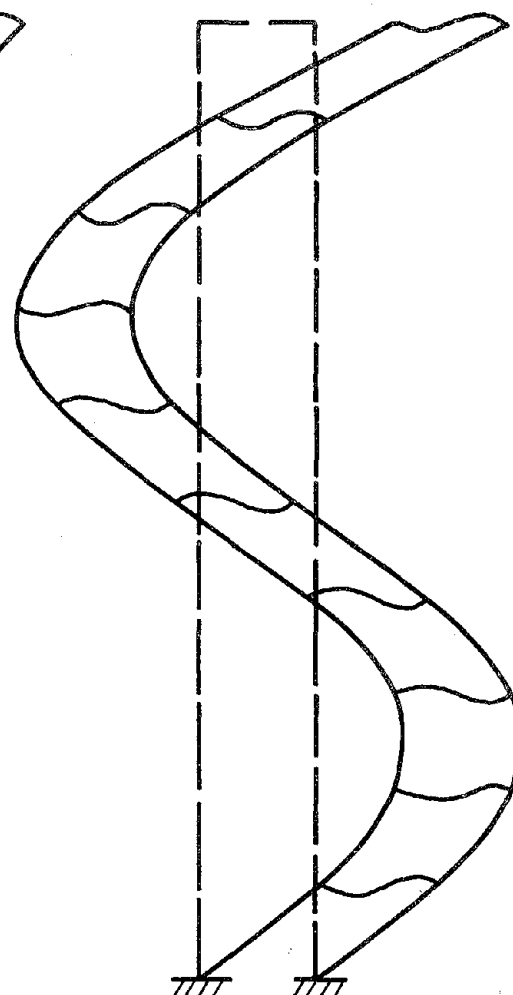
8

7

6

5

4

3

2

1

Base

(a) First Mode

(b) Second Mode

(c) Third Mode

Fig. 6.20   Modal Shapes for Model of Test Structure M ($\mu_b = 2$, $\mu_c = 4$)

328
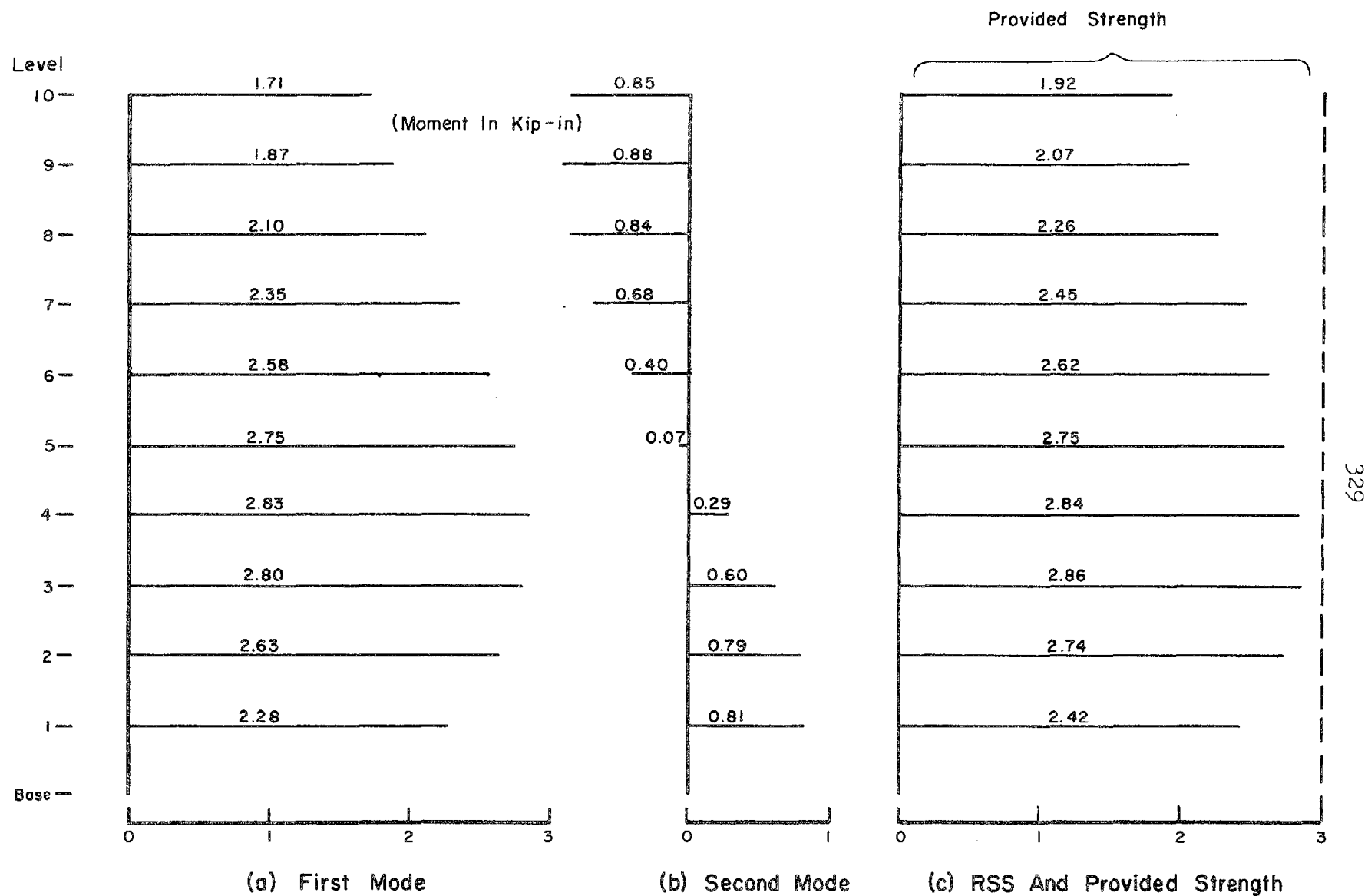
Fig. 6.21 Moments at Ends of Connecting Beams. Model of Test Structure M
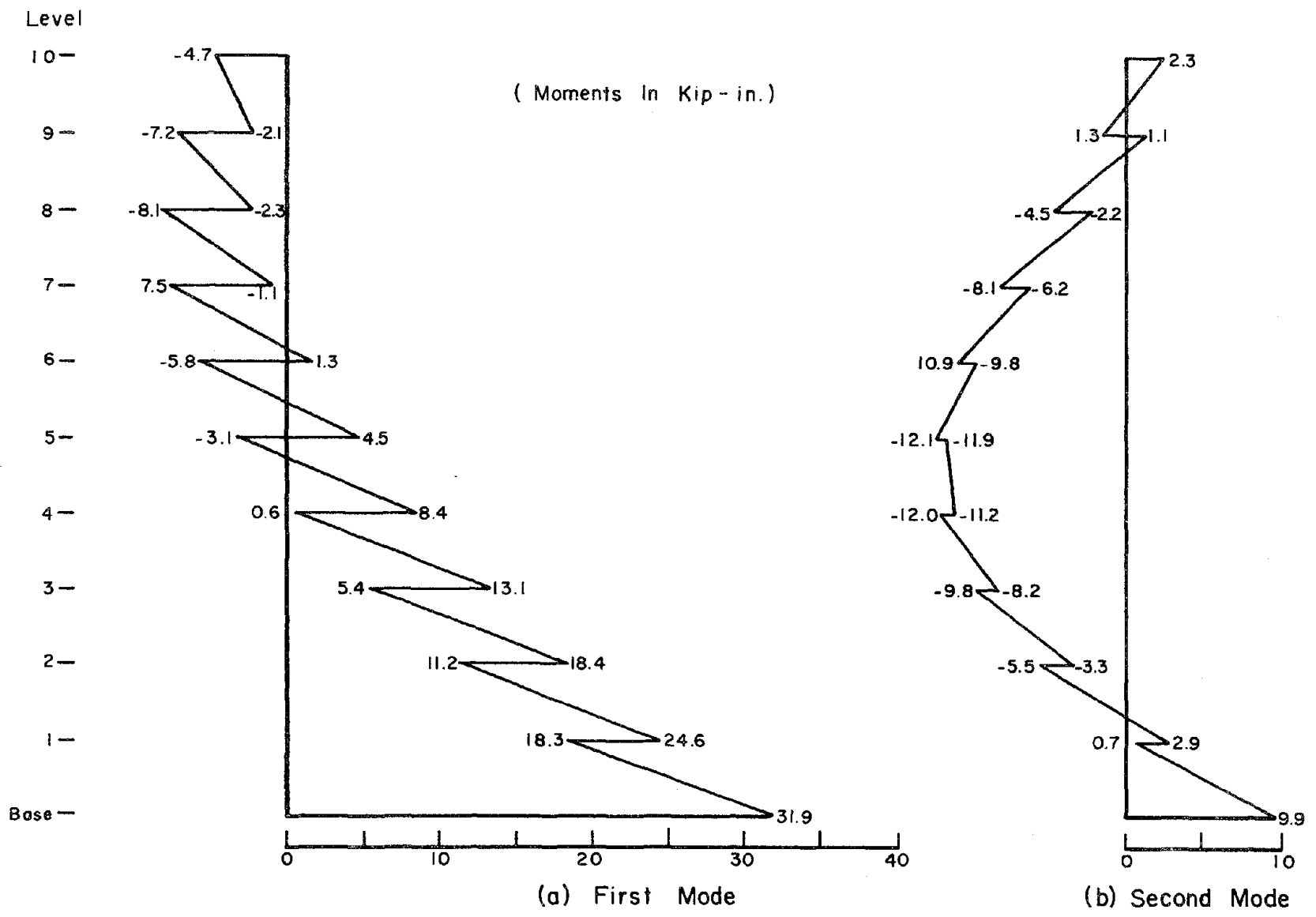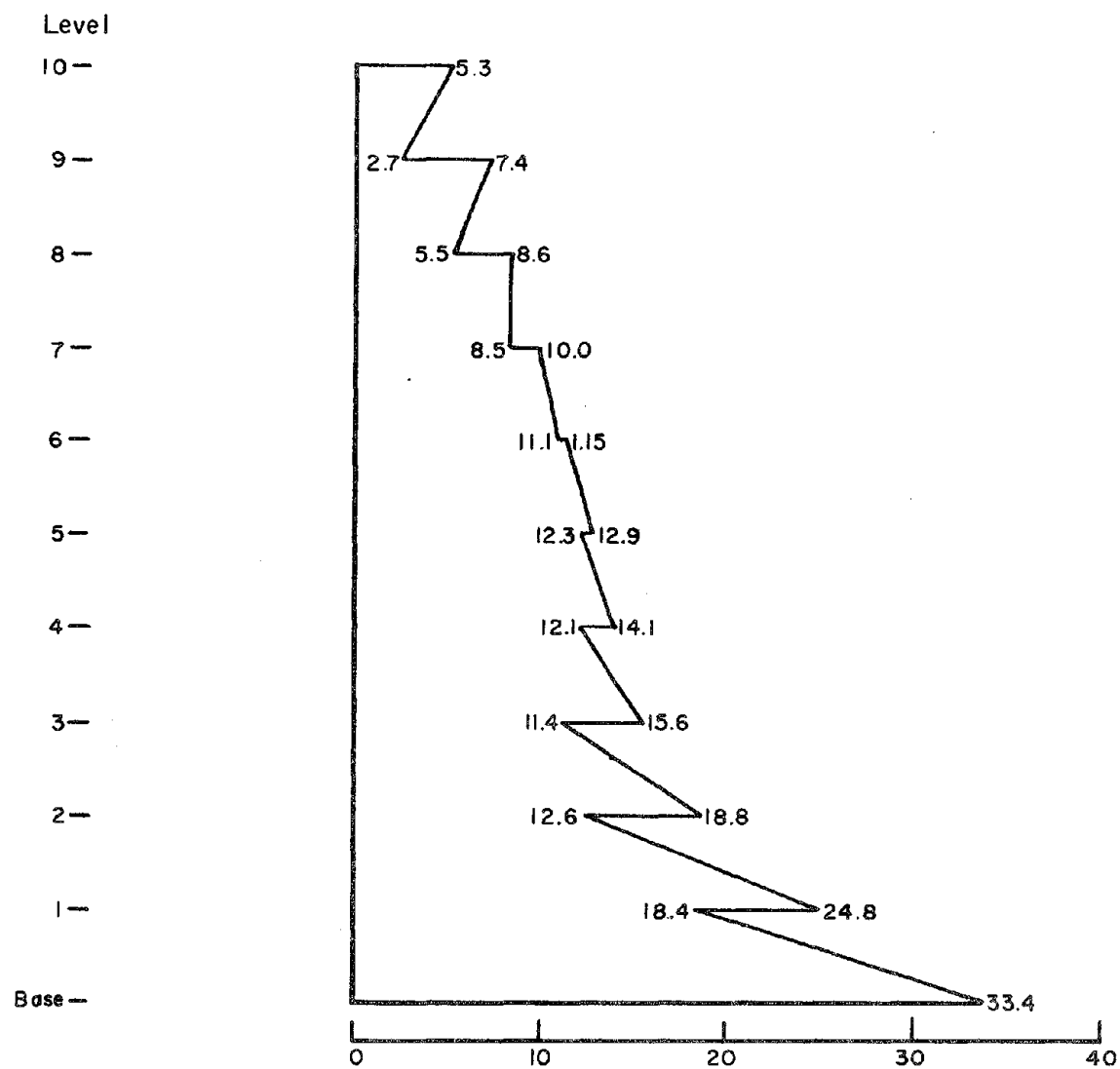
$$(\mu_b = 2, \quad \mu_c = 4)$$

Fig. 6.22 Flexural Moments over a Single Pier. Model of Test Structure M
$(\mu_b = 2, \mu_c = 4)$

330

(c) RSS (Three Modes)

Fig. 6.22 (Contd)   Flexural Moments over a Single Pier.   Model of Test Structure M

$(\mu_b = 2, \mu_c = 4)$

Fig. 6.23 Axial Loads in the Piers. Model of Test Structure M ($\mu_b = 2$, $\mu_c = 4$)

Level   Column

1.21	0.71	10 —	⑩
2.49	1.49	9 —	⑨
3.87	2.37	8 —	⑧
5.33	3.33	7 —	⑦
6.86	4.36	6 —	⑥
8.44	5.44	5 —	⑤
10.02	6.52	4 —	④
11.60	7.60	3 —	③
13.10	8.60	2 —	②
14.46	9.46	1 —	①
		Base	

10   5   0   5

← Compression   Tension →

(a) Axial Load (± RSS + Weights)

333

(b) Interaction Diagram Of Pier (Assuming ϵ_{cu} = 0.004 And $f_c^{'}$ = 4500 psi)

Fig. 6.24 Location of Calculated Forces for the Columns in the Interaction Diagram. Model of Test Structure M (μ_b = 2, μ_c = 4)

Fig. 6.25 Comparison of Maximum Obtained Displacements with Calculated Values. Model of Test Structure M ($\mu_b = 2$, $\mu_c = 4$)

Fig. 6.26 Comparison of Maximum Obtained Forces with Calculated Values. First Mode. Model of Test Structure M ($\mu_b = 2$, $\mu_c = 4$)

Fig. 6.27   Comparison of Maximum Obtained Forces with Calculated Values.
Model of Test Structure M ($\mu_b = 2$, $\mu_c = 4$)

Fig. 6.28   Moments at Ends of Connecting Beams. Model of Test Structure M ($\mu_b = \mu_c = 2$)
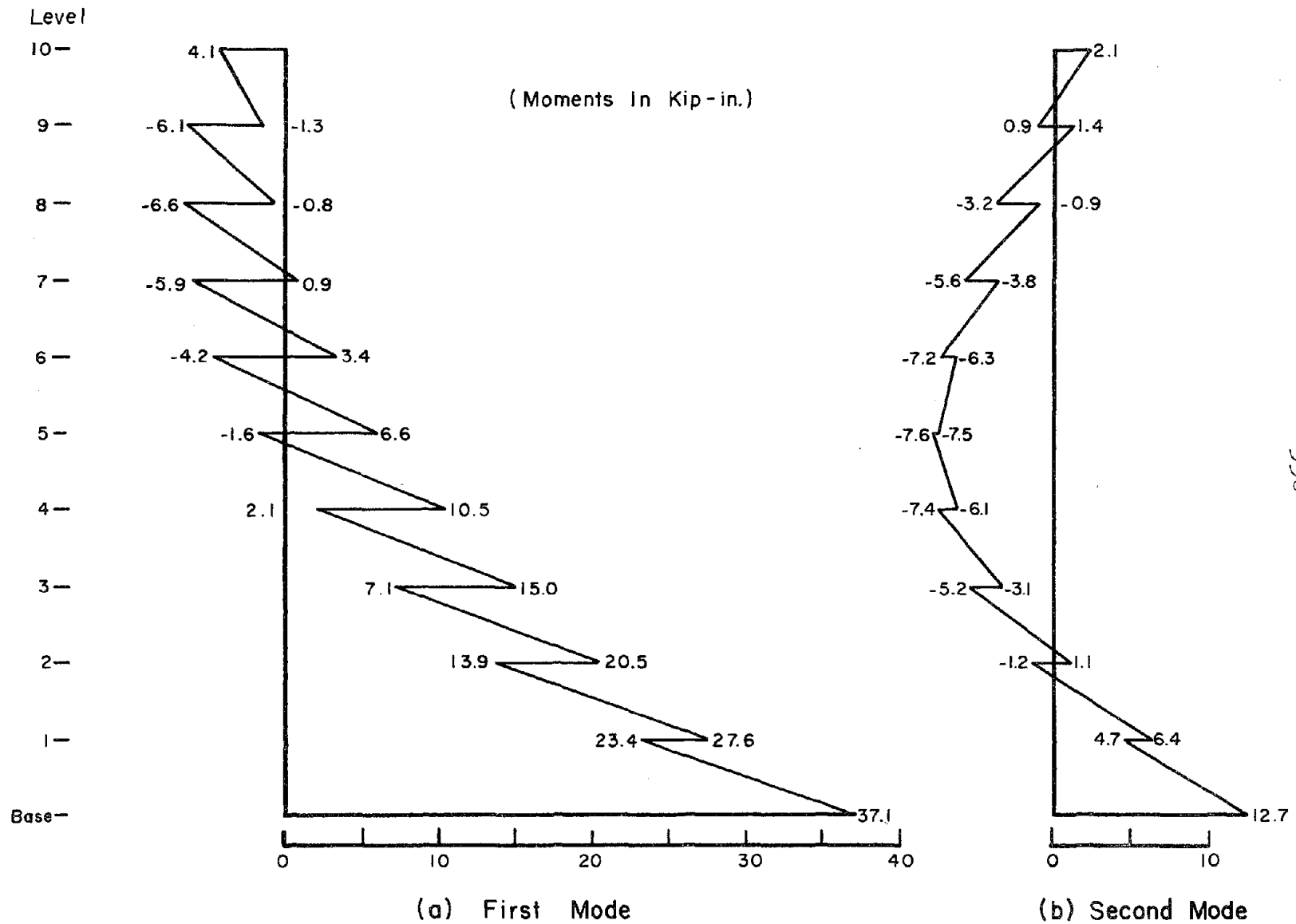
Fig. 6.29   Flexural Moments over a Single Pier.   Model of Test Structure M

$(\mu_b = \mu_c = 2)$.

338
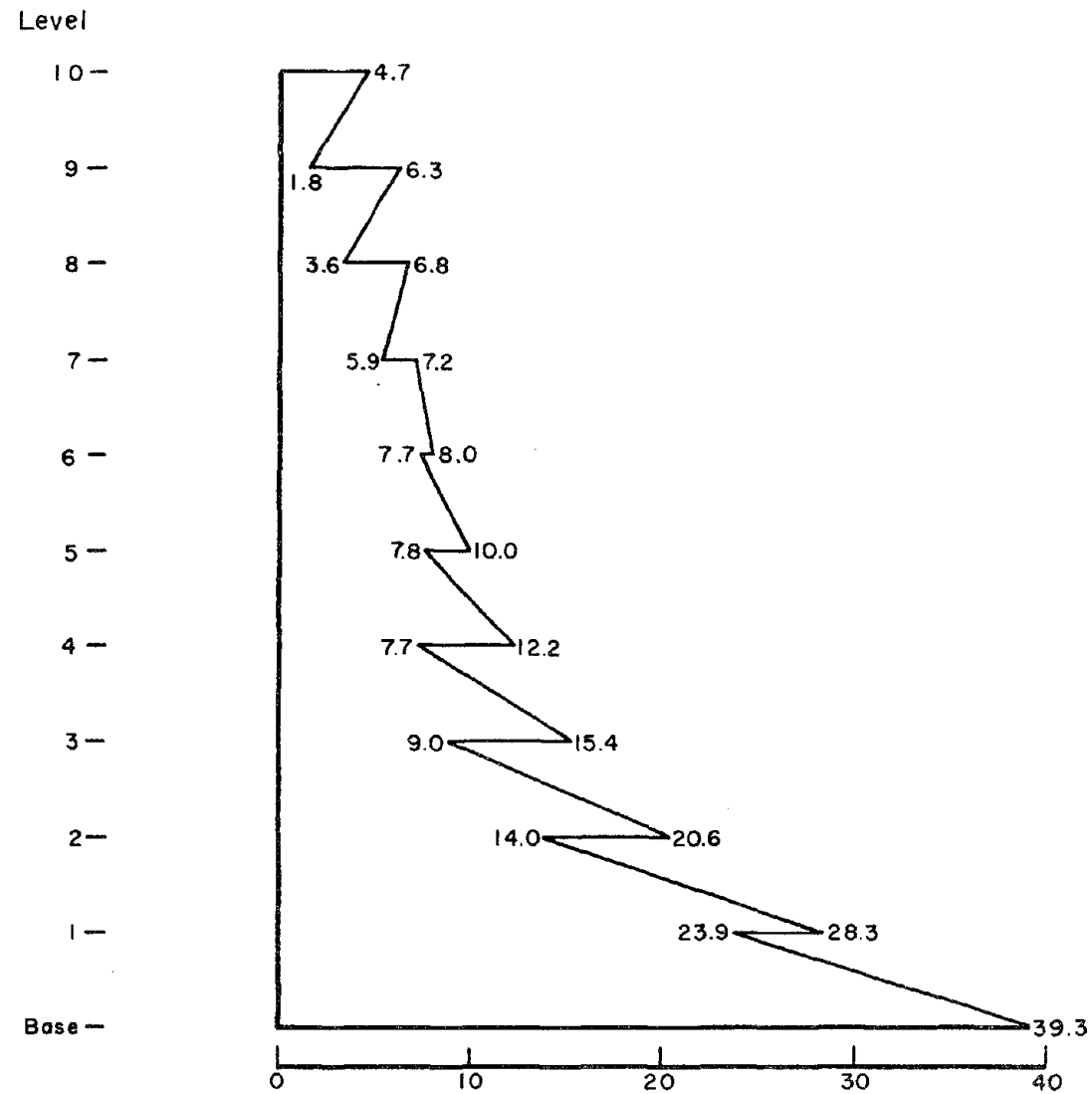
Fig. 6.29 (Contd) Flexural Moments over a Single Pier. Model of Test Structure M
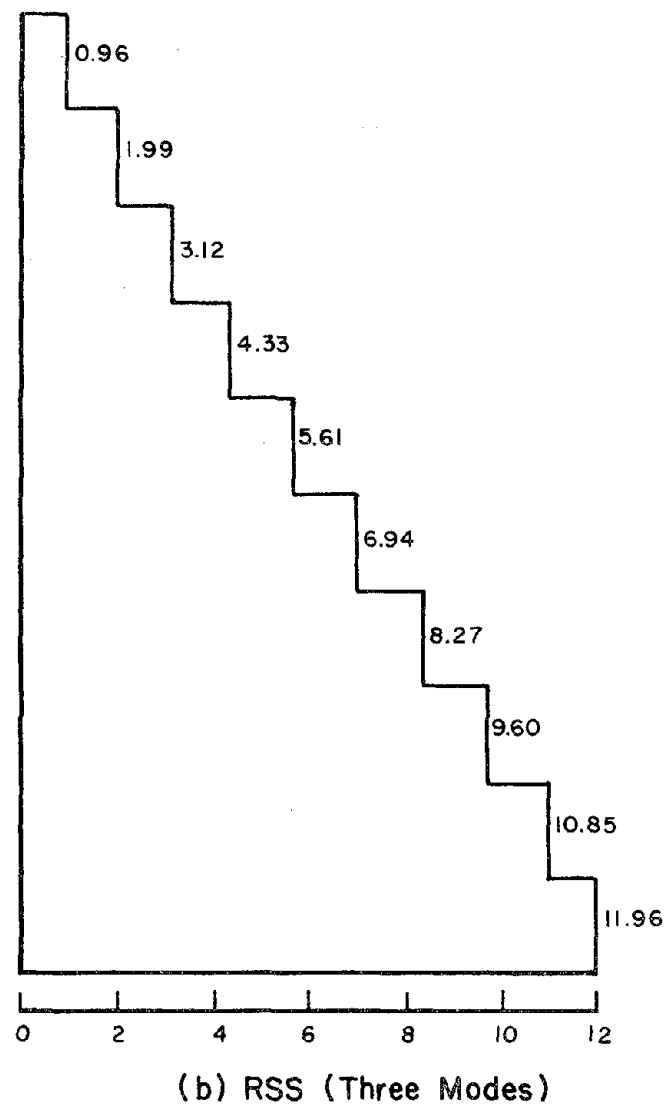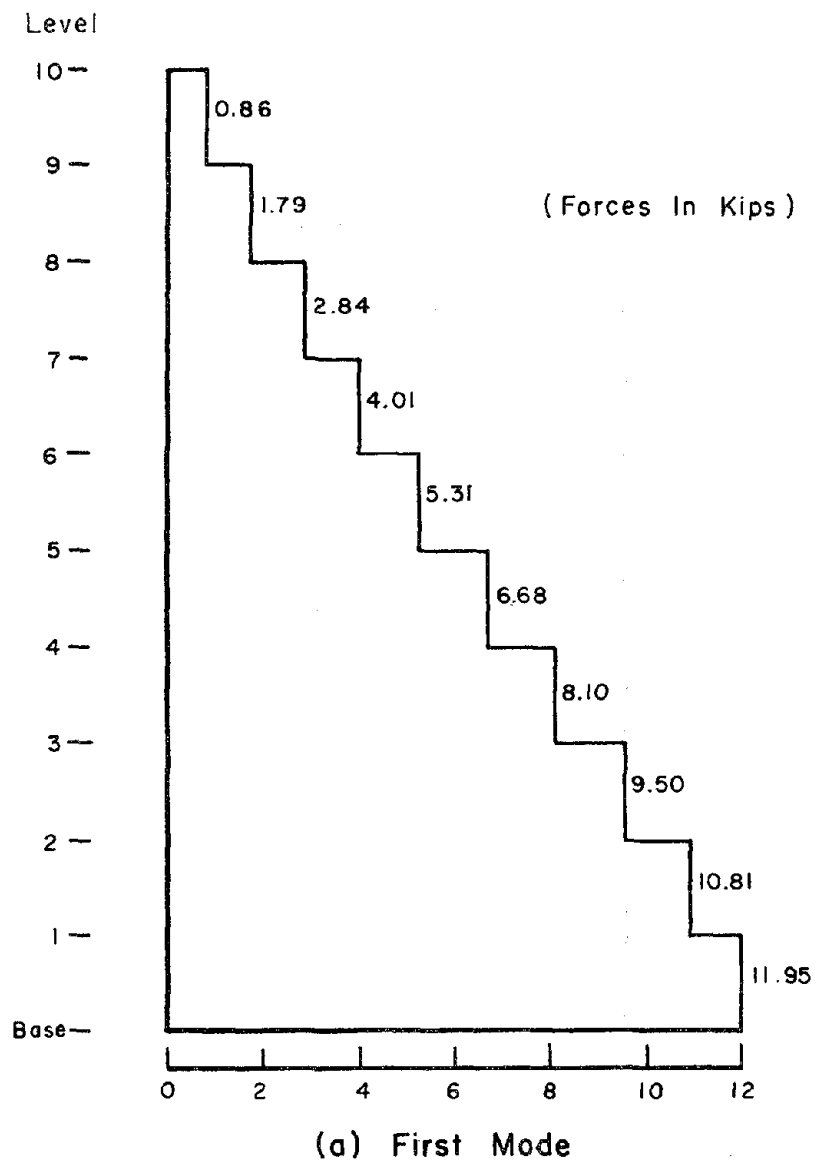$(\mu_b = \mu_c = 2)$
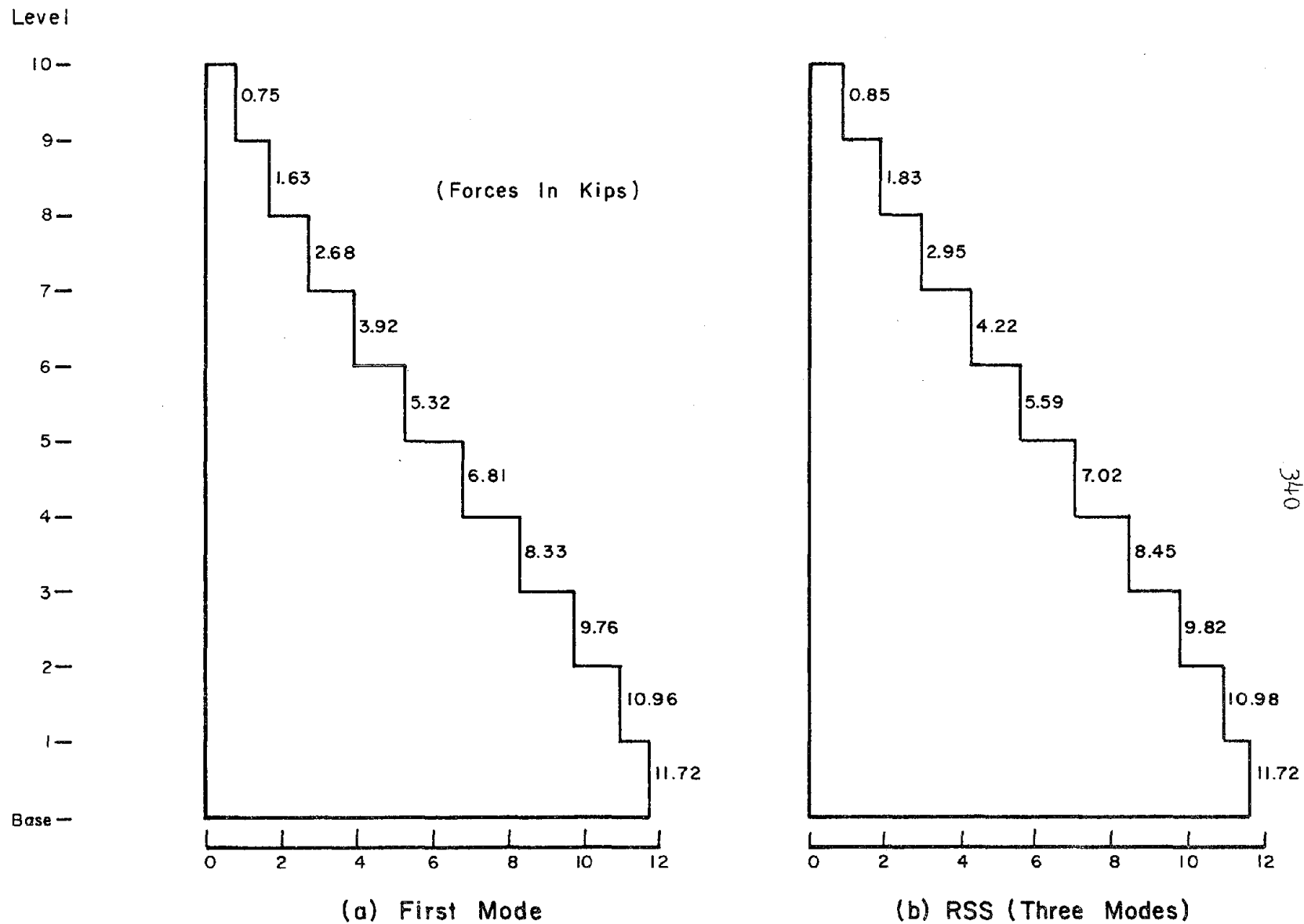
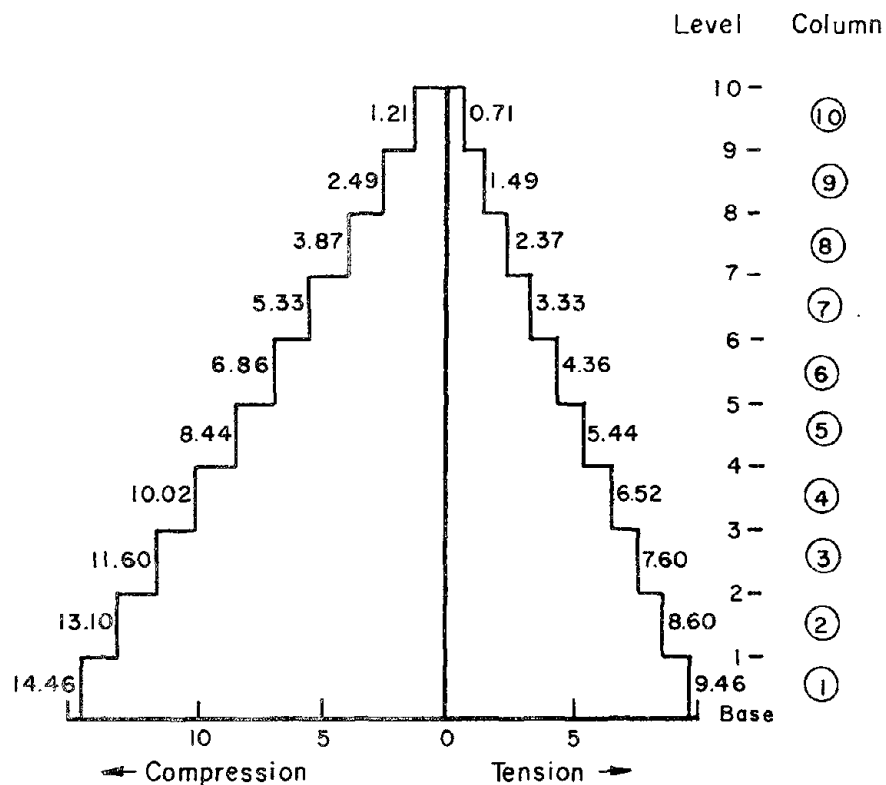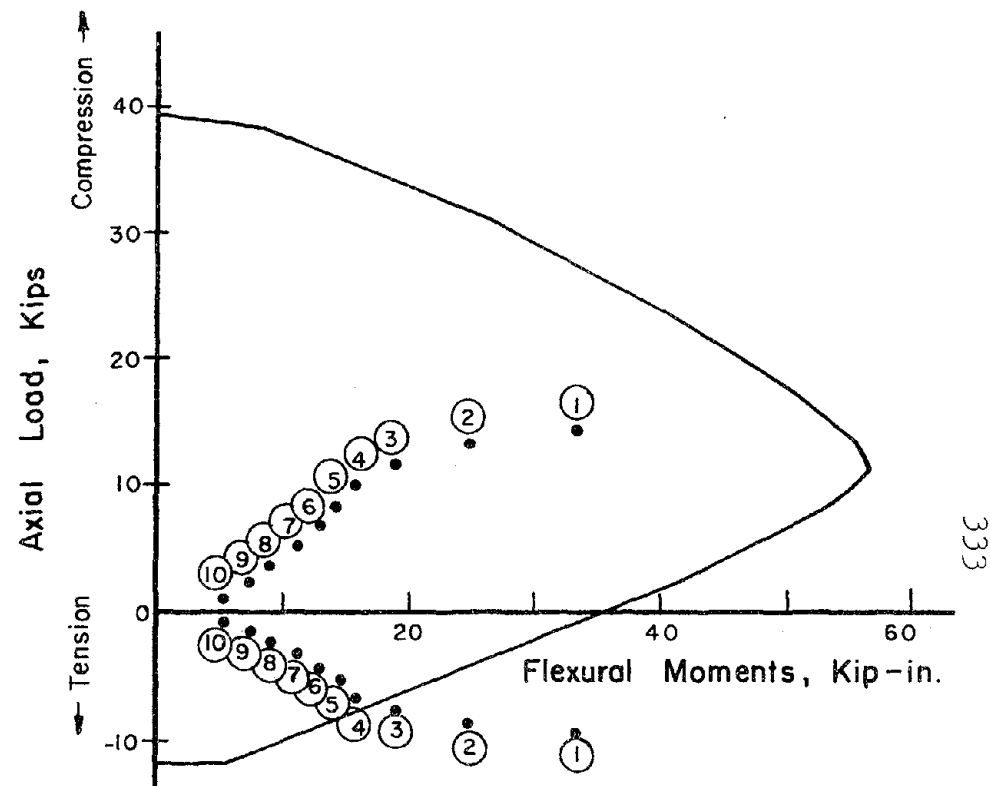Fig. 6.30   Axial Loads in the Piers.   Model of Test Structure M ($\mu_b = \mu_c = 2$)
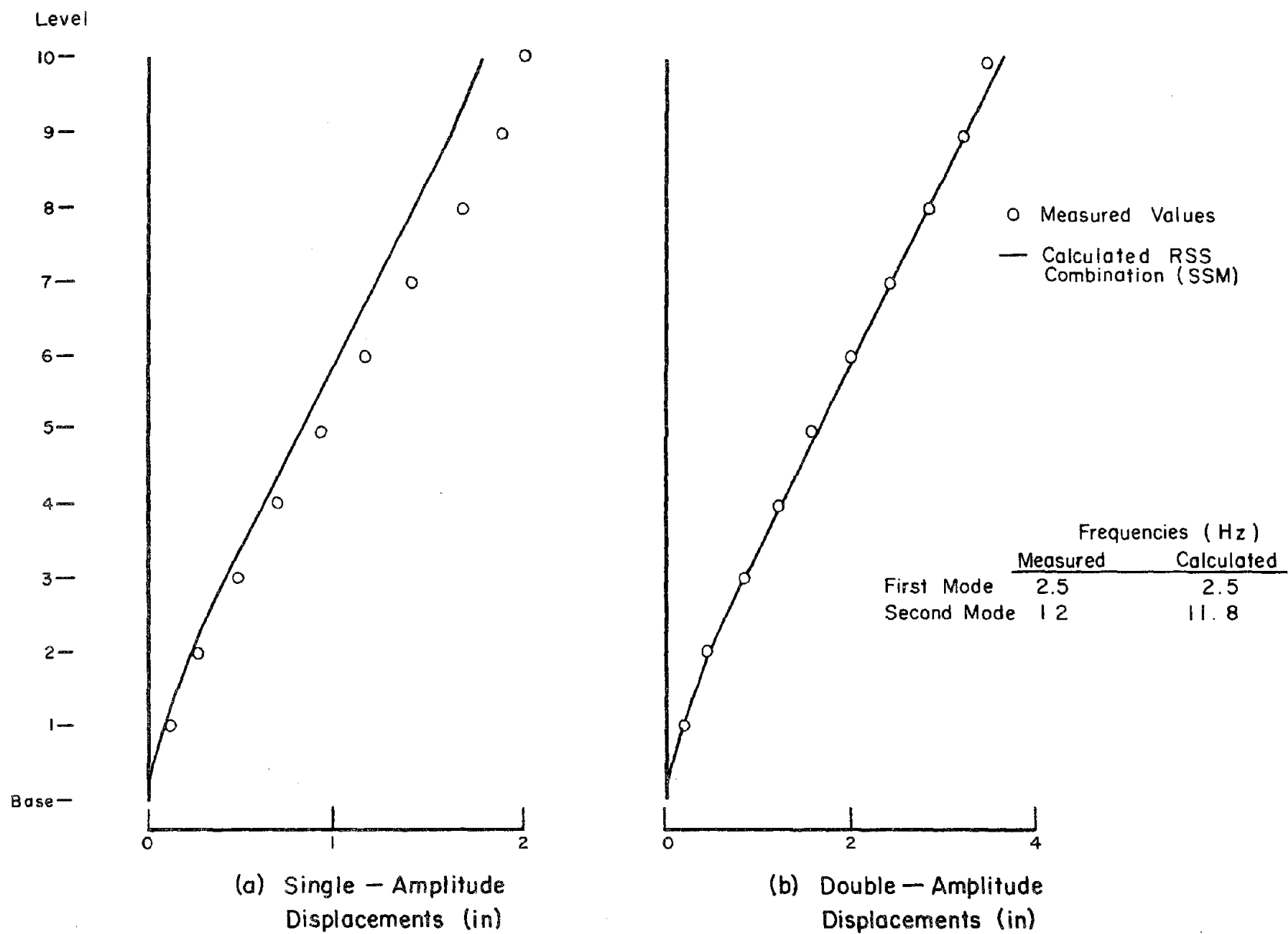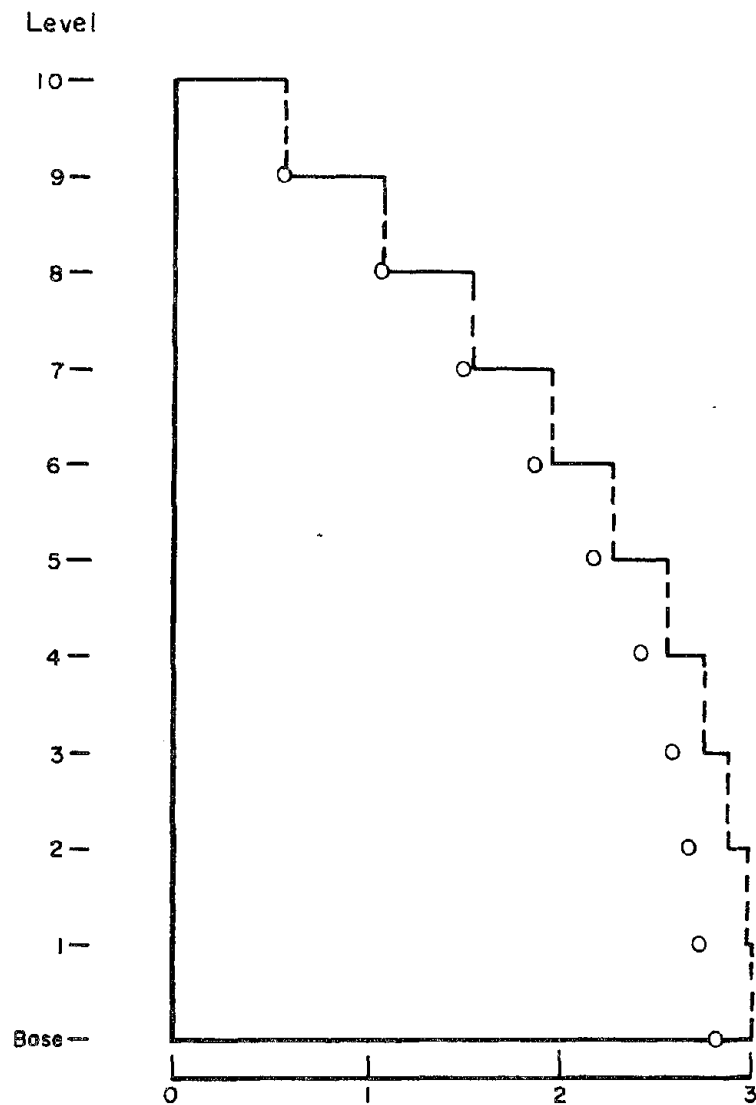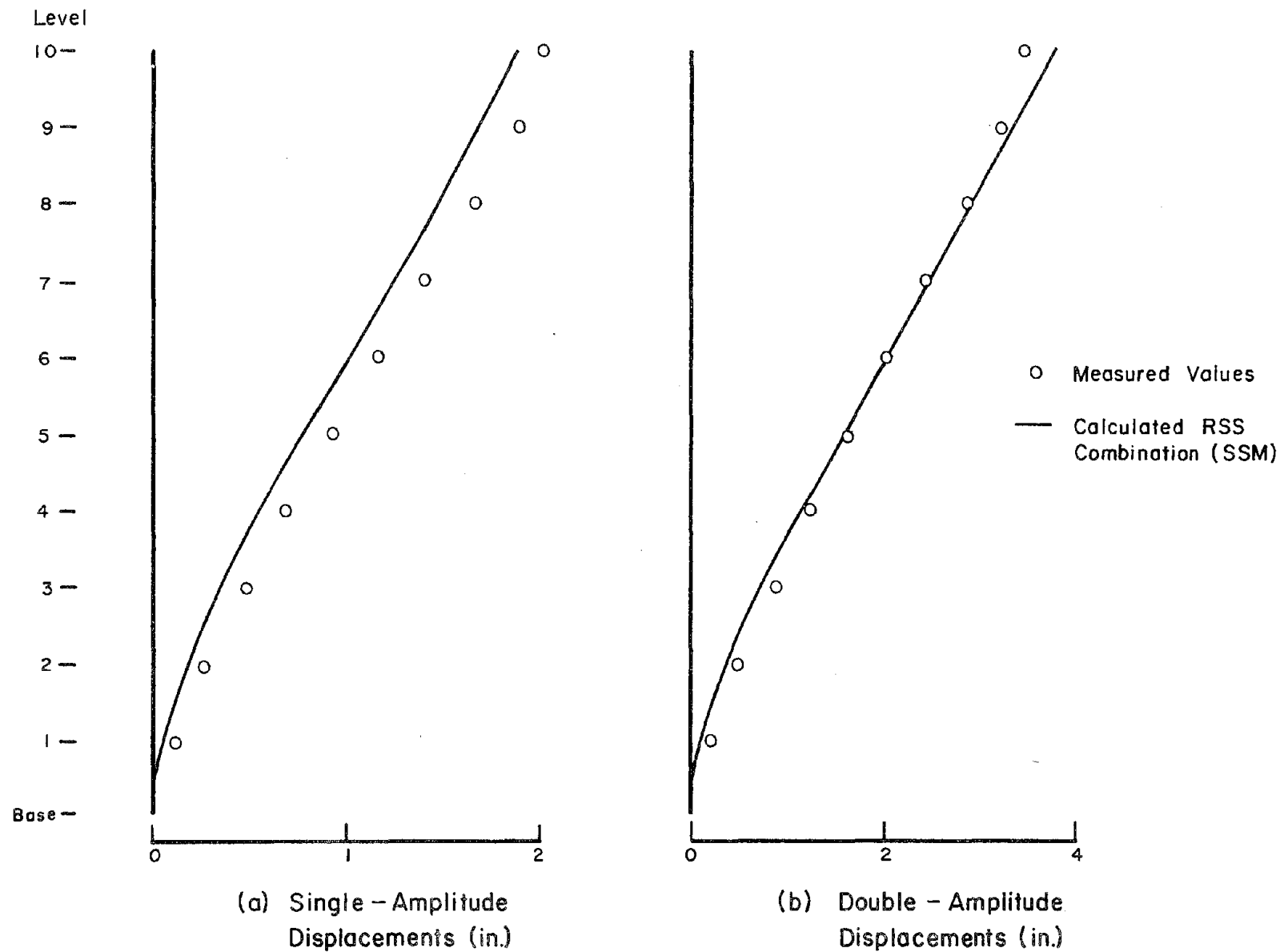
Fig. 6.31 Comparison of Maximum Obtained Displacements with Calculated Values. Model of Test Structure M ($\mu_b = \mu_c = 2$)

341
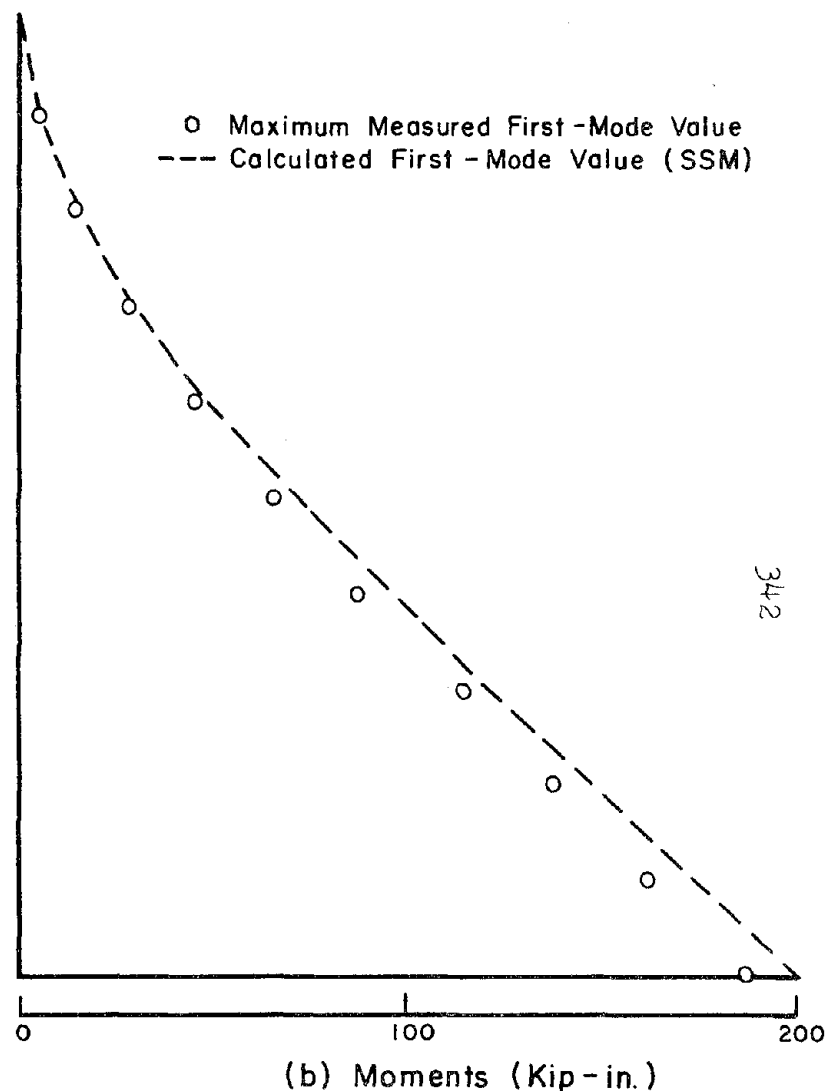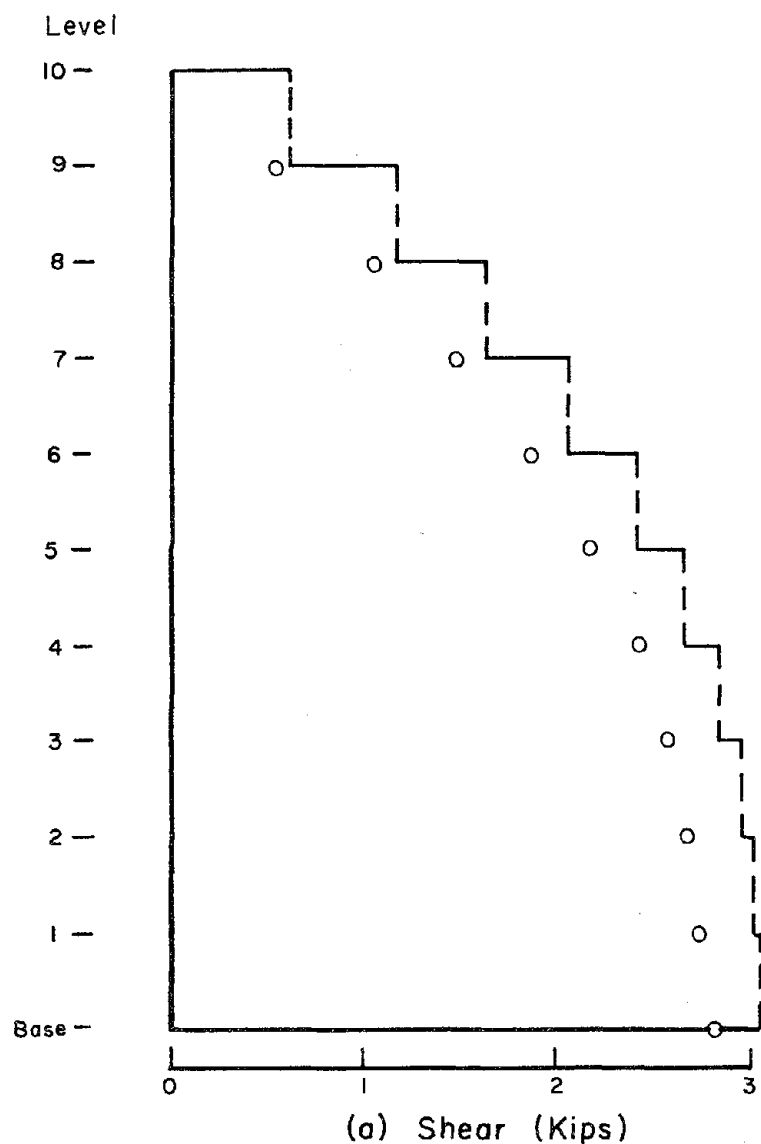
Fig. 6.32   Comparison of Maximum Obtained Forces with Calculated Values. First Mode.
Model of Test Structure M ($\mu_b = \mu_c = 2$)
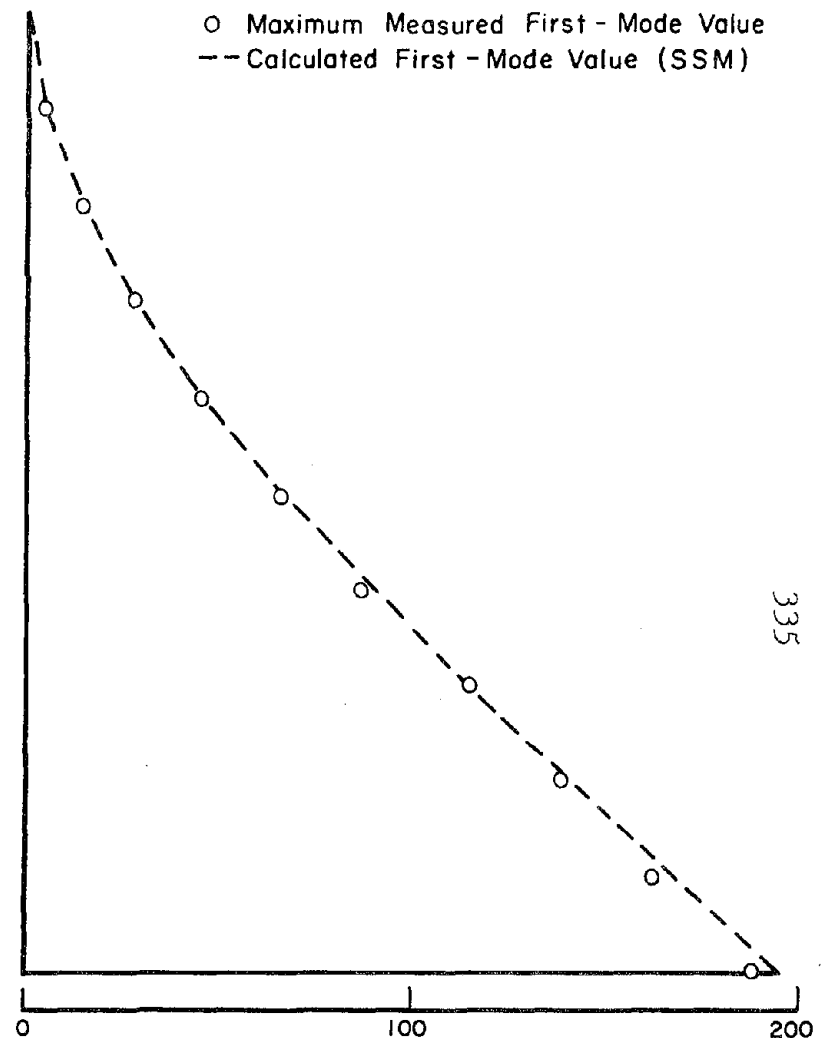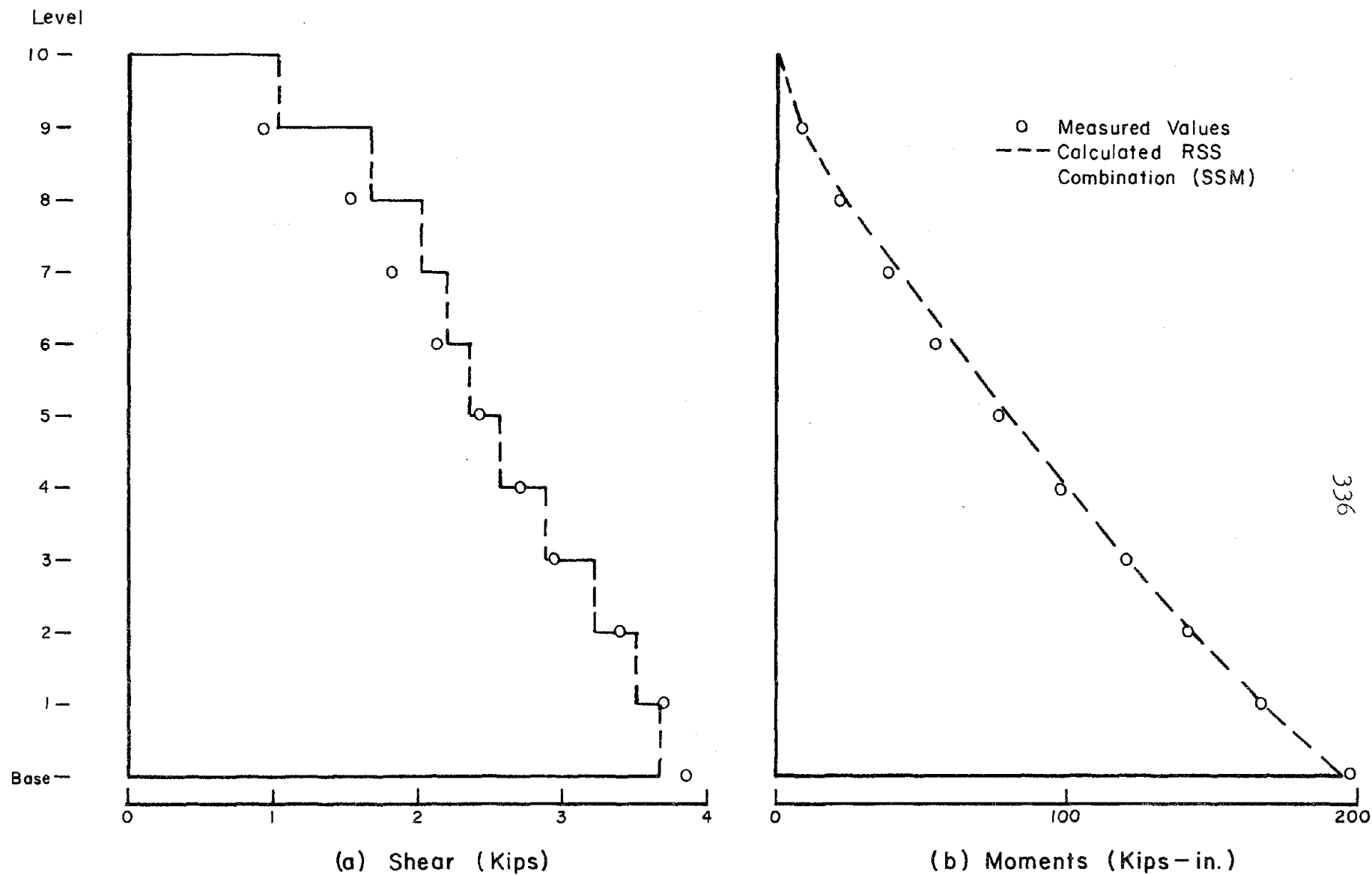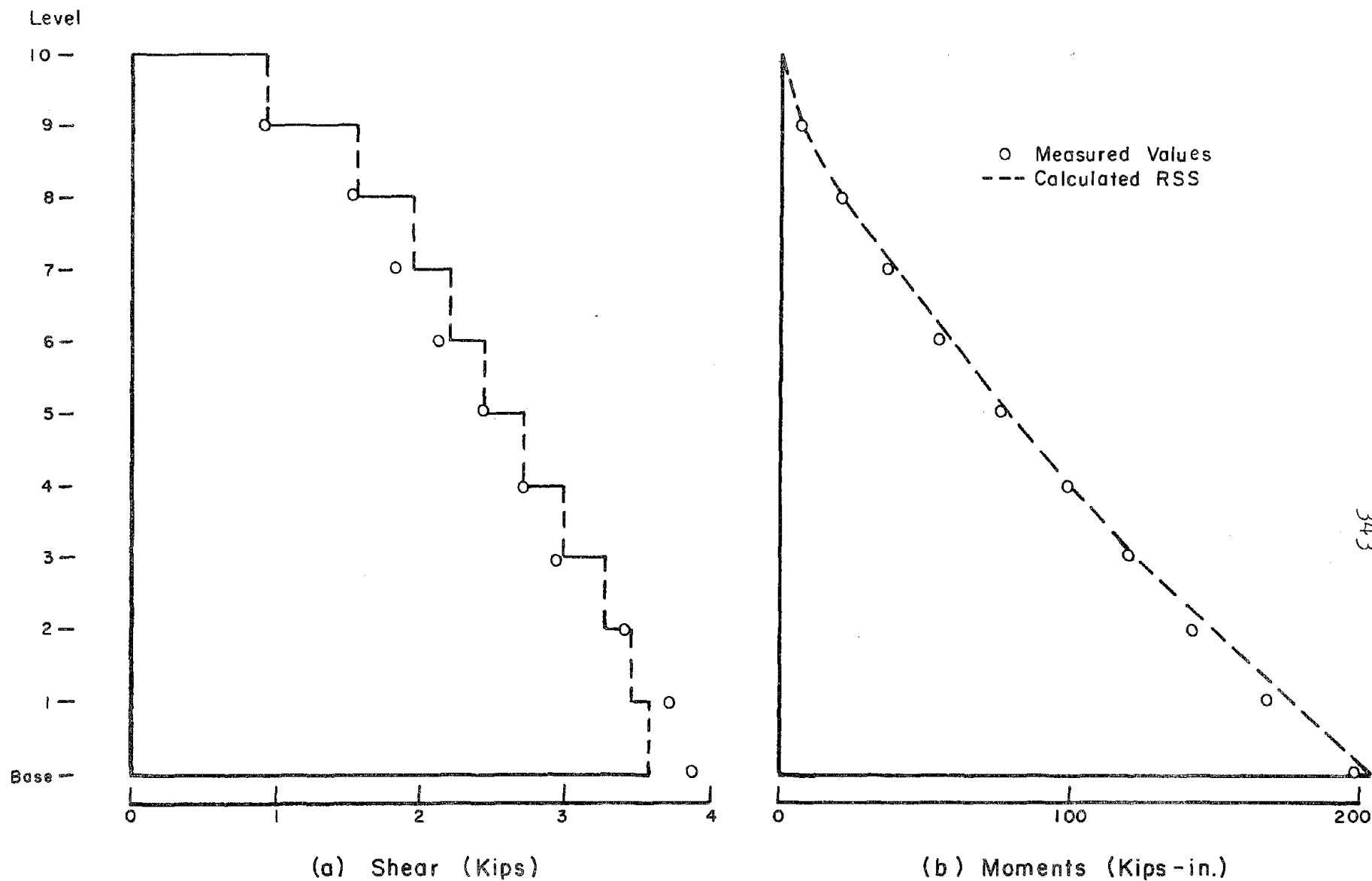
Fig. 6.33 Comparison of Maximum Obtained Forces with Calculated Values.
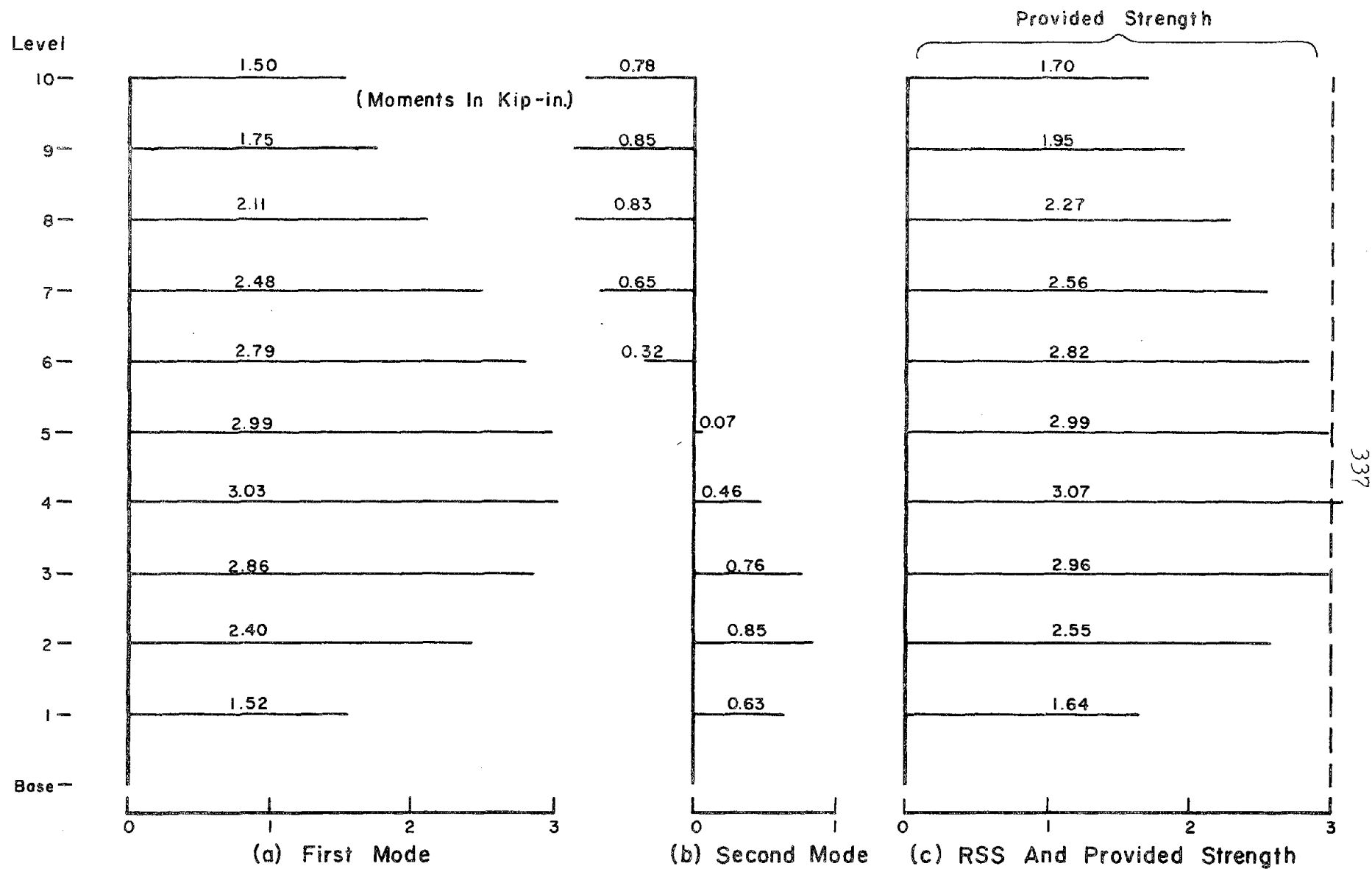Model of Test Structure M ($\mu_b = \mu_c = 2$)

APPENDIX A

DESCRIPTION OF EXPERIMENTAL WORK

A.1 Introductory Remarks

This appendix contains a description of the properties
of the materials used in the investigation, the physical char-
acteristics of the test frames, the experimental facilities
and the test procedures.

A.2 Materials

A.2.1 Concrete

The concrete used throughout this work was small-aggregate
concrete. High-early-strength cement (type III) was used in
casting all the test frames. Fine lake sand and wabash river
sand were used as fine and coarse aggregate. The mix propor-
tions by dry weight was 1:0.96:3.83 (cement:fine aggregate:
coarse aggregate). The water cement ratio was 0.80. This con-
crete was similar to that used in previous studies (Otani, 1974;
Gulkan, 1974) in the Structural Research Laboratory of the Civil
Engineering Departament of the University of Illinois, Urbana-
Champaign.

A couple of frames and control specimens were cast simulta-
neously from the same concrete batch. Mechanical properties of
the concrete were determined from the control specimens on the
same day that each test structure was tested. Three different
kinds of mechanical tests were performed: (1) compression,

(2) splitting and (3) modulus of rupture. Results of these tests for each test structure are summarized in Table A.1.

The compressive properties were determined by testing 4 by 8-in. cylinders using a 120-Kip universal machine. Strains were determined every 1 Kip up to 10 Kip and then every 2 Kip to maximum compressive load. They were measured using a 1/1000 in. mechanical dial gage with a 5-in. gage length. Due to the limi - tations of the testing equipment, the descending portion of the stress-strain relation was not obtained. The stress-strain re - latioships obtained for the concrete of each test structure are shown in Fig. A.1. The frequency distributions are shown in Fig. A.2.

The initial Young's modulus (E_c) of the concrete, taken as the average slope of the secant drawn from zero to 1000 psi, was determined for each compressive test. They are compared with the square root of compressive strength in Fig. A.3. All points fall between two lines described by $49 \sqrt{f_c'}$ and $36 \sqrt{f_c'}$.

The tensile strength properties were determined by splitting tests of 4 by 8-in. cylinders. The modulus of rupture was determined using 2 by 2 by 8-in. prisms loaded at midspan and simple supported at 3 in. The tensile strength and the modulus of rupture of the concrete are compared with the square root of the mean compressive strength in Fig. A.4. The relation between the tensile strength f_t and the average compressive strength $\overline{f_c'}$ was found to be approximately

$$f_t = 6.0 \sqrt{\overline{f}_c'}$$

and the relation between the modulus of rupture f_r and the average compressive strength $\overline{f}_c'$

$$f_r = 13.7 \sqrt{\overline{f}_c'}$$

The frequency distribution of the tensile strength (split cylinder) is plotted in Fig. A.5. The average from 18 splitting tests was 422 psi. The modulus of rupture is compared with the tensile strength in Fig. A.6. The apparent modulus of rupture was twice as large as the tensile strength. These results are similar to those obtained in previous studies (Otani, 1974).

A.2.2 Steel Reinforcement

Number 8 gage wire was used as flexural reinforcement. Number 16 gage wire was used as shear and shrinkage reinforce - ment.

An investigation was conducted to determine the effect of annealing temperature on the yield point of the steel reinforcement. The investigation was initiated because it was desired to lower the yield stress of the flexural reinforcement. The measured variation in the yield-point stress with annealing temperature is shown by Staffier (1975). The yield stress was taken at a 0.2% offset.

Tension tests of 9-in. coupons of the steel were perfomed using a 60-Kip universal testing machine (with a minimum load increment of 20 lb.). Strains were determined using an elec-

trical-resistance clip gage with a 0.5-in. gage length.

No special treatment was carried out to clean the surfaces of No. 8 and No. 16 gage wires. They came out free of impurities after the annealing process.

(1) Flexural Reinforcement: The steel used as flexural reinforcement throughout this study was No. 8 gage bright basic wire annealed at 900°F for two hours. The annealed steel was allowed to cool in the oven, and finally knurled using specially built machine. The cross-sectional dimensions of this wire were checked by micrometer readings. The nominal diameter was within 1% of the actual diameter. The nominal diameter and cross-sectional area are 0.162 in. and 0.0206 in.^{2}, respectively.

Results of the effects of strain rate on the yield stress on this steel are described by Staffier (1975), chapters 2 and 6. Coupons were subjected to strain rates ranging from 0.00017/sec to 0.1/sec. The measured load-strain curves of this steel did not display upper or lower yield at any strain rate and there was no significant increase of the yield point with increasing strain rate.

A total of 68 coupon specimens were taken at random from the same lot as was used in the test structures, and tested in tension. The frequency distributions are plotted for the yield stress (f_y) and the Young's modulus (E_s) in Fig. A.8 and A.9, respectively. The average yield stress at 0.2% offset was 72 Ksi with a standard deviation of 2.0 Ksi. The average Young's

modulus was 30.8×10^6 psi with a standard deviation of 2.4×10^6 psi. A typical stress-strain curve of this steel is shown in Fig. A.7. None of the stress-strain curves showed a flat yield plateau.

Welding was used on this steel at the anchorage plate in the base girder of the test frames (Fig. A.14) at the bar splice of the wall reinforcement between fifth and sixth levels (Fig. A.15) and at the ends of the bars of the beams of frames M (Fig. 2.20). Since the strength of the steel used as main reinforcement was very sensitive to high temperatures, as shown by the annealing temperature-yield stress plot (Staffier, 1975), welding was used only at those three locations described above which are far enough from the critical points, i.e. points where disturbances of the steel properties caused by the welding temperature would have a significant effect on the strength or behavior of the structural system. To study the effect of welding on the strength of the flexural steel, twenty coupon bars were taken at random from the same lot as was used for the fabrication of cages of the frames. From each two of these bars a welded splice was made in similar conditions to those encountered in the splice of the wall reinforcement (Fig. A.15), and tested in tension. The average ultimate stress was 67 Ksi, with a scatter range of 53 to 76 Ksi. This was equivalent to a loss of strength in the steel of 20%.

(2) Shear reinforcement: Number 16 gage plain wire an-

nealded at 900°F for two hours and oven cooled was used as transverse reinforcement throughout this study. The nominal diameter and cross-sectional area are 0.0625 in. and 0.00307 in.^{2}, respectively. A typical stress-strain curve is shown in Fig. A.10. The average yield stress taken from 5 coupons was 106 kips with a scatter range of 104 ksi to 108 ksi.

(3) Shrinkage reinforcement: Number 16 plain wire annealded at 1200°F for two hours and oven cooled was used as shrinkage and temperature steel along the center line of the walls of the standard frame (Fig. A.13). A typical stress-strain curve is shown in Fig. A.10. An average yield stress of 40 ksi obtained from 5 test coupons with a scatter range of 39 ksi to 42 ksi.

(4) Helical Reinforcement: Plain wire of 0.046-in. diameter and 20-ksi proportional limit was used for fabricating the helical reinforcement. This steel was received in rolls. The wire was then deformed by machine in a rectangular helix of 0.55 by 0.71 in. (Fig. A.13) and longitudinal spacing of 0.25 in. The average yield stress from 5 coupons of the wire as received and the average yield stress from four samples of the same wire straightened from the helix was 41 ksi as well.

A.3 Description of the Test Structures

Each test structure was made up of two frames (Fig. 2.1). Each frame comprised two walls connected at each level by beams. Two types of frames were constructed. These are referred to as

the standard test frame (type D) and the modified test frame (type M). Three structures of type D and one of type M were tested. The difference between these two structures was the amount of reinforcement in the connecting beams and in the top four columns of their corresponding frames.

The overall configuration of the test setup is shown in Fig. A.17.

(a) Dimensions

All the nominal dimensions were identical for both types of test structures and their corresponding frames. The overall nominal dimensions of the ten story test frame are given in Fig. 2.6a. The beams at every floor had identical section properties. The piers (walls) were continuous from the base to the top with the same nominal cross dimensions. The bottom end of the two piers were cast monolithically with a rigid base girder, as shown in Fig. 2.1.

The story height was 9.0 in. center-to-center of the beams. The top end of the piers protruded 4.0 in. from the center of the tenth-story beam.

A column had dimensions of 7.0 by 1.0 in. and was 94.0 in. tall measured from the top face of the base girder. Beams were 1.5 in. deep, 1.0 in. wide and 4.0 in. long. The base girder had a cross section of 9.0 by 12.0 in. and a length of 54 in. All the frames were built within a fabrication error of $^{+}_{-}0.02$ in. The base girder was built within a fabrication error of $^{+}_{-}0.05$ in.

In order to facilitate connection of the weights, holes were provided along the centerlines of each pier at each floor level beams, as shown in Fig. 2.1. These holes were reinforced with steel pipes (0.63 in. inside diameter and 0.02 in. thickness).

Four vertical holes were made in the base girders on 12.0 in. centers in order to fasten the test structure to the earthquake simulator platform. The holes were reinforced with steel pipes (1.5 in. inside diameter and 1/8 in. thickness).

(b) Beam Reinforcement

The amount and arrangement of steel in the connecting beams was a major variable in the experimental study. Arrangement of the steel reinforcement of the connecting beams for frames D and M are shown in Fig. 2.17 and 2.20.

The nominal flexural reinforcement ratios, based on the tensile steel area and the effective depth of the section, were 1.65% and 3.3% for frames D and M.

The nominal transverse reinforcement ratios, calculated as the ratio between the shear reinforcement area and the product of the thickness of the beam and the spacing of the shear reinforcement, were 1.53% and 3.06% for frames D and M.

The longitudinal reinforcement in the beams was extended all the way into the walls to develop anchorage. In frame-D beams only two No. 8 gage wires were used as flexural reinforcement located as shown in Fig. A.11. Whereas in frame-M beams

four No. 8 gage wires were used as shown in Fig. A.16. The anchorage provided for the beams was sufficient to develop the maximum strength of the beams (Abrams, 1976).

The flexural reinforcement of the frame-M beams were welded together at a distance of 5-in. from the interior face of the piers, as shown in Fig. 2.20 and A.16. This welding was provided to improve the anchorage of the longitudinal bars, since the provided nominal concrete cover was about 0.1 in.

(c) Wall Reinforcement

Arrangement of the wall reinforcement for frames D and M are shown in Fig. 2.15 and 2.18. Cross-sectional details of the walls are given in Fig. 2.16 and 2.19 for frames D and M. The amount of flexural reinforcement in the first six floors is identical in walls of frames D and M. The amount of flexural reinforcement in the walls of frame M was constant from top to bottom, whereas in frame D half of the bars were cut at a level between fifth and sixth levels.

The nominal flexural reinforcement of frame-D walls, calculated as the ratio of the total steel area to the gross area of the section, was 2.35% in the first five columns and 1.17% in the top five columns. For frame M, this ratio was 2.35% from top to bottom.

The nominal shear reinforcement ratios, calculated in the same way as for the beams, were 0.31% and 0.41% for the frame-D and frame-M walls, respectively.

Since the supplier cut the wire into 6 ft lengths, over-lapping of the flexural steel was required in the walls be-tween fifth and sixth floor levels (Fig. 2.15 and 2.18).

The flexural reinforcement in the walls was extended 7 in. into the base girder depth and welded to an anchorage plate as shown in Fig. 2.15 and A.14.

(d) Base Girder Reinforcement

Details of the reinforcement for the base girder are shown in Fig. 2.15 and 2.18. The nominal flexural reinforcement, as defined above, was 1.38%. A total of four #5 rebars grade 75 were used as shown by the figure. This longitudinal steel was provided such that the base could resist the maximum overturn-ing moment capacity of the frame without cracking.

(e) Casting and Curing

The two frames for each test structure were cast simulta-neously and cured under identical conditions, along with the control specimens (cylinders and prisms). The concrete was mixed in one batch in the laboratory.

The concrete was placed in the forms and vibrated using a mechanical stud vibrator. The vibrator was used inside the concrete for the base girder and against the formwork (outside the concrete) for the frame. Approximately one hour after placement, the concrete was struck off and then troweled smooth.

The two frames and the control specimens were covered with plastic sheets and allowed to cure overnight. One day after

casting, the sideforms were removed carefully since the concrete was still fresh. Then the frames, along with the control spec-imens, were covered with wet burlap and plastic sheets were placed over the wet burlap. The wet burlap and plastic sheets were removed a week after casting. The frames and the control specimens were then stored in the laboratory until time of test-ing.

Views of the formwork and the placement of the steel cage are given from Figure A.12 to A.15.

A.4 Test Structure Setup

This section describes the experimental facilities, the instrumentation and the test procedure used during the tests.

(a) The Earthquake Simulator

The test structures were tested on the Earthquake Simula-tor of the Structural Research Laboratory of the University of Illinois Civil Engineering Department. The overall configura-tion of the test setup is shown in Fig. A.17 and A.18.

The earthquake simulator system is an experimental facil-ity designed to subject small scale structures to vibratory base motions, of a regular or random character, in one horizontal direction.

The system consists of (1) a hydraulic ram equipped with a servomechanism, (2) a power supply, (3) a command center, and (4) a test platform.

The longitudinal axis of the ram is in the horizontal

plane. The ram reacts against the steel pedestal which is tied
to the test floor with prestressed 2 in. bolts. The operation-
al limits of the ram are: 75,000 lb capacity, four-in. double
amplitude displacement, 15-in. per sec. velocity, 7.5g accel-
eration, and 100 Hz.

The simulator platform measures 12 by 12 ft in plan and is
drilled and tapped for 1/2 in. bolts on 12 in. centers in both
directions. The platform is supported by series of flexure
plates, with flexure joints at each end. The flexure joints
act as hinges allowing free motion of the platform up to a dou-
ble-amplitude displacement of 5 in. The platform was designed
to carry specimens up to 10,000 lb.

The connection between the platform and the hydraulic ram
is provided by a flexural link, a steel shaft with two reduced
sections as shown in the figure. The flexure link is supposed
to transmit horizontal motion of the hydraulic ram to the plat-
form, at the same time allow the vertical movement of the plat-
form.

The earthquake simulator is activated by a command center
which can accept almost any signal in terms of electric volt-
age. Input form can be displacement, velocity and acceleration
time histories, although the motion of the hydraulic ram is con-
trolled by a displacement command, which can be acquired by
electronic integration from a velocity or an acceleration time
history.

Detailed description of the system hardware is given by Sozen et al. (1969); Sozen and Otani (1970); and Otani (1972).

(b) Instrumentation

Two different types of gages were used during each test: accelerometers to measure accelerations and linear voltage differential transformers (LVDT's) to measure displacements.

Accelerometers measured the absolute acceleration of the point of installation in the direction of the axis of the accelerometer. A $\pm$ 1.0g calibration signal was generated by changing the axis of the gage from the horizontal position to the vertical position.

Twenty-two accelerometers were installed to measure horizontal acceleration parallel to the imposed direction of motion: an accelerometer at the top of the base girder of each frame (Fig. 3.3), and an accelerometer on the longitudinal connections of the weights along the centerlines of the beams on both frames and at every floor level (Fig. 3.4).

LVDT's measured relative displacements with respect to a rigid steel frame fastened on the earthquake simulator platform in the direction of motion. These gages were mounted on the A shape steel frame (Fig. 3.2) which had a natural frequency of approximately 48 Hertz. Calibration factors were determined using metal gage blocks machined to either 1/4 in. or 1.0 in.

A total of twenty LVDT's were installed with their axis parallel to the imposed direction of motion: an LVDT along the

center line of the connecting beam of each floor level on both
walls.

(c) Test Procedure

Before installing the test frames on the platform, the
earthquake simulator was run several times to calibrate the ac-
tuator travel against maximum platform acceleration for the
particular waveform to be used in the tests. Waveforms of the
platform accelerations were examined for fidelity with respect
to the input waveform.

After the calibration of the earthquake simulator was
found acceptable, the two test frames were placed and bolted
down to the platform using longitudinal I steel beams and trans-
versal steel angles as shown by Fig. 3.1. Longitudinal and
transversal steel connections which carried the steel weights
were put in place one level at a time starting from the first
level.

Immediately after the ten weights and corresponding connec-
tions were placed and fastened to the frames any cracks in the
specimen were recorded. These could have incurred through
either shrinkage of handling. The frames were sprayed on the
surfaces with "Partek" P1-A Fluorescent (Magnaflux Corporation,
Chicago, Illinois) which is a fluid containing fluorescent par-
ticles penetrated into the concrete cracks and reflected "black
light" showing the crack patterns on the frames.

Immediately before any test, the tightness of all bolts on

the test setup were checked. The mounting and alignment of all sensors (gages) were rechecked.

The following steps were performed for each run of each test structure.

(1) The test structure was subjected to a low-amplitude free vibration by displacing the simulator platform very gently.

(2) The selected earthquake waveform was fed into the earthquake simulator to subject the test structure to the desired earthquake base motion at the desired acceleration level.

(3) During the run, the test data were all recorded on magnetic tape and the motion of the test structure was recorded using movie cameras and a video tape machine.

After each test run, cracks on the frames were marked with pencil and identified. Special attention was given to any spalling or crushing of the concrete in the structural members of the frames. Notes were made describing the nature and distribution of the damage caused on the structure.

Finally, the mechanical calibration of the LVDT's and accelerometers were performed. These calibration signals were recorded in a notebook. The calibration was made before and after the test to check the influence of temperature change on electronic devices.

A.5 Data Reduction

The response measurements of the test structures, as obtained during the test runs consisted of a series of instrument

(gages) responses in voltage units for various successive times. These responses were recorded by four analog magnetic tape recorders, each with a capability of recording thirteen voltage signals and one audio signal. A common signal (the input earthquake acceleration waveform) was recorded in channel one of all four units as a time reference so that data on the four tapes could by synchronized for interpretation of the test results.

For interpretation purposes the data was needed in digital form. The analog records were converted into digital records using the Spiras-65 computer of the Department of Civil Engineering. The digitation rate was 1000 points per second. The digitized data were also placed on magnetic tape.

The calibration factors and the zero levels recorded on tapes were read using a computer program. The calibration factors for the data were computed from the instrument response to known accelerations or displacements in terms of voltage units. The zero levels for each gage response was obtained by reading the portion of the data record immediately before the onset of the earthquake.

The organization of the data was then altered using a computer program. This program processed the data into its final form (series of response-time relations) applying the previously obtained zero levels and calibration factors of each gage. The data was finally in the form of a series of time histories in the units of either inches or g (gravity acceleration). The

final data (displacement and acceleration waveforms) were also placed on magnetic tape.

The shear-force and overturning-moment records at each level of the test frames were determined directly at each time from the measured acceleration signals combined with the story weight (0.5 Kip) and the story heights (9.0 in.). The overturning effect of gravity load acting through the sideway displacement was included in calculating the overturning moments at each level.

A computer program was written for the purpose of plotting response-time relations. This program plotted four waveforms per page (Chapter 4) and was used to plot large quantities of data.

The response spectra for the base acceleration waveforms were computed and plotted using a computer program. The program computes the response of a linear-elastic single-degree-of-freedom system to the measured acceleration record. The response spectra were plotted in tripartite (logarithmic) form and in arithmetic form.

A computer program was written to compute and plot the fourier transform spectrum of any waveform. The fourier transform (Fig. 5.1 and 5.2) is in effect a frequency decomposition of a record. The fourier transform plots show that there are certain frequencies, represented by the peaks, which are particularly important and predominant within the waveform. Only

information about amplitude was plotted.

To study the influence of the first-and higher-mode components in the waveforms, a computer program was written to separate the harmonic content from frequencies 0 to 5.0 Hz of the waveforms. This program makes use of the Fast Fourier transform (FFT) library subroutine.

Table A.1

Measured Average Strength of Concrete Control Specimens

Test Structure	Age (Days)	Secant* Modulus $\times 10^6$ (psi)	Compressive Strength (f'_c) (psi)	Tensile Strength	
				Splitting Test (psi)	Modulus Rupture (psi)
D1	71	2.7	4710	418	786
D2	60	2.9	5870	432	1137
D3	51	3.0	4950	447	988
M1	36	3.1	4750	392	983

* Measured at 1000 psi in compression test of 4x8-in. cylinders
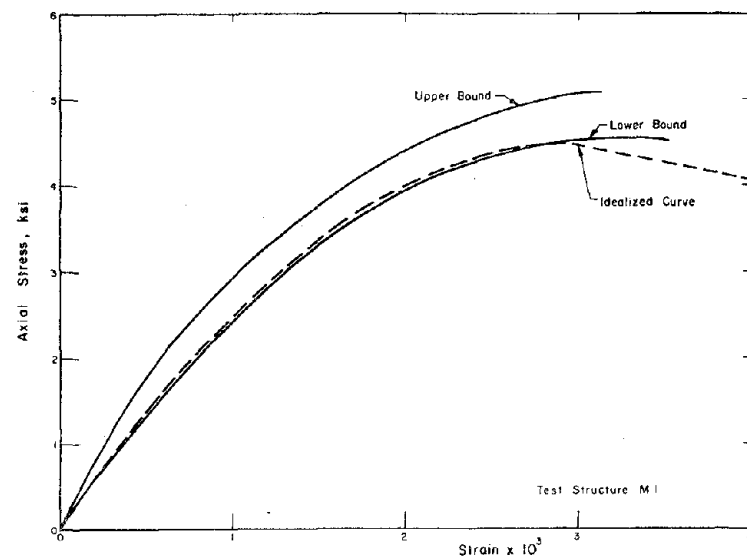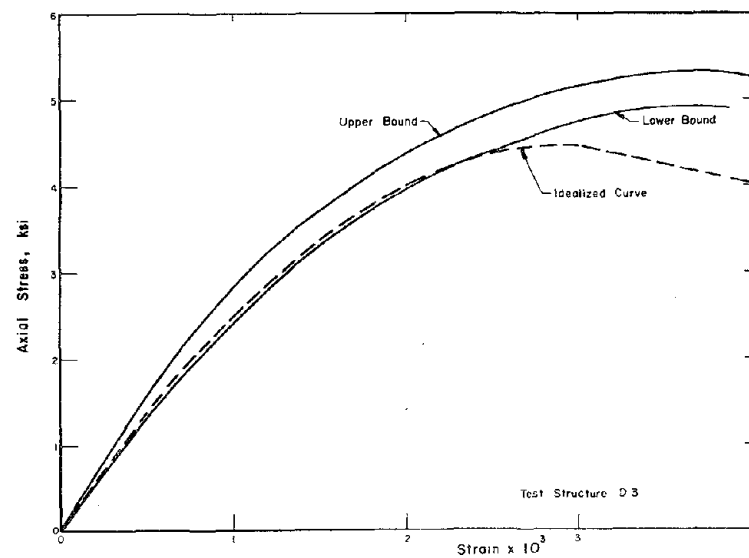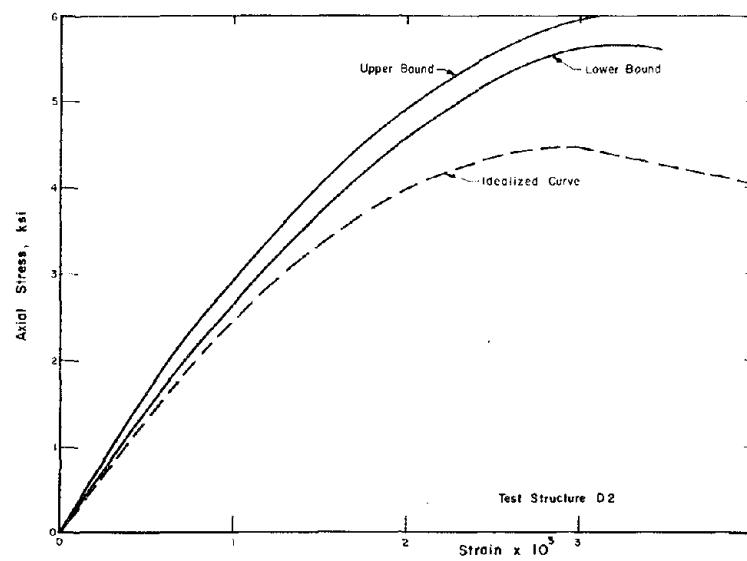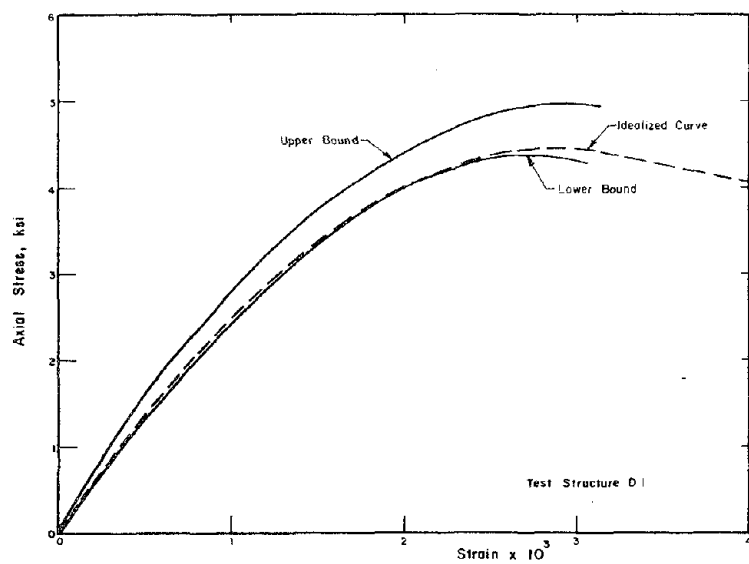
Fig. A.1   Bounds of Measured Stress-Strain Relationships for Concrete
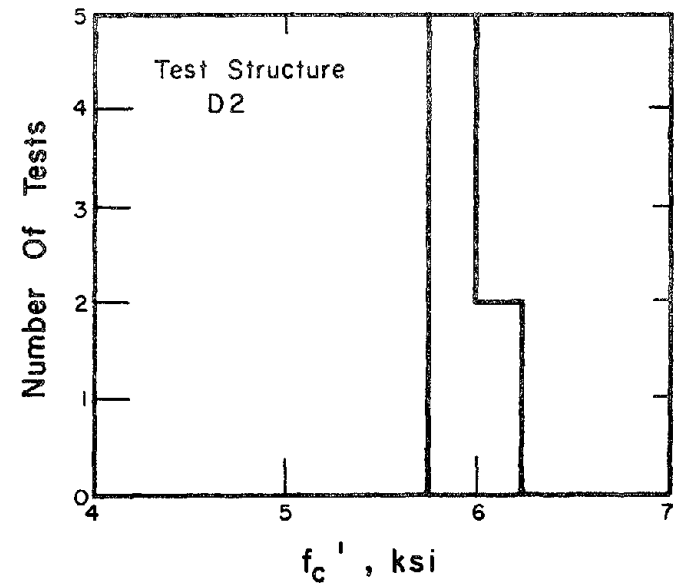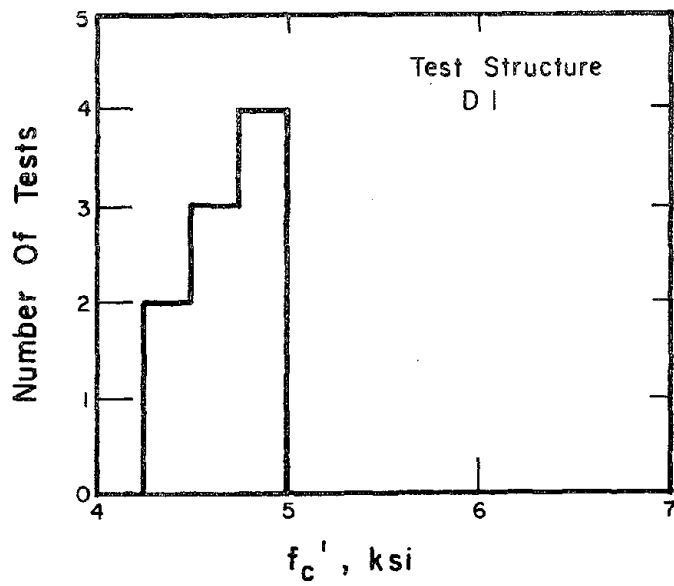
$f_c' = $ Compressive Strength Of Concrete
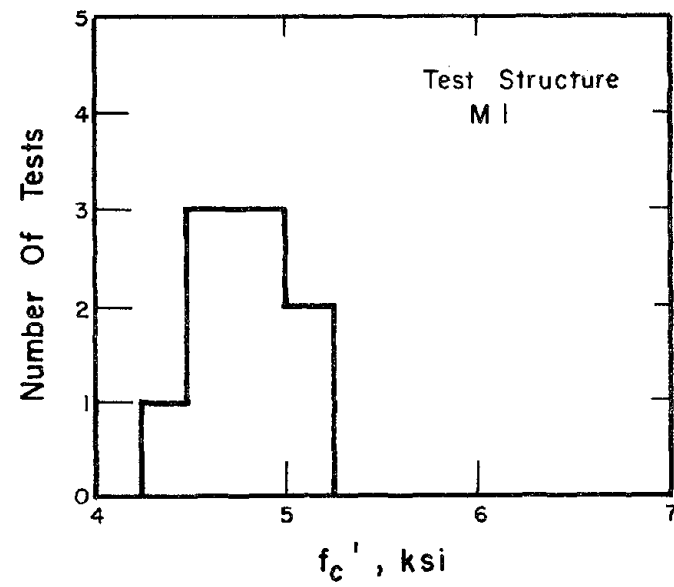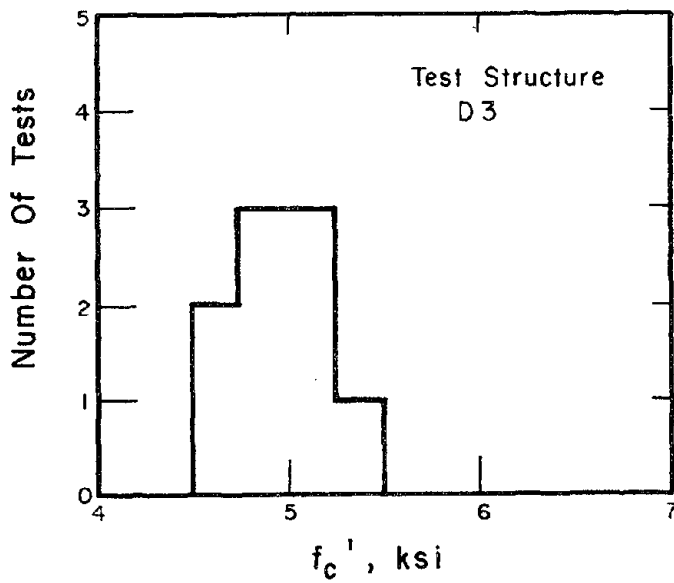
Fig. A.2 Distribution of Compressive Strength of Concrete
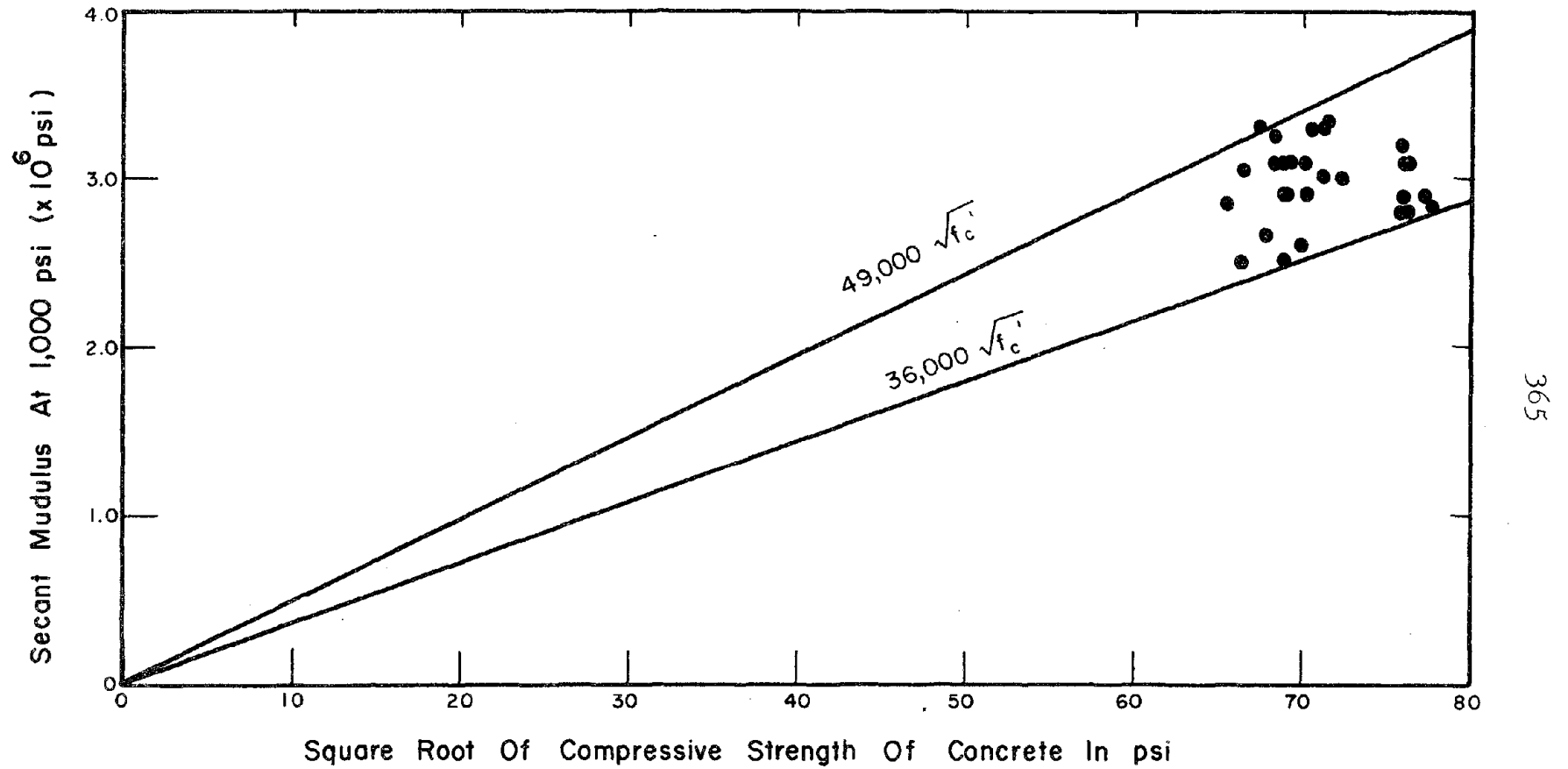
Fig. A.3 Variation of Secant Modulus with Square Root of Compressive Strength of Concrete
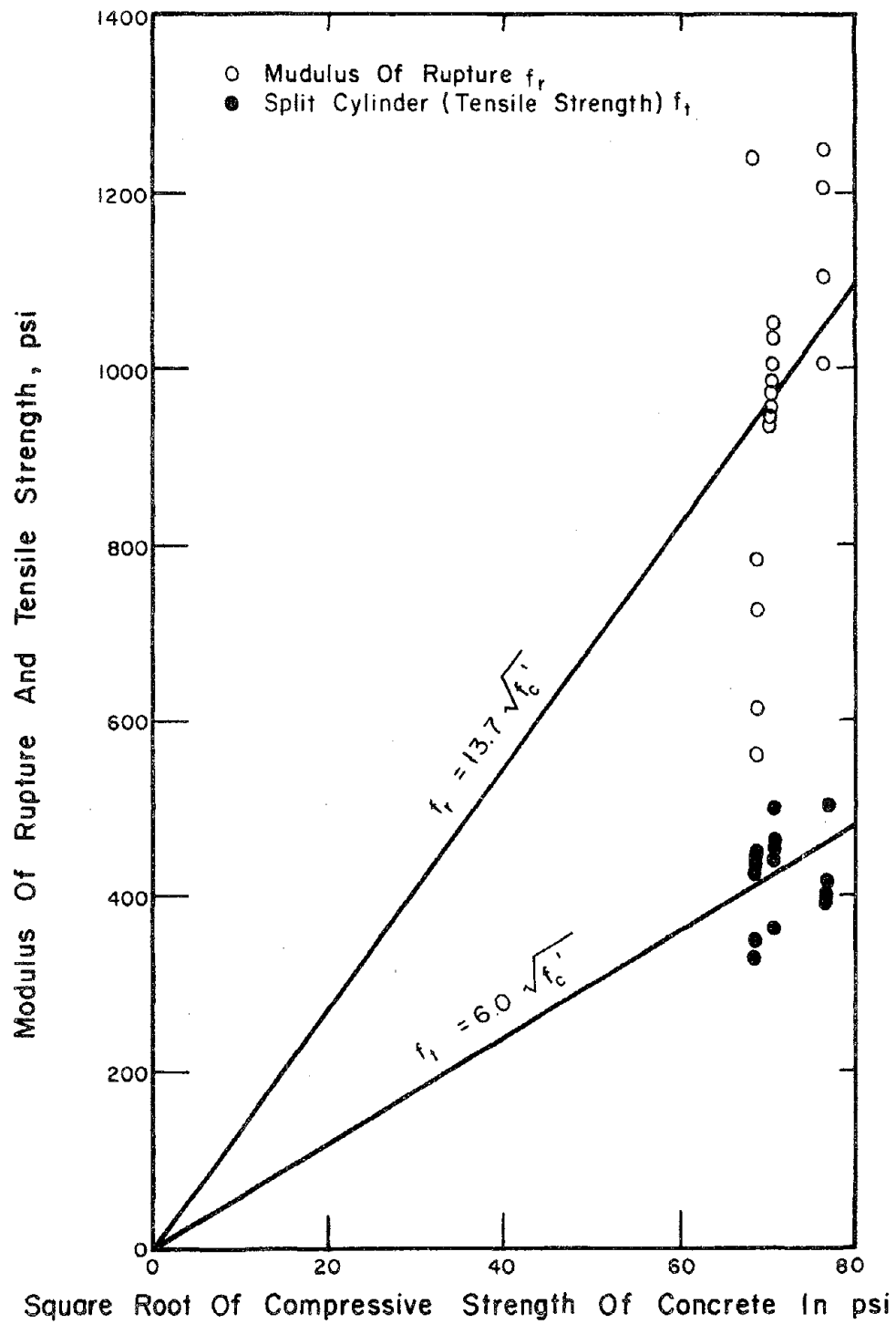
Fig. A.4   Variation of Tensile Strength and Modulus of
Rupture with Compressive Strength of Concrete
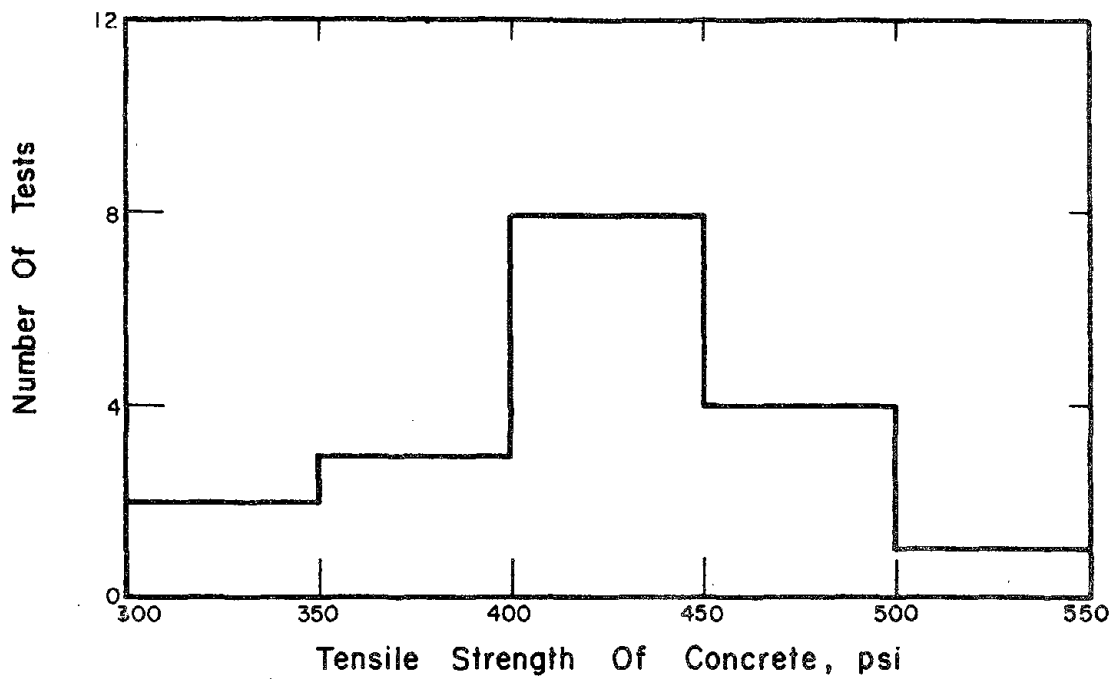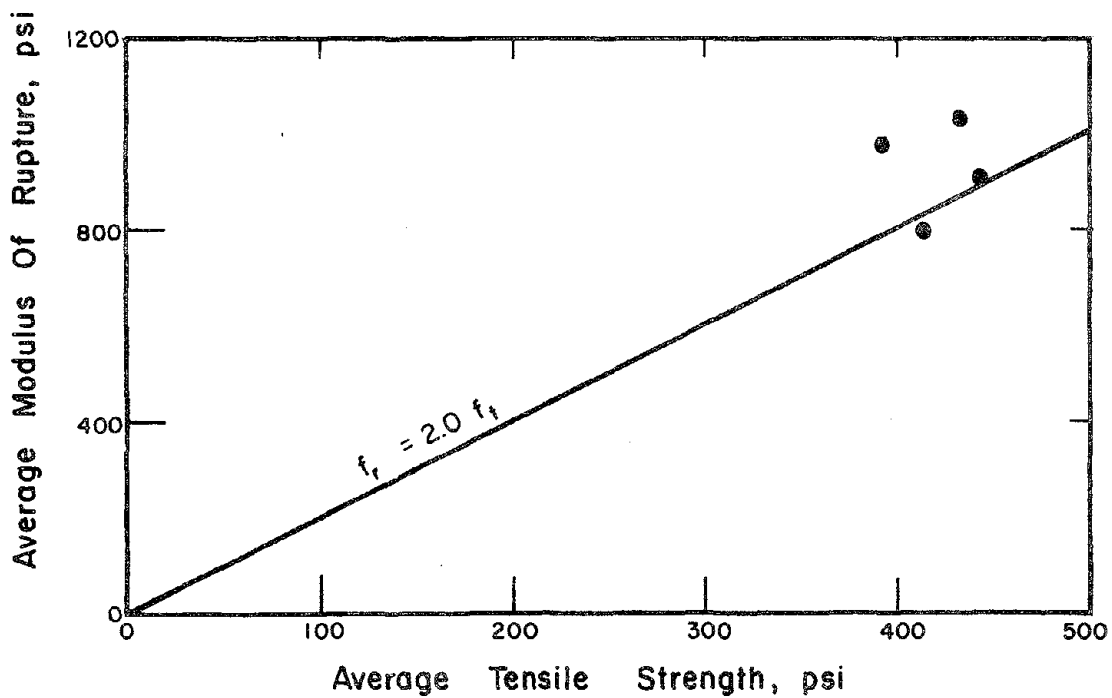
Fig. A.5 Distribution of Tensile Strength of Concrete
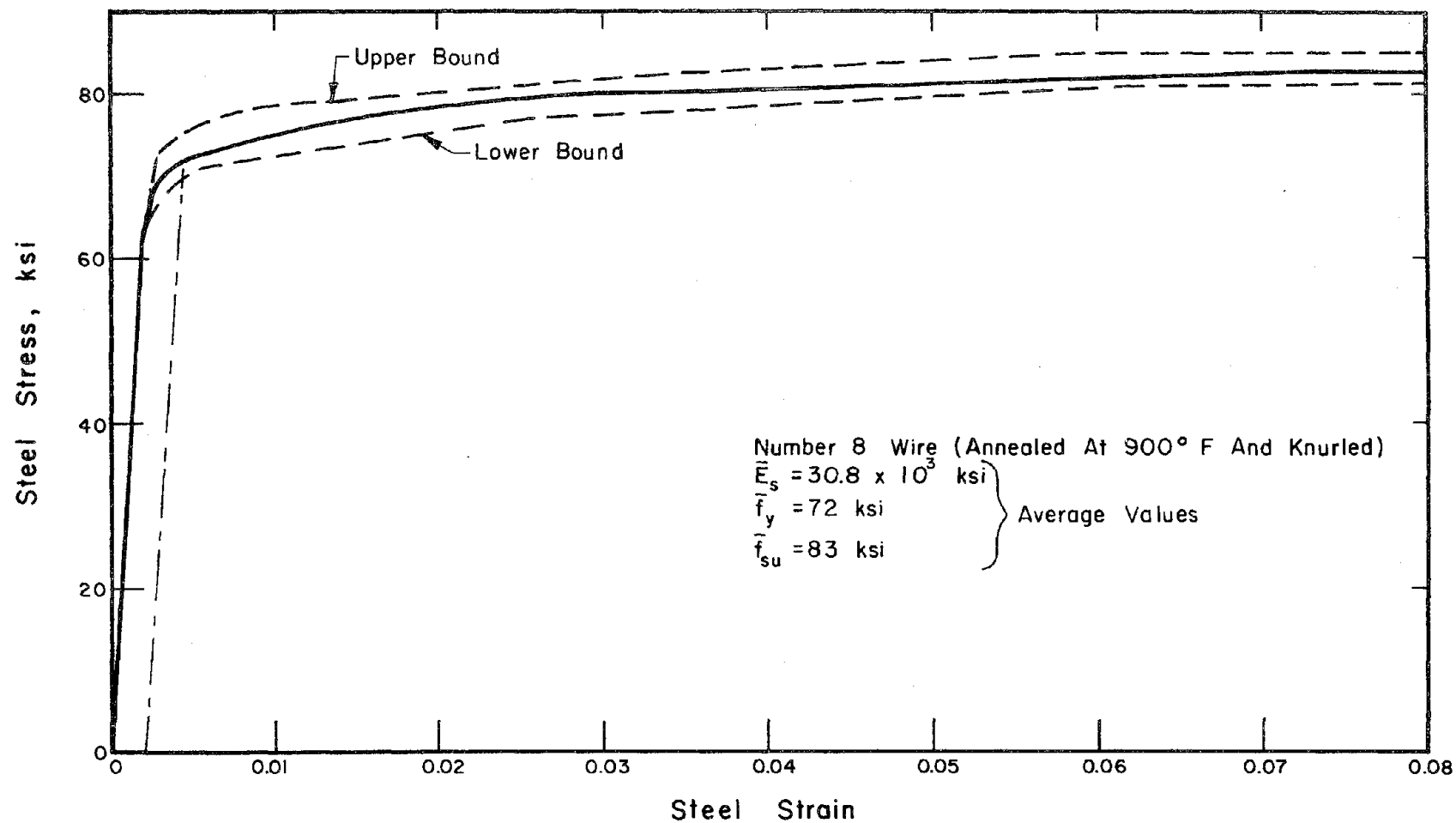

Fig. A.6 Comparison of Modulus of Rupture and
Tensile Strength of Concrete

Fig. A.7   Bounds of Measured Stress-Strain Relationships for No. 8 Gage Wire
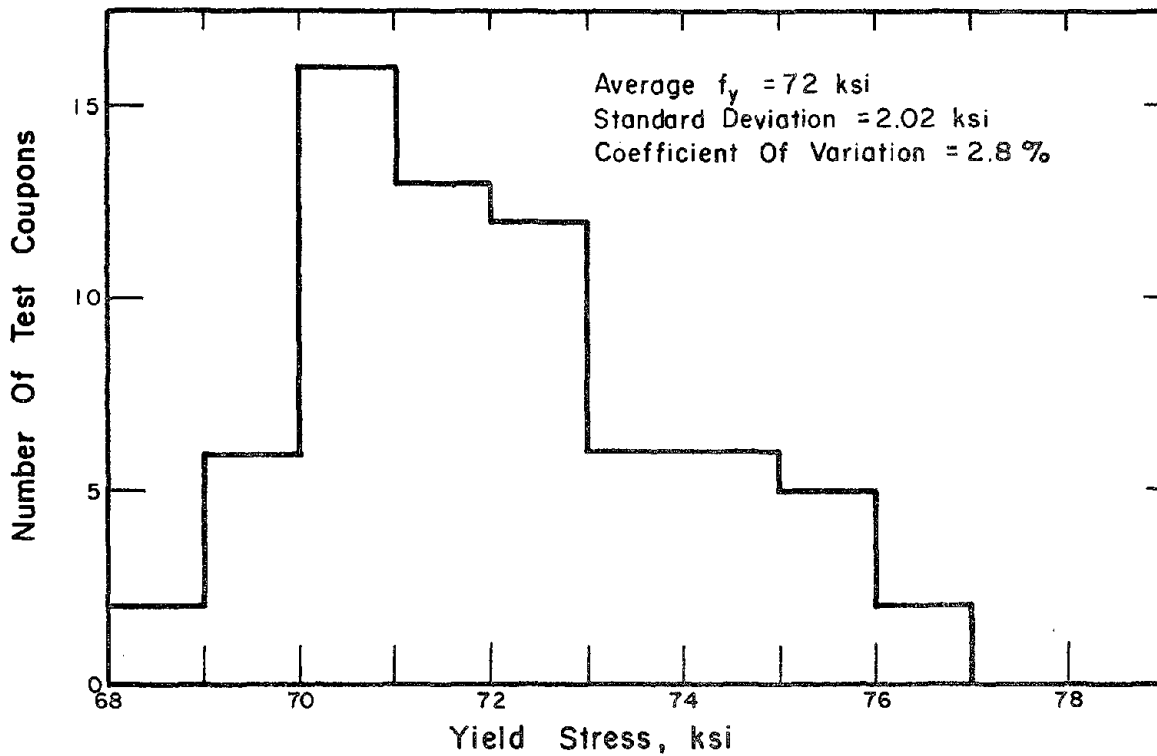
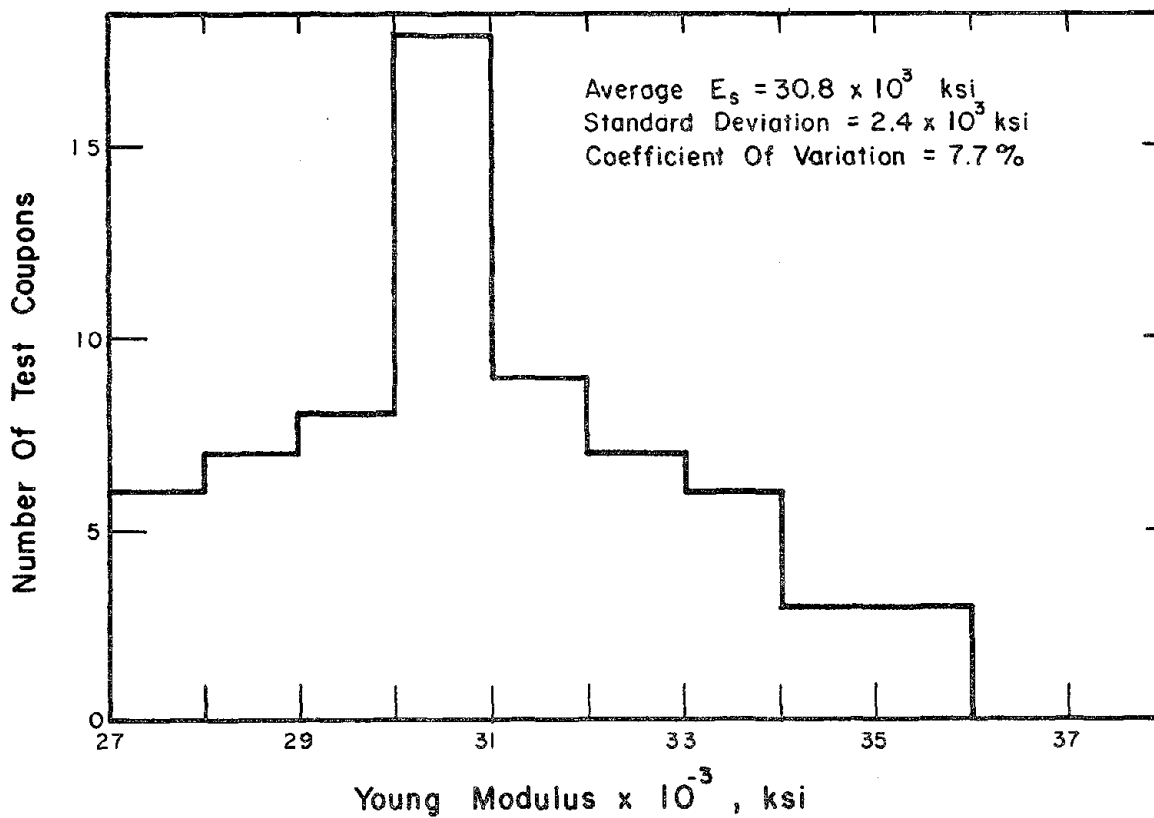Fig. A.8   Distribution of Measured Yield
Stress of No. 8 Gage Wire

Fig. A.9   Distribution of Measured Young's
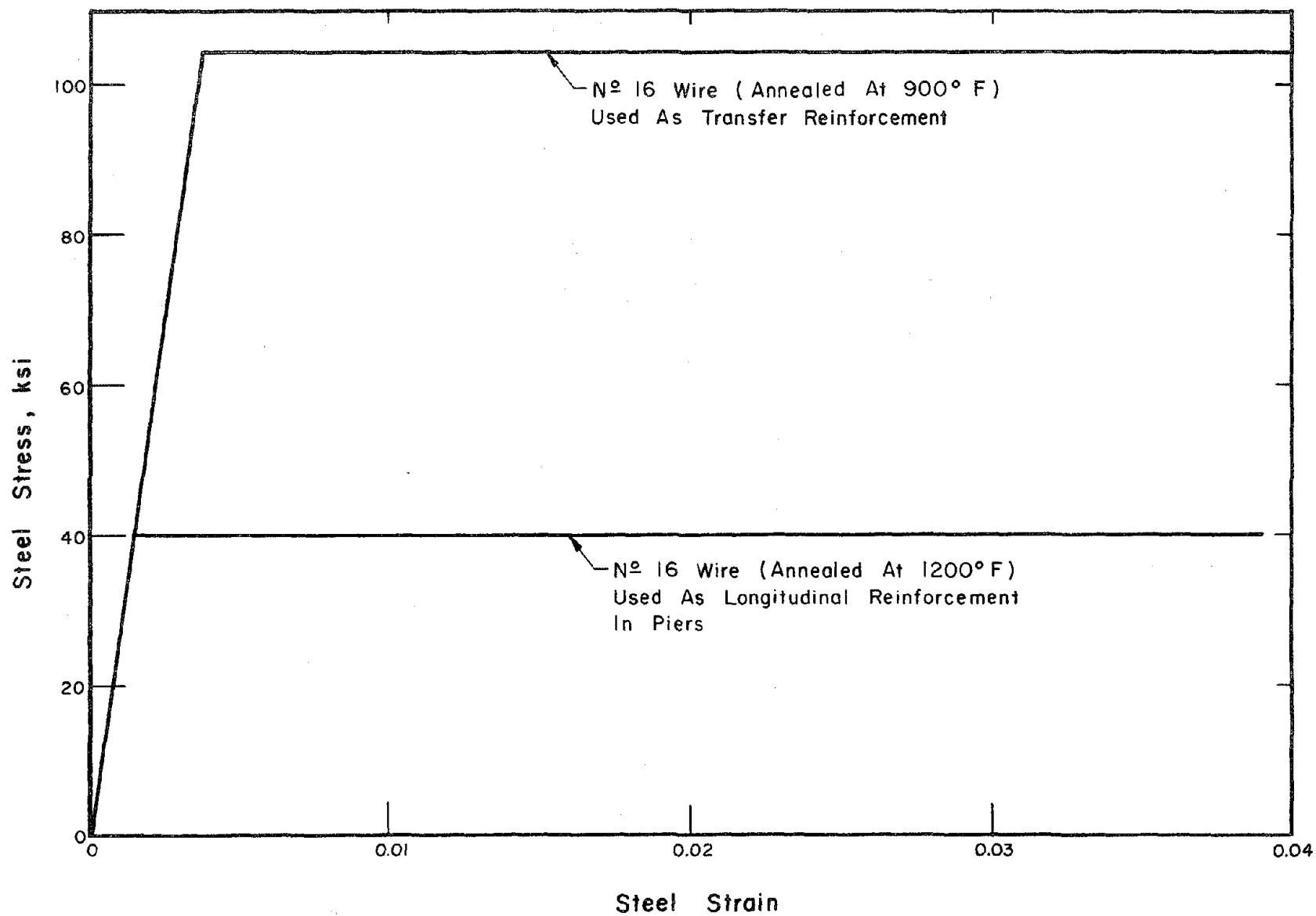Modulus of No. 8 Gage Wire

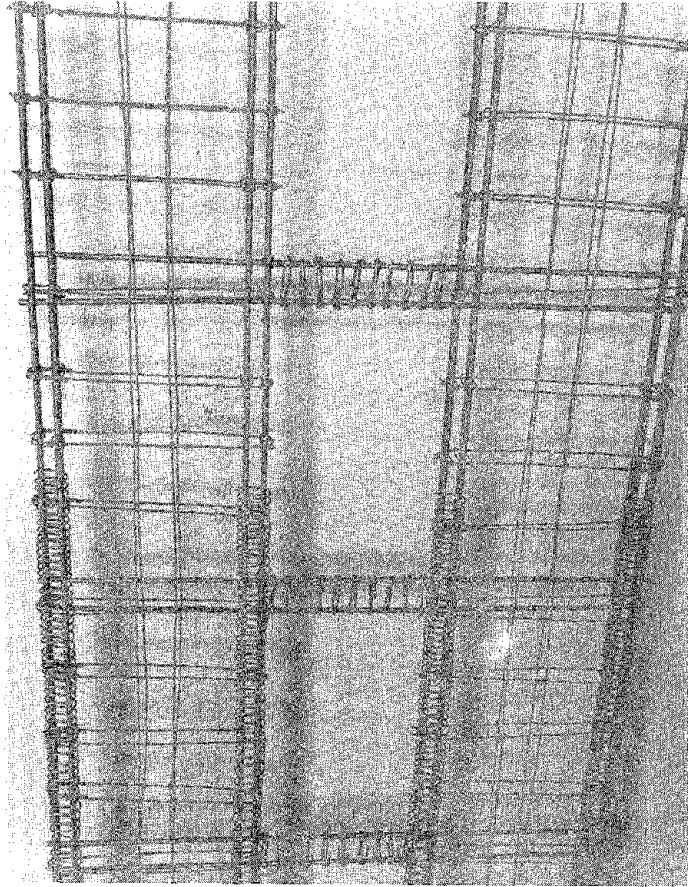Fig. A.10 Measured Stress-Strain Relationships for No. 16 Gage Wire

370

Fig. A.11   Beam and Wall Reinforcement (Frame D)
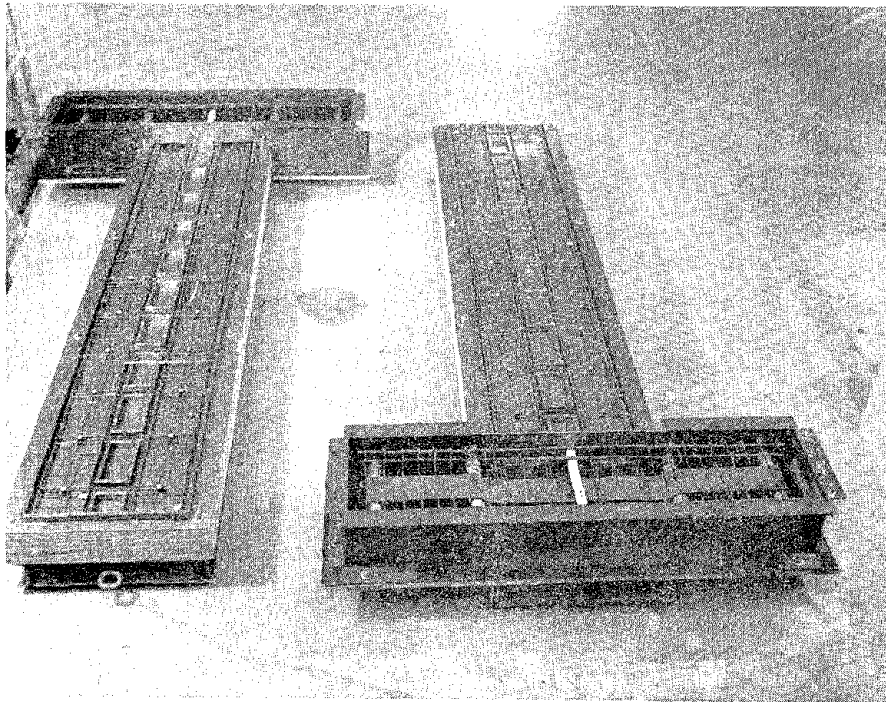

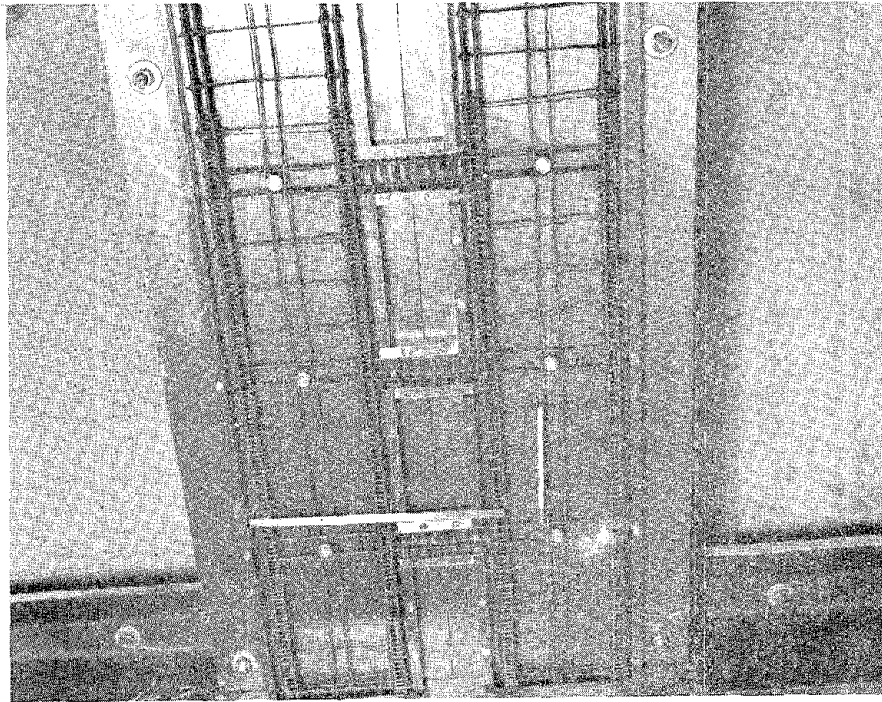Fig. A.12   A Typical Reinforcement Cage in the Casting Form

Fig. A.13   Detail of Reinforcement in the First
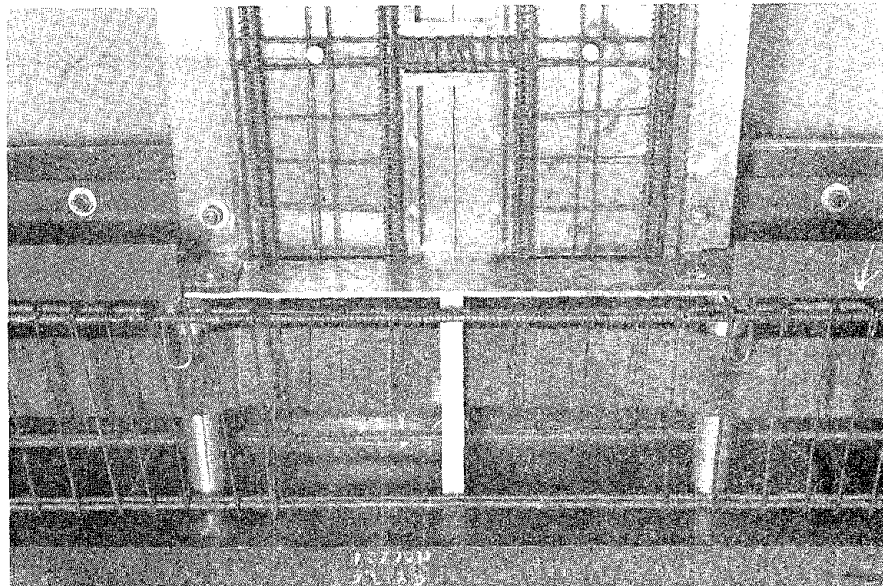   Three Levels (Frame D)

Fig. A.14   Detail of Base Girder Reinforcement
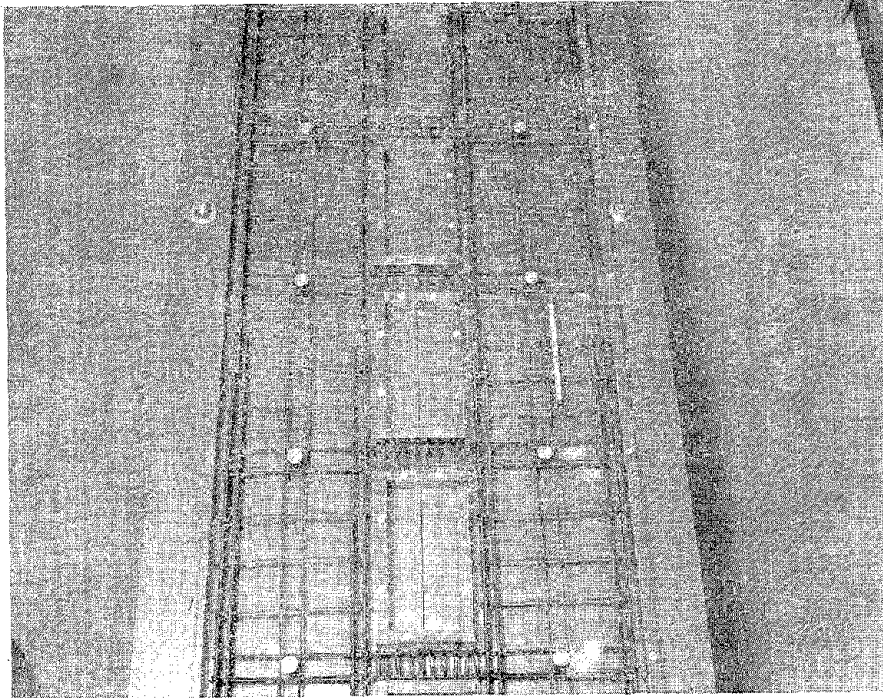
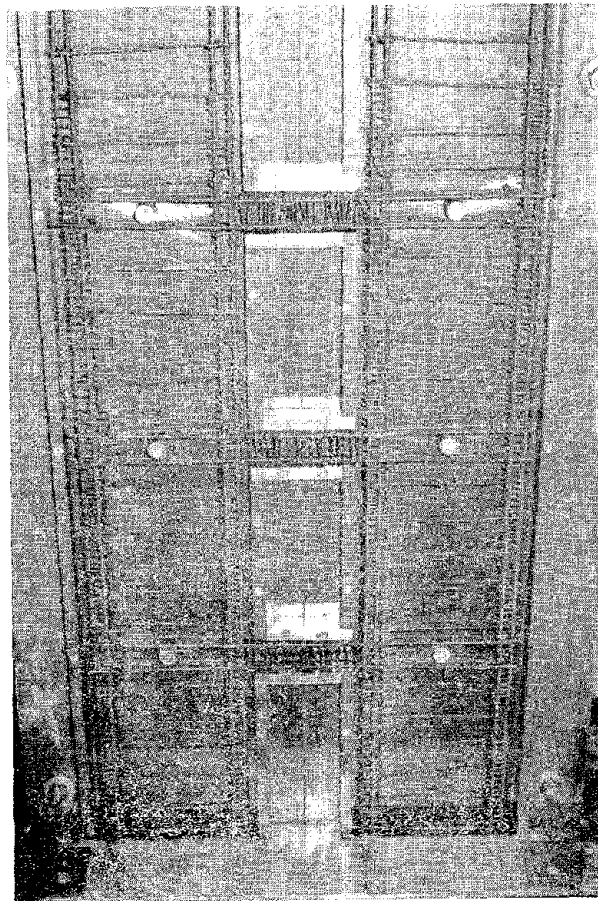Fig. A.15 Detail of Cutoff in Wall Reinforcement (Frame D)

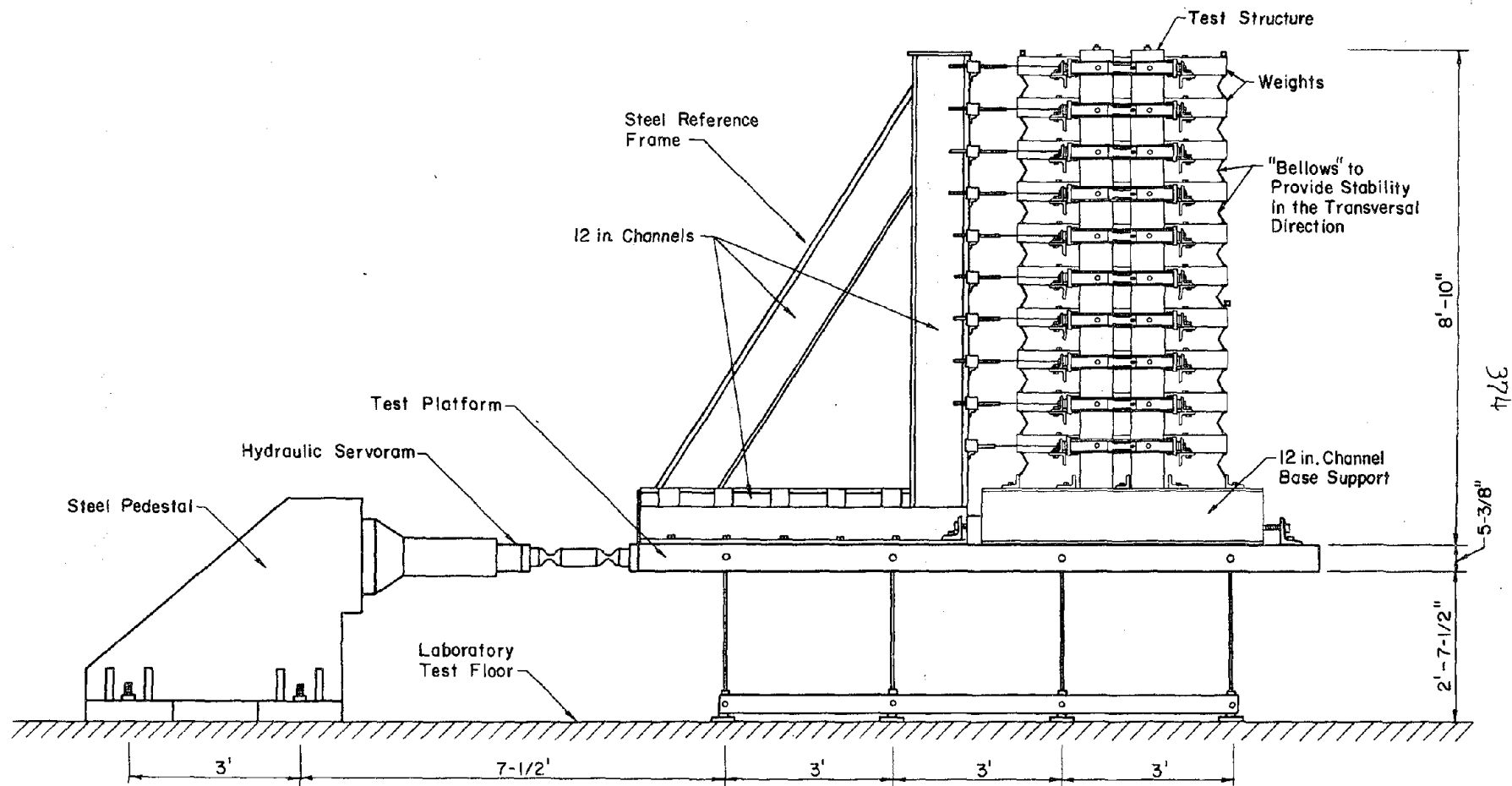Fig. A.16 Beam and Wall Reinforcement (Frame M)

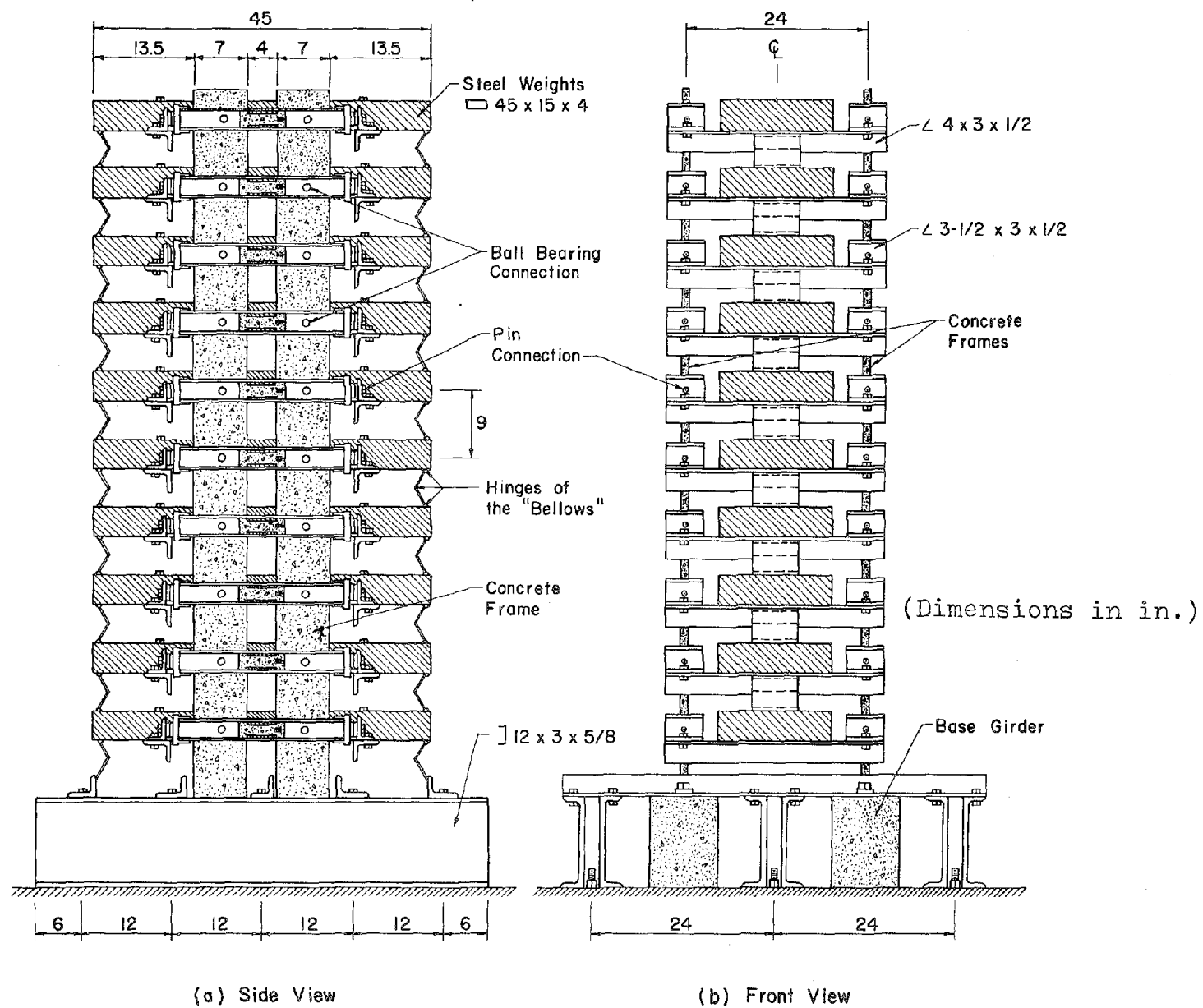Fig. A.17   Overall Configuration of the Test Setup

(Dimensions in in.)

(a) Side View   (b) Front View

Fig. A.18   Test Structure

APPENDIX B

THE FOURIER TRANSFORM PROGRAM

B.1 Introduction

This appendix contains a formal description of the computer program used to filter the response waveform records.

B.2 Definitions

The function S(w) defined for real w by

$$S(w) = \theta A(t) = \frac{1}{2\pi} \int_{-\infty}^{\infty} A(t)\, e^{-iwt}\, dt \quad \text{where } i = (-1)^{\frac{1}{2}} \quad (1)$$

is called the Fourier Transform of A(t); the operator θ is called the Fourier Transform operator. The inverse operator θ^{-1} is obtained by changing the sign of i, so that the equation above can be written

$$\theta^{-1} S(w) = \frac{1}{2\pi} \int_{-\infty}^{\infty} e^{iwt}\, S(w)\, dt = A(t) \quad (2)$$

Therefore

$$\theta^{-1}\theta\, A(t) = \theta\, \theta^{-1}\, A(t) = A(t) \quad (3)$$

What the Fourier operator does is simply a transformation from domain t to domain w, or more commonly from time (t) to frequency domain (w). The fundamental property of Fourier Transforms expressed by Eq. (3) makes possible to be used for filtering purposes of any real function A(t).

The following describes the numerical process used to find

the components between frequencies w_1 and w_2 of any record in the time domain. The method involves expressing $A(t)$ in terms of harmonic components, evaluating the response $A(t)$ to each frequency component, and then superposing the harmonic responses to obtain those corresponding between frequencies w_1 and w_2.

Equation (1) can be approximated by

$$S(w) \approx \frac{1}{2\pi} \delta \sum_{k=-N}^{N} A(k\delta) e^{-iwk\delta} \qquad (4)$$

where

$\qquad A(k\delta)$ = input vector

$\qquad \delta$ = time interval (or time increment)

$\qquad w$ = circular frequency

$\qquad N$ = number of points in array A

Equation (4) can be expanded as follows:

$$S(w) \approx \frac{1}{2\pi}\delta\, A(0) + \frac{1}{2\pi}\delta \sum_{k=1}^{N} A(k\delta)e^{-iwk\delta} + \frac{1}{2\pi}\delta \sum_{k=1}^{N} A(-k\delta)e^{iwk\delta}$$

$$\approx \frac{1}{2\pi}\delta\, A(0) + \frac{1}{2\pi}\delta \sum_{k=1}^{N} A(k\delta)e^{-2\pi ijk/N} + \frac{1}{2\pi}\delta \sum_{k=1}^{N} A(-k\delta)e^{2\pi ijk/N}$$

$$\approx \frac{\delta}{2\pi} \left[A(0) + FFTP_j + FFTP_{-j} \right] \qquad (5)$$

where

$$j = \frac{wN\delta}{2\pi}$$

$$FFTP_j = \sum_{k=1}^{N} A(k\delta)e^{-2\pi ijk/N}$$

$$FFTP_{-j} = \sum_{k=1}^{N} A(-k\delta)e^{2\pi ijk/N}$$

$FFTP_j$ and $FFTP_{-j}$ are evaluated using the library subroutine FFTP (Fast Fourier Transform program). For more information about this subroutine the reader is referred to the library functions Manual System/360 IBM.

The following FORTRAN program evaluates the harmonic components (P2) of a vector A between frequencies zero and FREQT (Hz).

```
      DO 3 I=1,NDT
      DUMMY= A(I)
3     DATA(I)= DCMPLX(DUMMY,0.000)
      CALL FFTP (DATA,NDT,IWK,IWK,IWK)
      DO 34 I=1,NDT
34    DATA(I)= DCONG(DATA(I))*DT
      DFREQ= 1./((NDT-1)*DT)
      I2= FREQPT/DFREQ
      I3= I2+1
      I4= 4096-I3
      DO 40 I=I3,I4
40    DATA(I)= DCMPLX(0.0D0,0.0D0)
      CALL FFTP (DATA,NDT,IWK,IWK,IWK)
      CONS= FLOAT(NDT)*DT
      DO 70 I=1,NDT
70    P2(I)= DREAL(DATA(I))/CONS
```

Where   NDT = number of data points (N)